

Understanding shoe-surface interactions in football

DRISCOLL, Heather Frances

Available from Sheffield Hallam University Research Archive (SHURA) at:

<http://shura.shu.ac.uk/17145/>

This document is the author deposited version. You are advised to consult the publisher's version if you wish to cite from it.

Published version

DRISCOLL, Heather Frances (2012). Understanding shoe-surface interactions in football. Doctoral, Sheffield Hallam University.

Repository use policy

Copyright © and Moral Rights for the papers on this site are retained by the individual authors and/or other copyright owners. Users may download and/or print one copy of any article(s) in SHURA to facilitate their private study or for non-commercial research. You may not engage in further distribution of the material or use it for any profit-making activities or any commercial gain.

102 040 950 9

Understanding shoe-surface interactions in football

Heather Frances Driscoll

A thesis submitted in partial fulfilment of the requirements of
Sheffield Hallam University
for the degree of Doctor of Philosophy

January 2012

Collaborating Organisation: adidas

ABSTRACT

One of the key aims of modern football shoe manufacturers is to find the balance between developing a shoe that improves performance but also minimises the risk of injury. Traction properties of the outsole play an important part in reaching this balance; high levels of traction are necessary to enable players to accelerate and change direction without slipping, but excessive traction can lead to stud fixation, a potential cause of injuries. The ability to accurately measure and assess the traction properties is essential in the design of outsoles, but appropriate test parameters need to be used in order for the assessment to relate back to the intended use. The purpose of the study was to develop a method to identify how the shoe interacts with the surface during realistic football movements and then to use observations from data collected to recommend appropriate test parameters.

A high-speed camera system was developed to capture the motion of the shoe in both a laboratory and natural turf environment. The cameras were calibrated using the checkerboard approach and filmed at 1000 Hz. Five markers positioned on the side of the shoe were tracked using a semi-automated algorithm developed using image processing techniques. Transposition matrices were used to identify the location of individual studs on the outsole of the shoe enabling the orientation, velocity and acceleration of the shoe to be calculated. Two data collection studies took place; firstly a single-participant study in the laboratory using a force-plate to relate kinematic results to kinetic information and secondly, a larger scale data collection outside on natural turf. Three movements representing scenarios requiring high levels of traction in football were assessed; acceleration, change in direction and braking. A representative trial for each movement was selected and full post-processing analysis was carried out. Information such as the orientation of the shoe on foot-strike, translation directions and centre of rotations during the transition phase and the number of studs in contact with the surface during push-off was obtained for each movement.

The period at which the player was at greatest risk of slipping was identified for each movement. The motion of the shoe during this period was used to suggest appropriate test conditions for mechanical and computational traction testing methods. The influence of the shoe-surface interaction on outsole design was also considered; with the observed translation directions and centre of rotations being used to suggest a design aiming to enhance translational traction, but minimise rotational resistance.

ACKNOWLEDGEMENTS

I would like to thank Professor Steve Haake, Harald Koerger and Dr Simon Goodwill for their support and guidance of this project. This thanks extends to all members of the Centre for Sports Engineering Research at Sheffield Hallam University; in particular Amanda Brothwell and Carole Harris for administrative support, Terry Senior for technical support, Dr John Kelley for his help in proof reading this document and Dr Tom Allen and Leon Foster for their encouragement and enthusiasm.

I am also grateful to adidas for the sponsorship of this project. The advice and expertise from Dr Bob Kirk, Dr Chris Holmes and Dr Daniel Price over the three years has been invaluable.

Finally I would like to thank Matthew Driscoll for proof reading the final document and my parents and Joseph Worsnip for their continual support.

CONTENTS

	ABSTRACT	ii
	ACKNOWLEDGMENTS	iii
	CONTENTS	iv
	LIST OF FIGURES	viii
	LIST OF TABLES	xvi
	NOMENCLATURE	xix
1	INTRODUCTION	1
1.1	Motivation for the research	1
1.2	Aim and objectives	4
1.3	Thesis structure	4
2	LITERATURE REVIEW	5
2.1	Introduction	5
2.2	Definition of traction	5
2.3	Measurement of traction	9
2.4	Surface classification	17
2.5	Biomechanics of football	24
2.6	Motion analysis	29
2.7	Photogrammetry	37
2.8	Chapter findings	45
3	ASSESSMENT OF CURRENT TRACTION TESTING METHODOLOGIES	47
3.1	Introduction	47
3.2	Aim and objectives	47
3.3	Mechanical traction testing	48
3.4	Surface shear stress analysis (Photoelasticity)	63
3.5	Modelling techniques	80
3.6	Chapter summary	90
4	METHODOLOGY FOR MOTION CAPTURE OF STUDED FOOTWEAR	92
4.1	Introduction	92
4.2	Aim and objectives	92
4.3	Stereo videogrammetry	93

4.4	Marker selection	103
4.5	Automated tracking methodology	107
4.6	Chapter summary	113
5	METHODOLOGY FOR POST PROCESSING AND VISUALISATION OF RESULTS	114
5.1	Introduction	114
5.2	Aim and objectives	114
5.3	Filtering techniques	115
5.4	Transformation to stud coordinates	122
5.5	Calculation of shoe orientation, velocity and acceleration	126
5.6	2D centre of rotation	132
5.7	3D helical screw axis	134
5.8	Chapter summary	135
6	VALIDATION AND ERROR ANALYSIS	136
6.1	Introduction	136
6.2	Aim and objectives	137
6.3	Reliability	137
6.4	Validation	142
6.5	Propagation of errors	146
6.6	Random errors	147
6.7	Chapter summary	148
7	TESTING PROTOCOL -----	149
7.1	Introduction	149
7.2	Equipment set-up	150
7.3	Definition of test movements	151
7.4	Notation	152
7.5	Indoor testing	152
7.6	Outdoor testing	153
7.7	Chapter summary	155
8	RESULTS AND ANALYSIS OF LABORATORY BASED DATA COLLECTION	156
8.1	Introduction	156
8.2	Results	157

8.3	Discussion	158
8.4	Defining impact and push-off	160
8.5	Identifying variables for comparison	163
8.6	Chapter summary	163
9	RESULTS AND ANALYSIS OF DONCASTER ROVERS FC DATA COLLECTION	165
9.1	Introduction	165
9.2	Results	167
9.3	Statistical analysis	170
9.4	Foot placement during kicking	178
9.5	Representative player trials	180
9.6	Analysis of representative trials	182
9.7	Chapter summary	205
10	INFLUENCE OF SHOE-SURFACE INTERACTIONS ON TRACTION TESTING PARAMETERS	210
10.1	Introduction	210
10.2	Mechanical traction testing	210
10.3	Analytical modelling	226
10.4	Computational modelling	228
10.5	Chapter summary	234
11	INFLUENCE OF SHOE-SURFACE INTERACTIONS IN OUTSOLE DESIGN	237
11.1	Introduction	237
11.2	Influence of shoe orientation at foot-strike and push-off	241
11.3	Influence of centre of rotation	244
11.4	Influence of translation vectors	246
11.5	Design suggestion	249
12	FUTURE WORK	251
12.1	Introduction	251
12.2	3D methodology development	251
12.3	Data collection and analysis	255
12.4	Influence of results on traction test methods and outsole design	256
12.5	Chapter summary	258

14	CONCLUSIONS	260
14.1	Assessment of current traction testing methodologies	260
14.2	Development and validation of 3D measurement system	261
14.3	Data collection and analysis	263
14.4	Influence of results	264
14.5	Limitations of the research	266
14.6	Future research	267
	REFERENCES	268
	PERSONAL BIBLIOGRAPHY	278
A	APPENDICES	279
A.1	Helical screw axis	279

LIST OF FIGURES

Figure 2.1	Schematic illustration of an interface, showing the real areas of contact (adapted from Persson 1998).	7
Figure 2.2	Composition of soil (adapted from Brouwer <i>et al.</i> 1985).	8
Figure 2.3	Causes of slips (adapted from Redfern <i>et al.</i> 2001).	9
Figure 2.4	Pendulum test foot in zero position (adapted from FIFA 2008)	10
Figure 2.5	Example traction curve.	11
Figure 2.6	Left: Influence of mass, radius and impact velocity on maximum force in a drop test with force platform. Right: Maximum force with two different shots on three surfaces (adapted from Nigg and Yeadon 1987).	19
Figure 2.7	Relationship between hardness, shoe-surface traction and other ground characteristics (adapted from Orchard 2001).	23
Figure 2.8	Force-plate with its reaction to applied force and vertical moment of force (adapted from Robertson <i>et al.</i> 2004).	30
Figure 2.9	Locomotion of a running horse captured by Muybridge (Kingston Museum and Heritage Service 2010).	38
Figure 2.10	Stroboscopic images by Edgerton, Left: "Densmore Shute bends the shaft"; Right: "Pitcher" (Edgerton, MIT Museum 2011).	39
Figure 3.1	Stud configurations on plate, from Left to Right: Copa Mundial, Pentagon, Tunit and World Cup.	50
Figure 3.2	Boots tested, from Left to Right: Copa Mundial, Predator, Tunit and World Cup.	50
Figure 3.3	Traction testing pitch locations, from Left to Right: Artificial turf (adidas TestCenter), Firm ground natural turf (Scheinfeld School) and Soft ground natural turf (Scheinfeld Football Club).	51
Figure 3.4	Investigation of testing parameters. Top left: Standard (adidas); Top right: No additional load; Bottom left: Faster translation; Bottom right: Longer displacement (mean \pm standard deviation).	51
Figure 3.5	Traction force displacement graphs for Top left: Copa Mundial; Top right: Predator; Bottom left: Tunit; Bottom right: World Cup shoes on natural firm ground turf (mean \pm standard deviation).	53
Figure 3.6	Force displacement plot for Copa Mundial on artificial turf. Left: Studded plate. Right: Full shoe.	57
Figure 3.7	Clegg hammer impact testing; voltage is directly proportional to impact force.	58
Figure 3.8	Maximum coefficient of traction (COT) against maximum torque for all shoe types on natural firm and soft ground conditions (mean \pm standard deviation).	60
Figure 3.9	Copa Mundial (shoe), force-displacement plot for all 5 repeats.	61
Figure 3.10	Stressed birefringent model viewed with two crossed polarisers (adapted from Dally and Riley 1991).	65
Figure 3.11	Fringe pattern in a frozen stress disk. Left: The dark isoclinic lines indicate the direction of the principal stresses. Right: The isochromatic fringe pattern indicates the areas over which the shear stress is constant. The reoccurrence of a colour or intensity can be used to determine the fringe order.	66

Figure 3.12	Experimental set-up in Sheffield.	68
Figure 3.13	Example of stress fringes generated in polyurethane using the studded plate.	69
Figure 3.14	Experimental set-up at Scheinfeld Top: Side-view; Bottom: Plan view (not to scale).	71
Figure 3.15	Image processing; the images were converted to greyscale and the background removed by calculation of the absolute difference method. The image properties were adjusted to produce a clearly defined stress patterns ($t = 0.20$ s).	72
Figure 3.16	Time series of stress patterns. Heel-strike and forefoot push-off photoelastic images during running in studded outsoles ($\Delta t = 0.04$ s).	73
Figure 3.17	Identifying maximum shear stress using greyscale intensity profiles. Top left: The intensity profile indicates clear peaks for the light fringes ($I \sim 255$) and troughs for the dark fringes ($I \sim 0$); Top right: Processed image - focussed on lower left forefoot; Bottom left: Calculation of shear stress using fringe order; Bottom right: The contour maps of the fringes indicate the increase in maximum shear towards the contact zone.	74
Figure 3.18	Stress trajectory and side view of shoe during heel-strike and forefoot push-off (white arrows indicate direction of motion of studs or growth of fringes).	75
Figure 3.19	Vector plot of first fringe location at time steps 0.02 s at 30° intervals around stud contact.	76
Figure 3.20	Force data for heel-strike.	77
Figure 3.21	Tracking locations for the right foot during heel-strike.	78
Figure 3.22	Springs in series modelling a drop hammer impact with a stud and ground.	82
Figure 3.23	Drop hammer soft and firm ground force deflection curves (red line) indicates simulated stiffness curves.	83
Figure 3.24	Instron® testing of Smart stud, force deflection curve.	83
Figure 3.25	Calculation of modified boundary conditions from literature results.	85
Figure 3.26	Analytical modelling – Top: Drop hammer boundary conditions - Left: Soft ground; Right: Firm ground - Bottom: Realistic loading conditions – Left: Soft ground; Right: Firm ground.	85
Figure 3.27	Verification of model; force-displacement results for FE model and Instron® testing.	87
Figure 3.28	Force displacement curves for drop hammer experiment and FE simulation.	88
Figure 3.29	Illustration of stud deformation on crushable foam surface.	88
Figure 3.30	Relative deformation of stud on soft ground conditions.	89
Figure 4.1	Assessment of optimal camera angle (adapted from Chen & Davis 2000).	93
Figure 4.2	Camera position and marker visibility.	94
Figure 4.3	High exposure and low frame rates can lead to blurring of markers during high velocity movement. Left: when the shoe is stationary the image is not blurred; Centre: during push-off, shoe velocity increases and details become blurred; Right: original heel marker shape and blurred marker shape could lead to error in centroid location.	96

Figure 4.4	Aliasing of original sine waveform by sampling lower than the Nyquist frequency. Top: Sampling at 2 Hz; Bottom: Sampling at 1.5 Hz. (Adapted from Olshausen 2000).	97
Figure 4.5	Vertical displacement data sampling at 1000 Hz and 60 Hz.	98
Figure 4.6	Mosaic of checkerboard images used to define the 3D test volume.	100
Figure 4.7	Extraction of checkerboard calibration pattern using grid square intersections.	100
Figure 4.8	Pixel re-projection error after calibration in a laboratory environment.	101
Figure 4.9	Global origin; participants run parallel to the y-axis, from right to left.	102
Figure 4.10	Foot anatomy and chosen shoe marker location.	103
Figure 4.11	Spherical reflective markers (Right: image from Quintic 2011).	104
Figure 4.12	LED markers in the laboratory and outside (exposure 40ps).	105
Figure 4.13	Retro-reflective top coating (adapted from Glowtec 2011).	105
Figure 4.14	Example test shoe with white retro-reflective markers.	106
Figure 4.15	Labelling and tracking of white objects after conversion to a binary image.	108
Figure 4.16	Left: Original binary image of a rectangular object 5×3 pixels; Centre: Square structuring element; Right: Dilating image adds the structural element to each side of the object.	108
Figure 4.17	Marker dilation. From left to right: original marker; marker at next time step; dilated marker; inversed dilated marker; overlap of dilated and marker at next time step.	109
Figure 4.18	Image cropped around selected marker coordinates and converted to a binary image; white objects are then labelled from left to right.	109
Figure 4.19	Predicting marker location using the difference between the previous two marker coordinates.	110
Figure 4.20	Differences in image brightness with changing light levels in outdoor testing.	111
Figure 4.21	Conversion to binary image. Top left: Dark, threshold 0.08; Top centre: Dark, threshold 0.12; Top right: Dark, threshold 0.18; Bottom left: Light, threshold 0.18; Bottom centre: Light, threshold 0.5; Bottom right: Light, threshold 0.6.	111
Figure 4.22	Using predicted method to estimate location of marker when obscured from view.	112
Figure 4.23	Visualisation of the results of tracking a marker from first frame to last selected frame.	112
Figure 5.1	Noise is amplified at each stage of differentiation.	115
Figure 5.2	Hypothetical frequency spectrum of a waveform consisting of a desired signal and unwanted higher frequency noise (adapted from Winter 2005).	116
Figure 5.3	Moving average filters applied to vertical displacement data (1000 Hz).	118
Figure 5.4	Plot of the residual between a filtered and an unfiltered signal as a function of the filter cut-off frequency (adapted from Winter 2005).	119
Figure 5.5	Left: Filtering using a Butterworth filter (85 Hz); Right: Residual value at varying cut-off frequencies.	120

Figure 5.6	Left: Filtering using a 7th order polynomial filter; Right: Effect of order on residual.	121
Figure 5.7	Assessment of filtering techniques.	122
Figure 5.8	Original marker position and chosen studs for transposition.	123
Figure 5.9	Defining Euler angles. Top left: Translating S1 to origin; Top right: Rotation about x axis = pitch; Bottom left: Rotation about z axis = yaw; Bottom right: Rotation about y axis = roll.	126
Figure 5.10	Schematic showing the orientation of the shoe.	128
Figure 5.11	Central differencing technique for calculating slope of curve at the Ah sample point (adapted from Winter 2005).	129
Figure 5.12	Calculating velocity using the central differencing approach from raw and filtered data (1000 Hz).	130
Figure 5.13	Calculation of acceleration using the central differencing technique from displacement and velocity data.	130
Figure 5.14	Plot of displacement and velocity from simulated data.	131
Figure 5.15	Reuleaux method (adapted from Baroon and Ravani 2006).	132
Figure 5.16	Example of centre of rotation from stud positions between 0.03 and 0.10 s after foot-strike.	133
Figure 6.1	Quality of data depends on both the accuracy and consistency (adapted from Maiwald 2011).	136
Figure 6.2	Three markers were tracked using the MAC system and semi-automated method.	143
Figure 6.3	Horizontal trajectory of marker tracked using the MAC system and semi-automated method.	145
Figure 7.1	Camera placement and axis system in field of view at Doncaster Rovers FC training ground.	150
Figure 7.2	Movement schematic for player testing. Left: Acceleration phase of sprinting; Centre: 45° lateral side-cut; Right: Long range kick.	151
Figure 7.3	Marker and axis notation. Top left: Marker positions on side of left shoe; Bottom left: Stud notation, aerial view; Top right: Axis orientation with respect to direction of motion, side view; Bottom right: Axis notation aerial view.	152
Figure 7.4	Surface condition after testing.	154
Figure 8.1	Position history for the metatarsal-phalangeal marker (P3) during a sprint movement (200 Hz).	157
Figure 8.2	Rotation angles for the rear-foot section during a sprint movement (200 Hz).	157
Figure 8.3	Example force-plate data for sprint movement (1000 Hz); Fz = vertical, +/- Fy = posterior/anterior, +/- Fx = medial/lateral; a = peak anterior force, b = peak lateral force, c = peak vertical force, d = peak posterior force.	157
Figure 8.4	Position of the metatarsal-phalangeal marker in terms of y and z displacement	159
Figure 8.5	Vertical displacement of marker P3, Left: Laboratory; Right: Natural turf.	161
Figure 8.6	Velocity and acceleration in the vertical direction (z) for marker P3, Left: Laboratory; Right: Natural turf.	161

Figure 8.7	Using horizontal force (red) and vertical displacement (black) of marker P3 to define push-off, Left: Laboratory (push-off at 0.146 s); Right: Natural turf (push-off at 0.113 s).	162
Figure 9.1	Relative frequency of pitch angle.	172
Figure 9.2	Relative frequency of yaw angle.	172
Figure 9.3	Relative frequency of roll angle.	173
Figure 9.4	Top left: Pitch and yaw angles; Top right: Yaw and roll angles; Bottom left: Pitch and roll angles; Bottom right: Possible groupings.	174
Figure 9.5	Scatter plots of kick impact angles after cluster groupings.	175
Figure 9.6	Position of support foot during the kick; lines represent distance from heel to toe studs (distance values in mm, ball centre positioned at 0,0).	179
Figure 9.7	Relationship between ball launch angle and position of the support foot.	179
Figure 9.8	Visual image of the left foot at 20% (0.03 s) intervals during the sprint movement from -20 to 120% contact time (motion from right to left).	184
Figure 9.9	Acceleration of marker P3 used to define time of impact (green marker indicates maximum vertical acceleration).	184
Figure 9.10	Position of marker P3 in the yz (horizontal-vertical) plane during the sprint movement (1000 Hz); green to red marker = foot-strike phase, red to blue marker = translation phase, blue to purple marker = push-off phase (arrows indicate shoe motion direction, total contact time = 0.15 s).	185
Figure 9.11	Horizontal (y) and vertical (z) displacement of marker P3 (1000 Hz; contact time = 0.15 s).	185
Figure 9.12	Orientation of the shoe (200 Hz; contact time = 0.15 s).	186
Figure 9.13	Velocity and orientation of shoe on foot-strike during sprint movement.	187
Figure 9.14	Position history of studs S3 and S11 in the yz plane during foot-strike phase (0 - 0.03 s) (Green markers indicate the time of initial foot-strike (0 s); red indicates 0.03 s after foot-strike; arrows represent stud motion direction).	187
Figure 9.15	Position of stud S3 in the horizontal (y) and vertical (z) directions (red markers indicate start of transition phase, 0.03 s and blue markers end, 0.09 s).	188
Figure 9.16	Relative positions of studs S11, S6 and S3 during contact phase (red markers indicates 0.03 s and blue markers 0.09 s after initial foot-strike; arrows indicate stud motion direction).	189
Figure 9.17	Plan view (xy) of forefoot stud positions and corresponding centre of rotation during the transition phase (0.03 - 0.09 s) of the sprint movement (shaded circle represents ± 1 SD of centre of rotation; arrow indicates rotation direction).	190
Figure 9.18	Motion path of studs S3 and S11 in the yz and xz planes (Blue marker indicates start of push-off phase, purple marker end of push-off phase).	191
Figure 9.19	Centre of rotation and resulting path of movement; blue markers indicate start of push-off (0.09 s) and purple markers end of push-off phase (0.15 s); dashed lines represent the motion path assuming a rigid system rotating about the calculated centre of rotation (red marker).	192

Figure 9.20	Fixed system rotation for forefoot during sprint movement in yz plane (blue indicates starting position and purple represents the position at the end of movement).	193
Figure 9.21	Visual image of the left shoe during the side-cut movement (from -20 to 120% contact time, at 20% (0.06 s) intervals; motion from right to left).	194
Figure 9.22	Orientation of the shoe during the side-cut movement (200 Hz); green to red markers = foot-strike phase, red to blue markers = transition phase, blue to purple markers = push-off phase.	195
Figure 9.23	Horizontal (y) displacement of stud S3 during the side-cut movement.	195
Figure 9.24	Vertical (z) displacement of stud S3 during the side-cut movement.	195
Figure 9.25	Horizontal (x) displacement of stud S3 during the side-cut movement.	196
Figure 9.26	Centre of rotation of the transition phase in the side-cut movement (shaded area indicates ± 1 SD for the calculation of the centre of rotation).	199
Figure 9.27	Position of studs S1, S3 and S11 in the xz and yz planes (blue markers indicate start of push-off (0.18 s) and purple markers end of push-off (0.28 s)).	200
Figure 9.28	Motion path of studs S11 and S3 during the push-off stage in the sprint and side-cut movements.	201
Figure 9.29	Visual image of planted left foot during the kick movement at foot-strike, ball contact, end of ball contact and end of movement (motion from right to left).	202
Figure 9.30	Pitch angle of the planted foot during kicking.	202
Figure 9.31	Summary of shoe motion during the sprint movement.	208
Figure 9.32	Summary of shoe motion during the side-cut movement.	208
Figure 9.33	Summary of shoe motion during the kick movement.	209
Figure 10.1	Percentage of absolute maximum for contributing grip factors in the sprint movement.	213
Figure 10.2	Resulting grip factor for the sprint movement with a safety factor of 2.	214
Figure 10.3	Percentage of absolute maximum for contributing factors in the kicking movement.	215
Figure 10.4	Resulting grip factor for kick movement with a safety factor of 2.	215
Figure 10.5	Slip of the planted foot during Hook's penalty kick during the Wales v France World Cup semi-final, 2011 (Screen shots taken from video from ITV pic. 2011).	216
Figure 10.6	Percentage of absolute maximum for contributing factors in the side-cut movement.	217
Figure 10.7	Resulting grip factor for side-cut movement.	218
Figure 10.8	Translation of shoe testing conditions to replicate motion during critical slip period during sprinting.	220
Figure 10.9	Translation of shoe testing conditions to replicate motion during critical slip period in the kick movement.	221
Figure 10.10	Translation of shoe testing conditions to replicate motion during critical slip period in the side-cut movement.	222
Figure 10.11	Test parameters for pendulum device.	226

Figure 10.12	Modified test conditions from player testing results.	226
Figure 10.13	Relative deformation of a Copa Mundial stud (10 mm forefoot, 12 mm heel) on firm ground conditions using input parameters derived from player testing of a sprint, kick and side-cut movement.	227
Figure 10.14	Illustration of stud penetration depth for each movement using new input parameters.	228
Figure 10.15	Coordinate position of stud S3 during the sprint movement (200 Hz).	230
Figure 10.16	Example boundary conditions for the foot-strike phase of the sprint movement applied to rigid body nodes on the studs S1, S2 and S3.	232
Figure 10.17	Position of the centre of rotation during the contact phase for a sprint trial.	233
Figure 11.1	Design cycle. Left: Traditional, player testing occurs after prototype development; Right: Modified, player testing is the starting point for idea generation.	237
Figure 11.2	Nike SENSE stud technology on the medial side of the forefoot on the Mercurial Vapor Superfly III (Nike INC. 2011).	238
Figure 11.3	Orientation and velocity vectors of the forefoot studs on foot-strike (sprint).	241
Figure 11.4	Orientation and velocity vectors of the forefoot studs at push-off (sprint).	242
Figure 11.5	Orientation and velocity vectors of the heel studs on foot-strike (kick).	242
Figure 11.6	Orientation and velocity vectors of the heel studs on foot-strike (side-cut).	243
Figure 11.7	Estimated centres of rotations (red markers) for the adidas F10 TRX AG outsole (adapted from adidas Group 2011); the dashed circles indicate the possible centre of rotation and corresponding motion path given the shape and orientation of the studs.	244
Figure 11.8	Left: Centre of rotation in sprint movement; Right: Centre of rotation during side-cut movement with Copa Mundial stud configuration; red markers indicate the observed centre of rotation from player testing and the dashed lines represent the corresponding motion path for the forefoot or heel about the calculated centre.	245
Figure 11.9	Position history of forefoot studs for the sprint movement.	246
Figure 11.10	Position history of all studs for the kick movement.	247
Figure 11.11	Position history of all studs for the side-cut movement.	247
Figure 11.12	Motion vectors for the sprint movement.	248
Figure 11.13	Motion vectors for the kick movement.	248
Figure 11.14	Motion vectors for the side-cut movement.	248
Figure 11.15	Outsole design suggestion.	249
Figure 12.1	Extended camera set-up for increased viewing area.	252
Figure 12.2	Use of <i>graythresh</i> function to identify appropriate binary conversion threshold.	253
Figure A.1	Left: Bisecting linear line complex; Right: The linear line complex of path normal (adapted from Eberhardter and Ravani 2006).	280

Figure A.2	Visual representation of the helical screw axis parameters; arrow represents the direction vector of the helical screw axis, radius of the cylinder relates to the angle of rotation and length of the cylinder to the displacement along the axis.	283
Figure A.3	Helical axis position for the sprint movement.	285
Figure A.4	Helical screw axis positions throughout kick movement (kick positions in red).	287
Figure A.5	Helical screw axis position for side-cut movement.	289

LIST OF TABLES

Table 2.1	Factors influencing shoe-surface traction.	8
Table 2.2	Observations and conclusions made by Nigg (1990) in relation to the traction assessment of shoes and surfaces.	14
Table 2.3	Soil properties (from Dixon <i>et al.</i> 2008).	20
Table 2.4	Proposed standards for playing performance (Canaway <i>et al.</i> 1990).	21
Table 2.5	Maximum permitted rainfalls for test results to be valid (Baker 1991).	22
Table 2.6	Summary of non-optical measurement methods (Orr and Shelton 1997).	36
Table 3.1	Assessment of testing parameters.	49
Table 3.2	Shoe properties.	50
Table 3.3	Traction force values for all shoes at set displacements during translation (mean \pm standard error).	54
Table 3.4	Ranking of traction values for translation movement for shoes on all surfaces (1 = highest).	55
Table 3.5	Tabular report of Analysis of Variance for all shoes on firm ground at 10 mm displacement.	55
Table 3.6	Tabular report of Analysis of Variance for all shoes on firm ground at 20 mm displacement.	55
Table 3.7	Tabular report of Analysis of Variance for all shoes on firm ground at 50 mm displacement.	56
Table 3.8	Mean difference analysis, * $p < .05$	56
Table 3.9	Assessment of differences between the plate and the shoe using f-tests for artificial surface.	57
Table 3.10	Clegg hardness values (mean \pm standard error).	59
Table 3.11	Significance of difference between firm and soft ground conditions using a Ftest.	59
Table 3.12	Average standard deviation in force over 50 mm displacement during translation movement.	61
Table 3.13	Advantages and disadvantages of mechanical traction testing.	62
Table 3.14	Optical and mechanical properties of polycarbonate and urethane (adapted from Dally and Riley 1991).	67
Table 3.15	Advantages and disadvantages of photoelastic testing.	79
Table 3.16	Advantages and disadvantages of computational (FEA) and analytical modelling.	81
Table 3.17	Derived stiffness equations for ground and stud.	84
Table 3.18	Iterative solution to equation of motion.	84
Table 3.19	Computational stud-foam model boundary conditions.	88
Table 6.1	Sources of error.	137
Table 6.2	Assessment of error in manual tracking.	138
Table 6.3	Assessment of error in semi-automated tracking.	138
Table 6.4	Assessment of errors in manual tracking after stereo-triangulation.	139

Table 6.5	Assessment of error in semi-automated tracking after stereo-triangulation.	139
Table 6.6	Significance of difference between manual and semi-automated tracking using a t-test (mean values are used from 5 repeats of 2 markers over 26 frames).	140
Table 6.7	Significance of difference between manual and semi-automated tracking methods using results set to the origin.	141
Table 6.8	Assessment of reliability using t-tests (velocity in ms ⁻¹).	142
Table 6.9	Mean and standard deviation of stationary marker.	143
Table 6.10	Variation in vertical displacement of moving marker.	144
Table 6.11	Roundness metrics of marker trajectory.	144
Table 6.12	Difference between measured and predicted stud position.	145
Table 7.1	Indoor data collection test conditions.	153
Table 7.2	Outdoor data collection test conditions.	154
Table 8.1	Orientation of the shoe on foot-strike.	163
Table 9.1	Player and movement trial terminology.	165
Table 9.2	Results collected from Doncaster testing.	165
Table 9.3	Results collected for complete shoe for representative player trials.	165
Table 9.4	Sprint results at foot-strike (N = 19).	167
Table 9.5	Sprint results at push-off (N = 12).	168
Table 9.6	Kick results at foot-strike (N = 34).	168
Table 9.7	Side-cut results at foot-strike (N = 21).	169
Table 9.8	Tabular report of analysis of variance for pitch angle.	170
Table 9.9	Tabular report of analysis of variance for yaw angle.	170
Table 9.10	Tabular report of analysis of variance for roll angle.	170
Table 9.11	Mean difference analysis for pitch angle.	171
Table 9.12	Mean difference analysis for pitch angle.	171
Table 9.13	Mean difference analysis for roll angle.	171
Table 9.14	K-means cluster method groups for kick movement.	174
Table 9.15	K-means cluster method groups for sprint movement.	176
Table 9.16	K-means cluster method groups for side-cut movement.	177
Table 9.17	Significant relationships using Spearman's rank analysis.	178
Table 9.18	Representative players for the sprint movement.	180
Table 9.19	Student's Best results for sprint group mean and representative player trial.	181
Table 9.20	Representative player trial for the kick movement.	181
Table 9.21	Representative player trial for the side-cut movement.	182
Table 9.22	Position of studs S3 and S11 and orientation of the shoe at push-off phase (position in mm, angle in °).	191

Table 9.23	Position of studs S1, S2 and S3 (in mm).	197
Table 9.24	Position of lateral (S1) and medial (S2) heel studs (inmm).	198
Table 9.25	Position of rear of forefoot (S3) and toe (S11) studs(in mm).	198
Table 9.26	Position of studs S1, S3 and S11 (in mm).	200
Table 9.27	Position of studs S1, S2 and S3 (mm).	203
Table 9.28	Orientation of the shoe (°).	203
Table 9.29	Position of studs S1, S2 and S3 (mm).	204
Table 9.30	Orientation of the shoe (°).	204
Table 10.1	Current test parameters and limits of the adidas traction tester, total load = 69.3 kg.	210
Table 10.2	Test parameters for rotation of forefoot and complete shoe replicating the sprint and side-cut movements (stud positions for size UK 9.5, distances in mm).	223
Table 10.3	Five testing parameters to represent translations and rotations observed in the sprint, kick and side-cut movements.	224
Table 10.4	Boundary conditions of 3 rigid nodes on the outsole during sprinting (displacements in mm, time increments in s).	229
Table 10.5	Boundary conditions for replication of impact motion for sprint, side-cut and kick movements (orientation represents pitch, yaw and roll angles respectively; stud velocities represent x, y and z components).	231
Table 12.1	Potential variables for investigation.	255
Table A.1	Helical screw axis parameters for the sprint movement (bold indicates dominant direction).	284
Table A.2	Helical screw axis parameters for the kick movement.	286
Table A.3	Helical screw axis parameters for the side-cut movement.	288

NOMENCLATURE

Abbreviations

ACL	Anterior cruciate ligament
AFL	Australian Football League
BMC	Bloomfield movement classification
BW	Body weight
COT	Coefficient of traction
DLT	Direct linear transformation
FC	Football club
FG	Firm ground
FIFA	Federation Internationale de Football Association
fps	Frames per second
GRF	Ground reaction force
MAC	Motion Analysis Corporation
RCOF	Required coefficient of friction
SG	Soft ground
SLR	Single lens reflex

Symbols

F	Frictional force	[N]
F	Coefficient of friction	
R	Normal reaction	[N]
	3D world coordinate vector	
X_t	Coordinate vector in camera reference frame	
T_c	Translation matrix	
R_c	Rotation matrix	
$n^{\wedge}n^2$	Principal indices of refraction	
	Principal stresses	[Nm ²]
c	Stress-optic coefficient	
A	Relative angular phase shift	
h	Material thickness	[m]
λ	Wavelength	[m]
N	Fringe order	

fa	Material fringe value	[Nm ⁻¹]
T_{-max}	Maximum shear stress	[Nm ⁻²]
F	Spring/mass force	[N]
m	Mass	[kg]
y	Spring/mass acceleration	[ms ⁻²]
y	Spring/mass displacement	[m]
k	Spring stiffness	[Nm ⁻¹]
I	Spring/mass impulse	[Ns]
fs	Sampling frequency	[Hz]
fc	Highest frequency	[Hz]
fn	Fourier frequency	[Hz]
(w,v)	Image coordinates	
R	Residual	
	Raw data at the zth sample	
$X'i$	Filtered data at the zth sample	
Pi	Shoe markers, where $i = 1-5$	
Si	Stud identification, where $i = 1-12$	
a	Pitch angle	
P	Yaw angle	
γ	Roll angle	
V;	Velocity	[ms ⁻¹]
«i	Acceleration	[ms ⁻²]
Xi	Displacement	[m]
$F_{x,y,z}$	Force in x, y or z direction	[N]
Q	Plucker coordinate direction vector	
V_o	Plucker coordinate moment vector	
SD	Standard deviation	
SE_m	Standard error of the mean	
SE_d	Standard error of the difference	
df	Degrees of freedom	
(S_{ix} , S_{iy} , S_{zz})	Stud coordinate position	
P/S,	Player l , where $l = 1-8$, Sprint trial j , where $j = 1-5$	
P/K,	Player l , where $l = 1-8$, Kick trial j , where $j = 1-5$	
P/C,	Player l , where $l = 1-8$, Side-cut trial j , where $j = 1-5$	

1 INTRODUCTION

The following chapters contain a three year study into the development and application of a measurement system to identify appropriate test parameters for traction testing of studded outsoles.

1.1 Motivation for the research

Football is one of the most popular sports in the world, with approximately 270 million people actively involved in the game (FIFA 2007). Secondary to the ball, football shoes play an important and influential role in the game. For many they are perceived as a footballer's tool (Torell 2011), forming the link between the ball and the player, and similarly between the pitch and the player. Football shoes were originally work boots, and although not fitted with studs, players would hammer nails or metal tacks into the sole of the shoe to increase the traction on the muddy pitches. By the 1920s football specific boot designs were being produced; for example the 'Mansfield Hotspur' was marketed as a boot offering "a rounded sole to edge preventing mud clogging and lock-riveted studs placed for improved grip and support" (Winner 2005). Shoe development progressed steadily and at the 1954 World Cup adidas gained international recognition with the innovation of interchangeable studs. During the final against Hungary, weather conditions turned causing the pitch to become muddy and waterlogged. At half time, the German team switched the studs on their boots to provide extra traction and went on to win the match whilst the Hungarian team struggled with the slippery conditions (adidas Group 2009). The 1954 World Cup was a wake-up call to the footwear industry with the notion that the design of the shoe can have a directed influence on the performance of players and the outcome of a game.

A wide selection of football shoes is now available on the market, targeted to meet the requirements of natural and artificial turf and indoor surfaces. With such a large choice available to consumers, pressure is on manufacturers to release innovative and exciting new designs. The current trend is for lightweight football shoes; during the build-up to the 2010 World Cup, the title for lightest football shoe changed hands four times with the winning shoe weighing only 150 g. Many players make a connection between the use of lighter shoes and the feeling of speed (Torell 2011) and lightweight shoes are often marketed towards fast and skilful players; starting with Ronaldo in 1998 wearing the Nike Air Mercurial (>200 g) and now Messi in 2011 wearing the adidas F50 adiZero

(165 g). The reduction of weight however, comes at a price; many players have experienced negative health related issues due to the lack of foot support or protection from impacts from the lighter weight shoes (Torell 2011). In 2000, the frequency of football injuries was estimated to be up to 35 per 1000 playing hours, with the majority of injuries occurring to the lower extremities (Dvorak and Junge 2000). Lack of support and lacerations from other player's studs are two potential injury causes; another significant contributor is stud fixation caused by excessive traction particularly during turning movements.

The traction between a football outsole and the surface was originally necessary to meet one goal; prevent the player from slipping over. If the available traction from the shoe-surface interaction was greater than the required traction for a particular movement, the player would not fall and the outsole would be deemed successful. The increase in the physical demands of players during a modern football game has influenced the demands of the outsole. Players want to be able to rapidly accelerate and quickly change direction meaning the required traction is greater. Stud configurations and profiles were changed in order to meet these demands. However, as mentioned, the increase in traction also has negative side-effects; improving traction to aid in acceleration may cause the shoe to fixate to the surface during turning movements leading to injuries.

One of the key aims of modern football shoe manufacturers is to find the balance between developing a shoe that improves performance but also minimises the risk of injury. Improvement in performance often takes the driving seat as it is can be easier to measure and validate biomechanically and then market to the consumers. Releasing a new design that claims to be safer than previous ones can often lead to the assumption that previous products are unsafe. The design of outsoles to reduce injuries therefore has to almost be unseen by the consumer, but is an important and often expensive aspect to consider, with the average cost for medical treatment per football injury estimated to be \$150 (Dvorak and Junge 2000).

The ability to accurately measure and assess the traction properties of the shoes plays a vital role in design. Appropriate measurement of the traction can give an indication to the expected performance of the shoe and its susceptibility to cause or prevent injury. It also allows new designs to be compared to successful past designs or competitor shoes. Traction measurement can be done computationally, mechanically or with players.

The sponsor of this project is the football division of adidas whose principal aim is to design and manufacture football shoes for both amateur and professional players. They use a combination of mechanical, computational and player testing to assess the traction of existing and prototype outsole designs.

In order for the traction assessment to bear any relevance on the intended use of the final product, appropriate test parameters need to be used. From the view point of the sponsor, 'appropriate' refers to the ability to produce traction results quickly and easily and produce results that can be compared with minimal analysis. 'Appropriate' also refers to the realism of the test parameters; the traction assessment needs to mimic the conditions seen by players during a game; this includes accurate kinematics and kinetics to represent player movements and also the use of representative test surfaces. This applies to all forms of traction testing.

The sponsor would like to improve the veracity of their traction assessment by incorporating realistic test parameters into both their mechanical and computational test methods. The intention of the project is to initially develop a method to identify how the shoe interacts with the surface during realistic football movements and then to use the observations to suggest appropriate test parameters. The full project aims and objectives are outlined below.

1.2 Aim and objectives

Aim

To define appropriate test parameters for traction testing of studded footwear.

Objectives

1. To identify the advantages and disadvantages of computational and practical traction assessment methods.
2. To select, develop and validate an appropriate measurement system for the motion capture of studded footwear.
3. To use the measurement system to obtain test parameters from realistic football movements in a laboratory environment and on natural turf.
4. To advise on modifications to current test methods to better represent measured test parameters.

1.3 Thesis structure

The chapters in this thesis form three main sections; methodology, results and discussion. The first stage of the project is to identify an appropriate methodology to capture the interaction between the shoe and the surface in 3D. Validation and error assessment of the method is required before data collection. The method is then trialled using a controlled study in the laboratory and a larger sample size outside on natural turf. The results from the trial studies are analysed in detail to provide an example of the expected test parameters. Potential uses of the test parameters in traction testing and design are discussed in the latter part of the thesis.

2 LITERATURE REVIEW

2.1 Introduction

The aim of the study is to identify appropriate testing conditions for the measurement of traction between a surface and a studded outsole with respect to football. In order for this aim to be fulfilled, recognition of current traction testing methods and their limitations is required. To identify appropriate test conditions the understanding of football player movement and methods of motion capture is also essential. This chapter provides an overview of relevant literature in the areas of traction measurement, surface classification, biomechanics of football and motion analysis techniques.

For consistency the following terminology will be used:

- Reports of frictional force, surface friction or resistance to sliding in relation to studded footwear will be described as traction.
- Cleats or traction outsoles will be referred to as studs.
- Soccer or association football will be referred to as football.
- Boots will be referred to as shoes.
- Boundary conditions or test conditions with respect to traction testing devices will be referred to as test parameters.
- Touchdown, impact or heel contact will be referred to as foot-strike.
- Toe-off or take-off will be referred to as push-off.

2.2 Definition of traction

The frictional adhesion between a player's outsole and the surface is known as traction. McNitt (2000) defined that with respect to shoe-surface interactions, the term friction applies to the interaction with smooth-soled footwear and the surface whereas traction applies to studded or spiked footwear. Although the classical laws of friction do not apply to outsoles sliding on natural or artificial surfaces (Valiant 1993), Barry and Milburn (1999) used research from tribology and soil mechanics to explain a mechanism for how traction is developed for footwear sliding on natural surfaces. The first stage to understanding traction is to identify the factors affecting frictional behaviour.

The resistance to motion of a body on a flat surface is a result of the frictional force acting between the two surfaces. Early investigations into friction were carried out by da Vinci, Amontons and Coulomb leading to what are now known as the laws of friction (Muncaster 1981):

1. The frictional force between the two surfaces opposes their relative motion or attempted motion;
2. Frictional forces are independent of the area of contact of the surfaces;
3. For two surfaces which have no relative motion, the limiting frictional force is directly proportional to the normal reaction;
4. For two surfaces which have relative motion, the sliding force is directly proportional to the normal reaction and is independent of the relative velocity of the surfaces.

The final two laws can be described by the simple equation:

$$F \leq$$

$$R p \quad \text{Equation 2.1}$$

where F is the frictional force, R is the normal reaction and p is the coefficient of friction.

When a body is placed on an inclined slope, but has no relative motion, the force that effectively holds the body in this position is known as the static frictional force. The static coefficient of friction is independent of the weight and surface area of the body. The dynamic coefficient of friction is the force resisting the movement of a body in motion (dynamic friction or sliding friction). It is generally considered that the dynamic coefficient of friction is lower than the static coefficient of friction. These definitions also apply to traction; values of dynamic coefficient of traction relate to the resistance of the surface when the shoe is in motion, whereas the static coefficient of traction relates to the resistance to motion.

For dry friction, when a body is placed on a surface, the actual area of contact is much smaller than the assumed surface area of the body; on a microscopic level, the surface of bodies are rough and consist of raised asperities. Hence, when the two surfaces are placed together, some regions on the surfaces will touch whilst other regions will be separated by a small distance (Figure 2.1).

**Figure 2.1 - Schematic illustration of an interface, showing the real areas of contact
(adapted from Persson 1998).**

How the asperities respond to each other when sliding occurs depends on their respective material deformation properties (Barry and Milburn 1999). It is assumed that plastic deformation occurs at the junctions created by two asperities as the surfaces come into contact; as such, the coefficient of friction becomes the ratio of the shear stress to yield stress. The complex molecular interaction between the two materials means that a number of factors can influence the resulting coefficient of friction. Coulomb hypothesised five contributing factors (Persson 1998):

1. The nature of the materials in contact and their surface coatings;
2. The extent of the surface area;
3. The normal pressure (or force);
4. The length of time the surfaces remained in stationary contact;
5. Ambient conditions such as temperature and humidity.

These factors are also thought to apply to the traction between an outsole and a natural turf surface. Natural turf consists of a particulate structure consisting of discrete un-bonded particles separated by pores of air or water (Figure 2.2) (Barry and Milburn 1999). Traditionally, when playing on natural turf, players will wear studded outsoles. When load is applied to the natural surface through the outsole the studs and soil particles act as asperities and develop contact forces at the junctions. The reaction of the particles to the contact forces varies; the particles may slide, compress or bend. Barry and Milburn (1999) hypothesised that sliding was the most common mechanism of soils under load and as such the theory used to explain dry friction also applies to soils. The ability of a particle to slide depends on the friction and bonding forces between it and neighbouring particles.

Natural turf is however a very complex structure consisting not only of soil, but also grass fibres, thatch, root zone and water pores (Mumford 2006). It is these factors and others (Table 2.1) that make the shoe-surface interaction a complex mechanism that is also highly dependent on the surface.

Influencing factors

- Grass type/species
- Thatch accumulation
- Soil texture, structure, compaction and strength
- Water content and water release characteristics
- Root growth
- Areas previously ploughed by studs

Table 2.1 - Factors influencing shoe-surface traction.

Traction plays an important part in the ability of a football player to perform at their best; a loss of traction can cause a player to slip and negatively affect their performance. Redfern *et al.* (2001) identified that in order for a person to avoid slipping due to loss of traction, the traction required by a person for that movement must be less than the traction available from the surface for that specific set of circumstances. The causes of the loss of traction leading to slips were identified by Redfern *et al.* and were said to be due to both environmental and human effects (Figure 2.3).

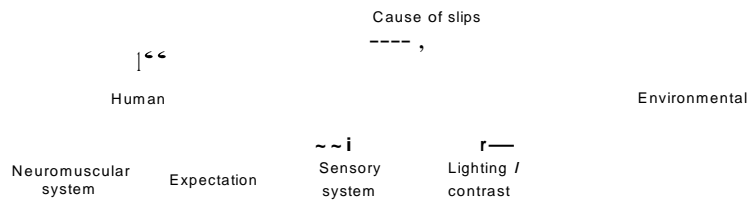


Figure 2.3 - Causes of slips (adapted from Redfern *et al.* 2001).

The negative connotations associated with loss in traction as well as the concerns over injuries caused by too much traction has meant that the measurement of the traction between a shoe and a surface is an area that is continually investigated. Section 2.3 outlines the most common methods used to measure traction and the improvements that can be made to ensure that the shoe-surface interaction is fully understood.

2.3 Measurement of traction

Traction testing measurements not only concern the shoe, but also the surface. Measurements can be used to compare studded outsole designs or as a classification measure for pitch quality. Mechanical, player and computational methods of measuring traction are reviewed.

2.3.1 Traction testing: Mechanical

Mechanical testing is one of the most commonly used methods to assess the traction between a studded plate or outsole and the surface. For evaluating a surface, a simple studded plate is normally used. Mechanical testing allows repeatable tests to be performed allowing quick assessment of the traction performance of outsoles or surfaces. In comparison, player testing is often found to be intrusive and suffer from poor repeatability, whereas mechanical testing has the advantage of being able to use fixed loading conditions leading to more repeatable results (Clarke and Carre 2010).

The Federation Internationale de Football Association (FIFA) guideline for the quality control of football turf has two tests that relate to the traction performance of a surface; the first measures the linear friction stud slide value and stud deceleration value and the second measures the rotational resistance (FIFA 2008). The first method uses a curved test foot with seven plastic studs (height 13 mm) attached to a pendulum arm (Figure 2.4). The arm is allowed to swing freely onto the surface and the peak deceleration due to the interaction of the studs with the surface is recorded. The second method uses a flat plate with six plastic studs weighing approximately 46 kg. The torque required to rotate the plate through 45° at 12 rev/min is recorded.

Figure 2.4 - Pendulum test foot in zero position (adapted from FIFA 2008).

The pendulum test method is recognised by the Health and Safety executive in the UK (Ferry 2005) but is not often used in research; instead horizontal translation of the whole shoe is used to represent sliding during a push-off movement. Translational traction testing devices can be simple; Vachon (2005) applied a 15.9 kg vertical load to a range of shoes and measured the horizontal resistance to motion using a load spring. The uncertainty in the measurements was between 10 – 15% of the mean suggesting poor repeatability in the measurements. The method of measurement was also susceptible to human error and the load non-representative of realistic conditions. More sophisticated devices use a motor to either drive or pull the shoe or plate across the surface. Haake *et al.* (2004) used a sled with a load cell to pull a studded plate across an artificial surface. The standard deviation in the measurements was only 2% of the mean indicating a much higher repeatability than the manually pulled device. The advantage of using mechanically driven devices is that the traction force can be measured

throughout the whole movement. Haake *et al.* measured the traction force at 100 Hz producing traction curves similar to Figure 2.5.

Figure 2.5 - Example traction curve.

The initial peak represents the static force and the lower value the dynamic force as the sled begins to move. Haake *et al.* used the mean dynamic value for comparison purposes; this is one of the shortcomings of the device, with Kirk *et al.* (2007) arguing that the shoe moves less than 10 mm during realistic sprinting movements and as such, the measurement of traction at distances greater than this are non-representative. A modified version of the traction sled was used by Clarke and Carre (2010) to assess the traction properties of different stud designs. The traction rig consisted of a high pressure pneumatic ram to drive a studded plate horizontally forwards. The device was capable of measuring the displacement of the studded plate as well as the resistive traction force. Although able to produce repeatable results, the use of a plate as opposed to a shoe outsole was a potential area of concern. The authors noted that when full stud penetration into the surface was possible, the friction between the plate and the surface was also a contributing factor to the resulting traction force. This was also observed by Haake *et al.* (2004), theorising that the total traction measured was:

$$\text{total traction} = \text{ploughing traction} + \text{plate skin friction} \quad \text{Equation 2.2}$$

Consequently, if the material and area of the plate is not illustrative of a shoe outsole the total traction measured will also not be realistic.

Devices that are able to use full or part shoe outsoles are also used for traction testing. McNitt *et al.* (1997) developed a device to measure both the linear and rotational

traction. A jointed leg and foot assembly capable of attaching full size football shoes was driven by pneumatic pistons in both rotation and translation. Although the movement and application of load was more representative than other devices, the authors acknowledged that it did not simulate actual movements. A similar device was developed more recently by Kuhlmann *et al.* (2009) that either pulled or pushed an artificial jointed foot along the surface. The traction force was measured continuously during the movement and produced an output similar to Figure 2.5 where there was a distinct static and dynamic traction phase. Kuhlmann *et al.* (2009) used the device to investigate the effect of vertical load on the traction performance of a range of studded outsoles. The results suggested that at vertical loads of less than 888 N, it was difficult to distinguish any differences between the traction behaviour of the shoes tested but at loads greater than 1776 N, the artificial turf test surface was permanently damaged. This highlights the problems of testing at loads that are potentially achievable during a sprinting movement.

The rotational resistance of a studded plate or shoe is a popular measurement of traction and is used to replicate a movement most commonly associated with lower limb injuries in football. Although mechanical advances have been made regarding the translational traction testing, many studies related to rotational testing use similar devices to the FIFA standard test device. Livesay *et al.* (2006) measured the peak torque and rotational stiffness of a range of different shoe designs, surfaces and vertical loads. The device used was similar in design to the FIFA device but included a biaxial load cell and goniometer to measure the torque and rotation angle during the measurements. This enabled torque graphs to be created similar to the translational traction graphs (Figure 2.5) displaying a peak torque and the dynamic rotational stiffness. The results indicated that as the vertical load increased, both the peak torque and rotational stiffness increased. Livesay *et al.* also observed that significant differences existed between shoe types and surface types but that the optimum torque and rotational stiffness was still undetermined, and as such it was difficult to comment whether a shoe that offers a lower torque and rotational stiffness was preferential to one that displayed higher values.

Andreasson *et al.* (1986) carried out one of the first studies that simultaneously measured the torque and traction when the shoe slides on the surface. The device used consisted of an artificial surface fixed onto circular rotating disc which was driven by an electric motor. An artificial test leg and foot assembly was positioned on the rotating

surface with a vertical force of 241 N supplied by a pneumatic cylinder. Strain gauges in the test leg were able to measure the torque and flexional stress, the reported value for comparison was the mean lever arm which was a ratio of the torque and traction. No degree of error or deviation of the results collected was given which means the repeatability of the device cannot be commented on. Although attempts were made to ensure that the position of the vertical centre of load of the shoe represented realistic conditions, the conditions were for a stationary stance and the vertical force actually applied had to be lower than observed due to the mechanical constraints of the test leg. The device allowed full outsoles to be tested but the choice of test surface was limited due to the fixation to the rotating disc.

Attempts to replicate realistic loading conditions have improved since the device used by Andreasson *et al.* in 1986 with the technical advancements of the test equipment available. Grund *et al.* (2007) proposed a complex list of requirements for a more realistic traction tester for high-risk loading scenarios:

- Replication of the full range of motion of the ankle;
- Application of forces and torques along the lower leg;
- Adjustable shoe-to-shaft positions and varying load conditions;
- Measurement of resultant forces and torques at the tibia position;
- Portable design to test the boots on different surfaces.

However, the criteria did not highlight the need for repeatable results that were also easy to interpret and compare. The test device developed by Grund *et al.* replicated the movement observed to cause anterior cruciate ligament (ACL) injuries and consisted of an artificial foot and ankle joint and shaft representing the lower leg. The movement of the leg was controlled by pneumatic cylinders and forces and torques around all axes of the leg were measured. Grund and Senner (2010) report results of the torque around the longitudinal axis of the lower leg for a range of different outsoles on natural turf. Despite the complexity of the movements performed by the test shoe on the surface, only two measurements were used for comparison; peak torque and effective peak torque. The results indicated that both the peak torque and effective torque depended on the loading conditions used and the outsole type. The order of the results for the outsoles changed depending on which loading condition was used. Although more representative loading conditions were used, the actual variable for comparison was still ambiguous and the results produced did not lend themselves to easy analysis.

Frederick (1986) highlighted that players have been observed to modify their kinematics as a result to changing surface conditions; this is not possible with mechanical traction testing and calls into question the traction characteristics of shoes and surfaces based only on mechanical testing.

This concern for the validity and relevance of traction characteristics based on mechanical tests only was also raised by Nigg (1990). Nigg reviewed the methods and results of using both mechanical and player testing and observed the following:

Observation	Conclusion
<ul style="list-style-type: none"> • Traction coefficient was dependent on material properties; 	<ul style="list-style-type: none"> • Both shoe and surface materials need to be representative;
<ul style="list-style-type: none"> • No correlation between rotational and translational traction values; 	<ul style="list-style-type: none"> • Both translational and rotational tests need to be performed;
<ul style="list-style-type: none"> • The order of translational traction coefficients on a range of surfaces changed depending on the vertical load applied; 	<ul style="list-style-type: none"> • Appropriate vertical loads need to be used;
<ul style="list-style-type: none"> • Mechanical and player testing traction results correlated for 6 out of the 7 surfaces tested. 	<ul style="list-style-type: none"> • Mechanical tests assess the shoe-surface interaction, player testing assesses the shoe-surface-player interaction; both are required to allow conclusions about the performance of a shoe-surface combination.

Table 2.2 - Observations and conclusions made by Nigg (1990) in relation to the traction assessment of shoes and surfaces.

2.3.2. Traction testing: Player

Despite the limitations of mechanical traction testing, there are few studies that attempt to use participants to measure the traction force during realistic movements. This is partially due to the negative connotations associated with player testing; increase in variability and potential for subjective outcomes, but also due to the complexities of measuring the traction force on a variety of surfaces.

To understand the interaction between the studs and the surface during player testing one of the most promising developments was the development of instrumented studs by Garcia *et al.* (1999) and Gonzalez *et al.* (2003) at the Institute of Biomechanics of

Valencia. Thirteen studs were instrumented with strain gauges attached to a steel spigot in the middle of the stud. Four gauges were positioned at 90° to each other to allow the measurement in the anterior-posterior and medial-lateral directions. The gauge cables passed through the shoe insole and were attached to an amplifier box sewn onto the side of the shoe. There was little data published on the results and accuracy of the system but initial analysis showed that significant differences can be seen between studs during different movements (Gonzalez *et al.* 2003). With the developments in wireless sensor technology, the disadvantages in the instrumented stud system of potentially hindering player performance will be minimised (Kirk 2008).

More details on player analysis techniques using force-plates, pressure insoles and high-speed cameras are given in section 2.6.

2.3.3 Traction testing: Modelling

Modelling techniques can also be used to evaluate the interaction between the shoe and the surface. Modelling allows prototype shoe designs to be assessed without incurring manufacturing costs. However, to ensure suitable results the model needs to accurately represent the surface, the shoe and the interaction between the two. To do this, understanding of the mechanical properties of the surface and modelling techniques used to represent them need to be understood. Natural turf is a complex material consisting of both soil and grass fibres. Modelling of soils is of particular interest in geotechnical engineering applications from earth penetration for tunnel and mining to the design of earth retaining structures (Sallam 2009).

With regard to the popularity in modelling soil using finite element applications, Brinkgreave (2005) reviewed a range of soil models to provide guidelines on selecting the most appropriate model for the given application. Brinkgreave initially identified five aspects of soil behaviour that soil models need to be able to replicate. Soil is a complex material that exhibits non-linear, anisotropic and time-dependent behaviour with respect to stress and strains. The characteristic soil aspects highlighted were:

1. *Influence of water on behaviour of the soil*. Pore pressure distribution can affect the total stress state in the soil.
2. *Soil stiffness is not a constant*. Stiffness can be affected by stress level, stress path, strain level, time, density, water, over-consolidation and direction.

3. *Soils irreversibly deform under loading*'. Soils only have a small elastic region and deform irreversibly from the onset of loading, however the soil does not fail.
4. *Shear strength is dependent*'. Soil shear strength can be influenced by loading speed, duration, density, undrained behaviour, over-consolidation and anisotropy.
5. *Soil exhibits time-dependent behaviour*. Pore-pressure and swelling which can influence soil stiffness and strength can decay in time.

The above list of soil characteristics is not exhaustive and demonstrates the highly complex nature of soil. It is therefore hardly surprising that the development of a computational finite element model to accurately represent the characteristics of soil would be complicated and time consuming. Attempts have been made to develop a soil model to measure the interaction between a shoe and the surface (Sun *et al.* 2005, Kirk 2008) however the focus has been on producing results that are able to give similar results to mechanical traction tests. The models also primarily represent the particulate nature of the soil and neglect the influence of grass fibres and root zones.

To accurately represent the interaction between the shoe and the ground, the shoe and human sections of the model also need to be represented. Mass-spring systems have often been used to model the dynamic impact between the body and the surface (Cavagna 1970, Blickhan 1989, Nigg and Liu 1999). The simplest model (Blickhan 1989) consists of a single linear spring. Over time more complex models were developed to represent both the body and the ground; for example, Nigg and Liu (1999) simulated the impact force during running using a spring-damper mass model consisting of four masses, six springs and four dampers.

Computational models used to model traction behaviour between a shoe and a surface are challenging to develop, but when used successfully can be a valuable tool in outsole design. The fundamental part of the model is the surface; natural turf is a complex medium and classification using mechanical measurements is one of the first stages in understanding its behaviour during shoe interaction.

2.4 Surface classification

During a typical sprinting movement in football, the motion can be described in three stages; impact, contact and push-off. The impact phase plays an important part in forming the first stage in the interaction between the studded outsole and the surface. Penetration depth of the studs has been shown to have a direct effect on the resulting traction properties (Clarke and Carre 2010). Being able to estimate the expected penetration of the studs can help inform players on the appropriate studded outsole for that surface. In the UK and the majority of Europe, natural turf can be generally grouped into two types; firm ground and soft ground. Firm ground is typically pre-season, end of season and the spring/summer months; soft ground usually occurs in the winter months (unless frozen which is then more representative of the firm ground hardness). However, the hardness is not the only parameter that affects the interaction between the stud and the ground; factors such as grass cover, root depth, moisture content, temperature, soil density and pitch construction all come into play (Canaway and Baker 1993). In winter, with soft ground conditions, it is expected that the stud would penetrate into the ground and thus give greater traction compared to in firm ground due to the enhanced contact area. However, firm ground in the spring months is likely to have greater grass cover and root strength, leading to improved traction through root-stud interaction. Completely different turf conditions are likely to be seen when playing in say Africa or Australasia. In essence, natural turf surfaces are geographically and temporally variable (Stiles *et al.* 2009) making categorisation of the surface difficult.

As described, the condition of natural turf surfaces can influence the traction properties of the shoe and as such it is important that when carrying out traction testing either mechanically or with players that the surface is appropriately classified. Stiles *et al.* (2009) defined three groups of mechanical testing methodologies that could be used to classify natural turf conditions:

1. Ball surface interactions;
2. Surface performance and aesthetics;
3. Player-surface interactions.

The FIFA quality concept for football turf handbook (FIFA 2008) outlines a set of ten tests that cover the topics suggested by Stiles *et al.* (2009):

1. Football rebound;
2. Angle ball rebound;
3. Ball roll;
4. Shock absorption;
5. Vertical deformation;
6. Rotational resistance;
7. Stud slide value and stud deceleration value;
8. Surface friction and abrasion;
9. Simulated wear;
10. Simulated weathering.

The tests relating directly to traction were discussed in section 2.3. Tests relating to surface hardness include a measure of the force reduction or shock absorption and vertical deformation of the surface. The shock absorption is measured using test apparatus known as an “artificial athlete”. A 20 kg falling weight is guided to fall smoothly onto a spring, load cell and test foot resting on the surface. The spring has a stiffness of 2000 N/mm and together with a load cell sampling at 500 Hz rests on a round steel plate weighing 3 kg acting as the test foot. The percentage reduction of the maximum force measured on the test surface relative to the maximum force measured on a concrete surface is reported as the force reduction. A similar test is used to measure the vertical deformation of the surface.

The device used by FIFA is also known as the Berlin Artificial Athlete. A modification to this test procedure is the Stuttgart Artificial Athlete which has an increased drop weight and reduced spring stiffness leading to a slight reduction in touch down velocity but an increase in the contact time of the test foot (Nigg and Yeadon 1987).

Nigg and Yeadon (1987) compared three mechanical drop tests; the Berlin Artificial Athlete, the Stuttgart Artificial Athlete and a standard drop test where an accelerometer is placed in a weight and dropped from a set height. The tests were repeated on a range of surfaces. For all tests, the ground reaction force and surface deformation were dependent upon the impact velocity and the radius and mass of the drop object. A change in one of the parameters not only changed the maximum force recorded, but also changed the ranking order of the group of tested surfaces. This is shown in Figure 2.6; the graph shows the results for the impact force peaks measured in a drop test on three different surfaces. Using the shot with mass 7.3 kg and radius 6.2 cm, surface A

recorded the lowest impact forces and surface C the highest. However, using a mass of 4 kg and radius 5.25 cm, the situation became reversed with surface C measuring the lowest impact forces and surface A the highest. This example highlights the need for a standardised method for the comparison of surfaces.

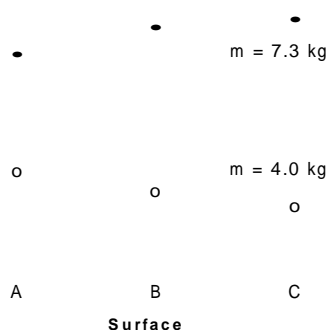


Figure 2.6 - Left: Influence of mass, radius and impact velocity on maximum force in a drop test with force platform. Right: Maximum force with two different shots on three surfaces (adapted from Nigg and Yeadon 1987).

The drop test described by Nigg and Yeadon (1987) is also known as the Clegg hammer. The Clegg hammer or Clegg Impact Soil Tester was originally designed to measure the suitability of soils as a base course for roads in Australia (Dr Baden Clegg Pty Ltd 2011) and has since been adopted by sports clubs and local councils as a standard test procedure for measuring the hardness of playing surfaces (Twomey *et al.* 2011).

Carre *et al.* (2006) assessed the performance of the Clegg impact hammer and the findings were used to develop a novel device to assess the performance of sports surfaces during ball impacts. The new system was designed to give consistent and accurate results for the hardness of a surface. Analysis of the Clegg impact hammer revealed inconsistencies relating to the uncontrolled drop of the impact mass, pressure build up in the tube as well as friction between the mass and the tube; leading to standard errors up to 30% for contact velocities for the same drop height. A new system was designed consisting of a hemispherical drop hammer on a linear bearing rail to give controlled motion. Further investigation revealed that a hemispherical drop hammer shape better represented impacts between sports balls and surfaces and gave better quality raw data than flat drop hammers. The device also included adjustable feet to aid in level set up and an electromagnetic drop mechanism to aid in accurate drop heights.

The new system gave standard errors of less than 5% and Carre *et al.* deemed that this was sufficiently accurate for use as a replacement for the Clegg hammer.

Despite the problems of the Clegg hammer for surface testing, it has often been used in research as a simple way to classify the hardness of natural turf surfaces. Dixon *et al.* (2008) investigated the loading within the shoe on a range of different surfaces. This required the soil surfaces to be characterised. The soil was characterised using two tests; the hardness was measured using a Clegg impact hammer (0.5 kg dropped from 0.55 m height) and the peak penetration resistance was measured using a cone penetrometer (130 mm² base area, 30° cone, penetration rate 30 mm/s) (Table 2.3).

Bulk density kg/m ³	Hardness (g)	Peak penetration (kPa)
1460	125	1200
1590	235	1500

Table 2.3 - Soil properties (from Dixon *et al.* 2008).

Dixon *et al.* (2008) observed the difference in hardness to be equivalent to the difference between complete sinkage of the studded sole to 50% stud penetration in static conditions for the median participant. The two surface conditions were thought to be representative of typical field conditions for 'soft' and 'hard' surfaces respectively. These peak hardness values correspond to measurements by Kirk (2008) used in the vertical interaction analysis (Chapter 3.5).

Baker (1991) at the Sports Turf Research Institute also used the Clegg impact hammer to investigate the effect of temporal parameters on the mechanical properties of natural turf football pitches. The mechanical properties chosen were deemed to be characteristic of playing quality and consisted of a measure of hardness and traction. The hardness was measured using a Clegg impact hammer; 0.5 kg, 50 mm diameter, dropped from a height of 0.3 m. The peak deceleration upon impact with the ground was recorded. The traction was measured using a studded plate with a torque wrench; in this case the force required to initiate rotational movement of the plate was recorded; similar to the standard FIFA test procedure for rotational resistance. Additional measurements were also made to help characterise the condition of the natural turf on the day of testing; these were:

- grass ground cover percentage,
- gravimetric moisture content,

- antecedent rainfall data.

Four different root-zone constructions were also used differing in the mixing ratio of soil to sand. Measurements were collected once a week from September 1986 to May 1987.

Results indicated that the moisture content was strongly influenced by root-zone composition and was particularly high in October and December 1986 in response to higher than average rainfall. The author postulated that the low moisture content in January and February 1987 was due to the increased evapotranspiration at the end of the playing season. The traction was found to decrease from September 1986 to May 1987; with the difference in traction on the varied root-zones negligible. In contrast, the hardness was found to vary significantly with the root-zone mixing ratio. Baker noted that in wet weather the root-zones with high soil content gave lower hardness readings compared to the sand; this was also reversed in dry conditions. In terms of temporal parameters; the traction was found to have little variation on a weekly basis, but simply decreased throughout the season with the wear of the turf. This was to be expected as traction is said to be related more strongly to the amount of root material present. The hardness was found to be very dependent on the moisture content of the turf; and as such was also strongly influenced by the antecedent rainfall (Baker 1991).

Giving reference to the proposed standards for playing performance (Canaway *et al.* 1990) (Table 2.4), Baker (1991) proposed grades of pitches defining under which circumstances they would be suitable for play. Basic grade pitches were deemed suitable for play in relatively dry conditions only with light rainfall expected to cause retention of surface water. Standard grade pitches were defined suitable under moderate rainfall intensities with high grade pitches expected to be playable under intense rainfall conditions. Baker (1991) also defined the maximum antecedent rainfall limits for mechanical test results to be valid (Table 2.5).

	Preferred range	Acceptable limits
Traction (Nm)	>25	>20
Surface hardness (g)	20-80	10- 100

Table 2.4 - Proposed standards for playing performance (Canaway *et al.* 1990).

Grade of pitch	Maximum permitted rainfall in the time period before testing (mm)			
	1 hour	6 hours	12 hours	24 hours
Basic	2	4	6	10
Standard	5	8	12	20
High	10	15	20	30

Table 2.5 - Maximum permitted rainfalls for test results to be valid (Baker 1991).

The results from Baker (1991) highlight the effects the temporal parameters can have on the surface condition and consequently the traction property of the shoe-surface interface. Rogers and Waddington (1989) revealed that the grass height can also affect the hardness and traction performance of a surface. The authors used a Clegg impact hammer to measure the hardness of a surface over a period of a year also noting the grass height and moisture content of the surface. The hardness using the 0.5 kg Clegg hammer were shown to be sensitive to the presence of verdure (top growth remaining after mowing) and grass height.

Fujikake *et al.* (2007) reported a similar sensitivity between the hardness and the grass type over a period of several months. Impact hammer test and traction tests were performed at 13 natural turf pitches and eight artificial turf pitches in Japan. The study focussed on mechanical differences between artificial and natural turf pitches and more importantly, how the change of season affected the mechanical characteristics of the pitches. From the results, of particular interest was the hardness index recorded for the same natural turf pitch over several months. The impact drop test was performed in August 2003 and then January, March, May, August and October of the following year. The authors recorded a significant difference in the hardness of the turf in March and October compared to the other months. The authors report that March was a transition period from rye grass to Bermuda grass and October was an 'overseeding period' which meant the amount of turf was less. Combined with an aeration process to allow nutrients and water to penetrate into the soil, Fujikake *et al.* concluded that in these months it was likely that the ground would be softer. This study again highlights the effects the grass type can have on the surface condition, but also the effect of ground maintenance.

An alternative measure of surface hardness is surface penetration. Penetrometers are more commonly used on horse racing circuits with the introduction of the GoingStick in 2006 (Brighton and Godwin 2006), they have however been extensively used by

Orchard (2001) in his study into the causes and effects of injuries in Australian Football League matches. One of the initial studies by Orchard (2001) was to use an objective measure of ground hardness to analyse the relationship between ground conditions and ACL injury rates in the Australian Football League (AFL). The ground hardness was measured using the Penetrometer. According to Neylan and Stubbs (1998, cited by Orchard 2001), the Penetrometer has better correlation with track hardness and race times than the Clegg hammer.

AFL injury surveillance data found that ACL injuries were less likely at Victorian (southern) venues and in games during the winter months (later in the season). However, the penetrometer study was unable to specify the particular characteristics of grounds that are responsible for the 'northern' and 'early-season' bias for ACL injuries. Orchard (2001) reported a non-significant trend towards more ACL injuries on harder grounds, as well as a similar trend where couch grass was the predominant species.

Orchard (2001) identifies the relationship between weather variables and surface conditions and in turn how these may ultimately affect the shoe-surface traction of players (Figure 2.7).

Figure 2.7 - Relationship between hardness, shoe-surface traction and other ground characteristics (adapted from Orchard 2001).

The range of surface measurements available together with the effect of additional surface conditions such as grass type, length, soil density and moisture content renders the task of classifying surfaces confusing and sometimes contradictory. Without consistency between surface measurements, a surface deemed hard by one study may be classed soft by another simply by using a different weight in a drop test.

2.5 Biomechanics of football

2.5.1 Biomechanics of football

One of the most comprehensive reviews of biomechanics in football was undertaken by Lees and Nolan (1998). They identified the biomechanical aspects of kicking, throw-ins and goalkeeping and also the influence of the ball, shoe and surface on player performance and injuries. The authors identified that ball speed could be used as a measure of kicking success. Using this notion, Sterzing and Hennig (2008) investigated the influence of the traction of the planted foot during kicking. The authors hypothesised that due to kinetic chain theory, the transfer of momentum to the ball is based on a whole sequence from foot strike of the planted foot to the end of the collision phase of the kicking leg, and as such, higher traction of the planted shoe will lead to an increased performance in ball velocity in kicking. The traction performance of four different studded outsoles was measured by observation of the ground reaction forces on impact. The ball velocity was measured using a radar gun. Player perception of both traction performance and ball velocity were also recorded. The results indicated that the shoes related to the highest ball velocity also recorded the highest maximum shear force and shortest reaction time. Perception ratings were variable; participants were able to differentiate different ball velocities but were unable to correctly rank the traction performance of the shoes. An interesting addition to this study would be the mechanical measurement of the traction values of the shoes and the comparison to functional performance and perception ratings.

Lees and Nolan (1998) also suggested that the placement of the planted foot during kicking may influence the performance. McLean and Tumilty (1993) identified for right foot kicks that participants (elite junior football players) positioned their support foot 373 ± 41 mm to the side of the centre of the ball and 81 ± 53 mm behind the ball. This was different to left foot kicks where the support foot was 451 ± 31 mm to the side

and 39 ± 91 mm behind the ball. Lees and Nolan (1998) postulate that the anterior-posterior positioning of the support foot is related to the type of kick and the intended trajectory; however there was no evidence to suggest that positioning the foot further or closer to the ball will cause it to go low or high.

The use of biomechanics in football shoe design has mainly been focused on shoe ergonomics and reduction in injury. Johnson *et al.* (1976) investigated how the design of the shoe affected stiffness. They hypothesised that the stiffness of the shoe in inversion and eversion could be related to the ankle injuries in football players. In the 1970's, shoe designs were introduced that had significantly lower profile in the ankle and these were often blamed for ankle injuries during football games. Johnson *et al.* compared a high ankle profile shoe and a low cut shoe by measuring the resistance to rotation in inversion and eversion of a participant's ankle while strapped in a leg brace. A third shoe in the low cut design but made from the same leather as the high ankle design was also tested. Results indicated that the high cut design was 50% stiffer than the new low cut shoe, but that the low cut shoe with old leather was 40% stiffer than the new design. The authors concluded that 80% of the differences between stiffness in shoe design could be attributed to a change in material rather than a change in shape. Lees and Nolan (1998) also identified that material selection played an important part in the biomechanical design of football shoes. Shoe-splitting was reported by 27% of professional players questioned, the authors estimated that during a game situation, the accumulated stress on the boot was three times greater than during training, and as such, the selection of material has to take into account both demands.

Sterzing *et al.* (2010) used player testing to evaluate a series of prototype designs specific for artificial turf. The study involved both biomechanical assessment and perception ratings from players. 47 players were asked to perform a slalom course on an artificial surface wearing a selection of artificial turf outsoles from a range of manufactures and a new prototype design. The time taken to complete the course was used as a comparative measure, combined with the perceived run time and traction rating of the shoe from the participants. Cutting and turning movements were also performed in the laboratory on a force-plate to measure the shear and vertical forces. Assessment of the prototype shoe compared to three shoes available on the current market revealed a faster run time round the slalom course and higher ratio of peak shear to peak vertical forces during the cutting and turning movements in the laboratory. From the results, the authors concluded that the new prototype exhibited a higher

functional traction (defined by ratio of horizontal to vertical force) than existing designs. This study demonstrates how player feedback and biomechanical assessment can be used to evaluate traction requirements without mechanical testing.

Brizuela *et al.* (1998) used pressure insoles to investigate the influence of stud position on performance and injury prevention. Participants were asked to perform an obstacle course wearing five different prototype outsole designs. The first design consisted of 15 studs distributed equally about the sole. The outsole designs were then modified by removing one or more studs. A final design mimicked a commercially available shoe with 13 studs. A goniometer was used to measure the inversion-eversion stability of the shoe and pressure insoles used to determine the pressure distribution under the foot during different movements. Player questionnaires were also used to obtain the comfort level of the shoe. Results indicated that stud position had a significant influence on the pressure distribution and stability of the shoe. Shoes with equivalent number of studs did not necessarily have the same comfort rating or high pressure areas indicating that the position of the studs is important. A more complete study would again be to investigate additional information such as mechanical traction values or ground reaction forces.

To date, the traction performance of outsoles has been highlighted as an important playing quality (Lees and Nolan 1998) but has predominately been investigated from the point of view of the surface rather than the biomechanical influence on stud design or configuration. Muller *et al.* (2010) identified that the stud configuration can influence the turning patterns; with players wearing an outsole with no studs displaying lower horizontal reaction forces compared to those wearing studded footwear. The observations from biomechanical studies are more commonly linked to the cause or reduction of injuries.

2.5.2 Injuries

The level of traction required by a player is a balance between injury prevention and performance enhancement; too much traction and the shoe can lock into the surface causing potential injuries to the lower limbs, too little traction and the player may slip compromising performance. The influence of traction on player injuries has always been a concern but has more recently been investigated with the increase in the number of artificial or portable grass surfaces, especially at elite competition level (Orchard *et*

al. 2008). As such, research on the influence of traction on injuries has predominately been focussed on surface characteristics rather than outsole designs. Orchard *et al.* (2008) hypothesised that portable natural grass may be a risk factor for knee injuries. Portable natural grass inherently has high resistance to shearing and as such has been linked to ACL injuries due to excessive shoe-surface traction. Orchard *et al.* identified a number of case studies of ACL injuries on natural grass and concluded that until further evidence is present, excessive shoe-surface traction is a likely cause, but random injuries can also occur that may or may not have any relation to shoe-surface interactions. The authors also observed that a succession of knee injuries occurring at one particular ground can cause an increase in media attention even when there is no quantitative evidence to suggest that the surface was the influencing factor.

The negative media association to injuries does not always focus on the surface. A succession of injuries occurring by players wearing a particular brand or style of football shoe or stud design can also cause the media to speculate that the shoe is the cause of the injury. Modern bladed studs are a prime example of a shoe design that is constantly under question from the media as to its safety for football players of all levels. In 2005, Sir Alex Ferguson raised one of the first public concerns for bladed studs, calling for a complete ban after injury to Roy Keane (BBC 2005). In 2010, Steve Bruce called for a conference on football player footwear and pitch conditions after a series of injuries caused by players wearing bladed footwear (Taylor 2010). Taylor (2010) reported that the fashion for players to wear bladed footwear over more conventional round studs was causing the shoe to stick in the surface leading to ACL injuries. The bladed stud also received negative press with respect to injuries caused by stud lacerations. Hall and Riou (2004) raised concern that the blades posed a greater threat to laceration injuries than rounded studs and that their use in youth football should be monitored.

The scientific evidence to support the claims that bladed studs posed a greater injury risk have also had mixed results. Kirk (2008) measured the resistance to rotation of both bladed and conventional round studded outsoles on natural turf. The results indicated that the rotational torque of the bladed designs was lower than the rounded studs. The author however, expressed concern that the type of stud must be appropriate for the surface; a shoe designed for soft ground conditions (longer stud profile) may pose an injury risk on other surfaces. Bentley *et al.* (2011) measured the pressure distribution on the foot when wearing bladed or round studded outsoles. The results

indicated that the pressure distribution on the lateral side of the foot during certain movements in the bladed shoe was significantly greater than the round studded shoe. This led the authors to speculate that the bladed shoe posed a greater risk to injury.

As mentioned by Kirk (2008) the players' selection of studded footwear has significant influence on both their performance and susceptibility to injury. There is little information on the relationship between surface condition and player footwear selection perhaps leading to a lack of education in players on appropriate footwear. Rennie (2010) measured the Clegg impact hardness of the football pitch before every match and training session for Leicester City Football Club to investigate relationship between hardness and incidence of injury. The seasonal variability of pitch hardness was also investigated. However, the author reported that the players were not made aware of the pitch hardness and as such it did not influence their footwear selection. A player's ability to perceive the hardness and traction properties of the surface plays an important role in selection of footwear and ultimate media portrayal.

2.5.3 Perception

The evaluation of player perception has always played an important part in sports shoe design and research. A player's ability to perceive information such as surface hardness or traction properties can lead to a more informed selection of footwear. Muller *et al.* (2010) undertook an evaluation of player-surface interaction on artificial surfaces investigating both mechanical, performance and perception results. Players wore a range of studded outsoles and performed slalom and acceleration movements to gauge both the performance of the shoes and the players' ability to perceive the traction performance. The perceived ranking of traction performance correlated with the course times used as a performance indicator. These also matched well with mechanical measurements taken for the traction performance of the shoes. The authors concluded that the combination of perception, performance and mechanical testing was a successful way to ensure a comprehensive understanding of the shoe-surface interactions.

Perception of loss of traction, or slipping has more readily been investigated with respect to heel slide during walking (Redfern *et al.* 2001, Gronqvist *et al.* 2001, DiDomenico *et al.* 2007). Redfern *et al.* (2001) stipulated that the kinematics of the heel as it contacts the floor has a high potential for slips; the heel rapidly decelerates just

prior to contact and then there is a slight sliding motion along the surface at impact. Leamon and Li (1990, cited by Redfern *et al.* 2001) stated that during normal walking gait, it was expected for there to be some sliding observed at and just after heel contact. This was termed a microslip and was said to be in the order of 10 mm. A microslip greater than 30 mm was then termed a slip. Perkins (1978) reported that slip distances up to 30 mm can occur without being perceived. Information on perceived slip distances can affect the realism of traction testing devices. If translation distances of greater than 30 mm are tested, it is likely that the player would have perceived this slip and monitored their movement to compensate for it. This will have compromised their performance and as such questions the translation distances mechanical tests should measure to.

As suggested, players are able to adapt to the surface conditions and adjust their movements according to the shoe-surface interaction at the time (Hennig 2011). On a soft, wet surface, Hennig (2011) observed that players ran more cautiously and performed movements slower. Changing the footwear caused a 3% difference in performance whereas a change in the surface caused up to 20% difference in performance. The ability to observe the shoe-surface interaction and the resulting effect on the player performance during different movements on a range of surfaces can help further the understanding in traction requirements in order to improve performance but reduce the likelihood of injuries.

2.6 Motion analysis

Nigg (1990) stressed the importance of understanding the shoe-surface-player interaction as well as just using mechanical measurements to assess traction performance. To do this, knowledge of the loading conditions and movement of the shoe during motion is required. Motion analysis techniques for human movements are used to obtain measurements and understanding of the following areas:

- Force and pressure (loading conditions);
- Rate of movement (velocity and acceleration);
- Position: displacements and angles of an object or person.

Techniques used for motion analysis can be classified into two areas; intrusive and non-intrusive data collection methods.

2.6.1 Intrusive

Intrusive data collection involves making modifications to the test environment in order to measure the desired parameter. The changes could be major, such as moving the test environment to a laboratory rather than an outside playing field, or minor such as adding tracking markers to a player or piece of equipment (Kelley 2011).

a) Information of loading conditions

Force-plates (or platforms) are one of the most commonly used methods for obtaining loading information during player testing. Modern force-plates usually consist of four pedestals instrumented with either strain gauges or piezoelectric crystals. Each pedestal measures forces and bending moments that result from loading of the top plate; they are instrumented to measure in three directions (Figure 2.8) operating on the principle that no matter how many objects apply the force, there is only one resultant ground reaction force vector (GRF) (Robertson *et al.* 2004).

Centre
of pressure

**Figure 2.8 – Force-plate with its reaction to applied force and vertical moment of force
(adapted from Robertson *et al.* 2004).**

Shorten *et al.* (2003) used a rubber coated force-plate to investigate the shoe-surface traction of American football players during cutting movements. The surface normal and surface tangential forces were measured for players performing 45°, 90° and 180° changes of direction whilst wearing rubber soled shoes. The traction requirement of the movement was defined as the ratio of normal to horizontal force. Shorten *et al.* also

investigated the available traction and resistance to rotation of a range of studded outsoles on an artificial turf surface using a motor driven mechanical rig. Comparisons were made between available and required traction, noting that the available traction exceeded the 95th percentile of required traction. However, one of the major limitations of this study was that the required traction measurements were made on a different surface with flat soled shoes.

Kaila (2008) used a combination of a force-plate and gait analysis system to investigate the effect of different style studded outsoles on the loading of the knee during cutting movements. The study built on previous work by Shorten *et al.* (2003) by installing an artificial turf surface over the force-plate and test area. Although the required traction (ratio of vertical to horizontal) was not calculated, the results suggested that differences between stud types could be seen in the knee loading during cutting movements but not straight running. This suggests that limiting traction testing to just one movement may not be representative of the interactions likely to occur during football.

One of the limitations of force-plate testing is that they are often restricted to a laboratory. Portable force-plates are available, for example the Kistler multicomponent plate (type 9286B), but have a reduced measurement range and lower natural frequency compared to a standard embedded force-plate (type 9281E) (Kistler 2011). They also sit above the surface, either requiring the player to step onto the plate, or need to be imbedded into the test surface requiring modification to the test area.

An alternative to force-plates that allows testing away from the laboratory on realistic playing surfaces are pressure insoles. The use of pressure insoles as an alternative to force-plates was validated by Barnett *et al.* (2000). The study concluded that the accuracy of the pressure insoles was sufficient enough to warrant its use in clinical applications. Ford *et al.* (2006) used pressure insoles to compare the in-shoe loading patterns on natural and artificial turf. Participants performed a slalom course wearing studded football shoes with pressure insoles. The advantage of the pressure insoles over the force-plate was that the pressure could be measured for the whole course, rather than just in one discrete location. The results showed that the total force time integrals for the artificial and natural surfaces were not significantly different, but that differences did exist between the plantar loads at specific foot regions. During the cutting move, the medial forefoot region had a higher relative load on natural grass compared to the artificial surface. A standard force-plate would not be able to detect these differences.

Queen *et al.* (2007) undertook a similar study to Ford *et al.* (2006) but also varied the outsole design as well as the surface. The experiment took place in a laboratory with participants wearing pressure insoles and performing a slalom style course. The authors concluded that significant differences existed between the forefoot loading patterns of different studded outsoles but that there was no conclusive evidence to suggest that players should select one design over another in order to minimise the risk of injury.

Pressure insoles are limited to only measuring the effect of the vertical forces. Force-plates have an advantage in that they are capable of measuring both the shearing and vertical forces, but only give the resultant force; there is no information about the location of forces as provided by pressure insoles. Davis *et al.* (1998) designed a device to simultaneously measure the vertical pressure and the shearing forces in the anterior-posterior and medial-lateral directions under the plantar surface of the foot. The device consisted of sixteen transducers comprised of a cylindrical column with an S-shaped cantilever. The column contained eight rosette strain gauges equally spread around the surface; these strain gauges measured the shearing forces. The S-shaped cantilever had four rosette strain gauges and measured the vertical forces acting on the transducer. The transducers were arranged in a 4 x 4 array giving a surface area of 10.5 cm x 10.5 cm. This area was only large enough to cover the forefoot and not the entire plantar surface area of the foot. The results validated well against force-plate data but were limited by the size of the test area. It was thought that the transducer area was likely to underestimate the true peak pressures. The results were able to identify areas of maximum shear and maximum pressure within the forefoot. The device was also limited to sampling at 37 Hz; coupled with the small test area this also restricted the range of movements that can be performed on the device.

Aside from force-plates and pressure mats, plantar foot pressure can also be measured by optical techniques. This is most commonly seen in the medical industry where optical methods are used to identify high pressure areas in the foot plantar surface of diabetic patients. The Pedobarograph was a major development in the field of foot pressure sensing (Chodera 1960, cited by Urry 1999). A Pedobarograph uses the principle of critical light reflection along a glass plate. The glass plate is covered with a thin rubber mat and illuminated from the side. When no pressure is applied to the rubber surface, the light is internally reflected along the glass plate. When pressure is applied, the rubber surface is pushed against the glass deforming the microscopic surface asperities (Urry 1999). This alters the critical angle and light is transmitted out

of the glass. The higher the applied pressure, the greater the intensity of light transmitted. As such, when viewed from below a pressure profile is seen in which the pressure is proportional to the intensity of light. Although beneficial for identifying pressure, the Pedobarograph is unable to measure shear forces.

An alternative optical method to measure shearing forces is photoelasticity. The theory of photoelasticity is outlined in Chapter 3.4. The use of photoelasticity to measure foot pressure was first proposed by Arcan and Brull in 1976. The device was later used by Rhodes *et al.* (1988) to determine ground foot reaction forces and by Nishizawa *et al.* (2006) to investigate the contact pressure distribution in Down syndrome infants. The underlying method behind the device makes use of the principle of photoelasticity. Photoelasticity is a stress analysis technique and is commonly used to identify maximum shear forces in mechanical structures. The device used consisted of a sheet of photoelastic material on a rigid transparent support. A flexible sheet with contact points was on the top of the surface upon which the pressure was applied. When illuminated from below stress fringes were visible in the photoelastic material. The outer fringe of each contact point was calibrated against the applied pressure. In essence, a relationship was derived between the outer fringe diameter and the pressure; the higher the pressure, the greater the diameter of the fringe. Rhodes *et al.* (1988) indicated that the set-up produced high resolution results with a good accuracy. One of the problems of using a photoelastic method alone is that there is no information on the vertical pressure applied to the plate which can cause out-of-plane shear forces. A potential solution to this would be to combine the principles of the Pedobarograph and photoelastic methods.

b) Information of position

Optical methods

To obtain information on the position of an object or player in the test environment using intrusive methods requires the addition of a tracking marker. Markers can be passive or active:

- Passive markers reflect electromagnetic radiation;
- Active markers emit electromagnetic radiation.

Many visual 3D motion analysis systems use passive markers; Ehara *et al.* (1995, 1997) reviewed a range of 11 commercially available systems assessing them on the measurement error and processing time. The position of two markers placed a fixed distance apart were moved around the test environment and tracked by the camera systems. The accuracy of the re-projection of the markers was evaluated. The most accurate system had a mean error of 0.53 mm and standard deviation of 0.31 s and took 47 s to process. The least accurate system had a mean error of 18.42 mm and took 16 min to process. The longest processing time was 28 min and the shortest only 10 s. The review highlighted the differences between commercially available systems in both the level of accuracy that can be achieved and also the time taken to process data.

Many commercially available motion analysis systems also require an external light source. This increases the amount of equipment necessary to collect data and can make test environments more complex to set up. Many laboratories have one system installed eliminating the need to set-up and take down the systems. To reduce the amount of equipment, commercially available systems that also combine the sensor and light source are available. The Motion Analysis Corporation system (MAC) (Motion Analysis Corporation 2011) uses a red light and sensor with a red light filter to detect passive spherical reflective markers.

Potthast (2010) used four high-speed cameras filming at 100 fps to capture the kinematics of the lower extremities during kicking on natural and artificial turf surfaces. A commercial video analysis package was used to track the marker positions and create an anatomical model. The data was filtered using a second order Butterworth filter with a cut-off frequency of 20 Hz. Two artificial turf surfaces were tested; one with sand and rubber infill and one with just rubber infill. Results indicated that for five variables evaluated (deceleration, maximum foot pronation, backwards inclination of the leg at impact, ball velocity and percentage of good shots) that there were significant differences between the artificial surfaces and the natural surface, but also between the two artificial surfaces. Potthast commented that these results indicated that the classification of pitches into just two categories: natural and artificial, is perhaps an oversimplification of the situation. A low sampling rate was used which could also affect the calculation of the angle of leg on impact.

Muller *et al.* (2010) investigated the lower extremity kinematics and kinetics during turning movements for four different studded outsole shoes. Eight high-speed cameras

sampling at 500 fps were used to capture the reflective tracking markers on the leg and shoe of participants. A commercial processing package was used to filter the data (Butterworth 30 Hz) and generate the 3D coordinates of the markers. The foot and shank orientations (plantarflexion, abduction and eversion) were used as variables for comparison. The results indicated that the outsole with no studs was observed to show an increase in foot translation during contact which could increase the risk of slipping, but also a decrease in the turning moments at the knee and ankle joints minimising the risk of injuring during rotation. The increase in risk of slipping was perceived by the participants, with a slower approach speed and significantly reduced horizontal ground reaction force. Movement adaptations prior to and during landing for the three studded outsoles were not observed.

Although many commercially available systems include software to automatically detect and track the markers in the test environment they are also very susceptible to noise and are unable to differentiate between a marker and a rogue reflective object. Non-commercial systems involve the use of high-speed cameras and photogrammetry to identify the position of a tracking marker and generate its location with respect to a global axis system whether in 2D or 3D. High-speed photography, photogrammetry and studies using non-commercial motion analysis systems are discussed in more detail in section 2.7.

Non-optical methods

Orr and Shelton (1997) identified three non-optical methods that could be used to determine the position of a body segment or piece of equipment. The three methods were goniometry, accelerometry and magnetic tracking devices; the advantages and disadvantages of each method are highlighted in Table 2.6.

Ahmadi *et al.* (2010) compared the accelerations calculated by a commercial laboratory based optical system to those found from gyroscope sensors for a participant performing an overhead tennis serve. The results showed good agreement between the calculated and measured results, indicating that the gyroscope sensors mounted on the arm, chest and hand were accurate in obtaining the angular velocity required to monitor player skill (Ahmadi *et al.* 2010). This allows measurements to be taken during play in the field rather than being restricted to a laboratory setting.

Method	Advantages	Disadvantages
Goniometry	Cheap; Lightweight; Possible for use for remote activities.	Cannot make absolute measurements; Sensitive to mounting error; Generally 2D; Electronic devices require electrical power and cables attached to the participant.
Accelerometry	High natural frequency; Very sensitive; Very accurate devices; Velocity and position obtained by integration, reducing noise; Can get 3D motion measurement.	Difficult to relate motion to global axis system and force-plate; Sensitive to mounting/placement; Delicate; Expensive; Suffers from drift; Needs minimum 6 per segment; Requires electrical power and cables.
Magnetic tracking	Gives absolute movement of segments; Gives 3D motion measurement.	Limited volume; Needs separate unit per segment; Sensitive to presence of some metals – produces artefact; Requires electrical power.

Table 2.6 - Summary of non-optical measurement methods (Orr and Shelton 1997).

2.6.2 Non-intrusive

Non-intrusive motion analysis allows players to be observed in their natural environment without the distractions of additional markers or based in a laboratory setting. Non-intrusive techniques are often used for either live analysis of the game to provide player information to commentators, or post game analysis to aid coaches in the review of player performances. In football, one of the most successful match analysis systems is Prozone. Prozone is used by over 100 sporting organisations world-wide from schools to professional clubs such as Arsenal and Real Madrid (Prozone 2009). Prozone offers services in four areas of analysis:

1. Performance: live analysis
2. Feedback: post-match analysis
3. Evaluation: trend analysis
4. Preparation: opposition analysis

The player tracking system provided by Prozone (PROZONE3) consists of 8 cameras positioned around the pitch. Di Salvo *et al.* (2006) validated the velocity measurement of players using the Prozone system against light-gate recordings. Results revealed good correlation between measurements, with a Pearson product moment correlation coefficient greater than 0.9 for all run distances trialled. The run trial that showed the most discrepancy was the 20 m sprint with left and right turns. One of the drawbacks of the system is the installation cost, estimated to be around £100 000 for a stadium system (Setterwall 2003). The system also requires skilled manual operators and full analysis of a match can be timely (Bradley *et al.* 2007).

Bloomfield *et al.* (2004) used the 'PlayerCam' facility provided by Sky Sports Interactive Service to undertake motion analysis of individual players in a game of football. Footage of six players tracked individually for 15 mins was analysed manually by eight observers. Player movement was designated using the 'Bloomfield Movement Classification' (BMC) and consisted of a behaviour and a modifier. Examples of behaviours ranged from sprint, fall, swerve, shoot and dribble. Modifiers were used to identify the direction: forwards, backwards, up, left, etc. The data entry process was very time consuming due to the combination of movements given in the BMC but the concept allows the physical demands of each player or position to be identified (Bloomfield *et al.* 2007).

2.7 Photogrammetry

Photogrammetry is the method of obtaining information from a single or series of photographs. Videogrammetry is an extension of photogrammetry, using recorded video footage to generate a series of images and then extracting the information.

Photogrammetry for motion analysis uses high-speed photography. High-speed photography allows information from images to be processed that are too fast for a human eye to register. One of the first motion sequences of animals in locomotion was taken by Muybridge in 1872 (Kingston Museum and Heritage Service 2010). Muybridge used 12 cameras activated with electro-switches and timers to capture images of a running horse (Figure 2.9). These images showed that photography was not just an art form but had the potential as a tool for scientific analysis leading to the field of photogrammetry.

Figure 2.9 - Locomotion of a running horse captured by Muybridge (Kingston Museum and Heritage Service 2010).

Photogrammetry can either be carried out with a single camera for 2D analysis or with multiple cameras for 3D analysis. Examples of both techniques being used for analysis of player or equipment motion are given below.

2.7.1 Single camera photogrammetry

For sports analysis, one of the most popular photogrammetry examples is the stroboscope. The electronic stroboscope is said to have been invented by Edgerton in 1931; using a flash strobe light, a camera with an open shutter was used to capture images showing the high-speed movement of objects (MIT Museum 1998). Figure 2.10 shows the use of stroboscopic effects to capture the swing of a golf club and the launch of the ball from a baseball pitcher. Stroboscopic images are often used to measure the characteristics of sports balls (Haake 1991, Carre *et al.* 1998), but their use has fallen due to the increased availability of high-speed video cameras.

**Figure 2.10 - Stroboscopic images by Edgerton, Left: “Densmore Shute bends the shaft”;
Right: “Pitcher” (Edgerton, MIT Museum 2011).**

Kirk *et al.* (2007) used a single high-speed camera to observe the shoe-surface interaction of players on a natural turf surface. A 2 x 2 m zone was captured by the camera filming at 1000 fps. This frame rate was significantly higher than that used in other studies using commercially available systems (Muller *et al.* 2010, Potthast 2010). Tracking of the shoe was carried out manually at 500 fps using features on the shoe to define two rigid segments. Using a single camera, the results were susceptible to parallax error when the test object moved out of the plane of the camera. To ensure these effects were minimised, the authors positioned the camera approximately 10 m from the test area and used a large focal length. The velocity and orientation of the shoe on impact was calculated using the tracked shoe position. The results of the study were subject to high variability and as such no significant differences between the angle or velocity of the shoe during impact on different surfaces was observed. Additional information such as the orientation of the stud on impact was however able to be found from the high-speed footage. The study was also limited to movements in a single plane; rotations or cutting movements were not able to be investigated due to the 2D analysis restrictions. The author concluded that an extension of the study using 3D analysis techniques would be beneficial to identify potential shoe-surface interactions that can be replicated in mechanical test devices.

As highlighted, one of the weaknesses of single camera photogrammetry is the potential for high error when the tracked object moves out of plane. One solution is to use an additional camera and capture the movement of the object in 3D.

2.7.2 Multiple camera photogrammetry

Two or more cameras can be used to obtain 3D position information about objects in the field of view; this is known as stereo-photogrammetry.

There have been very few studies using multi-camera non-commercial analysis systems to monitor player movement in football; more recent developments have been in tennis, using a two camera approach to identify the impact characteristics between the ball and racket. Choppin *et al.* (2011) positioned two high-speed cameras either side of the net line to capture a 2 x 2 x 2 m volume at the centre of the baseline. The cameras were calibrated using the checkerboard technique. To track the position of the racket, five high contrast tape markers were placed on the rim of the racket; only three markers were necessary to define the racket position but an additional two were added to allow for marker occlusion. Choppin *et al.* developed a MATLAB™ graphical user interface to digitise the marker locations in 2D, transform the data to 3D coordinates and return shot characteristics. The characteristics obtained were ball and racket velocity in three dimensions, racket angular velocity around three axes, ball-to-racket impact position and ball spin. The error in tracking the 3D position of the racket was ± 2.5 mm. By using bespoke software, the authors were able to track the position of the racket and also the location of the ball. The ball did not include any specific tracking markers and as such, is unlikely that commercial analysis programmes used to track the reflective markers on the racket would be able to locate the ball as well.

a) Tracking algorithms

The limitation of non-commercial tracking systems is the additional time required to digitise the location of the marker. Kelley *et al.* (2010) validated a bespoke automated analysis tool by using a tennis ball launcher to fire balls which were recorded by two high-speed cameras at 1000 fps. The cameras were positioned one in front of the other and the balls launched at angles of 10°, 45° and 90° to the cameras. To validate the software tool, the ball speed and spin rate were measured manually and then compared to the automated measurements. Kelley *et al.* used image processing techniques to firstly locate the ball in the test volume and then identify a marker on the ball that can be used to define the spin rate.

Kelley (2011) identified five potential image processing techniques that could be used for object detection from high-speed video:

1. Thresholding;
2. Image differencing;
3. Morphological operators (erosion and dilation);
4. Hough transform;
5. Edge detection.

Thresholding and image differencing are two of the simplest methods to apply. Thresholding involves converting the image to a binary image (black and white) where each pixel in the original image is compared to a threshold value. If the pixel value is above the threshold it is assigned a value of 1 (white) and otherwise 0 (black). The threshold value can be modified to leave only the tracking object white and the background black. This technique works best when the tracking object is high contrast compared to the background.

Image differencing is simply the difference between two images when one is subtracted away from the other. This technique can be used to remove the background; if an image consisting only of the background and not the tracking object is subtracted from an image of both background and tracking object, the resulting image will contain only the tracking object.

Erosion and dilation can be used to make an object smaller or larger respectively. Erosion removes pixels from the edge of an object and dilation adds pixels. If the distance between tracking objects from one image to the next is small, object dilation can be used to increase the size of the object in the first image, and use only this area to locate the object in the next image. This technique can be used to minimise the search area of the tracking object.

The Hough transform is used to detect parametric shapes such as straight lines or circles. Its use in tracking can be in detecting lines on the side of the pitches or courts to determine the field of play or detecting the circular ball. Edge detection potentially has more use than the Hough transform and essentially detects sharp changes in the image brightness and displays them as a binary image (Kelley 2011).

Colour can also be used in image processed tracking. Agbinya and Rees (1999) used colour histograms to develop an object tracking programme for use in player tracking in

a range of televised sports. The method works by first identifying the colour histogram of the object to be tracked, M and then the histogram of the whole image, I . The ratio $(M/I_i, 1)$ is then calculated where i denotes a particular colour. The ratio is a measure of how much colour i is in the image. The image is then converted to greyscale using the threshold scaled by the colour ratio. Objects which match the colour of the initial tracked object then appear brighter (white) compared to the background image. This technique can be used to identify players of the same team on a playing field by identify just one player in the first image. Agbinya and Rees investigated the success of tracking players from televised footage of a game of football. The success rate over 80 frames was 88%. The limitations of the method are mostly based on object occlusion. If a player is partially obscured from view, for example if their colour shirt was not visible, they are unlikely to be identified by the tracking software.

Utsumi *et al.* (2002) also used colour based tracking to analyse football games from single camera video footage. The method firstly detected the playing field, then detected objects on the field, it tracked the objects and finally labelled the individual players and monitored their performance. The method had an overall detection rate of 64.9% when including tracking occluded players and 94.1 % for non-occluded players.

To overcome the problems associated with player occlusion, Figueroa *et al.* (2006) developed a player tracking algorithm using multiple cameras. Image differencing and thresholding was used to segment the players as *blobs* in the image. Morphological filtering was then used to remove noise. Information on the size of the blobs was then determined by using its contour information:

- Width and height: size of the bounding rectangle of the blob;
- Area: the number of pixels in the blob;
- Perimeter: the number of pixels around the edge of the blob;
- (x,y): the coordinates of the centre of the blob.

This information was then used to split the blobs so that one blob was associated to just one player, and then provide information on its position on the field and its movements over a period of time.

Most of the image processing and tracking work in football has been on tracking the location of a player or ball rather than more in depth motion analysis of body segments or individual limbs. To derive the testing conditions for a traction tester, Grund *et al.*

(2007) analysed the video footage of a player in an injury causing scenario. A 3D skeletal model was superimposed over the player in the video to define the body into distinct segments. Using the mass of the player and the acceleration of the body segment, the approximate reaction force during the injury time was calculated. These reaction forces and body segment angles were used to inform the testing conditions for the traction tester. This approach is a promising development towards mechanical tests mimicking injury scenarios but the data collection method relied on using an approximate model for the body segments rather than exact measurements. The data collection process was also lengthy, taking several months to analysis one scenario.

b) Calibration techniques

When obtaining object information using photogrammetry methods calibration of the cameras is required. Calibration allows 2D image coordinates to be transformed to 3D coordinates in the test space. Zhang (1999) identified the two types of calibration techniques:

1. Photogrammetric calibration: Calibration is performed by observing an object whose geometry in 3D space is known with accurate precision.
2. Self-calibration: Moving the camera in a static scene provides constraints on the cameras' parameters.

Photogrammetric calibration is the most commonly used approach in biomechanics, and in most cases, the direct linear transformation (DLT) method is the preferred approach (Robertson *et al.* 2004). The DLT method was first described by Abdel-Aziz and Karara in 1971. The calibration involves positioning an object in the control volume consisting of a number of points with known relative position on the object. At least 6 non-coplanar points are required. The 2D image coordinates of the control points, n from each camera are then found. From the 2D image coordinates a set of $2n$ equations are found for each camera. Solving these equations leads to 11 DLT parameters that are used to describe the 3D system.

An alternative method of calibration was developed by Zhang (1999). The technique requires the camera to view a 2D planar pattern from at least two orientations. Either the camera or the planar pattern can be moved. The planar pattern typically used is a checkerboard pattern with known number and size of grid squares. Bouguet (2010)

developed a MATLAB™ toolbox implementing the planar calibration algorithms. The method works by defining a camera reference frame attached to the planar pattern in which the coordinates of the pattern coordinates are found. The coordinate vectors of the pattern in the camera reference frame (X_t) relate to the 3D world coordinate vector (X_w) in the test volume through an unknown rigid motion transformation consisting of a translation (T_c) and rotation matrix (R_c):

$$X_w = R_c X_t + T_c \quad \text{Equation 2.3}$$

The unknowns are solved by matching the observed corners on the image with the final projection of their position using the calibration parameters.

Whyld (2004) and Choppin (2008) assessed the accuracy and ease of use of both the DLT method and the planar calibration technique. The methods were assessed by calibrating two cameras using both techniques. The positions of a set of known points were found using both techniques and the average and maximum error calculated. Whyld and Choppin concluded that the most versatile camera calibration method was the planar calibration technique; the errors were lower than the modified DLT method and only slightly greater than the standard DLT method. However the added flexibility of the calibration object being easy to manufacture and use gave it the advantage over the DLT method.

2.8 Chapter findings

Each section can be summarised as follows:

Measurement of traction: Mechanical traction tests provide a quick and repeatable assessment of the translational or rotational shoe-surface interaction but care must be taken over the test parameters used. They can be used to either assess the surface or the outsole design but changing the load or translation distance can affect the traction rating of the surface or shoe. The lack of bio-fidelity in mechanical traction tests has raised concerns over the sole use of mechanical tests to understand the shoe-surface interaction (Frederick 1986). Player testing has the advantage that loading conditions are representative, but can produce results with high variability and also can be subjective. Computational modelling offers scope to accurately represent the surface and the loading conditions but to fully develop a representative natural turf model is challenging and subject to many assumptions that can affect its realism. Nigg (1990) concluded that both mechanical and player shoe-surface measurements were needed to fully understand the situation.

Surface classification: Natural turf surfaces are complex and variations in hardness, soil composition, grass type and water content have all been shown to affect the traction performance (Baker 1991). Accurately classifying the test surface allows traction results to be compared on a more even level.

Biomechanics of football: The literature on the biomechanics of football predominantly focuses on the factors effecting kicking performance (Lees and Nolan 1998). Support foot position and traction have both been shown to relate to the ball speed (Sterzing and Hennig 2008). Identification of injury mechanisms related to shoe-surface interactions has always been an important research area with both too much and too little traction having the potential to cause injuries. Player testing in this area is difficult due to ethical reasons, but injury statistics over a playing season can be used to hypothesise causes of injury. In many cases, ACL or lower limb non-contact injuries were caused by non-related means, these however can be misinterpreted by the media leading to speculations over surfaces or stud designs (Orchard *et al.* 2008). Players have been shown to modify their movements to adapt to different surfaces (Hennig 2011). This makes player testing difficult and relevant only to the specific surface conditions. However, the ability of the player to perceive the surface conditions or potential of slips is important. Player perception of the hardness or traction properties of a surface leads

to their choice of footwear. Incorrect perceptions can lead to unsuitable footwear being worn increasing the susceptibility to injury. Literature showed that humans were unable to perceive slip distances smaller than 30 mm, but after 30 mm are likely to make modification to their movements (Perkins 1978). This raises the question of how far should mechanical traction tests move the shoe in translation; greater than 30 mm and the player is likely to have modified their movement and hence compromised performance.

Motion analysis: Two types of motion analysis techniques were identified; intrusive and non-intrusive. Intrusive techniques involve modifications either to the player, equipment or environment. Many force sensing measurement devices require the testing to take place in the laboratory or use of pressure insoles. Both devices are likely to affect natural movement. Optical measurements are primarily used to track movements of equipment or body segments. Many commercial systems are available but generally require either use of a laboratory with external light sources, or large tracking markers. Non-intrusive methods have the advantage that observations can be made during match conditions. It is difficult to obtain accurate information of exact kinematic data using intrusive methods. Development of custom motion analysis systems allow greater control over which variable are measured and smaller markers can be used reducing the impediment to the players.

Photogrammetry: Photogrammetry is the use of images to obtain information on position or movements. 2D and 3D photogrammetry methods have been successfully used in sports analysis to track the movement of equipment or players (Kirk 2008, Choppin 2008). Custom tracking algorithms make use of image-processing techniques to identify the target object in the video footage. Calibration techniques used in stereo-photogrammetry were assessed with the planar checkerboard technique identified as offering both high accuracy and ease of use.

3 ASSESSMENT OF CURRENT TRACTION TESTING METHODOLOGIES

3.1 Introduction

Traction testing methodologies were assessed in order to highlight the problems associated with experimental testing. Three different methodologies were chosen; traditional mechanical traction testing, a new approach to identify surface shear stresses and a modelling method using analytical and computational techniques. The three methods were selected as they covered a range of the potential advantages and disadvantages of experimental traction testing; mechanical traction testing can be carried out on realistic surfaces but the movements are limited, surface shear stresses can use realistic movements, but the surface is not representative, and modelling uses an approximation of both surface and movement.

The adidas traction tester was chosen for the investigation into mechanical traction testing. A range of stud configurations on both shoes and studded plates were assessed on three different surfaces and the traction values produced were discussed. For the second methodology, a bespoke photoelastic experiment rig was assembled in order to identify and analyse the surface shear stresses generated during running. Surface shear stresses are rarely measured when assessing traction however they can provide more information on how individual studs interact with the surface. Two modelling techniques (analytical and finite element analysis) were used to highlight the advantages and disadvantages of predicting the traction computationally.

3.2 Aim and objectives

Aim

- To assess the methods used in experimental traction testing.

Objectives

- To test a range of methodologies including:
 - Mechanical traction testing;
 - Identification of surface shear stress;
 - Computational modelling.
- To identify the advantages and disadvantages of each method.

3.3 Mechanical traction testing

3.3.1 Introduction

As reported in Chapter 2 there is a range of mechanical traction testers used to either measure the translational or rotational resistance to movement on a playing surface. These devices range from a complex robotic leg said to replicate an injury loading movement (Grund and Senner 2010) to a simple pendulum swing test (FIFA 2008). For the assessment of mechanical traction testing, the adidas tester was used. The adidas traction tester as described by Kirk (2008) replicates the acceleration during sprinting by posteriorly translating the forefoot of a shoe. The traction tester can also represent a rotational movement of the forefoot. The traction tester consists of an electric motor and two separate load cells enabling the rotational and translational traction to be measured; rotational speeds up to 200°s^{-1} for a range of up to 180° , and translational speeds up to 300 mms^{-1} over a distance of 450 mm are achievable. This type of device was selected for assessment as it allows an easy and direct comparison of shoe designs and surface types.

The traction tester is compatible with both full shoes and studded plates. Studded plates are often used to assess new stud configurations or shapes (Clarke and Carre 2010). The purpose of the assessment was also to identify the limitations of the studded plate by testing stud configurations similar to the shoes being tested.

A range of surfaces was also tested to highlight the differences between testing indoors on an artificial turf sample compared to outside on firm or soft natural turf.

3.3.2 Aim and objectives

Aim

- To assess the testing properties of the adidas traction tester.

Objectives

- To assess the effect of changing the standard test parameters (load, speed and displacement);

- Test a range of stud configurations using a studded plate and a selection of shoes;
- Test three surfaces, firm and soft natural turf and artificial turf;
 - Classify the ground condition using a Clegg impact hammer.

3.3.3 Experimental procedure

The effect of load, displacement and speed on traction were assessed using the Copa Mundial shoe on an artificial surface (Table 3.1). Standard test parameters as used by adidas were:

- Translation: 50 mm at 10 mms⁻¹
- Rotation: 60° at 12V¹
- Total load: 69.3 kg

The carrier load on the traction tester was 34.3 kg; an additional 35 kg was added to the traction tester to increase to the standard load of 69.3 kg.

Test condition	Load	Displacement	Speed
1 - Standard	69.3 kg	50 mm	10 mms ⁻¹
2 - Load	34.3 kg	50 mm	10 mms ⁻¹
3 - Speed	69.3 kg	50 mm	100 mms ⁻¹
4 - Displacement	69.3 kg	100 mm	10 mms ⁻¹

Table 3.1 - Assessment of testing parameters.

Four adidas shoes were used for the traction testing assessment. The Copa Mundial, Predator (FG), Tunit and World Cup were selected for the range in stud shape, number and material. Shoe (UK size 8.5) and plate configurations are shown in Figure 3.1 and Figure 3.2; the plate configurations matched the shoe outsole configurations as closely as possible. Due to the bladed profile of the Predator studs, a plate configuration was not designed. An additional pentagon shaped stud configuration was also tested with the plate. Rubber studs, 12 mm in length were used in the plate. The shoes were positioned with a heel angle of 18.1° to ensure only the forefoot was in contact. The stud configurations were tested using the standard testing parameters (total load = 69.3 kg, translation 50 mm at 10 mms⁻¹, rotation 60° at 12V¹). Stud characteristics were identified as shown in Table 3.2).

Shoe	No. of studs	Stud profile	Stud height	Stud material	Surface
Copa Mundial	8	Round	10 mm	Rubber	FG
PREDATOR® Absolado TRX FG	0	Bladed	14 mm	Moulded TPU	FG
F50 i TUNiT	6	Round	10 mm	Plastic	SG
World Cup	4	Round	14 mm	Metal	SG
Plate	4-7	Round	12 mm	Rubber	-

Table 3.2 - Shoe properties.

Five repeats of each test condition were carried out. This provided enough data to enable repeatability to be analysed, but ensured the test surface was not 'over tested'.

Figure 3.1 - Stud configurations on plate, from Left to Right: Copa Mundial, Pentagon, Tunit and World Cup.

Figure 3.2 - Boots tested, from Left to Right: Copa Mundial, Predator, Tunit and World Cup.

Three surfaces were used for testing; artificial, natural firm ground and natural soft ground. The artificial turf was tested in the adidas Test Center. The firm ground was tested at the Scheinfeld School sports field; no additional conditioning was applied to the pitch. The soft ground was tested at the Scheinfeld Football Club pitch; approximately 1.5 l of water was added to an area of 0.25 m² (equivalent to 6 mm of

rain) between each shoe or plate set of tests. Pitch conditions are shown in Figure 3.3. Each test surface was tested with the Clegg impact hammer (0.5 kg, 0.3 m drop height, 50 mm diameter) to provide an estimation of the surface hardness. Impact tests were taken before and after testing.

Figure 3.3 - Traction testing pitch locations, from Left to Right: Artificial turf (adidas TestCenter), Firm ground natural turf (Scheinfeld School) and Soft ground natural turf (Scheinfeld Football Club).

3.3.4 Results and discussion

a) Investigation of testing parameters

Figure 3.4 - Investigation of testing parameters. Top left: Standard (adidas); Top right: No additional load; Bottom left: Faster translation; Bottom right: Longer displacement (mean \pm standard deviation).

After reviewing the results (Figure 3.4), the standard testing parameters currently used by adidas produced a smooth curve with minimum variation between repeats. Although maximum traction may not necessarily be reached after 50 mm, results showed good repeatability with smaller standard deviation between repeats and allowed more results to be performed on the same size test section compared to other parameter combinations. The following observations were made from Figure 3.4.

- Using the standard testing parameters it was not possible to see whether maximum traction was reached after 50 mm displacement, however results displayed good repeatability and no oscillations during translation.
- Reducing the additional load enabled the maximum traction value to be reached after approximately 40 mm but it was thought that the load was not high enough to be representative of realistic conditions (Representing only 0.4 BW for an 80 kg player).
- Increasing the speed of the displacement introduced oscillations in the initial displacement and increased the variability between results.
- Increasing the length of displacement enabled the maximum traction value to be reached but values after this point tended to show more variation.
- Increasing the length of displacement also increased the area required for testing.

The standard adidas test conditions were used for the next stages of testing; this also allowed the potential for results to be compared to previous tests carried out on the traction tester.

b) Translation of shoe results

Figure 3.5 - Traction force displacement graphs for Top left: Copa Mundial; Top right: Predator; Bottom left: Tunit; Bottom right: World Cup shoes on natural firm ground turf (mean \pm standard deviation).

Currently, the traction value at the end of translation (50 mm) is used for comparison (Table 3.3). In most cases, this is the maximum traction reading for the movement. However, when comparing the force-displacement curve for the translational movement it becomes apparent that the shoes that display the highest traction values at 50 mm do not always have the highest traction prior to this point.

Artificial	Force (N) at 10 mm	Force (N) at 20 mm	Force (N) at 50 mm
Copa Mundial	374.2 ± 3.5	595.3 ± 7.6	994.0 ± 20.6
Predator	415.7 ± 7.7	656.9 ± 10.2	843.6 ± 20.1
Tunit	359.5 ± 8.6	551.8 ± 7.7	901.2 ± 17.9
World Cup	389.2 ± 9.7	588.3 ± 9.8	881.2 ± 38.4

Firm Ground	Force (N) at 10 mm	Force (N) at 20 mm	Force (N) at 50 mm
Copa Mundial	433.9 ± 5.9	631.7 ± 8.7	1005.3 ± 18.5
Predator	457.4 ± 6.4	662.0 ± 10.8	1046.2 ± 22.0
Tunit	415.3 ± 12.1	586.3 ± 18.1	976.4 ± 25.8
World Cup	442.9 ± 11.5	613.1 ± 25.8	953.2 ± 55.0

Soft Ground	Force (N) at 10 mm	Force (N) at 20 mm	Force (N) at 50 mm
Copa Mundial	369.7 ± 9.0	548.1 ± 13.1	906.5 ± 32.3
Predator	409.1 ± 15.0	590.1 ± 17.6	930.5 ± 29.8
Tunit	390.0 ± 14.4	582.2 ± 24.2	965.7 ± 52.3
World Cup	399.3 ± 2.9	579.2 ± 9.0	918.4 ± 22.7

Table 3.3 - Traction force values for all shoes at set displacements during translation (mean ± standard error).

Table 3.4 illustrates the variation between traction rankings depending upon the displacement value used for comparison. For all surface conditions, the ranking order at 10 mm displacement differs from the final 50 mm displacement reading. The most extreme example is the Predator shoe on artificial turf; at 10 mm and 20 mm displacement, the shoe exhibits the highest traction force out of the 4 shoes. However, only using the traction value at the end of the translation (50 mm) for comparison causes the traction result for the Predator shoe to then be the lowest.

Artificial	Rank at 10 mm	Rank at 20 mm	Rank at 50 mm
Copa Mundial	3	2	1
Predator	1	1	4
Tunit	4	4	2
World Cup	2	3	3

Firm Ground	Rank at 10 mm	Rank at 20 mm	Rank at 50 mm
Copa Mundial	3	2	2
Predator	1	1	1
Tunit	4	4	3
World Cup	2	3	4

Soft Ground	Rank at 10 mm	Rank at 20 mm	Rank at 50 mm
Copa Mundial	4	4	4
Predator	1	1	2
Tunit	3	2	1
World Cup	2	3	3

Table 3.4 - Ranking of traction values for translation movement for shoes on all surfaces (1 = highest).

An ANOVA F-test was used to see if there were any significant differences between the shoes on the same surface.

Source of variance	Sum of squares	<i>df</i>	Mean square	<i>F</i>	<i>p</i>
Between groups	4660.93	3	1553.64	3.52	< .05
Within groups (error)	7065.24	16	441.58		
Totals	11726.18	19			

Table 3.5 - Analysis of Variance for all shoes on firm ground at 10 mm displacement.

Source of variance	Sum of squares	<i>df</i>	Mean square	<i>F</i>	<i>p</i>
Between groups	15213.62	3	5071.21	3.43	<.05
Within groups (error)	23668.07	16	1479.25		
Totals	38881.70	19			

Table 3.6 - Analysis of Variance for all shoes on firm ground at 20 mm displacement.

Source of variance	Sum of squares	<i>df</i>	Mean square	<i>F</i>	<i>p</i>
Between groups	24165.03	3	8055.01	3.06	<.10
Within groups (error)	42050.13	16	2628.13		
Totals	66215.16	19			

Table 3.7 - Analysis of Variance for all shoes on firm ground at 50 mm displacement.

Results suggested that at 10 mm and 20 mm significant differences ($p < .05$) existed between the shoes on the same surface. To assess which shoes differ significantly, the raw score mean differences between each shoe were calculated for the 10 mm displacement.

	Copa Mundial	Predator	Tunit	World Cup
Copa Mundial	0.0	23.6	18.5	9.1
Predator		0.0	42.1*	14.5
Tunit			0.0	27.6
World Cup				0.0

Table 3.8 - Mean difference analysis, * $p < .05$.

Tukey's honestly significant difference test was used to determine which shoes were significantly different. Tukey's test indicated that only the Tunit and the Predator were significantly different at the 10 mm displacement reading (Table 3.8). The Predator was the only bladed shoe tested whereas the Tunit was a round studded shoe. The Tunit also had fewer forefoot studs than the Copa Mundial shoe and a shorter stud height compared to the World Cup shoe. This combination of factors lead to the Tunit shoe showing the lowest traction value for 10 mm and the Predator shoe displaying the highest. The absence of significant differences between the World Cup and Predator shoe indicates that although the World Cup was targeted for soft ground conditions and the Predator firm ground; both display high traction values on firm ground conditions.

General observation for translation movements:

- On firm ground, the Predator and Copa Mundial displayed the highest traction values.
- On soft ground, the Tunit shoe displayed the highest traction value at 50 mm but also had the largest standard deviation between repeat testing.

- The World Cup shoe designed for soft ground fell in the lower half of the group on all surfaces after 20 mm, but showed high traction results in the 0–20 mm range.
- The Copa Mundial shoe designed for firm ground gave high traction resistance on both artificial and firm ground conditions, but ranked low on soft ground turf.
- The Predator shoe, the only bladed stud outsole tested showed high traction values on all surfaces over the initial 0–20 mm displacement, but fell slightly when comparing traction values at 50 mm.

c) *Plate and outsole comparison*

Figure 3.6 - Force displacement plot for Copa Mundial on artificial turf. Left: Studded plate. Right: Full shoe.

A plate was used as a comparison to the shoe outsole to investigate whether a plate was a suitable alternative to an outsole when researching the effect of stud configurations. The advantages of using a plate would mean easy alteration and assessment of new stud designs and configurations. ANOVA *t*-tests were used to compare the Copa Mundial configuration of the plate and shoe on artificial turf.

	Mean (N)	<i>SD</i>	<i>SE_m</i>	<i>sed</i>	<i>t</i>	<i>p</i>
Plate at 10 mm	420.8	30.0	13.4	13.9	3.36	<.01
Shoe at 10 mm	374.2	8.0	3.6			
Plate at 20 mm	656.1	61.3	27.4	28.4	2.15	<.05
Shoe at 20 mm	595.3	16.9	7.6			
Plate at 50 mm	1109.1	69.8	31.3	37.3	3.08	<.01
Shoe at 50 mm	994.0	45.9	20.5			

Table 3.9 – ANOVA *f*-test assessment of the plate and shoe on the artificial surface.

Significant differences were seen between the plate and the shoe. The traction values for the plate at 10 mm and 50 mm were significantly higher ($p < .01$) than the shoe at the same position. The difference seen may be accounted for by a number of reasons:

- The plate allowed all forefoot studs to be in contact and imbedded up to the same depth. It was difficult to test only the forefoot of the shoe without a high heel angle which was not always possible without a deformable last; as such, at certain configurations the heel may also be in contact.
- The plate was expected to have higher traction values due to a greater surcharge pressure as it has a larger area.
- The plate displayed poor repeatability due to the edge of the plate interacting with the surface. A solution to this would be to have a curved front edge to mimic the toe of the shoe.
- Comparisons between rotational results cannot be drawn as the shoe and plate have a different point of rotation.

d) Surface hardness

The Clegg impact hammer was used to measure the surface hardness. The device was modified to read the voltage for the complete impact. The voltage was directly proportional to the force being measured (Figure 3.7).

Figure 3.7 - Clegg hammer impact testing; voltage is directly proportional to impact force.

Artificial	Natural firm ground	Natural soft ground
80±1g	105 ±3 g	79 ±4 g

Table 3.10 - Clegg hardness values (mean ± standard error).

The artificial and soft ground conditions displayed similar maximum hardness values and force curves. The firm ground was approximately 25 g harder than the other surfaces. A r-test was used to ensure that there was a significant difference between the hard and soft ground surfaces.

	Mean	SD	sed	t	P	
Firm	105	3	1.34	2.23	11.6	<.01
Soft	79	4	1.79			

Table 3.11 - Significance of difference between firm and soft ground conditions using a t-test.

A f-test indicated a significant difference between the firm and soft ground conditions ($p < .01$). The values of surface hardness for all three surfaces were within the upper limits of the guidelines issued by Canaway *et al.* (1990); values of 10 to 100 g were set as acceptable limits. This indicates that the soft ground condition, although statistically different from the firm ground condition, may not best represent soft surfaces.

The standard deviation of the maximum impact force for the natural turf conditions was greater than the artificial turf. This highlights the problems with testing natural surfaces due to the lack of consistency in surface properties across the test area.

e) Surface comparison

The shoes tested were marketed as being suitable for a range of surfaces; the Predator and Tunit were designed for firm ground conditions, the World Cup for soft ground and the Copa Mundial suitable on all surface conditions. The suitability of a shoe on a surface depends not only on the translational traction value, but also on the rotational traction value. The coefficient of traction (COT, traction force at 50 mm divided by vertical load) was calculated for each shoe on soft and firm natural ground conditions at 50 mm displacement. The torque for each shoe was also calculated at 60° rotation. Figure 3.8 displays the maximum coefficient of traction (COT) value for all shoe configurations on both firm and soft ground conditions. The COT value is plotted

against the maximum torque for internal rotation. In previous work, Kirk (2008) proposed an acceptance zone of COT and torque values; values of COT between 1.35 and 1.9 and torque between 54 and 77 Nm defined the limits of the zone. The values were obtained from traction assessment of the Copa Mundial shoe on dry natural turf, a bladed stud design on dry natural turf and the World Cup shoe on wet natural turf. Values above the zone were seen as extreme, and below as insufficient. Values of extreme torque but insufficient traction were classed as the danger zone. Although the exact values of acceptance cannot be used for comparison due to the differences in surface conditions, the concept can still be applied to Figure 3.8 using the Copa Mundial, World Cup and Predator shoe to define the acceptance zone.

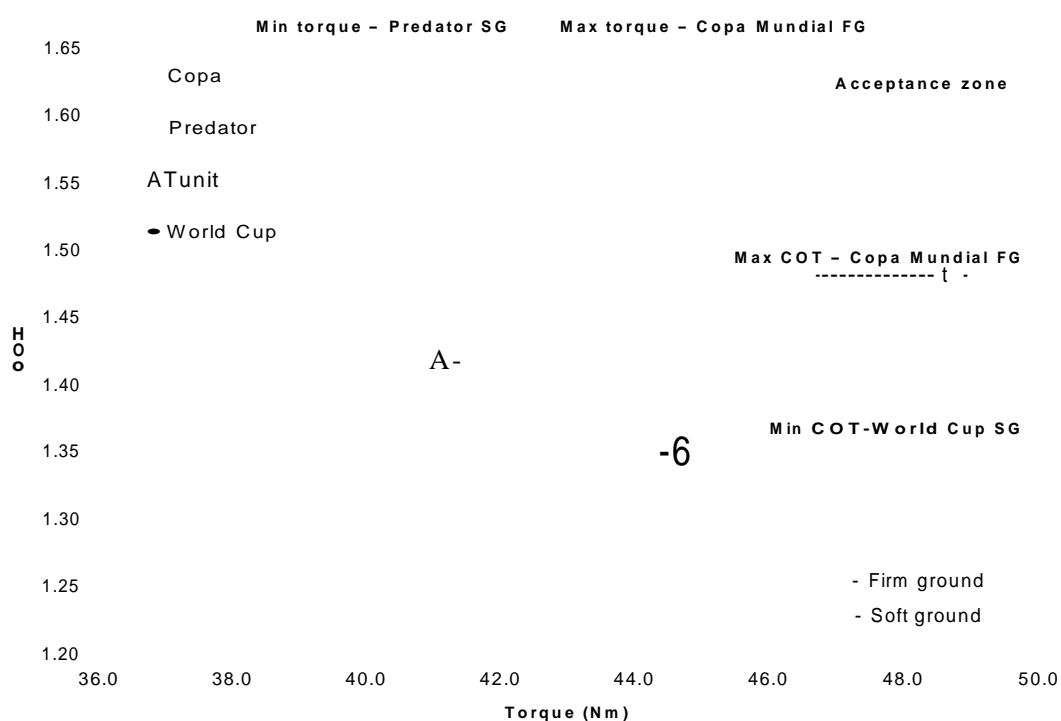


Figure 3.8 - Maximum coefficient of traction (COT) against maximum torque for all shoe types on natural firm and soft ground conditions (mean ± standard deviation).

The following observations were made from Figure 3.8:

- The World Cup shoe showed a low COT value but reasonably high torque on soft ground surfaces; for a shoe designed for soft ground, a higher COT would have been expected.
- The World Cup on firm ground was positioned at the centre of the group, with both moderate COT and torque.

- Both the Predator and Copa Mundial shoes exhibited high COT and torque values for firm ground conditions, but had significantly reduced performance on soft ground conditions.
- The COT value for the Tunit shoe did not vary between firm and soft ground and only exhibited a slight change in maximum torque. This could suggest that the Tunit is a good all round shoe, with an unchanging mid performance on both surfaces.
- A high standard deviation of all results was seen highlighting the problems of testing on natural surfaces.

f) *Repeatability*

Figure 3.9 - Copa Mundial (shoe), force-displacement plot for all 5 repeats.

The average standard deviation of force for five repeats over the 50 mm displacement ranged from 20 to 70 N. This was approximately 2-7% of the traction at 50 mm and 4-15% of the traction at 20 mm. All the shoe configurations on soft ground displayed higher standard deviations than the other surfaces. This again highlighted the difficulties in outdoor testing of realistic surface conditions.

	Artificial (N)	Firm Ground (N)	Soft Ground (N)
Copa Mundial	25.3	28.9	39.3
Predator	32.4	35.6	44.6
Tunit	22.4	48.9	69.8
World Cup	42.3	54.4	28.1

Table 3.12 - Average standard deviation in force over 50 mm displacement during translation movement.

3.3.5 Summary

The results provided a suitable database of traction values to use for comparison for either future experimental testing or to validate analytical models. Differences were shown between firm and soft ground conditions, but high deviations between soft ground repeats highlights the issues involved in testing realistic conditions.

Further research is required to find the most suitable traction values for comparison. Results showed that using the traction value at 50 mm was not representative as to how the shoe performed during the early stages of translation. A comparison at 10 or 20 mm may provide better indication of how the shoe will behave during the initial stages of slip.

The following advantages and disadvantages were identified:

Advantages	Disadvantages
<ul style="list-style-type: none">• Controlled, repeatable test;• Use of standard testing protocol allows results to be compared over a period of time;• Can test realistic surfaces;• Non subjective testing.	<ul style="list-style-type: none">• Non-realistic loading conditions;• Testing on natural surfaces introduces variability;• Difficult to control surface consistency;• Use of a plate to test shoe configurations is non-representative.

Table 3.13 - Advantages and disadvantages of mechanical traction testing.

3.4 Surface shear stress analysis (Photoelasticity)

3.4.1 Introduction

In previous work, the overall resistive force (traction) between the studded outsole and the surface was measured by use of mechanical test equipment (traction tester). The limitation of this approach was that little is known about the effect the individual studs have on the overall traction; particularly under realistic loading conditions. One way to enable more information to be gathered is to analyse the shear stresses arising between the studded outsole and the surface. The purpose of the study was to develop a low cost but high resolution system to enable the shear stresses between individual studs in the outsole and the surface to be identified. This was done by the use of photoelasticity. The advantages and disadvantages of this approach were also assessed; focussing on its potential for repeatable testing and comparison of outsole designs.

3.4.2 Aim and objectives

Aim

- To identify the shear forces between the shoe and the surface during football specific movements using photoelasticity.

Objectives

- Undertake a pilot study at Sheffield Hallam University to design and make a small scale experiment to produce a method of displaying and measuring the shear forces in a polyurethane plate;
- Use the successful method on the glass force plate at the adidas test centre and collect photoelastic images of participants running over the plate in studded footwear;
- Analyse photoelastic images using image processing techniques.

3.4.3 Theory of photoelasticity

Photoelasticity is an experimental stress analysis technique utilising the optical phenomenon of birefringence (or double refraction) which occurs in some stressed, transparent materials.

Birefringence nominally occurs in non-cubic crystals which due to their atomic structure are optically anisotropic. When a light ray is incident on an optically isotropic material, the speed of light is the same in all directions. However, when a light ray is incident on a birefringent material it splits into two rays; the ordinary ray and the extraordinary ray (Tipler and Mosca 2004). The two rays travel at different velocities, and depending on the orientation of the material they can also travel in different directions. The rays emerge with a phase difference that depends on the thickness of the material and the wavelength of the incident light; in essence, this results in the material having two refractive indices. The same phenomenon occurs in some transparent materials when under stress. As the material deforms the internal structure of the material changes and the material-light interaction alters resulting in the change in the refractive index (Klamecki 2001). A material that was initially optically isotropic when free of stress becomes optically anisotropic when stressed (Dally and Riley 1991). When the incident light on a stressed birefringent material is polarised, again two light rays emerge travelling at different velocities and perpendicular to each other but they are also orientated to the direction of principal stress (Strainoptics Inc. N.D.). If the resulting light is viewed through a second polariser orientated at 90° to the first, the stress patterns in the material can be seen.

The change in the indices of refraction (retardation) of a birefringent material under stress is linearly proportional to the loads and thus related to stresses and strains (Maxwell 1853). This gives rise to the stress optic law. For plane-stress situations ($\sigma_3 = 0$), using the change in refractive index this can be expressed as:

$$n_1 - n_2 = c(\sigma_1 - \sigma_2) \quad \text{Equation 3.1}$$

where; n_1 and n_2 = principal indices of refraction

σ_1 and σ_2 = principal stresses

$c = c_1 - c_2$ = relative stress-optic coefficient (Dally and Riley 1991)

Figure 3.10 - Stressed birefringent model viewed with two crossed polarisers (adapted from Dally and Riley 1991).

By relating the relative retardation (relative angular phase shift, A) to the change in the indices of refraction in a stressed material of thickness h , the stress optic law can be written as:

$$A = \frac{2\pi r / C}{C_0 - 1 - 0.2} \quad \text{Equation 3.2}$$

This can be simplified to:

$$\text{Equation 3.3}$$

where the fringe order, N :

$$\text{Equation 3.4}$$

and the material fringe value is:

Equation 3.5

The maximum shear stress can be found from the difference between the two principal stresses;

$$\tau_{max} = \frac{\sigma_1 - \sigma_2}{2}$$

Equation 3.6

Hence, the maximum shear stress can be simply obtained from measuring the relative retardation or fringe order, N apparent in the resulting fringe pattern.

Two fringe patterns result in the stressed birefringent material; isoclinic fringes and isochromatic fringes. Isoclinic fringe patterns appear as dark lines on the material, they are used to determine the direction of the principal stress. The isochromatic fringe patterns gives the lines along which the principal stress difference is equal to a constant (Dally and Riley 1991) and appear as coloured lines when white incident light is used. The colour or intensity of the isochromatic fringes is indicative of the shear stress present in the material. By counting the reoccurrence of a particular colour or intensity, the fringe order can be determined; this can be used in Equation 3.6 to calculate the shear stress. A quarter-wave plate can be used at 45° to the polarisers to remove the isoclinic fringes; this can aid in the identification of the isochromatic fringe order.

Figure 3.11 - Fringe pattern in a frozen stress disk. Left: The dark isoclinic lines indicate the direction of the principal stresses. Right: The isochromatic fringe pattern indicates the areas over which the shear stress is constant. The reoccurrence of a colour or intensity can be used to determine the fringe order.

3.4.4 Method

a) Experimental design

Preliminary testing was investigated in Sheffield to find appropriate materials, apparatus set-up and methodology to capture the dynamic photoelastic images before transferring the pilot study to Germany.

An 8 mm acrylic sheet was used at the support surface and placed in a 500 x 500 x 500 mm wooden frame. Acrylic is non-birefringent and hence provides a suitable rigid support surface. Two photoelastic materials were chosen for initial analysis; a rigid polycarbonate sheet and a flexible polyurethane sheet. A summary of the optical and mechanical properties of the materials are shown in Table 3.14.

Property	Polycarbonate	Urethane rubber
Time-edge effect	Excellent	Excellent
Creep	Excellent	Excellent
Machinability	Poor	Poor
Modulus of Elasticity	2480 MPa	3 MPa
Poisson's ratio	0.38	0.46
Proportional limit	34.5 MPa	0.14 MPa
Stress fringe value	7.0 kNm ⁻¹	0.18 kNm ⁻¹
Sensitivity index	4.92 ram ⁻¹	0.78 mm ⁻¹

Table 3.14 - Optical and mechanical properties of polycarbonate and urethane (adapted from Dally and Riley 1991).

If the top surface of the material is reflective, a single polariser can be used; this is known as 'reflective photoelasticity' and allows the stress pattern to be viewed from the same side as the incident light. Silver spray paint was applied to the top surface of the polycarbonate providing a reflective coating when viewed from below. However, spray paint would not adhere to the polyurethane surface; instead an additional layer of polyester with silver spray was used. The photoelastic material was placed on the top surface of the acrylic support sheet. A polarising film and a quarter-wave plate were placed between the photoelastic material and the acrylic. The quarter-wave plate was aligned such that the isoclinic lines were removed from the image. A frozen stress disk

was used to align the plates and confirm the polarising axis of polariser sheet (Figure 3.11).

In order for the photoelastic image to be viewed, the material was illuminated from below and a camera focussed on the underside of the acrylic. Numerous lighting and camera set-ups were experimented with to obtain the best image for post processing. Reflections on the underside of the acrylic were one of the most difficult issues to resolve; all support frames and camera components were covered with black material to help reduce the problem.

A round plate with 5 rubber studs was used to localise the shear forces on the photoelastic material. A 30 kg load was applied to the studded plate and moved in translation and rotation on the surface to instigate shear forces. Figure 3.12 shows the final set-up system at Sheffield that provided a suitable quality image.

Reflective surface
Photoelastic material
Circular polariser

Wooden frame

Black coating

High-speed video camera

Floodlights

Figure 3.12 - Experimental set-up in Sheffield.

Using the studded plate, it was difficult to generate fringes in the polycarbonate material; the friction between the studs and the surface was not sufficient enough to create shear forces in the material. In comparison, the fringe patterns from the polyurethane material were clear and there were sufficient fringes outside the contact zone (out of plane shear fringes) to indicate shear stresses in the material (Figure 3.13).

Figure 3.13 - Example of stress fringes generated in polyurethane using the studded plate.

3.4.5 Final experimental procedure

The images obtained from the preliminary work in Sheffield gave proof that the shear stresses could be obtained dynamically from the photoelastic material. As such, the experiment was moved to the adidas Test Center in Scheinfeld. An elevated glass force plate was used as the support surface in replacement of the acrylic sheet. The glass force plate allowed the photoelastic images to be viewed but also allowed force plate data to be recorded in synchronism with the photoelastic work.

Again, reflections were the main problem when trying to obtain a high quality image. The camera had to be removed from directly under the plate and repositioned outside of the support frame. The camera was focussed on the photoelastic plate via a mirror angled at 45°. The lights used to illuminate the surface had to be cold lighting to prevent the glass plate from overheating and cracking. This however meant the image appeared very blue and washed out. This colouring was hindered further by the blue tint to the glass plate. These issues were overcome by adjusting the contrast, brightness and gamma values of the camera. Again, the support frame was covered with black material to prevent unnecessary reflections. Diffusers were also placed over the lights to soften the lighting. A high-speed camera (Photron APX-RS) was used to record the photoelastic images at a frame rate of 50 fps and resolution 1024 x 1024. Given the low frame rate, ideally an SLR camera could have been used at a higher resolution; however, there was no external trigger for the camera meaning the image had to be

manually taken from under the plate at the correct time of the movement. This was deemed unreliable and not practical; as such the high-speed camera with external trigger was used.

The reflective surface, polyurethane, polariser and quarter-wave plate were layered on the top surface of the force plate. Another problem encountered was the fixation of the sheets to the glass surface. Tape was used as the fixation had to be temporary and not leave permanent marks on the glass. Slippage of the sheets was a problem that could have been overcome by an external frame supporting the polyurethane; this unfortunately was not possible given the time constraints.

Dynamic photoelastic images were recorded for two different loading scenarios. The first method made use of the adidas traction tester to horizontally move a studded plate and football shoes across the surface. Four stud configurations and four football boots were used to vary the stud placement and number. No additional load was applied to the traction testing given a vertical load of 34.3 kg. The studded plate and shoes were moved in translation 50 mm across the surface at a speed of 10 mms⁻¹. Images were also recorded for rotation, 60° at 12°s⁻¹. Photoelastic images and traction data were recorded for all tests.

The second loading condition aimed to replicate more realistic movements. Participants wearing World Cup adidas football boots with rubber studs ran across the photoelastic material, with the heel-strike landing in the centre of the image. The photoelastic camera was synchronised with the force plate and an additional camera focussed on the side view of the heel-strike. The second camera (VDS Vosskuhler HCC-1000) recorded at 200 fps and a resolution 1024 x 512 pixels. The two cameras were triggered by a light-gate sensor set up 2 m before the force plate and photoelastic material. The force plate was triggered by a falling edge trigger on impact and sampled at 1000 Hz for 0.5 s.

Shear stresses were produced in the material when the outsole came in contact. Studded outsoles (4 studs in the forefoot and 2 studs in the heel) were used to localise the shear stress and minimise the interference from out-of-plane stresses. Each foot-strike had a ground contact time of approximately 0.5 s, producing 25 photoelastic images. The start and end of contact was defined visually through the side-view images and validated against the force-plate results.

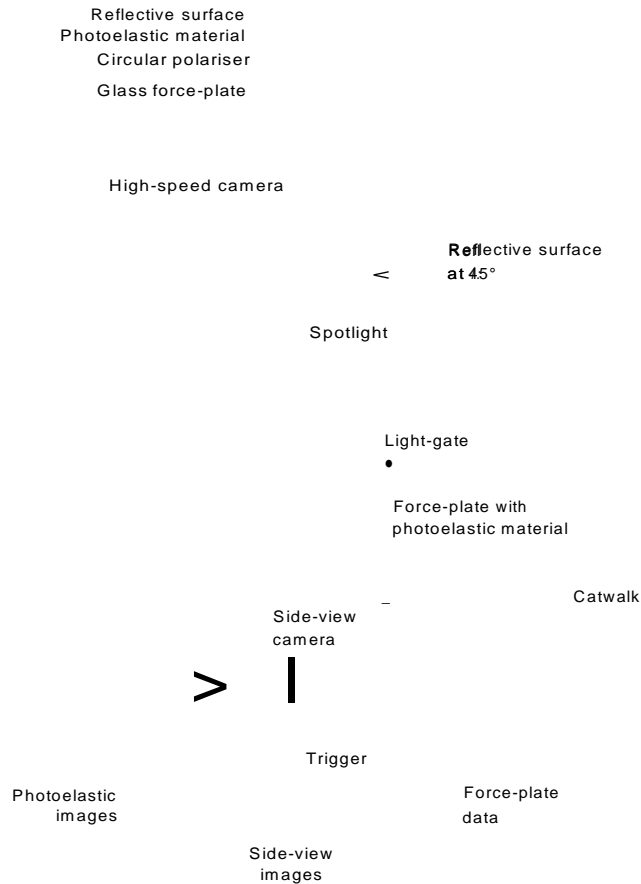


Figure 3.14 - Experimental set-up at Scheinfeld. Top: Side-view; Bottom: Plan view (not to scale).

3.4.6 Image processing

Dynamic images were recorded and saved as individual image files using the Photron software. This allowed post-processing of the images to be carried out. The aim of the post-processing was to convert the images into a form from which the fringes could be easily counted, and the movement or growth of a fringe tracked. The image toolbox in MATLAB™ was used to do this. Background subtraction, histogram equalisation, L*a*b* K-mean clustering segmentation and contour mapping of the greyscale image were all investigated.

The images were initially converted into greyscale (0 - 255) and the background removed by the calculation of the absolute difference between the stressed image and a non-stressed image. Figure 3.15 shows the original and processed image captured at $t = 0.2$ s during the foot-strike. The two heel studs and three of the forefoot studs were in contact; i.e. the foot was in transition between heel-strike and forefoot push-off. Figure 3.15 displays the isochromatic fringes (loci of constant maximum shear stress); when

viewed in colour, the repetitions of green and red bands were the most prominent. When converting to greyscale the maximum shear stress loci become visible as bands of constant greyscale intensity. The green and red bands formed the lightest and darkest fringes respectively and it was their reoccurrence that was used to identify the fringe order (N). Due to the set-up and processing, the background of the images appeared dark ($N = 0$), as such the first fringe detected was a light fringe ($N = 1/2$) and the next a dark fringe ($N = 1$). The processed results were then used to evaluate the subsequent maximum shear stresses.

Original Greyscale imabsdiff imadjust

Figure 3.15 - Image processing; the images were converted to greyscale and the background removed by calculation of the absolute difference method. The image properties were adjusted to produce a clearly defined stress patterns ($t = 0.20$ s).

3.4.7 Results

Figure 3.16 shows the growth of the photoelastic fringes for the foot-strike. Upon the initial heel-strike, the shear stresses radiated from the stud contact points along the direction of motion. When the forefoot came into contact, the influence of the heel shear stresses decreased, and the fringes around the forefoot studs grew indicating maximum shear stresses acting predominately in the opposing direction to motion.

Figure 3.16 - Time series of stress patterns. Heel-strike and forefoot push-off photoelastic images during running in studded outsoles ($\Delta t = 0.04$ s).

3.4.8 Analysis

a) Fringe identification

To identify the location of the fringes, greyscale intensity profiles were drawn radiating from the centre of each stud on the image. The intensity profiles showed clear peaks for the light fringes and troughs for the dark fringes. A contact zone directly beneath the stud placement was defined. This was the region in which the stresses were no longer directly related to out-of-plane shear stresses, and were instead a result of stresses arising from the normal force during contact. The contact zone produced a large number of fringes tightly spaced together; as such, the fringes could not be easily distinguished on the intensity profile and the overall zone was instead identified.

Figure 3.17 illustrates the intensity profile for one stud in the forefoot during a translational movement (push-off after heel-strike, $t = 0.2$ s). A profile line 45° to the direction of motion was chosen as the distinction between fringes was clearly observed.

Distance along profile, d (pixels)

Figure 3.17 - Identifying maximum shear stress using greyscale intensity profiles. Top left: The intensity profile indicates clear peaks for the light fringes ($I \sim 255$) and troughs for the dark fringes ($I \sim 0$); Top right: Processed image - focussed on lower left forefoot; Bottom left: Calculation of shear stress using fringe order; Bottom right: The contour maps of the fringes indicate the increase in maximum shear towards the contact zone.

The fringe orders determined in Figure 3.17 can be used to estimate the maximum shear stress by use of the stress-optic law (Equation 3.6). Further calibration of the material is required to determine the stress fringe coefficient (f_o), however using an estimation of 0.20-0.28 kNm⁻¹ (Dally and Riley 1991, Doyle 2004), rudimentary analysis of the fringe pattern suggested that shear stresses of 0.12-0.16 MPa were evident in the heel-surface during initial impact and approximately 0.08-0.12 MPa at the forefoot-surface during push-off.

b) Stress trajectories

An alternative method of analysis involves plotting the "stress trajectories" of the fringes. These are lines indicating the maximum distance a shear stress fringe radiates from the point of contact (stud). This is a useful visualisation tool as it indicates the direction the material is likely to fail. Figure 3.18 shows the stress trajectories for a heel-strike in the World Cup boot. The images are coupled with the side-view stills to show how the position of the boot relates to the fringe patterns.

Figure 3.18 - Stress trajectory and side view of shoe during heel-strike and forefoot push-off (white arrows indicate direction of motion of studs or growth of fringes).

The vector plot shown in Figure 3.19 was created by tracking the growth of the first fringe at each time step at 30° intervals around the point of stud contact. The overall growth pattern suggests the direction in which the shear stresses are acting at that moment in time. A symmetrical vector plot suggests a predominately vertical force being applied, whilst one which is significantly more prominent in one direction (i.e. aspect ratio of horizontal to vertical diameter > 1) would indicate a shear force acting in that direction.

- 1
- 2
- 3
- 4
- 5
- 6
- 7
- 8
- 9
- 10
- 11
- 12
- 13
- 14
- 15

Figure 3.19 - Vector plot of first fringe location at time steps 0.02 s at 30° intervals around stud contact.

The vector plot indicated a shear force acting along the direction of motion upon heel-strike contact. This was also consistent with the force data shown in Figure 3.20; a noticeable force in the anterior (-F_y) direction was observed. The propulsive force on push-off (+F_y) was not as prominent as the impact forces. This was also seen in the vector plot; the vectors radiating from the forefoot studs on push-off were uniform in

shape with no dominant shift in the aspect ratio. The force data was representative of a typical heel-strike run; an initial first peak in the Fz direction represents the full body weight being transferred to the loading in the foot and the second peak occurring at push-off. The net negative impulse in the Fy direction indicates a slight deceleration. It is anticipated that during an acceleration movement, there will be a notable shift in the aspect ratio of the vector pattern occurring opposite to the direction of motion on the forefoot studs.

Figure 3.20 - Force data for heel-strike.

c) Kinematic analysis

The medial heel stud (Figure 3.21) on the right foot was tracked at 200 fps using the footage from the side-view high-speed camera. The pixel coordinates (w , v) were converted to x and y coordinates using the length of the adidas stripe for calibration (1 pixel = 0.41 ± 0.09 mm). The velocity of the heel stud was calculated using the finite differencing numerical method, the average for the 5 frames before impact was taken. The resultant velocity and the velocity vector were calculated from the u and v components.

The resultant velocity of the heel on impact was 2.6 ms^{-1} at an angle of 61° to the horizontal. This is similar in magnitude to the values collected by Kirk *et al.* (2007); $2.90 \pm 0.13 \text{ ms}^{-1}$. However, the velocity angle was significantly higher than Kirk *et al.* (2007); $16.81 \pm 1.86^\circ$. This could be attributed to the surface the participant was running on; the surface was perceived to be more susceptible to slipping than a natural grass surface which could lead to reluctance to load the foot.

Figure 3.21 - Tracking locations for the right foot during heel-strike.

3.4.9 Summary

The photoelastic method was suitable for obtaining dynamic photoelastic images but more work is required to deal with discolouration of the fringes and selection of a top reflective surface to provide more traction. Image processing methods were successfully used to identify the first fringe for tracking to produce the vector plots. Surface shear stresses in the material were also calculated, but further calibration of the material was required in order to validate the values.

During the course of the experimental testing, concerns were raised about the suitability of using the method for traction testing purposes:

Main concerns

- Players cannot perform realistic movements (due to surface and length of catwalk after force-plate);
- Difficult to distinguish out-of-plane shear contact pressure from the true shear stresses;
- Shear patterns around the stud on the photoelastic material is likely to be different to that expected in soil.

Possible solutions

- Use a stronger adhesive, such as spray rather than tape to fix the photoelastic material to the glass-plate. This will give a more stable surface and allow participants more confidence when running over the surface. An alternative reflective layer could also be used to give a higher friction surface. Reflective

foils and sprays containing micro-particles of silver are available and may be a better solution than the polyester layer. Achieving natural movements of a player in any laboratory environment is difficult; but the movements performed by a player can also be analysed against movements undertaken in real game situations to assess the realism of the study.

- A calibration method similar to the work by Nishizawa *et al.* (2006) and Arcan and Brull (1976) where the outer fringe diameter was related to the normal load could be used to distinguish the contact stresses from the direct shear stresses. Once calibrated, the force plate data at each time frame could be correlated to a fringe diameter for the vertical load. This would provide a masking area around each stud, outside of which the fringe patterns could be said to be due to direct shearing forces only.
- It is difficult to know the exact shear patterns that occur in soil. Models have been presented (Godwin and Spoor 1977 cited by Kirk 2008) using the empirical observations of soil failure patterns; crescent failure and lateral failure. However, it is difficult in any model to truly replicate the soil conditions; this is also true for computational modelling. The photoelastic work should be treated as another modelling tool that gives a suggestion of the shear stresses; it may be possible to verify the stresses by use of a computational simulation, but even this would have to be based upon assumptions.

The overall advantages and disadvantages of the system with respect to traction testing were identified:

Advantages	Disadvantages
<ul style="list-style-type: none"> • Realistic player movement; • Knowledge of influence of individual studs; • Produces identifiable visual images. 	<ul style="list-style-type: none"> • Non-realistic surface; • Complex analysis is timely and not suitable for large scale testing; • Use of players introduces subjectivity into results.

Table 3.15 - Advantages and disadvantages of photoelastic testing.

3.5 Modelling techniques

3.5.1 Introduction

Modelling the interaction between an outsole and surface is complex and a suitable model is required for both the surface and the shoe. Modelling the interaction of the shoe and surface can be thought of as a two stage processes, first impact and penetration and then translation along the surface. This section introduces two techniques attempting to mimic the impact phase (penetration) of studs. The associated problems and benefits of the techniques are acknowledged.

The vertical interaction between the stud and the ground can have a significant effect on the level of traction provided by the shoe. Stud penetration is fundamentally dependent on two conditions; the stiffness of the stud and the stiffness of the surface. Consequently, three types of outsoles exist; soft ground, firm ground and hard ground. The stud material and length depends on the target ground condition. Modelling the predicted penetration of the stud on different surfaces types can help determine the suitability of the stud. To investigate the potential of analytical and computational modelling techniques, an adidas prototype stud known as the “Smart Stud” was used. The Smart Stud was an exploratory new product design that began at adidas in 2005. The initial concept and design stage was carried out by Kirk (2005), with preliminary mechanical testing and evaluation undertaken by Koerger (2007) and Price (2008). The principal aim of the stud was to provide a suitable level of traction on any hardness of playing surface. This was to be done by deforming the stud by different amounts dependent on the hardness of the surface; ultimately, maximising the outsole to surface contact area.

Two different approaches were used to model the vertical interaction between the stud and the ground; analytical and computational modelling. Table 3.16 summarises the advantages and disadvantages of each modelling approach.

Analytical modelling	Computational modelling
<i>Advantages</i>	<i>Advantages</i>
Short run time	Uses correct stud geometry
Computationally efficient	Changes can be made to the stud geometry
Ground or stud stiffness is easily modified	Both simple and complex analysis of the model can be run
Control over underlying maths	Can use material parameters
<i>Disadvantages</i>	<i>Disadvantages</i>
Stud shape not considered	Requires material parameters for the studs
Many simplifications	Ground conditions are approximated
Need to tune damping coefficients	Lengthy process to accurately model the ground
	Stud is strain-rate sensitive requiring dynamic material analysis
	Computationally inefficient
	Long run time
	Limited control over underlying maths

Table 3.16 - Advantages and disadvantages of computational (FEA) and analytical modelling.

3.5.2 Aim and objectives

Aim

- To evaluate the effectiveness of analytical and computational modelling using an adidas prototype stud design.

Objectives

- To develop an analytical model to represent the impact of a single stud with two surfaces (soft and firm);
- To develop a computational finite element model using accurate stud geometry of the impact of the stud with soft ground.

3.5.3 Analytical modelling

The first method was an analytical (theoretical) process and involved modelling the stud and ground as mass spring systems. By modelling the stud and the ground as non-linear springs in series (Figure 3.22), the relative deformations of the ground and the stud were estimated. Newton's second law was applied to give the equation of motion for undamped free vibration:

$$F = m\ddot{y} = -ky \quad \text{Equation 3.7}$$

where k is the spring stiffness.

For the ground, two conditions were modelled analytically using non-linear stiffness spring equations; $k = f(y)$. Initially, experimental data from a hemispherical drop hammer test (mass 1.52 kg, kinetic energy 2.30 J), (Kirk 2008) was used to yield the force-displacement curves for both firm and soft ground conditions. Firm ground was natural turf tested in the UK in September; soft ground was created by adding 8 mm of water to the test area. Third order polynomial equations were fitted to the results, and the equations differentiated to produce stiffness curves; stiffness $k = dF / dy$. Both stiffness curves were non-linear and followed a quadratic function; $k = ay^2 + by + c$.

Figure 3.23 - Drop hammer soft and firm ground force deflection curves, red line indicates simulated stiffness curves.

A similar differential approach was used to estimate the spring constant of the stud. Instron® testing was used to produce the force-deflection curve for the deformation of the stud on a rigid metal plate. The Instron® test was displacement driven at 100 mm/s to a maximum compression of 4 mm. At present, one of the major drawbacks in using this data in conjunction with the drop-hammer results for the ground condition is that two different testing methods have been used to generate the initial force-displacement data. Again a polynomial equation was fitted to the curve; however, the curve was split into three regions and separate equations derived for each (Figure 3.24).

Figure 3.24 - Instron® testing of Smart stud, force deflection curve.

The resulting stiffness equations (Table 3.17) for the stud and the ground were used with the equation of motion to estimate the relative deformation of each part when under load.

Ground stiffness	Stud stiffness
	IF $y_s < 2.7$ $k_s = a_2 y^2 + b_2 y_s + c_2$
$= a_1 y^2 + b_1 y_g + c_1$	IF $2.7 < y_s < 3.8$ $k_s \sim C_3$
	IF $y_s > 3.8$ $k_s = a_3 y^2 + b_3 y_s + c_4$

Table 3.17 - Derived stiffness equations for ground and stud.

An iterative approach (Table 3.18) was used to solve the equation of motion for two non-linear stiffness terms.

	i	$i+1$
t	0	dt
y	0	$y_i + y_i dt$
y_i	0	$F_{j+i} \sim P_j$ $ku + y_u$
y_z	0	$F_{j+i} - F_j$ $k_{2i} + y_{2i}$
y	v	$y_i + y_{t+i} dt$
y	0	F_{i+i}/m
		$Z(y_i(i+i))$
*2	$f(y_{2i})$	$/(y_{2(i+i)})$
	i	i
k		$\wedge^{(i+1)} \quad \wedge^{(i+1)}$
F		$k_{ty} dt + F_t$

Table 3.18 - Iterative solution to equation of motion.

The input variables mass (m) and initial velocity (v) were initially the same as the drop-hammer tests; $m = 1.52$ kg and $v = 1.7$ ms⁻¹. Using the same iterative model, the boundary conditions were also modified to replicate a heel-strike during running. The boundary conditions were drawn from literature (Cavanagh *et al.* 1984); estimating that two studs would be in contact during a heel-strike and that the impact force would be evenly distributed between the two.

Figure 3.25 - Calculation of modified boundary conditions from literature results.

Figure 3.26 - Analytical modelling. Top: Drop hammer boundary conditions - Left: Soft ground; Right: Firm ground. Bottom: Realistic loading conditions - Left: Soft ground; Right: Firm ground.

Results (Figure 3.26) showed that on soft ground, the predicted deformation of the stud upon impact was 4 mm and the ground 7 mm. On firm ground, the deformations were more equal; 4.2 mm for the stud and 4.4 mm for the ground. From the plot of the total displacement, it can be seen that on the soft ground the major contributing factor was the ground; whereas on the firm ground, both the stud and the ground deformed at similar rates until the stud reached maximum deformation, after which the ground deformed at a quicker rate. This has been termed the equilibrium point; for firm ground this should ideally occur early on in the interaction enabling a greater surface area of stud to be in contact with the ground, thus maximising traction.

For the modified boundary conditions ($m = 19 \text{ kg}$ and $v = -0.7 \text{ ms}^{-1}$), results predicted that for a heel-strike on firm ground the stud would deform 4.4 mm and the ground 6.8 mm. This would leave a 0.8 mm sole-plate to ground clearance. For soft ground, the stud deformation was 4.2 mm and the ground was 10.7 mm suggesting there would be complete contact between the sole-plate and the ground surface.

A MATLAB™ Simulink model was developed using the iterative approach to produce an interactive model enabling various ground conditions and stud types to be interpolated and extrapolated from the existing experimental data. For example, the interaction between a stud and the ground condition "medium" (interpolated between soft and firm) could be estimated. This provides feedback into the expected stud deformation during vertical impact.

a) Summary analytical modelling

The analytical model was able to accurately simulate the deformation of the stud and the surface individually using the test load conditions. However, the combined stud and surface model needs further validation using appropriate loading conditions as the penetration between the stud and the ground can only be assumed from the relative deformation of each material; further experimental testing would be required to confirm the accuracy.

3.5.4 Finite element analysis

The alternative approach was to use finite element analysis (FEA) and computationally model the interaction. A quasi-static model of the stud was produced and validated against experimental results. The stud comprised of five individual parts; seal, structure, tip, rails and base unit. The CAD files for the stud were imported into Hypermesh and the individual parts meshed with a 0.4 mesh size, refined to 0.3 around more detailed areas to avoid over-closure issues. The parts were then exported into a FE modelling programme, Abaqus. First order tetrahedral C3D4 elements were used. The material properties used were isotropic, elastic approximations for four of the five materials and a hyperelastic, Mooney Rivlin model for the seal. A linear step amplitude of 5 mm in the vertical direction was used to model the deflection of the stud. This was representative of the mechanical Instron® test which was used to evaluate the accuracy of the model.

Results (Figure 3.27) indicated that the FE model accurately represented the stud when loading at the same rate of compression as the Instron® testing. However, the materials used in the stud are strain-rate dependent; without using dynamic material models, the FE simulation will not reflect this.

Figure 3.27 - Verification of model; force-displacement results for FE model and Instron® testing.

The interaction between the stud and the surface was modelled by simulating the soft ground conditions. The drop-hammer test used to provide the force-deflection curves in the analytical modelling approach was again used to define the ground characteristics. The soil was modelled as crushable foam with initial material parameters from soil test

data (Kirk 2008). The parameters were then tuned until the simulated drop-hammer force-deflection results matched those from experimentation (Figure 3.28).

Figure 3.28 - Force displacement curves for drop hammer experiment and FE simulation.

The quasi-static stud model and the crushable foam soft ground model were combined together (Table 3.19) to simulate the interaction.

Foam model	Stud model	Stud - foam interaction
Rigid analytical body mass 1.52 kg	Quasi-static	Quasi-static
Dynamic explicit step 0.005 s	Smooth amplitude loading 0.005 s	Smooth amplitude loading 0.005 s
Rigid analytical body velocity 1.74 ms ⁻¹	5 mm displacement of rigid bottom plate	5 mm displacement of stud Crushable foam replaces rigid bottom plate

Table 3.19 - Computational stud-foam model boundary conditions.

Figure 3.29 - Illustration of stud deformation on crushable foam surface.

Further experimental work is required to validate the combined stud and crushable foam model. However, when comparing the relative deformation of the stud and the ground

(Figure 3.30) it was seen that similar response curves were produced for both the FE model and the analytical approach.

Figure 3.30 - Relative deformation of stud on soft ground conditions.

b) Summary computational modelling

The limitations of the computation modelling were similar to those expressed in the analytical modelling. The components used in the model are only validated individually and under different loading conditions. The viscoelastic behaviour of the stud and particulate nature of the soil do not always lead to predictable loading conditions, further increasing the complexity of the required model.

3.6 Chapter summary

The results from mechanical traction testing revealed a number of findings; firstly the complexities of testing on natural turf conditions were highlighted, with results displaying a greater standard deviation in both hardness and traction readings. Secondly, when using a studded plate to replicate studded outsole configurations, the test did not produce similar results or shape of traction curve as the counterpart shoes. This was potentially due to the difference in orientation of the plate and shoe to the surface and the additional surcharge pressure from the increase in surface area of the plate. The final important finding was the change in traction ranking order when comparing the shoes at different displacements. Typically, the traction value at 50 mm is used for comparison, however concerns were raised that this was not representative of a typical movement and that traction values at lower displacements maybe more realistic.

Photoelasticity was used to identify the shear stresses between a surface and a studded outsole. Image processing techniques were successfully used to identify the individual fringes and show the change in position over time. Although these types of images had not been previously done before and they had potential to aid in stud shape design, the non-realistic surface restricted the use of the technique for traction analysis. Post processing methods were also time consuming and large sample size testing would not be possible using the current system. Although the system used participants to ensure the movements on the surface were representative, the surface may have caused participants to modify their movement style from that on natural turf. Full 3D kinematic analysis of the participant and the studded shoe on natural turf compared to the photoelastic surface would allow any differences in movements to be recognised.

The Simulink analytical model and the FE simulation provide a useful tool for estimating the likely vertical interaction between the stud and the ground during varying loading conditions. However, although individual sections of each model were verified against experimental data; namely drop hammer tests and Instron® force-displacement results, the complete interaction between the stud and the surface was not validated. The use of appropriate impact loads and velocity also needed to be validated. The computational models developed are also only the first stage towards developing a modelling tool that can be used to predict the traction between a prototype outsole and a range of surfaces.

The overall observation from the range of experimental methods investigated is that prior knowledge of realistic testing conditions would help to provide a more detailed and accurate analysis of the traction interaction; with the leading question raised from this study being:

What are the testing parameters that can be used to develop a testing protocol to produce repeatable results but also remain representative of actual football movements?

Chapter 4 aims to address this issue by developing a test methodology to identify realistic test parameters from player movements.

4 METHODOLOGY FOR MOTION CAPTURE OF STUDED FOOTWEAR

4.1 Introduction

In order to better understand the conditions needed for realistic testing, the behaviour of the shoe in contact with the surface needs to be examined. This can be achieved by capturing how the shoe interacts with the surface using 3D analysis.

A range of 3D motion capture techniques were outlined in Chapter 2. Stereo videogrammetry was highlighted as the most suitable method with its potential to be used both in the laboratory and outside on the field. It is also relatively easy to use and its results can be analysed directly, rather than relying on intermediate processing systems. Using a system that is self-developed enables it to be customised to suit the environment and applications it is designed for rather than having to make compromises with an existing motion capture system. A methodology review was carried out to ensure correct choices were made in terms of camera set-up, marker selection and marker tracking.

4.2 Aim and objectives

Aim

- To develop an experimental methodology to track the position of a shoe in 3D.

Objectives

- To develop a system that is:
 - Portable,
 - Of minimal intrusion to the players,
 - Suitable for use in both a laboratory and outside,
 - Able to achieve high marker re-projection accuracy.
- To convert the tracked image coordinates to 3D global coordinates.

4.3 Stereo videogrammetry

Stereo videogrammetry or stereo photogrammetry is the technique of using two or more cameras to reconstruct points on an image in a 3D coordinate system. This technique was chosen over the more commonly used commercial motion capture systems due to the ease of use and versatility that enables the technique to be applied in a wider range of scenarios.

4.3.1 Camera placement

Stereo videogrammetry requires the use of two cameras in order to triangulate the position of an object in 3D. The placement of the cameras can have significant effects on the error present in the 3D measurements. Error can be introduced into the system from poor image resolution or target occlusion (Chen and Davis 2000) and it is important that the cameras are placed such that effects of these are reduced. Considering only image resolution, Chen and Davis (2000) found that the optimal angle between the cameras was 90° , with acceptability between 40° and 140° . Camera angles of less than 40° or greater than 140° tended to greatly increase the uncertainty in the 3D measurement (Figure 4.1).

Figure 4.1 - Assessment of optimal camera angle (adapted from Chen & Davis 2000).

When target object occlusion was considered, the optimal camera placement was when they were orientated to be facing each other as this increased the likelihood that at least one camera was seeing the target object (Chen and Davis 2000). The markers used on the tracking shoe were positioned on one side of the shoe only so it was anticipated that an angle between cameras of 0° would in fact be optimal when considering marker occlusion. Static marker occlusion can be compensated for before filming by adjusting

the angle of the cameras in order to ensure that both cameras were able to see all the markers on the shoe during the likely range of motion of the foot. To assess this, two cameras were originally set at 90° focussing on a stationary shoe. The shoe was rotated and the number of markers visible in the left and right cameras was recorded. The angle between the cameras was then adjusted in order to find the optimal angle in which all five markers could be seen for the greatest range of rotation.

At an angle of 90° between cameras, the markers were occluded at shoe rotation angles of 30° . Reducing the angle to 70° enabled the markers to remain visible until 45° rotation of the shoe. Further reducing to 50° and the markers became excluded from the right camera at internal angles of over 60° . This indicated that an angle of 50 to 70° was suitable to reduce the influence of marker occlusion, yet still remain in the range for low error due to resolution.

4.3.2 Camera properties

The quality of the recorded images can directly influence the accuracy of the calibration and final data collection. Two high-speed Phantom v4.3 video cameras were used to form the basis of the stereo videogrammetry technique. It is important that the camera settings do not change between calibration and data collection and so an optimum setting to satisfy both requirements is needed. Camera settings that were adjusted were:

- Focus and zoom level
- Resolution
- Exposure

- Synchronisation
- Frame rate

a) Focus and zoom level

The size of both the squares on the checkerboard and the markers to be tracked affect the accuracy of the results. As such, an appropriate zoom level was needed to ensure they filled the maximum possible field of view of the cameras. However, due to the inherent variability in foot placement during participant data collection, a sizable volume was required. A volume 1.5 x 1.5 x 1 m was chosen for calibration. At this size, the markers occupied 1-2% of the volume size. Although small, they could easily be detected at this size and eccentricity effects were minimised.

The focus of the camera was important for calibration in order to successfully identify the intersection between grid squares. A poorly focussed image increased the re-projection error of the intersections.

b) Resolution

The image resolution influenced both the level of detail detectable in the image and the computational efficiency of the data capture. For player testing, it was important that the files could be quickly saved and the next data capture started to ensure the participants were not kept waiting. The time to save compared to reduction in image size was assessed and a resolution of 512 x 386 selected. The files took between 15 and 20 s to save and required approximately 85 MB for 400 frames.

c) Exposure

The exposure time or shutter speed controls the amount of light allowed to enter the captured image. For high-speed video work, a high exposure or long shutter speed can result in blurring in the captured image leading to error and inaccuracies in tracking the target markers. Ideally, the exposure needed to be as low as possible in order to improve the quality of the tracked markers. The contrast of the markers and the level of lighting on the test area therefore influenced the exposure setting. The test system was designed to work both in the laboratory under artificial lighting and outside with natural lighting. In the outside environment, additional lighting sources were avoided as it

increased the complexity of the testing system. In the laboratory, additional lighting was readily available and could be used to reduce the camera exposure. The level of exposure was also dependent on the frame rate. Testing both in the laboratory and outside suggested that an exposure time of 70 μ s at 1000 fps was suitable to avoid blurring, show the markers clearly and also show image background details that may be required in subsequent analysis.

Figure 4.3 - High exposure and low frame rates can lead to blurring of markers during high velocity movement. Left: when the shoe is stationary the image is not blurred; Centre: during push-off, shoe velocity increases and details become blurred; Right: original heel marker shape and blurred marker shape could lead to error in centroid location.

d) Synchronisation

The two cameras were synchronised so one camera triggered internally and the other externally. A remote manual trigger was used to activate the internal camera when the player entered the filming zone. Automated triggering options such as light-gates were considered but complications arose when capturing different player movements. In the laboratory, the cameras were triggered from a falling edge trigger on activation of a force-plate in the filming zone.

e) Frame rate and sampling theorem

The frame rate of the cameras determines how many images can be captured during the movement; it essentially sets the resolution for the smallest detectable movement. Using a set of data captured at 1000 Hz the Nyquist sampling theory was applied to assess the lowest frame rate that could be used. The Nyquist sampling rate theory states

that the process signal must be sampled at a frequency at least twice as high as the highest frequency present in the signal itself (Winter 2005). Expressed mathematically as:

$$f_s > 2f_c \quad \text{Equation 4.1}$$

where f_s is the sampling frequency and f_c is the highest frequency expressed in the sample (Olshausen 2000).

This concept is clearly illustrated in the sampling of a standard sine wave of frequency 1 Hz (Figure 4.4).

Figure 4.4 - Aliasing of original sine waveform by sampling lower than the Nyquist frequency. Top: Sampling at 2 Hz; Bottom: Sampling at 1.5 Hz. (Adapted from Olshausen 2000).

Sampling at 2 Hz or greater as indicated by the Nyquist theorem is sufficient to capture the signal, but sampling lower, at 1.5 Hz not only misses important information from the original signal, but also creates an entirely new waveform (Olshausen 2000).

This theory is easy to apply when sampling simple waveforms, but as the signal becomes more complex, identifying the Nyquist frequency also becomes more difficult. One solution is to consider the Fourier theory, in that any signal can be recreated from a series of sine and cosine waveforms of varying frequencies (Manal and Buchanan 2004). Fourier transformations of periodic signals can be used to identify the frequencies present in the signal. This approach can be easily applied using the fast Fourier transform (FFT) function in MATLAB™. However, real movement data as collected from the marker coordinates is non-cyclic and therefore does not satisfy the FFT conditions.

The principle that any signal can be comprised of sine and cosine waveforms gives rise to the Fourier series equation:

$$h(t) = a_0 + \sum [b_n \cos(2\pi r f n t) + c_n \cos(2\pi r / n t)] \quad \text{Equation 4.2}$$

This was applied to a set of coordinate data for the sprint movement in the z axis, sampled at 1000 Hz. A Fourier order of 6 was required to fit a curve with an R value of 0.98 to the raw data set. The minimum frequency was 4.7 Hz (1/t) and the maximum was 28.3 Hz (6/t). This suggests that the Nyquist sampling frequency needs to be greater than 60 Hz (2/6).

Figure 4.5 - Vertical displacement data sampling at 1000 Hz and 60 Hz.

Figure 4.5 illustrates the resulting data set from sampling at the Nyquist frequency of 60 Hz compared to 1000 Hz. The primary shape of the data curve is the same for both sampling rates suggesting that a sampling rate of 60 Hz may be sufficient for that example. However, slight differences are evident approaching 0.05 s; this is near the point of contact and hence it is important the detail is correct at this time. The Fourier

approach will also produce varying frequencies for each set of coordinate data (x, y and z) and to sample at different frequencies for each is not possible. Analysis of pilot study data shows that in the running direction, a displacement of 5 mm was seen over a time of 0.045 s. This indicates that in 0.009 s, the shoe moved 1 mm. Setting 1 mm as the smallest displacement resolution, this means a frequency of over 100 Hz is required.

In the past, the Nyquist sampling frequency was necessary to allow data to be collected at the lowest sampling rate possible but yet still maintain accurate results. This was due to the high computational and operational requirements of recording at higher sampling rates. With the increase in computer performances and the availability of high-speed video cameras, sampling up to or over rates of 1000 Hz is no longer considered unachievable. Filming at a rate higher than the Nyquist sampling rate also allows more advanced filtering techniques to be used without running the risk of masking important details in the data.

A sampling rate of 1000 Hz was chosen for the high-speed video capture with a minimum tracking sample rate of 200 Hz. Both are sufficiently above the Nyquist frequency and allow further filtering methods to be used to reduce the effect of noise.

4.3.3 Calibration

After reviewing potential calibration techniques, the planar (checkerboard) approach was chosen. This method has been shown to work well by Choppin (2008) in calibrating a large volume on a tennis court. The advantages of the checkerboard technique, as outlined in Chapter 2 were that a large volume can be defined and it is inexpensive and easy to carry out.

a) Image collection

In order to reduce the error in the calibration 15 or more images of the checkerboard are required (Zhang 1999). The checkerboard needs to occupy as much of the image as possible so that it is composed of more pixels and it is easier to resolve the intersections (Choppin 2008). Twenty images of the checkerboard were collected at a range of angles from both cameras, defining a volume approximately $1.5 \times 1.5 \times 1 \text{ m}$

Figure 4.6 - Mosaic of checkerboard images used to define the 3D test volume.

b) Camera parameters

The MATLAB™ camera calibration toolbox (Bougout 2010) was then used to extract the grid corners. For both the left and the right cameras, the four corners of the checkerboard are selected, and the individual grid squares are identified by interpolating along black or white interfaces.

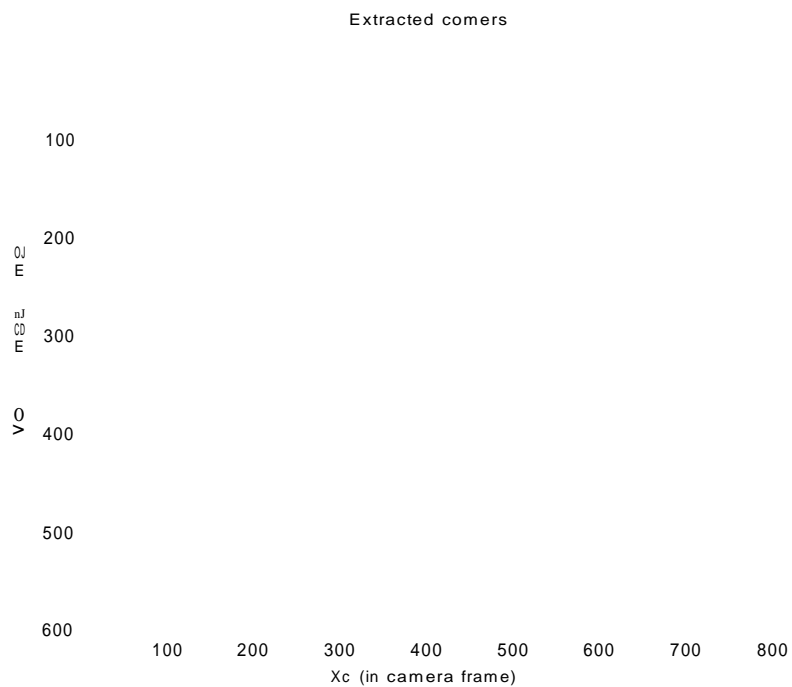


Figure 4.7 - Extraction of checkerboard calibration pattern using grid square intersections.

Distortion factors can be applied if the grid square corner location does not match the exact image. Once this process is repeated for each checkerboard image, the calibration parameters are generated. Calibration produces first a set of intrinsic parameters that relate the individual cameras to the calibrated volume, and secondly a set of extrinsic parameters that describe the relationship between the two cameras. The intrinsic parameters are (Bouget 2010):

- Focal length
- Principal point
- Skew coefficient
- Distortions

The extrinsic parameters are:

- Translation matrix
- Rotation matrix

The intrinsic parameters can be used to re-project the grid coordinates back onto the original checkerboard images. The re-projection error is calculated from the distance between the re-projected grid coordinate and the original point extracted. The error indicates the accuracy of the calibration and the detected intersection points (Choppin 2008). If the re-projection error appears to be large, further distortion factors can be applied to reduce the error.

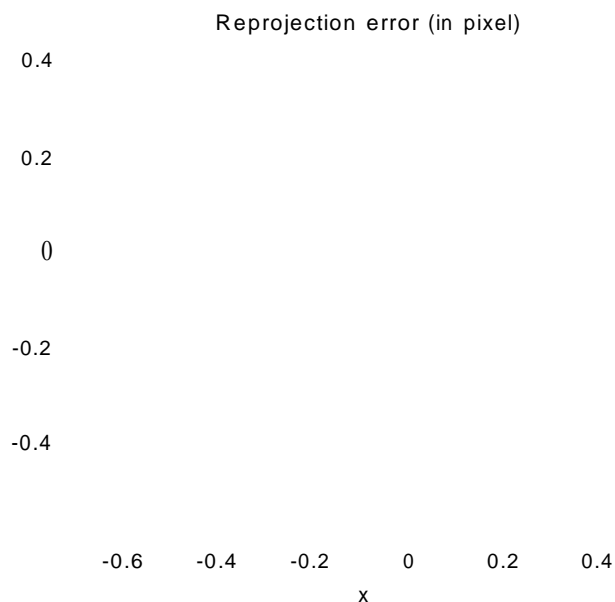


Figure 4.8 – Pixel re-projection error after calibration in a laboratory environment.

c) Origin definition and stereo-triangulation

The calibration procedure automatically produces a coordinate system relative to the left camera. However, for the purpose of analysing the position of the shoe in 3D, a global origin position is advantageous. To define the new axis system, the checkerboard was laid flat in the calibrated volume, with one edge aligned in the running direction of the participants. The edge at 90° was aligned away from the cameras. The third, vertical axis is created from the cross-product of the two axes.

Figure 4.9 - Global origin; participants run parallel to the y-axis, from right to left.

The camera parameters are then used with the global origin position to generate a transformation matrix used to convert image coordinates from the left and right views into 3D coordinates.

4.3.4 Summary

The methodology review indicated that just two Phantom v4.3 high-speed video cameras could be used to capture a 1.5 x 1.5 x 1 m volume on a natural turf football pitch and in a laboratory environment. The volume was sufficient enough to capture the inbound and outbound foot trajectory with compensation for differences in foot-strike location. To ensure the shoe was visible throughout a range of movements within the test volume, the optimal camera placement in terms of marker occlusion and 3D reconstruction errors was approximately 5 m perpendicularly away from the foot-strike zone at an angle of 70° to each other. The checkerboard technique can be successfully used to calibrate the cameras; using approximately 20 images of a checkerboard from the left and right cameras to determine both intrinsic and extrinsic camera parameters. Camera settings of 1000 fps for 0.6 s at a resolution of 512 x 382 pixels and a low exposure of 70 ps were chosen to reduce save time but allow high quality images to be recorded.

4.4 Marker selection

Copa Mundial football shoes (sizes UK 8-11) were used for testing. The Copa Mundial shoe has 6 moulded studs on the forefoot and 4 on the heel. The Copa Mundial was first released in 1979 but is still considered one of the most popular football shoe designs more than 30 years on. It is also considered a suitable stud configuration for natural turf on the firm to soft hardness borderline as anticipated at the time of testing (October, early season in UK).

Five markers were required on the left shoe. The markers were used to define two rigid bodies representing the rear-foot and forefoot sections of the shoe. The differences between markers on the shoe and on the foot has been well researched (Robertson *et al.* 2004) and marker placements have to be carefully considered so not to introduce unnecessary errors into the system. The natural pivot point of the foot is thought to be near the metatarsal-phalangeal joint and as such, a marker (P3) was placed as close to this location as possible. Two further markers were used to form the rear-foot section; one near the heel (P1) and one near the ankle (P2). Markers on the upper forefoot (P4) and toes (P5) were used to define the forefoot section.

Navicular

Forefoot

Rear-foot

Figure 4.10 - Foot anatomy and chosen shoe marker location.

Requirements for the system were that it could be used for outside testing; thus in potentially long grass environments. The selection of the type of marker used on the side of the shoe was important in order to have a marker that could be easily tracked (high visibility), have low re-projection error (centre easy to find) and was of minimum intrusion to the players. To minimise the image processing required to identify the marker from the background, the marker also needed to be high contrast. This also allowed a lower camera exposure to be used, improving the quality of the image and allowing a lower frame rate to be used, thus reducing memory requirements.

4.4.1 Spherical markers

Spherical reflective markers are typically used in biomechanical motion capture and are attached to the tracking object with adhesive tape. Due to their spherical shape they are easily tracked as the centre of the marker can always be found regardless of the orientation to the camera. However, after trialling the markers on the shoe, a number of limitations were found:

- They sit off the surface of the shoe which was intrusive to the players,
- They had difficulty staying attached during high velocity movements,
- They were easily knocked off or moved when the shoe was in contact with long grass or artificial fibres.

Figure 4.11 - Spherical reflective markers (Right: image from Quintic 2011).

4.4.2 LEDs

Electronic active markers were investigated to see if the gain from the high contrast marker outweighed the limitations of requiring an external power source. A strip of LEDs were tracked both in the laboratory and outside in natural light. The camera exposure was adjusted until only the LEDs were visible; reducing the image processing required to extract the markers from the background during the analysis stage.

An exposure of 40 ps was required both in the laboratory and outside compared to 70 ps required using retro-reflective markers. Despite the advantages gained from the high contrast markers, it was thought that the limitations were still too great to use this method. A power source would have to be worn on the top of the shoe and a series of wires would have to run to each LED. This would be very intrusive for the player and likely to impede their performance.

«

Figure 4.12 - LED markers in the laboratory and outside (exposure 40ps).

4.4.3 2D white circles

The third type of tracking marker tested was a simple 7 mm white circle painted onto the shoe using white oil based gloss paint. To increase the visibility of the markers a retro-reflective top coating (Glowtec 2011) was applied over the white paint. Retro-reflective surfaces return light directly to the source reducing the scattering effect (Figure 4.13).

Embedded glass microbeads

Reflective top coat

White gloss layer

Original surface

Figure 4.13 - Retro-reflective top coating (adapted from Glowtec 2011)

The advantages of these markers were that they were applied directly to the shoe and were not able to be displaced during movement of the shoe. The markers were also of negligible mass and as such, not intrusive to the players.

Most 3D marker systems use spherical markers as the centre of the marker is independent to the viewing direction. The problem of the 2D circular markers is that the marker appears elliptical in all viewing planes with the exception of an image plane that is directly parallel to the camera viewing plane. The ellipse centre differs from the centre of the projected circle depending on the angle and the displacement between the circle surface and the image plane; this effect is known as eccentricity (Bobrowitsch *et*

al. 2011). However, the eccentricity error is typically less than the image measurement accuracy (Ahn *et al.* 1999) for small circles. The pixel diameter of the markers in the image to be tracked is approximately 6 pixels in an image size of 512 x 384 pixels. The marker therefore comprises less than 1-2% of the total image size and as such, it is expected that the error from eccentricity will be negligible.

4.4.4 Summary

Despite the potential error due to eccentricity, a simple white painted circle was chosen over the spherical markers due to its robustness in natural turf, ease of tracking and lack of intrusion to the players. A retro-reflective coating was applied over the white circles to increase the contrast in directional light conditions. This specifically applied in the laboratory where additional light sources positioned behind the cameras could be used. This increased the contrast of the markers compared to the base shoe, and allowed a lower camera exposure to be used. Applying the markers directly to the surface of the shoe with a permanent paint eliminated the likelihood of the markers moving with respect to the surface of the shoe during testing, and also between testing during transportation of the equipment. The markers added negligible mass to the shoe, and as such were of minimum intrusion to the participants.

Figure 4.14 - Example test shoe with white retro-reflective markers.

4.5 Automated tracking methodology

A semi-automated tracking method was developed to allow fast and efficient acquisition of results. For each trial captured, approximately 400 frames required analysis. Obtaining the 3D coordinates from each marker thus required 2000 data points to be gathered per camera, per trial; the intention of the automated process was to speed up the data processing. Manual digitisation methods that have been previously used for similar applications (Choppin 2008) were available, but to manually select 2000 points for each trial would be very time consuming.

The MATLAB™ image processing toolbox was used to develop an algorithm that can automatically return the image coordinates of a selected marker. Three methods were trialled to assess their ease of use, accuracy and efficiency. For all methods, the first stage was to convert the video file created by the high-speed Phantom (v4.3) cameras to *.avi* files which could then be read into MATLAB™. The first and last frames to be analysed were then defined and the section of the video file between these frames converted to individual images. This allowed each time frame to be analysed sequentially using a *loop* function to move through the frames. The methods are described as follows.

a) Object labelling method

Each frame was converted to a binary black and white image with the threshold dependent on the light level of the image. Noise was removed using the *bwareaopen* function. This function removes objects from a binary image that have less than a chosen number of pixels. A successful resulting image contained only the five markers to be tracked (Figure 4.15).

The white objects (markers) remaining in the image were then labelled from left to right (*bwlabelV*). A separate tracking loop for each marker was defined, and the coordinates of the centroid (centre of mass) of the white object were returned as marker coordinates using the *regionprops* function.

The success of the tracking was highly dependent on the quality of the thresholding and amount of noise remaining in the converted image. If noise was detected as a valid object, the numbering order of the markers changed and the tracked trajectory shifted to the new object location. Using a predicted trajectory based on previous marker position,

it was possible to re-allocate the trajectory to the correct marker position, but this required user intervention and increased the complexity of the automated approach. The advantage of this system was that when successful, it was able to track all five markers simultaneously.

Figure 4.15 - Labelling and tracking of white objects after conversion to a binary image.

b) Object dilation method

Since the success of the object labelling method was highly dependent on the noise removal, modifications were made to the technique in order to improve the accuracy. The modified algorithm used the same steps as the object labelling method, using *bwlabel* to identify objects in the image. The object number of the marker to be tracked was selected and its coordinates returned. The selected marker was then dilated using *imdilate* with a square shaped structuring element (*streb*) (Figure 4.16).

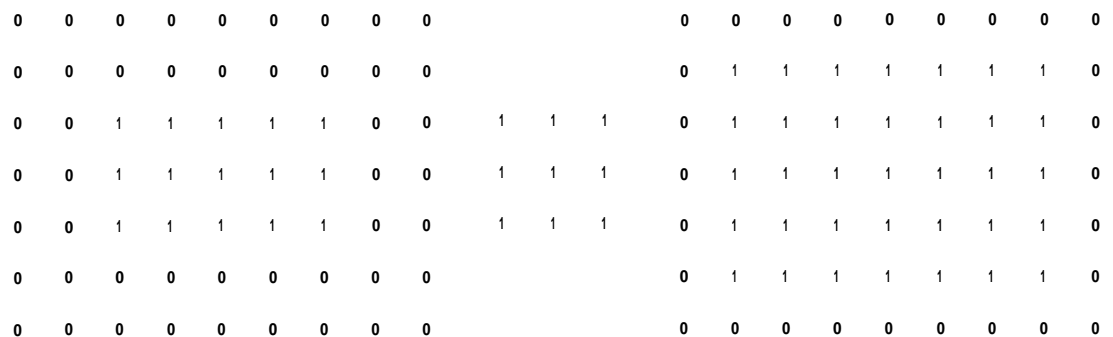


Figure 4.16 - Left: Original binary image of a rectangular object 5x3 pixels; Centre: Square structuring element; Right: Dilating image adds the structural element to each side of the object.

The dilated marker image was then inverted; for binary images the zero value pixels become value 1. The inversed dilated marker image was then subtracted from the next frame leaving the marker that was overlapped by the original marker (Figure 4.17).

Figure 4.17 - Marker dilation. From left to right: original marker; marker at next time step; dilated marker; inversed dilated marker; overlap of dilated and marker at next time step.

This method was computationally time consuming and success depended on the size of the marker after conversion to a binary image. If the marker decreased in size due to a change in viewing angle or if an external object was masking the marker, the dilated marker was also smaller. This reduced the likelihood of the markers overlaying in the next time frame.

c) Tracking window method

The third automated method used a tracking window to reduce the search area of the target marker. Rather than using the object labelling function to select the marker to be tracked, the method allowed the user to select in the first frame, the location of the marker. The pixel coordinates were then returned and an area 20 x 20 pixels was cropped about the centre of the marker (approximately four times marker diameter) in the next image frame. The cropped area was then converted to a binary image and noise removed. The white objects remaining in the cropped image were then labelled (Figure 4.18).

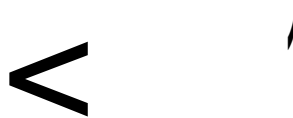


Figure 4.18 - Image cropped around selected marker coordinates and converted to a binary image; white objects are then labelled from left to right.

An *if loop* was then used to identify which object was the marker. If more than one object was identified, the difference between the centroid of the objects and the

predicted marker location was calculated. The predicted marker location was calculated using the previous marker position and the expected trajectory (Figure 4.19).

Figure 4.19 - Predicting marker location using the difference between the previous two marker coordinates.

The object with the minimum difference between the centroid and the predicted marker location was selected. If no objects were detected due to the marker not being visible in the image frame, the predicted marker location was used. The image coordinates of the new marker were then converted from the cropped coordinates to the original image coordinates. The process was then repeated about the new marker position until the end frame. The complete marker coordinates were displayed after the last frame allowing the final trajectory to be checked. At each stage an image was saved showing the cropped marker position for both the original and binary image. This allowed the user to check the algorithm was returning coordinates for the marker, and not noise.

The advantage of returning both the original and binary cropped image was that the threshold conversion to binary can be easily modified by the user if the lighting conditions change during filming. This is especially important when testing outside as changing light conditions due to cloud cover and time of day can affect the contrast of the markers. This could be overcome by changing the exposure of the cameras, but compensation during the post processing enables the capture method to remain simple. Figure 4.20 shows the differences in images during one day of testing outside; during sunny intervals, a binary threshold of 0.5 was used to identify the markers, whereas during times of cloud cover, a higher threshold of 0.08 was needed. Using a too high or too low threshold can affect the quality of the converted image and decrease the success of tracking the markers (Figure 4.21). The highest threshold used for the dark image to

identify the heel marker was 0.18. When this threshold was used on the sunlight images, the markers were not distinguishable from other white objects in the image.

Figure 4.20 - Differences in image brightness with changing light levels in outdoor testing.

J!

Figure 4.21 - Conversion to binary image. Top left: Dark, threshold 0.08; Top centre: Dark, threshold 0.12; Top right: Dark, threshold 0.18; Bottom left: Light, threshold 0.18; Bottom centre: Light, threshold 0.5; Bottom right: Light, threshold 0.6.

Using the predicted marker position during frames where no marker was detected worked well when the marker became obscured for short periods of time. An example of this is when the markers are being tracked outside on natural turf (Figure 4.22). Soft ground conditions and long grass can cause the markers nearer the sole of the shoe to become obscured when in contact with the ground. However, during this time little movement of the marker is expected enabling the predicted position to keep the search

area in the same location until the shoe moves vertically upwards and the marker becomes visible again.

Figure 4.22 - Using predicted method to estimate location of marker when obscured from view.

4.5.1 Summary

The chosen tracking algorithm used the self-windowing technique and appeared to be able to track the markers effectively (Figure 4.23). The advantages of using the tracking window were that there was a reduced search area to find the next marker location and it was not influenced by the level of noise outside the tracking window. The threshold level for conversion to a binary image allowed the markers to be identified in changeable light conditions without the need to adjust the exposure of the cameras.

Figure 4.23 - Visualisation of the results of tracking a marker from first frame to last selected frame.

4.6 Chapter summary

The methodology review revealed that two Phantom v4.3 filming at 1000 Hz with a resolution of 512 x 386 pixels was appropriate for capturing a 3D volume in both a laboratory and on a natural turf football pitch. Calibration by the checkerboard technique was selected as the most appropriate for the size of volume and ease of use.

The most suitable marker in terms of ease of tracking, robustness in natural turf and of minimal intrusion to the players was a white retro-reflective circle painted on the shoe. Due to the size of the marker in the test volume, potential errors due to eccentricity that do not occur with spherical markers are negligible.

The self-windowing technique was chosen as the tracking algorithm as the reduced search area made it computationally more efficient and accurate than other methods trialled.

The above method allows the shoe to be tracked and image coordinates of the chosen markers to be returned with minimal user involvement. The image coordinates can be converted to 3D coordinates of a global coordinate system predefined in the calibration procedure. The 3D coordinates are then suitable for post processing techniques in order to better understand the interaction of the studs with the surface.

Chapter 6 details the validation and error propagation of the proposed 3D measurement system.

5 METHODOLOGY FOR POST PROCESSING AND VISUALISATION OF RESULTS

5.1 Introduction

The analysis of 3D motions can generate large amounts of data; visual interpretation is often seen as the most appropriate way to convey the most important aspects of the results. Visual interpretation can range from a simple series of 2D images such as those created by Marey or Muybridge, to a more complex representation of the instantaneous helical screw axis (Keefe *et al.* 2008). When working with industrial sponsors visualisation of the results is important in order for the results from the study to be easily understood and interpreted. This has particular significance when transferring the results to other test forms such as mechanical traction testing or finite element simulations. This chapter outlines the post processing techniques used to analysis the 3D coordinate data obtained from stereo videogrammetry.

5.2 Aim and objectives

Aim

- To develop a range of post processing techniques to aid in the understanding of results collected.

Objectives

- To select a suitable filter reduce the influence of noise;
- To identify features on the shoe that are compatible with other systems and to determine their position from 3D data;
- To use the tracked 3D results to determine the orientation, velocity and acceleration of the shoe;
- To identify methods to describe the movement of the shoe.

5.3 Filtering techniques

Systematic and random errors in the extraction of the 3D coordinate position ultimately results in a level of noise present in the raw data. If the raw displacement data was used unprocessed to calculate the velocity and acceleration, at each calculation, the level of noise would be amplified and the true results would be difficult to identify (Figure 5.1). Consequently, before further analysis of the raw data occurs, it must be first smoothed to reduce the level of inherent noise.

Figure 5.1 - Noise is amplified at each stage of differentiation.

Filters can be used to reduce the effect of noise and smooth the data signal. Care has to be taken when choosing a filter as they can either reveal the true signal by suppressing noise or distort the true signal by altering or eliminating important information. The quality of the original signal also affects the success of the filter; if the data has not been captured at a high enough sample rate, the filter is more likely to have a negative affect and mask important information.

5.3.1 Digital filters

Filtering techniques typically fall into two classes:

- 1) Analogue filters
- 2) Digital filters

Analogue filters such as resistors and capacitors are applied to the input signal to filter it before it is recorded. Digital filters comprise of the mathematical procedures that are applied after data collections.

Digital filters primarily work by analysing the frequency spectrums of both the signal and the noise (Winter 2005). Figure 5.2 illustrates the overlap between the true signal and the noise. The role of a filter is to reject the frequencies of the noise, or to attenuate the frequency of the signal. The cut-off frequency of the filter is the overlap between the signal and the noise, f_c this is also the highest frequency seen in the signal, i.e. half the Nyquist sampling frequency.

A m p l i t u d e

Figure 5.2 - Hypothetical frequency spectrum of a waveform consisting of a desired signal and unwanted higher frequency noise (adapted from Winter 2005).

Digital filters were needed to smooth the results from the marker coordinate data before further processing to velocity or acceleration. Three types of filters were selected for analysis:

- 1) Moving averages
- 2) Butterworth
- 3) Polynomial

Their ease of use, accuracy, aliasing and suitability were assessed with the final filtering technique used on the collected 3D coordinate data. For each filter type, the z axis positional data from the marker P3 during a sprint movement was used for analysis. The data was collected using the semi-automated tracking method at 1000 Hz.

The residual fit of the smoothed data to the original data was calculated using:

$$R = \frac{\sum_{t=1}^n (X_t - \hat{X}_t)^2}{\sum_{t=1}^n X_t^2} \quad \text{Equation 5.1}$$

where X_t is the raw data at t 'th sample and \hat{X}_t is the filtered data at the t th sample (Winter 2005).

a) *Moving averages*

A moving average filter is one of the most basic digital filters and is often considered more of a smoothing tool than a digital filter. The advantages of the technique are that it is very easy to implement, especially on large data sets and it can be effective in smoothing noisy signals. However, the moving average filter is not able to distinguish signals from noise and by the nature of the technique, is strongly influenced by noisy signal values (Robertson *et al.* 2004).

A 5 point moving average is found by replacing each value X_t , with \bar{X}_t :

$$\bar{X}_t = \frac{1}{5} (X_{t-2} + X_{t-1} + X_t + X_{t+1} + X_{t+2}) \quad \text{Equation 5.2}$$

Using this technique there will be undefined results at the start and end of the data series. This can be compensated for by collecting a larger data set than required.

Figure 5.3 - Moving average filters applied to vertical displacement data (1000 Hz).

The moving average filter is easy to apply using Excel™ and can be applied directly to the raw collected data without any prior processing. Figure 5.3 shows the effect of the filter applied to the vertical displacement data collected at 1000 Hz. As the number of points used increases, the signal becomes smoother, but it begins to lose some of the details of its original shape. A 5-point moving average filter with this set of data smoothed the noise whilst maintaining the shape of the data curve.

b) Butterworth filter

The Butterworth filter is one of the most widely used filters in biomechanical studies and is essentially regarded as a sophisticated moving average filter. Butterworth filters can be low-pass, high-pass or band-pass filters. A low-pass filter attenuates high frequency noise but passes the low frequency signal unattenuated (Winter 2005). Conversely, a high-pass filter passes high frequencies unchanged but removes low frequency noise. A band-pass filter either passes or rejects frequencies between two cut-off frequency values.

The noise present in movement data is typically high frequency compared to the underlying signal; as such, a low-pass Butterworth filter is required. A low-pass Butterworth filter takes the format:

$$X'(nt) = a_0X(nt) + a_1X'(nt - t) + a_2X'(nt - 2t) + \dots + a_nX'(nt - nt) + b_1X'(nt - t) + b_2X'(nt - 2t)$$

Equation 5.3

where the filter coefficients a_0, \dots, b_2, \dots depend on the order of the filter, the sampling frequency, f_s and the cut-off frequency, f_c (Winter 2005). The order of the Butterworth filter also defines the sharpness or how much the signal is attenuated in the region of the cut-off frequency (Manal and Buchanan 2004).

The filter coefficients can be found from:

$$a, c = \tan(\hat{})$$

$$K_1 = \sqrt{2a/c}, \quad K_2 = a$$

$$a_0 \sim a_2 \sim \frac{1}{1 + f_1 + f_2} \quad c_1 = 2a,$$

$$b_1 = -2a_0 + K_3, \quad b_2 = 1 - 2a_0 - K_3$$

The cut-off frequency, f_c is sensitive to the input signal and although can be estimated from the Nyquist frequency, it is best found by assessing the residuals between the raw data and the Butterworth filter at varying cut-off frequencies.

Residual

Figure 5.4 - Plot of the residual between a filtered and an unfiltered signal as a function of the filter cut-off frequency (adapted from Winter 2005).

Butterworth filters cause phase distortion on the filtered data; the smoothed data shifts right. This could affect timings of events concluded from the data so is important that this is compensated for. One approach is to cancel the shift by back filtering in the opposite direction (Seeley 2009). This effectively converts a 2nd order filter into a 4th order, but does prevent the data from shifting.

A 2nd order Butterworth filter was applied to the raw data over a range of cut-off frequencies (250 Hz to 25 Hz). The cut-off frequency is typically less than one quarter of the sampling rate giving the highest cut-off frequency assessed as 250 Hz. The Butterworth filter was applied in MATLAB™ using the *butter* function.

```
[b, a] = butterfn, a)^
```

```
filt = filter(b, a, seriesl)
```

where n is the order of the low-pass filter and a/n is the normalised cut-off frequency ranging from 0 to 1 where 1 is the Nyquist frequency in n radians per sample. The Butterworth filter was then applied again in the opposite direction to reduce the shifting, but converting the filter to a 4th order.

Figure 5.5 - Left: Filtering using a Butterworth filter (85 Hz); Right: Residual value at varying cut-off frequencies.

The residual limit from the intercept on the vertical axis in Figure 5 is approximately 0.4. This is achieved by using a cut-off frequency of 85 Hz. This value is slightly higher than the Nyquist limit found from Fourier analysis but still well below half the sampling frequency.

The Butterworth filter is straightforward to apply using a MATLAB™ function but the selection of the cut-off frequency may vary depending on the data collected.

c) Polynomial filter

Polynomial filters are also known as curve fitting techniques and are based on the notion that any set of n data points can be fitted with a polynomial of degree $n - 1$ of the form:

$$Q(t) = CLt + d2^4 + 4^3 + 4^2 + 4^1 + C(t) \pm t$$

Equation 5.4

This polynomial will go through each of the n data points with no smoothing (Robertson *et al.* 2004).

Smoothing can be applied by removing the higher order terms, restricting the polynomial to lower frequency changes. The coefficients are typically found using a least-squares method. The *polyfit* function in the curve-fitting toolbox in MATLAB™ was used to assess the residuals of a series of polynomials ranging from 4th to 9th order. It is thought that data from movement analysis can be described by polynomials of the order 9th or lower (Robertson *et al.* 2004).

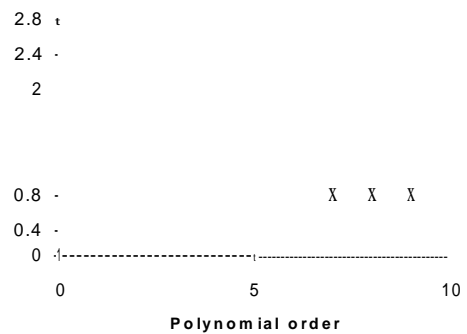


Figure 5.6 - Left: Filtering using a 7th order polynomial filter; Right: Effect of order on residual.

The 7th order polynomial provided the best fit in terms of smoothing but yet still maintaining the integral shape of the original data curve.

Polynomial fits have the advantage that the resulting equation can be used to calculate the derivative for velocity and then acceleration. However, it is unlikely that these would be very accurate (Seeley 2009). There is also little control on the amount of smoothing, especially if only one region of the graph is complex.

5.3.2 Summary

For the first stage of smoothing the raw displacement data, the Butterworth filter and moving average technique produce very similar results (Figure 5.7). The polynomial filter excessively smoothed the results and was the most complex to apply requiring a new polynomial function for each set of data. The moving average filter could easily be

applied to large data sets in Excel™ which was the primary source for data storage. The Butterworth filter required MATLAB™ and although was simple to apply, the coefficients of the filter were thought to be sensitive to the signal data. A different set of coefficients may be necessary for the x, y and z components of the displacement data. In light of this, the first choice for filtering the data was the 5-point moving average filter.

Figure 5.7 - Assessment of filtering techniques.

5.4 Transformation to stud coordinates

The marker locations on the side of the shoe were specifically chosen to aid in tracking and to ensure two distinct rigid bodies could be defined. However, it is difficult to accurately pin-point their position when moving to different shoe sizes. The stud positions on the outsole of the shoe scale accurately between shoe sizes, therefore the three studs on the outsole of the shoe were chosen as comparable locations. The studs selected (lateral posterior heel, S1, medial posterior heel, S2 and lateral metatarsal-phalangeal joint, S3) also form a right-angled triangle on the outsole of the shoe (Figure 5.8). By knowing the position of the studs during the movement, the number and location of the studs in contact with the surface can also be inferred. This is not possible from direct observation of the video footage as the studs are often obscured from view in the grass.



Figure 5.8 - Original marker position and chosen studs for transformation.

A transformation matrix consisting of a translation and three rotation matrices was used to convert the marker coordinates obtained from tracking to stud coordinates used for analysis. All 12 studs on the outsole can be located using the following method, although for ease of explanation, only the three target studs have been described.

The following method was used:

- 1) The coordinates of the markers and studs were measured by positioning the shoe on a flat surface with a coordinate system such that stud S1 was at the origin, S2 was on the x axis and S3 was on the y axis. This was termed the “neutral” position of the shoe. The respective coordinates were measured using digital callipers.
- 2) The transformation matrix required to translate marker P1 to the origin, rotate marker P3 to lie on the y axis and rotate marker P2 to lie on the xy plane from the neutral position was defined.
- 3) The transformation matrix was applied to the neutral stud coordinates to determine the transformed stud position.

Steps 1-3

Neutral marker and stud positions:

$$\begin{array}{l}
 P1x \\
 P1y \\
 P1z \\
 \dots 1 \dots
 \end{array}
 ; P2 = \begin{array}{l}
 P2x \\
 P2y \\
 P2z \\
 \dots 1 \dots
 \end{array}
 ; P3 = \begin{array}{l}
 P3x' \\
 P3y \\
 \vdots \\
 0z \\
 \vdots \\
 1
 \end{array}$$

$$S1 = \begin{bmatrix} S1x \\ S1y \\ S1z \\ 1 \end{bmatrix}; S2 = \begin{bmatrix} S2x \\ S2y \\ S2z \\ 1 \end{bmatrix}; S3 = \begin{bmatrix} S3x \\ S3y \\ S3z \\ 1 \end{bmatrix}$$

a) Translate to set P1 to origin:

$$T = \begin{bmatrix} 1 & 0 & 0 & -P1x \\ 0 & 1 & 0 & -P1y \\ 0 & 0 & 1 & -P1z \\ 0 & 0 & 0 & 1 \end{bmatrix}$$

$$P1a = T * P1; P2a = T * P2; P3a = T * P3$$

b) Rotate so P3 lies on the xy plane, rotation about x:

$$\alpha = \text{atan2}(P3az, P3ay)$$

$$R1 = \begin{bmatrix} 1 & 0 & 0 & 0 \\ 0 & \cos \alpha & \sin \alpha & 0 \\ 0 & -\sin \alpha & \cos \alpha & 0 \\ 0 & 0 & 0 & 1 \end{bmatrix}$$

$$P1b = R1 * P1a; P2b = R1 * P2a; P3b = R1 * P3a$$

c) Rotate so P3 lies on the yz plane (y axis), rotation about z:

$$\beta = \text{atan2}(P3bx, P3by)$$

$$R2 = \begin{bmatrix} \cos \beta & -\sin \beta & 0 & 0 \\ \sin \beta & \cos \beta & 0 & 0 \\ 0 & 0 & 1 & 0 \\ 0 & 0 & 0 & 1 \end{bmatrix}$$

$$P1c = R2 * P1b; P2c = R2 * P2b; P3c = R2 * P3b$$

d) Rotate so P2 is on the xy plane, rotation about y:

$$\gamma = \text{atan2}(P2cz, P2cx)$$

$$R2 = \begin{bmatrix} \cos \gamma & 0 & \sin \gamma & 0 \\ 0 & 1 & 0 & 0 \\ -\sin \gamma & 0 & \cos \gamma & 0 \\ 0 & 0 & 0 & 1 \end{bmatrix}$$

$$P1d = R3 * P1c; P2d = R3 * P2c; P3d = R3 * P3c$$

e) Transformation matrix:

$$M = R3 * R2 * R1 * T$$

f) Stud position after transformation:

$$SIM = M * SI ; S2M = M * S2 ; S3M = M * S3$$

- 4) A new transformation matrix was generated for each time step from the tracked marker coordinates.
- 5) The inverse transformation matrix was multiplied by the stud positions to determine the new stud coordinates.

Steps 4 and 5

g) Input coordinate data from tracking of markers for each time-step, i:

$$\begin{matrix} 'P1x(i)' & & P2x(i)' & & 'P3x(i)' \\ P1y(i) & ; P2\{i\} = & P2y(i) & ; P3\{i\} = & P3y(i) \\ P1z(i) & & P2z(i) & & P3z(i) \\ \cdot & 1 & \cdot & & \cdot & 1 & \cdot \end{matrix}$$

h) Repeat steps a-e as above for each time-step generating new transformation matrices:

$$M\{i\} = R3\{i\} * R2\{i\} * R1\{i\} * T\{i\}$$

i) Calculate new stud coordinates using the inverse transformation matrix and stud positions from step f:

$$S1_{new}\{i\} = \quad * SIM$$

$$S2_{new}\{i\} = M\{i\}^{-r} * S2M$$

$$S3_{new}\{i\} = \quad * S3M$$

A MATLAB™ program was written to run the above calculations using the marker coordinate data from the semi-automated tracking program. The program outputted the 3D stud coordinate data in Microsoft Excel™ format.

5.5 Calculation of shoe orientation, velocity and acceleration

The stud coordinates were then used to define the orientation, velocity and acceleration of the shoe.

5.5.1 Orientation

The orientation was defined using the local axis system on the shoe set by the three stud positions (Figure 5.8).

The three Euler angles (pitch, yaw and roll) were used to determine the orientation of the shoe at any given time step. Initially a direction cosine matrix was defined, this performs the coordinate transform of the stud vectors onto the x, y and z axes. As the studs formed a right-angled triangle, three rotations were required. The first rotated the shoe about the x axis through the pitch angle (α), second a rotation about the z axis through the yaw angle (P) and lastly, a rotation about the y axis through the roll angle (γ); giving order of rotation XZY.

Figure 5.9 - Defining Euler angles. Top left: Translating S1 to origin; Top right: Rotation about x axis = pitch; Bottom left: Rotation about z axis = yaw; Bottom right: Rotation about y axis = roll.

Two sets of Euler angles can be defined due to the fact there is always more than one sequence of rotations about the three principal axes that results in the same orientation of an object (Slabaugh 1999). In the case where the yaw angle is equal to 90° the angle of pitch and roll become linked. This phenomenon is known as Gimbal lock. In this

instance the foot has to be in either internal or external rotation of 90°. Although not unusual for this to occur in rotation movements in football, it was thought unlikely it would occur during sprinting, lateral side-cut or on the planted foot in kicking. A range of $-7t < \alpha, \gamma < 7t$ was also assumed. The calculation of Euler angles can therefore be simplified to obtaining just one solution (Slabaugh 1999).

The following steps were taken to generate the Direction Cosine Matrix:

Stud positions derived from marker coordinates

$$S_{new} = \begin{matrix} 'S1_{newx}' \\ S1_{newy} \\ S1_{newz} \\ \dots 1 \dots \end{matrix} ; S2_{new} = \begin{matrix} 'S2_{newx}' \\ S2_{newy} \\ S2_{newz} \\ \dots 1 \dots \end{matrix} ; S3_{new} = \begin{matrix} 'S3_{newx}' \\ S3_{newy} \\ S3_{newz} \\ \dots 1 \dots \end{matrix}$$

a) Translation to set S_{new} to the origin

$$T = \begin{matrix} "1 & 0 & 0 & -S1_{newx}' \\ " & 0 & 1 & 0 & -S1_{newy} \\ " & 0 & 0 & 1 & -S1_{newz} \\ " & 0 & 0 & 0 & 1 \end{matrix}$$

$$S1a = T * S1_{new} ; S2a = T * S2_{new} ; S3a = T * S3_{new}$$

b) Rotate so $S3$ lies on the xy plane, rotation about x (pitch):

$$a = \text{atan2}(S3_{az}, S3_{ay})$$

$$R_x = \begin{matrix} "1 & 0 & 0 & 0" \\ " & 0 & \cos a & \sin a & 0 \\ " & 0 & -\sin a & \cos a & 0 \\ " & 0 & 0 & 0 & 1 \end{matrix}$$

$$S1b = R_x * S1a ; S2b = R_x * S2a ; S3b = R_x * S3a$$

c) Rotate so $S3$ lies on the yz plane, rotation about z (yaw):

$$p = \text{atan2}(S3_{bx}, S3_{by})$$

$$R_z = \begin{matrix} " \cos \beta & -\sin \beta & 0 & 0" \\ " & \sin \beta & \cos \beta & 0 & 0 \\ " & 0 & 0 & 1 & 0 \\ " & 0 & 0 & 0 & 1 \end{matrix}$$

$$S1c = R_z * S1b ; S2c = R_z * S2b ; S3c = R_z * S3b$$

d) Rotate so $S2$ is on the xy plane, rotation about y (roll):

$$y = \text{atan}(S2cz/S2cx)$$

$$D \begin{pmatrix} \cos y & 0 & \sin y & 0 \\ 0 & \mathbf{1} & \mathbf{0} & 0 \\ -\sin y & 0 & \cos y & 0 \\ \mathbf{0} & 0 & 0 & 1 \end{pmatrix}$$

$$Sid = Ry * Sic ; S2d = Ry * S2c ; S3d = Ry * S3c$$

e) Euler angles

$$(pitch, yaw, roll) = (a, (3, y))$$

The pitch of the forefoot was calculated using the change in angle between marker P1 and marker P5 about marker P3. The yaw and roll were assumed to remain the same for the forefoot and rear-foot section.

The pitch, yaw and roll angles are non-commutative and must be applied in that order. In biomechanics terms, the pitch, yaw and roll can be thought of as:

+/- Pitch = Toe-up/Toe-down

+/- Yaw = Toe-in/Toe-out

+/- Roll = Inward roll/Outward roll

+ Yaw = Toe-in - Yaw = Toe-out

+ Pitch = Toe-up

- Pitch = To

- Roll = Inward

+ Roll = Outward

Figure 5.10 - Schematic showing the orientation of the shoe.

5.5.2 Velocity and acceleration

a) Velocity

Provided the displacement data has been suitably smoothed, the velocity and acceleration can be calculated using the central differencing technique. Differencing over just two consecutive time steps gives the velocity at a point in between time steps which can lead to errors when matching the timing of events from velocity and displacement data. The central differencing technique uses the preceding and following data values and as such has the advantage that the velocity is given at exact time steps using the average of the preceding and following values:

$$v_i = \frac{X_{i+1} - X_{i-1}}{2\Delta t} \quad \text{Equation 5.5}$$

This approach assumes the slope of the line connecting the two displacement values is the same as the slope of the tangent (Figure 5.11).

Figure 5.11 - Central differencing technique for calculating slope of curve at the Zth sample point (adapted from Winter 2005).

If there is still some degree of noise present in the smoothed displacement data, the central differencing technique can be applied over a greater range of time steps, essentially reducing the sampling frequency of the displacement data. For example, central differencing over five time steps gives:

$$v_i = \frac{X_{j+2} - X_{j-2}}{4\Delta t} \quad \text{Equation 5.6}$$

Central differencing calculations were applied to the raw and filtered displacement data to evaluate which approach yielded the best results in terms of accuracy and noise reduction. Both the 5-point moving average and Butterworth filters were evaluated.

Time (s)

Figure 5.12 - Calculating velocity using the central differencing approach from raw and filtered data (1000 Hz).

b) Acceleration

The acceleration values can either be calculated from the velocity or the displacement data:

$$a_{CLi} = \frac{V_{j+i} - v_{j-1}}{2\Delta t} \quad a_{CLi} = \frac{x_{i+1} - 2x_j + x_{i-1}}{\Delta t^2} \quad \text{Equation 5.7}$$

For our data set, the importance of obtaining the acceleration data is to be able to identify the peak acceleration which occurs on impact of the shoe with the surface. This was then used to normalise all the data sets from different trials and enables the contact time to be calculated. The acceleration values calculated using both the velocity and the displacement data were evaluated.

Time (s)

Figure 5.13 - Calculation of acceleration using the central differencing technique from displacement and velocity data.

The filtering and central differencing techniques were also demonstrated on a set of simulated data at 1000 Hz where artificial random noise was added. The simulated displacement data represents a quadratic curve, consequently giving predictable velocity and acceleration curves in the further analysis.

Figure 5.14 - Plot of displacement and velocity from simulated data.

The simulated signal (Figure 5.14) demonstrates that as the smoothing level increases, the signal better represents the quadratic signal before the addition of noise. However, if the original shape of the signal is unknown as in the coordinate data, it is important not to smooth the data too far for fear of missing important features.

5.5.3 Summary

The final velocity of the shoe was derived using the central differencing method over five time steps. The velocity data was then smoothed using a 5-point moving average. Acceleration was then found from the un-smoothed velocity data using a 3-point central differencing method. These techniques were found to best represent the underlying data without losing the original features of the data.

5.6 2D centre of rotation

During contact of the forefoot with the ground the foot can be seen to move in translation and rotation. When the movement of the shoe is purely in rotation, the location of the centre of rotation is of interest in defining the test parameters for mechanical traction testing. The rotation of the shoe plays an important role in limiting the injury to the knee, when the traction between the shoe and the surface is too high and the foot becomes locked in place and rotation instead occurs at the knee joint. On the other hand, if the traction is too low, the player will not get any purchase off the rotation movement and could slip. As such, an acceptance level was described by Kirk (2008) in which the resistive torque to rotation should lie.

Mechanical traction testing methods use the centre of the forefoot as the centre of rotation but the exact location of the rotation has not previously been accurately measured. Using the stud positional data obtained from 3D tracking of the shoe, an estimate of the centre of rotation over consecutive time steps can be found.

5.6.1 Reuleaux method

The approach to find the centre of rotation is based upon the Reuleaux method. The displacement of any rigid body in 2D using two points from P_i to P_i' and P_2 to P_2' can be carried out with a rotation of angle α about the pole of displacement, I (Eberharther and Ravani 2006) (Figure 5.15).

Figure 5.15 - Reuleaux method (adapted from Baroon and Ravani 2006).

The eight forefoot studs were assumed to form a rigid body lying on the x-y plane. Time steps at 100 Hz (0.01 s) were used to ensure there was sufficient rotation to evaluate. The Reuleaux method over one time step was applied using a MATLAB™ program in the following stages:

- 1) Determine the equation of the line connecting the original (S) and displaced (S') stud positions (repeat for all studs).
- 2) Calculate the equation of the perpendicular bisector between S and S'.
- 3) Find the intersection of all the perpendicular bisectors.
- 4) Calculate the standard deviation and 95% confidence interval and remove values outside the interval.
- 5) Determine the mean value of intersection points and new standard deviation.

The method produces a common point of rotation for all forefoot studs as well as an assessment on the accuracy using the standard deviation (Figure 5.16).

Figure 5.16 - Example of centre of rotation from stud positions between 0.03 and 0.10 s after foot-strike.

5.7 3D helical screw axis

One of the assumptions in calculating the 2D centre of rotation is that the displacement in the z-direction is assumed to be zero. This is obviously not always the case. During the sprint movement, the shoe is observed to both rotate and translate. This movement can be described using a helical screw analysis. The helical screw motion is a method of describing the motion of a rigid body from one point to another in 3D. The helical screw axis itself represents the line in space in which the rigid body simultaneously rotates around and translates along (Baroon and Ravani 2009). The motion can be defined by a rotation matrix and a translation vector, or by the position of the screw axis, the angle of rotation about the axis and the translation along the axis; also known as the screw parameters (Spoor and Veldpaus 1980).

Defining motion of a rigid body using the helical screw axis is an elegant solution for movements that undergo significant amounts of rotation and translation and where the motion path of the rigid body is not important. For this reason, the helical screw axis method is well suited to defining joint moments where certain degrees of freedom limit the motion of the body (Keefe *et al.* 2008). However, for describing the motion of the shoe during different movements, the helical screw axis parameters can vary significantly at each time-step. This is partially due to the anticipated small changes in displacement and rotation which can lead to errors in the helical screw parameter calculations (Robertson *et al.* 2004). An example helical screw axis was calculated for each movement (Appendix A.1).

The resultant helical screw axes allowed comparisons of each movement to be made, but were limited in terms of use for visualisation and aiding in understanding on the shoe motion due to the fact that the shoe does not actually follow the motion path of the helical screw axis. The parameters described by the helical screw axis as such do not always relate to a representation of shoe motion that is meaningful, but is more suited as a way to describe the new coordinate position of a rigid body with respect to its previous location. As such, full details on the calculation and application of the helical screw axis analysis on the movement data is given in Appendix A.1 but have not been included in the description of shoe-surface interactions for each movement (Chapter 9).

5.8 Chapter summary

The first stage of the post processing is to filter the results in order to reduce the amplification of noise when performing further calculations. The 5-point moving average filter was chosen as it was easy to apply and did not require prior calculation of filter coefficients.

Using the filtered marker positions, the coordinates are transformed to the stud positions. A transformation matrix consisting of a translation and three rotation matrices for each time step is derived and used with the shoe geometry to give the coordinates of the 12 outsole studs.

A similar rotation matrix approach is used to define the orientation of the shoe. The pitch, yaw and roll angles for the rigid rear-foot section of the shoe can be found at each time step representing the rotation about the x, z and y axis respectively.

The final velocity of the shoe was derived using the central differencing method over five time steps. The velocity data was then smoothed using a 5-point moving average. Acceleration was then found from the un-smoothed velocity data using a 3-point central differencing method.

The Reuleaux method was used to find the 2D centre of rotation of the shoe. The intersection of the perpendicular bisectors of the displacement of the studs from one time position to another gives rise to the centre of rotation. The approach can be used to show how the centre moves over time and where it is positioned in relation to the shoe.

The post processing methods outlined in this chapter will enable the results to be visualised and graphically represented. The next stage is to validate and quantify the accuracy and reliability of the proposed 3D measurement system and analysis tools.

6 VALIDATION AND ERROR ANALYSIS

6.1 Introduction

The quality of collected data can be assessed by considering its validity and reliability; essentially how accurate are the results and how consistent is the measurement method. The dartboard analogy (Figure 6.1) demonstrates how data can be consistent but not accurate, or accurate but not consistent and as such, the importance of being able to quantify both aspects of quality.

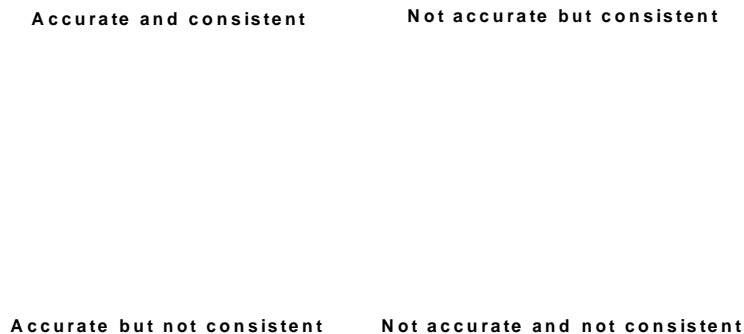


Figure 6.1 - Quality of data depends on both the accuracy and consistency (adapted from Maiwald 2011).

Systematic measurement errors introduced into the system affect the accuracy of the results whilst random errors influence the reliability. Identification of these errors can help in increasing the quality of the data.

The validity or accuracy of the measurement method can be assessed by comparing the results collected to those obtained using a 'gold standard' technique. The reliability can be evaluated by investigating how repeatable each stage of the method is. The magnitude of the error and how it propagates in further calculations is also considered.

6.2 Aim and objectives

Aim

- To assess the validity and reliability of the proposed 3D measurement system.

Objectives

- To identify potential sources of error;
- Assess the error involved in tracking the markers;
- Quantify the reliability error;
- Validate the method by comparison to a 'gold standard' technique;
- Quantify the effect of error propagation in further processing steps;
- Identify sources of random error and suggest ways to minimise their effect.

6.3 Reliability

6.3.1 Sources of error in determining marker location and stud position

The error in determining the position, angle and velocity of the studs on the shoe were thought to arise from the following sources:

	Source	Method	Systematic error	Random error
Data collection	Tracking of markers in left and right images.	Camera set-up and calibration; MATLAB™; Check3D.	Calibration; Camera position; Marker eccentricity; Marker tracking (in pixels).	Change of shoe shape and thus marker location due to foot distortion; Changes in camera position post calibration;
	Conversion to global 3D coordinates.	MATLAB™.	Propagation to position error (mm)	Incorrect shoe size used in
Data processing	Transform to stud positions.	MATLAB™; Manual measuring of studs.	Error in measurement of stud position relative to markers; Error propagated from marker position.	transformation of markers to studs; Out of plane movement of participant.
	Calculation of Euler angles and velocities.	MATLAB™.	Propagation from previous steps	

Table 6.1 - Sources of error.

6.3.2 Error in tracking of markers

The sources of errors in tracking the markers arose from error in the calibration of the cameras, eccentricity error and error in the determination of marker location (either manually or automated). Choppin (2008) assessed the error in the software calibration point selection to be ± 0.1 mm.

The human error in manual tracking was obtained from tracking two points on the shoe over 26 frames and repeating five times for both the left and right camera images. The standard deviation between the five repeats before stereo-triangulation was averaged to give the mean standard deviation in pixels.

	U-Coordinate	V-Coordinate	Mean
Mean standard deviation	0.33	0.32	
Maximum standard deviation	0.71	0.62	0.32 pixels
Minimum standard deviation	0.00	0.00	

Table 6.2 - Assessment of error in manual tracking.

The overall error due to human marker tracking was concluded to be ± 0.5 pixels.

A similar approach was used for the semi-automated tracking method using the same images; two markers were tracked over 26 frames and repeated five times.

	U-Coordinate	V-Coordinate	Mean
Mean standard deviation	0.26	0.23	
Maximum standard deviation	0.66	0.61	0.24 pixels
Minimum standard deviation	0.16	0.14	

Table 6.3 - Assessment of error in semi-automated tracking.

The overall error due to semi-automated marker tracking was concluded to be ± 0.25 pixels.

The error in human marker tracking was higher than in semi-automated tracking. The only error introduced in the semi-automated tracking was from the initial selection of the starting marker.

a) *Propagation of error after stereo-triangulation*

The stereo-triangulation values used in the conversion to 3D global coordinates are dependent upon the calibration of the two cameras, and thus their position relative to the shoe. The location of the cameras relative to the filming area was approximately the same throughout all tests, although some variability is inevitable due to the non-permanent set-up.

The sets of marker image coordinates were converted to 3D global coordinates using the stereo-triangulation method. The manual tracking method used the Check3D program; this had an inbuilt conversion to 3D global coordinates using the data obtained from calibration. The same approach was used in MATLAB™ to convert the semi-automated marker image coordinates to 3D global coordinates. The standard deviation of the *x*, *y* and *z*-coordinate data was then analysed to give the propagated error in mm.

	X-Coordinate	Y-Coordinate	Z-Coordinate	Mean
Mean standard deviation	0.89	0.48	0.42	
Maximum standard deviation	1.49	0.89	0.80	0.60 mm
Minimum standard deviation	0.33	0.11	0.14	

Table 6.4 - Assessment of errors in manual tracking after stereo-triangulation.

The ± 0.5 pixel error in manual tracking propagated to an error of ± 0.6 mm. The error was greatest in the *x*-direction. This was to be expected as it is the axis heading away from the camera and is the most difficult to obtain in a 3D system.

	X-Coordinate	Y-Coordinate	Z-Coordinate	Mean
Mean standard deviation	0.72	0.36	0.29	
Maximum standard deviation	1.40	0.81	0.49	0.46 mm
Minimum standard deviation	0.38	0.23	0.13	

Table 6.5 - Assessment of error in semi-automated tracking after stereo-triangulation.

The ± 0.25 pixel error in semi-automated tracking propagated to an error of ± 0.5 mm.

b) *Comparison between manual and automated tracking*

The 3D global coordinates of the two marker points from each of the 5 repeats were averaged for each frame for both the manual and semi-automated tracking results. The averages from the manual and semi-automated methods were then compared. The mean absolute difference between the manual and semi-automated method was 3.3 mm.

A t-test was used to determine whether this difference was significant.

	Mean	<i>SD</i>	SE _m	<i>sed</i>	<i>t</i>	<i>P</i>
Manual	-152.04	0.595	0.266	0.344	10.8	<.01
Automated	-154.36	0.242	0.204			

Table 6.6 - Significance of difference between manual and semi-automated tracking using a t-test (mean values are used from 5 repeats of 2 markers over 26 frames).

The r-test indicated that the difference between the manual and the semi-automated tracking method was significant at $p < .01$.

This suggests that results obtained from tracking manually cannot be directly compared to those tracked using the semi-automated method, as any differences that arise may be due to the change in method. However, the significance of a 3 mm difference in terms of a percentage of each coordinate depends on the position of the origin. Setting marker 1 to be 1 m away from the origin would suggest a 3 mm difference was equivalent to a 0.3% change between the manual and the semi-automated method. Alternatively, setting marker 1 to be 1 mm away from the origin yields a 300% change between the two methods. However, the important feature being measured from the results is not always where the marker is in space, but how far it moves between frames. The movement between frames is used to calculate the velocity of the marker as well as determine if there is any slippage during the ground contact phase of the movement.

To assess the accuracy in the movement of the marker, the origin (0, 0, 0) was set to the marker position in the first frame of each result set. The difference between the marker positions at each frame was then calculated.

The absolute mean difference between the manual and the semi-automated tracking method after resetting the origin was reduced to 1.2 mm. Again a r-test was used to assess the significance of this difference.

	Mean	SD	SEM	SED	t	P
Manual	-2.09	0.85	0.38	0.54	1.97	<.10
Automated	-2.83	0.83	0.37			

Table 6.7 - Significance of difference between manual and semi-automated tracking methods using results set to the origin.

The f-test indicated that the difference was significant at the $p = .10$ level. Taking all coordinate results into consideration rather than using the average of each marker at each frame, an co test was used to determine the importance of the mean difference and the f-test result. This test is often used when the number of results is large and the standard deviation for each method is small and statistical significance is found using the f-test when the means are close in value.

The $co2$ value was 0.16. This indicates that 16% of the differences between the manual and the semi-automated method is due to the change in method, whilst 84% is due to unidentified factors and error of measurement.

The comparative analysis of results from the manual and semi-automated tracking methods suggests that after stereo-triangulation, differences do occur between the two methods, but their statistical significance is small ($p < .10$). To minimise the chances that the differences between data sets are due to the tracking method rather than other effects, comparative result sets will either be tracked using the semi-automated or the manual method exclusively. In the situation where comparisons need to be made between two sets of data tracked using different methods, before a f-test is used to analyse the differences between results, the mean absolute difference after the origin is reset must be greater than 1.5 mm. This control value has been chosen from the mean absolute difference between the manual and the semi-automated method assessed above.

6.3.3 Repeatability study

To assess the error arising from changes in test conditions, camera position and participant repeatability, a reliability study was carried out over two separate days. The same participant was used for both tests wearing Team Mundial shoes with three markers defining the rear-foot section. The participant performed 5 sprint movements in the laboratory on a carpet surface with artificial turf on the test area. The same

cameras were used for testing and although the camera position was approximately the same, they were not constant between the two test days. This was deliberate to assess the reliability of changes in camera set-up which will occur when testing in different locations. The tests were performed at 10 am on both days and the participant was given a 10 min warm-up period before testing.

The velocity of the marker P3 (metatarsal-phalangeal) in the z direction at foot-strike was used as a comparison variable. Foot-strike was defined as the point where the acceleration of marker P3 was at a maximum (Chapter 8). Marker P3 was used as the participant landed forefoot first in all trials. A t -test was used to compare the two sets of data (Table 6.8). Results from the t -test indicated that there was no significant difference between the impact velocity at the $p = .10$ level. The absolute difference between the two mean values was 0.18 m/s.

	Mean	<i>SD</i>	<i>SE_m</i>	<i>sed</i>	<i>t</i>	<i>P</i>
Day 1	-0.76	0.19	0.087	0.098	1.89	>.10
Day 2	-0.58	0.08	0.047			

Table 6.8- Assessment of reliability using t -tests (velocity in m/s¹).

The slight difference that did occur may be due to the differences in the camera set up, or the participant was more accustomed to the technique required – indicating that more repeats or a longer warm-up period is required. Changes in participant fitness, climatic conditions and camera set-up can all lead to differences arising between test results when staged over two separate days. However, results indicated that the differences were not statistically significant ($p > .10$).

6.4 Validation

6.4.1 3D marker position

To validate the 3D global coordinates produced from stereo-triangulation after tracking, three markers were initially tracked using the Motion Analysis Capture (MAC) system. The MAC system is considered to be the ‘gold standard’ in marker tracking in biomechanical analysis. A whirly-gig device was used to move three markers about the image frame with a constant rotational velocity. The reflective markers were tracked with the MAC system using infrared cameras. The same markers were tracked using the

semi-automated method with the same global coordinate system. The coordinates provided by the MAC system were then compared to the results obtained from the semi-automated tracking method after stereo-triangulation.

Figure 6.2 - Three markers were tracked using the MAC system and semi-automated method.

One of the markers tracked was stationary throughout the movement. The consistency of the returned coordinates of this marker was evaluated over 500 frames for both the MAC system and semi-automated tracking. The mean marker position and standard deviation was obtained along with the difference in means (Table 6.9).

	X(mm)	Y (mm)	Z (mm)
MAC	-11.79 ±0.464	-11.61 ±0.352	333.87 ±0.082
Automated	-12.10 ±0.568	-9.74 ± 0.793	335.38 ±0.402
Difference in means	0.31	1.87	1.51

Table 6.9 - Mean and standard deviation of stationary marker.

The semi-automated tracking method displayed slightly higher deviation over the 500 measurements (maximum standard deviation of 0.793 mm compared to 0.464 mm) but the difference in mean values between both measured values was less than 2 mm for all three coordinate directions.

Both of the other markers moved around the centre of the object with a circular trajectory of fixed radius and fixed vertical displacement. The variation in the vertical displacement of the markers measured with both the MAC system and the semi-automated method was calculated.

	MAC	Automated	Difference
Mean (mm)	334.93	336.05	1.12
Standard deviation (mm)	2.23	1.49	

Table 6.10 - Variation in vertical displacement of moving marker.

Table 6.10 shows that the absolute difference between means was 1.12 mm but the standard deviation in the vertical displacement measured by the MAC system was greater than that obtained from the semi-automated tracking method.

The circular trajectory of the moving marker was assessed by measuring the radius of the trajectory and circle roundness metric. The tracked horizontal coordinates were used to find the circumference of the trajectory and area bound within it. The roundness metric was calculated using the following equation:

$$\text{Metric} = \frac{47rA}{C} \quad \text{Equation 6.1}$$

where A is the area and was calculated using the MATLAB™ function *polyarea* and C is the circumference and was found using the sum of the difference between adjacent values. The radius was then found from the calculated value of the area.

	MAC	Automated
Roundness metric	0.997	0.991
Radius (mm)	398.72	397.16

Table 6.11 - Roundness metrics of marker trajectory.

Both roundness and radius values were less than 1% away from their true roundness values; the semi-automated value was slightly further from the true value than the MAC system (difference of 1.5 mm).

Figure 6.3 - Horizontal trajectory of marker tracked using the MAC system and semi-automated method.

6.4.2 Stud position

The matrix transformation from marker location to stud position was validated by using an image in which the three reference studs were visible as were the three rear-foot markers. The 3D coordinates of the studs were obtained from manual selection of the studs using Check3D and compared to the predicted coordinates from matrix transformation.

	S1x	S1y	S1z	S3x	S3y	S3z
Measured	-301.6	325.3	36.4	-337.5	313.7	13.0
Predicted	-303.7	321.9	36.8	-335.2	313.9	15.3
Difference	2.1	3.4	0.4	2.3	0.2	2.3

Table 6.12 - Difference between measured and predicted stud position (mm).

The average absolute difference between the measured and predicted stud position was 1.8 mm.

6.5 Propagation of errors

6.5.1 Propagation of errors to stud position

In the first stage of transforming the marker coordinates to stud coordinates, the stud position relative to the marker position was measured when the shoe was in a neutral position. Stud SI (lateral rear heel) was positioned at the origin of a measuring grid. Stud S2 (medial rear heel) was positioned on the x-axis and stud S3 (lateral metatarsal-phalangeal) on the y-axis. The remaining studs and markers were measured relative to the measuring grid. The measurements were considered accurate to ± 1 mm.

The neutral stud positions were then used to determine the stud position after the initial matrix transformation. These values were used with the raw 3D global coordinate marker data to calculate the position of the studs at each time-step.

The sources of error in this step of the process occurs firstly from the measurements of the neutral stud positions (± 1 mm) and secondly from the marker tracking (± 0.5 mm).

Using the Taylor (1997) method for propagation of errors, the combined effect of the errors arising from the measurements of the stud location and uncertainties in marker tracking lead to a maximum error of ± 2.2 mm. If a more conservative assessment of the measurement error of 2 mm is used, the maximum propagated error is 3.3 mm.

Using the Taylor (1997) method, the resulting propagated error is dependent upon the initial global coordinates of the tracked markers and as such will vary for each time-step. The closer the marker is to the set origin, the smaller the propagated error. The maximum propagated error of ± 2.2 mm was calculated when the marker P1 was at a distance of 250 mm from the origin in all dimensions. This was considered to be the furthest from the origin that it would be necessary to track a marker given that the origin is reset to the point where the marker first contacts the ground. The propagated error at the origin was ± 1.6 mm.

6.5.2 Propagation of errors to Euler angle and velocity calculations

Using the Taylor (1997) method for propagation of errors arising from the errors in stud transformation; the systematic errors in the angle and velocities were calculated to be:

$$\text{Stud position} = \pm 2.2 \text{ mm}$$

- Pitch = $\pm 2.7^\circ$
- Yaw = $\pm 1.5^\circ$
- Roll = $\pm 3.8^\circ$
- Velocity = $\pm 0.3 \text{ ms}^{-1}$

These errors were calculated for the upper limit of the results expected. Again, given the nature of the Taylor (1997) method, the closer the stud to the origin, the closer the angle to 0° or velocity to 0 ms^{-1} , the smaller the propagated error becomes. The above were calculated for the most extreme scenario at angles of 60° and a velocity of 5 ms^{-1} . Using a more conservative velocity of 2 ms^{-1} the propagated error is only 0.05 ms^{-1} (approximately 0.25%). Similarly, selecting only an initial pitch angle of 30° reduces the error to only $\pm 1.3^\circ$.

6.6 Random errors

Random errors in the results were thought to arise from:

- Change of shoe shape and thus marker location due to foot distortion.
- Changes in camera position post calibration.
- Incorrect shoe size used in transformation of markers to stud position.
- Out of plane movement of participant.

The error due to an out of plane movement in the sprint was reduced by advising participants to run alongside a set of cones parallel to the global axis. Results were rejected from further analysis if it was noticeable that the participant was moving out of plane. The error due to out of plane movement in a 3D camera system is not as significant as in a 2D system. It was further reduced by ensuring the two cameras were at an angle of approximately 90° to each other. The effect of a change in camera position was minimised by recalibrating midway through testing. The cameras were also fenced off with warning cones to reduce the risk of them being accidentally knocked.

The three markers on the side of the shoe were assumed to form a rigid body. However, as with any marker system on the human body, deformation between markers is expected. To assess the degree of deformation, the vector length between marker P1 and P2 and marker P1 and P3 was calculated over a series of 230 frames. The standard deviation between the vector lengths was 1.1 mm. This was considered small when taking into account the systematic error of $\pm 0.5 \text{ mm}$ in 3D global coordinate data.

However, if due to deformation the marker positions changed by 2 mm, this would propagate to an error in the stud position of 6 mm. The standard deviation of the vector lengths over each result set will therefore be used as a control to limit the effect of shoe deformation. If the standard deviation is greater than $\pm 2\text{mm}$, the data set will be excluded from further analysis.

The use of the wrong shoe size in the stud transformation calculations was minimised by creating individual MATLAB™ files for each shoe size. The vector distances between the studs in each result set were also compared to those of the shoe size worn by the participant. If there was a significant difference, the transformation was carried out again.

6.7 Chapter summary

The 3D measurement system and tracking algorithm were assessed in terms of reliability and validity. The reliability was an assessment of the consistency of the results; the semi-automated tracking method (± 0.24 pixels) was shown to be more consistent than the previously used manual tracking method (± 0.32 pixels). The repeatability was assessed by performing the same trial with the same participant on two separate days. A Z-test was used to compare the vertical velocity of the P3 marker from each trial. Results from the Z-test indicated that there was no significant difference between the impact velocity at the $p = .10$ level. The method was validated by comparison with the MAC system. The difference in means of a tracked object was less than 2 mm although the MAC system displayed a slightly lower standard deviation.

The errors identified in the reliability and validity analysis were propagated using the Taylor (1997) method to give a stud position error of ± 2.2 mm for the most extreme scenario. Random errors were reduced by careful selection of testing equipment and using known distances between markers or studs as a verification check.

The 3D measurement system was concluded to have suitable levels of accuracy and reliability compared to a commercial system allowing test data on the shoe-surface interface to be collected. Two data collection approaches were identified; firstly a small controlled study based in the laboratory and secondly a larger participant group on a natural turf surface. The next chapter details the testing protocol used for both data collection studies.

7 TESTING PROTOCOL

7.1 Introduction

Two data collection studies were identified to demonstrate the use of the 3D measurement system in analysing the shoe-surface interaction within different environments. The first study was a controlled test using a single participant in a laboratory environment. The second study expanded the data set using a cohort of eight youth team players from Doncaster Rovers FC. The reasoning behind the two data collection studies were:

1. Laboratory study: Using a single participant allowed the testing to be more controlled without the organisation and time pressure of working with a larger group. More time could be allocated to testing to ensure that every trial collected met the testing criteria. The surface used was not representative of a natural playing surface but was consistent between tests. The size of the laboratory restricted the movements that could be performed without impedance but had the advantage that the climate and light conditions were constant. The laboratory also had the benefit that a force-plate could be used to allow simultaneous collection of visual 3D information and force data. One of the aims of the laboratory study was to use the force data information to identify events within the movements that could then be determined using the visual information when the force-plate was not available.
2. Doncaster Rovers study: A larger group size potentially led to more variability within the results but allowed a wider range of player types to be studied. The natural surface was representative of a match and training situations but was inherently more variable and difficult to characterise. Testing outside provided a larger environment for the players to warm-up while testing was taking place. No confinement on space also gave more freedom on the movements analysed and provided a natural environment for the participants to minimise the influence of performance changes when being observed. A larger group size placed more pressure on the time allocated to each player for data collection in order for all results to be collected in one session to minimise the impedance to the players' schedules. The sample size was not large enough to represent the

population, but provided an indication on the type of data that can be collected and analysed in the future.

Full institutional ethics approval from Sheffield Hallam University was granted for the use of participants in experimental testing.

7.2 Equipment set-up

Two Phantom v4.2 high-speed video cameras were used to capture a 1.5 x 1.5 x 1 m volume both in a laboratory and on a natural turf football pitch. The volume was sufficient enough to capture the inbound and outbound foot trajectory with compensation for differences in foot-strike location. The cameras were placed 5 m perpendicularly away from the foot-strike zone at an angle of approximately 75° to each other. Using this orientation of cameras, the shoe was visible throughout all three test movements. The cameras filmed at 1000 fps for 0.6 s at a resolution of 512 x 382 pixels and a low exposure of 70 ps. These settings were chosen to reduce download time but allow high quality images to be recorded. The cameras were synchronised and triggered manually when the participant entered the filming zone, or triggered externally by the force-plate when testing in the laboratory. The checkerboard technique was used to calibrate the cameras. The checkerboard was positioned flat in the foot-strike zone and was used to define the origin and global axis system. The same camera arrangement and calibration procedure was used in both the laboratory and outside testing.

Field of view

Left camera

Right camera

Figure 7.1 - Camera placement and axis system in field of view at Doncaster Rovers FC training ground.

7.3 Definition of test movements

Three movements were selected to represent scenarios that required high levels of traction; acceleration, change in direction and braking. The transition between a jog and a sprint was used to represent an acceleration movement; with the emphasis on a forefoot propulsion during the sprint phase. A 45° lateral side-cut was used to represent a change in direction; before testing it was unknown whether players would land in a toe-down or toe-up position and if they would rotate the forefoot during the movement. The planted foot during a right-footed long range kick was used to represent a braking movement. It was anticipated that players would land heel first in contrast to the sprint movement.

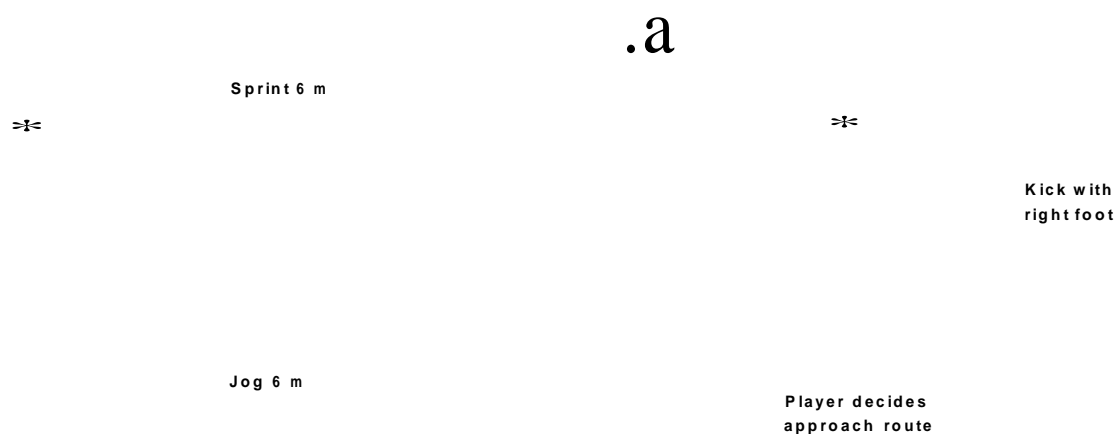


Figure 7.2 - Movement schematic for player testing. Left: Acceleration phase of sprinting; Centre: 45° lateral side-cut; Right: Long range kick.

The sprint consisted of a 6 m jog followed by a 6 m sprint; the filming zone was at the transition between jog and sprint. For the 45° side cut, participants first undertook a 45° medial side-cut before undertaking the lateral side-cut in the filming zone. The kick was a stationary long-range kick where participants were asked to aim at a target 50 m away. Participants took a free run-up to the kick from any location and at their choice of trajectory. Cones were set-up within the test area to mark the sprint distance, side-cut course and approximate film location.

7.4 Notation

The following figures illustrate the terminology used for the axis directions, marker notation and stud notation.

S7 S3 S4 S1

Figure 7.3 - Marker and axis notation. Top left: Marker positions on side of left shoe; Bottom left: Stud notation, aerial view; Top right: Axis orientation with respect to direction of motion, side view; Bottom right: Axis notation aerial view.

7.5 Indoor testing

One player participated in the laboratory study. The high-speed cameras were set up as described in section 7.2 with the addition of a force-plate. The test conditions are described in Table 7.1. The participant wore Copa Mundial football boots and performed the acceleration phase of sprinting (6 m jog, 6 m sprint) onto the force-plate covered with artificial turf. The force-plate was triggered by a falling edge signal on foot-strike. The trigger from the force-plate was used to activate the two synchronised cameras. This allowed timings of events to be matched from force-plate and video data. The participant was made aware that the left foot needed to land onto the force-plate; but was given sufficient practice time to ensure that this movement was natural.

<i>Participant:</i>	Ex-academy level football player
<i>Movement:</i>	Acceleration phase of sprinting, five repeats
<i>Footwear:</i>	Copa Mundial, size UK 8.5
<i>Surface:</i>	Carpet with artificial turf covering the force-plate (0.6 x 0.4 m area)
<i>Camera:</i>	Phantom v4.3
	Recording frame rate = 1000 fps
	Analysis frame rate = 200 fps
	Exposure = 50 ps
	Resolution = 512 x 256 pixels
<i>Force-plate:</i>	Sample rate = 1000 Hz
	Trigger above level
	10% pre trigger
	Shear range = 1331 N
	Vertical range = 5246 N

Table 7.1 - Indoor data collection test conditions.

The laboratory study was used as an example of the level of detail that can be gained from the position history of the shoe markers combined with force-plate data. Features in the results that will enable a larger data set to be analysed were highlighted. Using the force-plate data, key timings such as foot-strike and push-off were identified, and compared to events in the position history to allow results to be normalised to aid in post processing.

7.6 Outdoor testing

A cohort of 8 Youth Team players participated in the study. Participants were given a selection of Copa Mundial football shoes (sizes UK 8 – 11) and asked to pick the size they would chose for a regular training session. Participants were given a 30 minute warm-up period to become accustomed to the footwear. All of the three movements were tested; sprint, long range kick and 45° side-cut. Before testing began participants were given practice attempts at each movement until they felt confident. Five repeats were made of each movement.

Participants: Doncaster Rovers Youth Team
 16.6 ± 0.5 years
 3 x Midfield, 3 x Forward, 1 x Defence, 1 x Keeper

Movements: Acceleration phase of sprinting
 Long range kick
 45° lateral side-cut

Footwear: Copa Mundial
 2 x UK 8, 2 x UK 8.5, 3 x UK 9.5, 1 x UK 10.5

Surface: Natural turf, 40% FIFA rebound

Camera: Phantom v4.3
 Recording frame rate: 1000 fps
 Analysis frame rate: 1000 fps and 200 fps
 Exposure = 70 ps
 Resolution = 512 x 384 pixels

Table 7.2 - Outdoor data collection test conditions.

Testing took place at the Doncaster Rovers FC training ground in October 2010. The surface was a natural turf of fibre length approximately 40 mm. A FIFA standard ball bounce test was performed on the surface prior to and after testing. The rebound height was 40% of the initial drop height; this value was within the accepted hardness range (20 - 50%) as identified by Canaway *et al.* (1990).

Figure 7.4 - Surface condition after testing.

The test area was moved half way through testing to ensure the grass condition did not deteriorate significantly between participants.

Weather information was obtained for the week before testing from the Doncaster weather station, approximately 4 miles from the test location (Doncaster Weather Station 2010). An average temperature of 12°C and humidity of 22% was recorded on the day of testing which was consistent with the previous 7 days. No rainfall was recorded over this period.

7.7 Chapter summary

Two data collection studies were carried out to obtain information on the shoe-surface interaction within a controlled laboratory environment and outside on natural turf. The primary aim of the two studies was to provide an example of the type of results that can be collected using the proposed 3D measurement system. In both studies the left shoe (Copa Mundial) was filmed using two high-speed video cameras using the stereo-videogrammetry method and analysed using the bespoke marker tracking tool.

In the first study, data collection of a single participant in a laboratory was carried out. The participant was asked to perform the acceleration phase of sprinting movement on an artificial turf surface. The filming zone coincided with a force-plate allowing both visual and force data to be collected.

For the second study, a larger sample size of 8 participants was undertaken at Doncaster Rover's training ground on a natural turf pitch. The participants performed three movements, sprint, kick and side-cut with five repeats of each movement.

Using the data collected, the next stage of both studies was post processing of the results to provide an example of how the shoe-surface interaction can be analysed.

8 RESULTS AND ANALYSIS OF LABORATORY BASED DATA COLLECTION

8.1 Introduction

The aim of the player based data collection studies was to initially evaluate the 3D measurement system developed in Chapter 4 and to use the results to provide an example of the level of detail that can be obtained to aid in the understanding of the shoe-surface interaction. The first study looked to address the initial aim, using a single participant in a laboratory environment. The controlled nature of the study hinders the realism of the results collected, but allows the measurement system to be assessed with the aid of additional force-plate data.

An ex-academy level football player performed the acceleration phase of sprinting onto a force-plate covered with artificial turf. Five repeats of the movement were captured after a sufficient warm-up period. Two high-speed video cameras were synchronised with a force-plate and triggered by a falling edge trigger when the participant made contact with the force-plate. The cameras filmed at 1000 fps. A five-point moving average filter was used to smooth the results before velocities and accelerations were calculated. For the initial stage of testing, the position history of marker P3 placed near the metatarsal-phalangeal joint was used. Additional information using the force-plate data was also found, with the intention to identify features in the results that could help classify event timing without the use of a force-plate. Variables that could aid in improving the efficiency of analysis of a larger sample size were also investigated.

8.3 Discussion

For this participant, notable yaw angles (toe-out) of the foot prior to and during foot-strike was observed from the recorded video footage. During the movement the foot rotated approximately 5° . This gave rise to a peak lateral force of -232 ± 37 N occurring 0.04 ± 0.01 s after impact (Figure 8.3 *point b*). This indicated that the foot was still rotating upon foot-strike. Results indicated that the metatarsal-phalangeal joint (P3) was moving posteriorly prior to foot-strike (seen in the negative y displacement gradient prior to $t = 0$ s in Figure 8.1). For the preceding 0.02 s prior to foot-strike as triggered from the force-plate, the P3 marker travelled an additional 5 mm in advance of the impact point. After foot-strike, the P3 marker continued to travel posteriorly for 0.15 s until moving anteriorly. The total posterior movement during surface contact was 4.8 ± 0.4 mm. A large net impulse in the posterior direction was also seen in Figure 8.3 indicating the participant was accelerating away from the force-plate with little energy wasted on the transfer between impact and push-off. Slower or less successful acceleration movements are expected to display a more neutral net impulse with equal impact to push-off phases.

The posterior motion of the P3 marker was due to the rotation of the foot about the ankle joint. The increase in pitch angle (rotation about the x-axis) suggested that the foot was moving from a slight toe-up position during transition through the air to a toe-down position at foot-strike. The rotation of the P3 marker about the ankle joint without a substantial increase in the y displacement caused the P3 marker to move posteriorly relative to its initial position. This was seen in Figure 8.4 which shows the relative position of the P3 marker in terms of the y and z position.

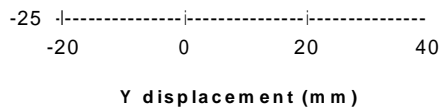


Figure 8.4 - Position of the metatarsal-phalangeal marker in terms of y and z displacement.

The maximum vertical force occurred 0.103 ± 0.002 s after foot-strike (Figure 8.3 *point c*); this did not relate to maximum vertical displacement of the P3 marker which occurred at 0.021 ± 0.005 s after foot-strike. The maximum vertical force occurred during the push-off stage of the sprint movement. The maximum vertical displacement of the P3 marker occurred when the foot was transitioning between the foot-strike and the push-off stage. The maximum horizontal force (in the y direction) occurred during the push-off at 0.144 ± 0.002 s after foot-strike (Figure 8.3 *point d*). This coincided with the moment at which the P3 marker ceased to travel posteriorly and instead moved anteriorly. This was considered the peak push-off time.

Calculation of the ratio of horizontal to vertical force showed that it was greatest at the end of the sprint movement, occurring 0.199 ± 0.001 s after foot-strike. At this moment, only the very tip of the shoe was in contact with the ground. This highlighted the possible need for an additional stud at the tip of the forefoot, as during this time period, no studs were in contact with the ground. Upon impact with the ground, the foot was at an angle of $7.2 \pm 0.3^\circ$ to the horizontal. An additional stud on the tip would not affect the traction properties of the shoe upon foot-strike.

At foot-strike the resultant velocity of the P3 marker was $1.18 \pm 0.02 \text{ ms}^{-1}$ (averaged over the preceding 0.012 s). The marker at this instance was moving posteriorly, as such the velocity along the y-axis was $-0.12 \pm 0.02 \text{ ms}^{-1}$. The z-axis motion was the most dominant with a velocity of $-1.01 \pm 0.03 \text{ ms}^{-1}$. There was also significant motion in the x-axis as indicated by the yaw angle (toe-out) of the foot in Figure 8.2; a velocity of $0.56 \pm 0.04 \text{ ms}^{-1}$ was calculated.

During the study the participant communicated that they felt safe running in the footwear on the chosen surface. A posterior movement of the metatarsal-phalangeal joint marker of $4.8 \pm 0.4 \text{ mm}$ was observed during the movement. It is difficult to tell whether this was caused by the foot slipping, or by the rotation of the rear-foot about the metatarsal-phalangeal joint as the participant transitioned between foot-strike and push-off. During normal walking, a heel slide of greater than 30 mm occurring at and after heel-strike is considered a slip (McGorry *et al.* 2007). Below this 30 mm threshold it is considered to be a microslip and often occurs without being perceived (Perkins 1978). As such, a displacement of $4.8 \pm 0.4 \text{ mm}$ would not be considered a slip and therefore the traction requirement of the participant on that surface was achieved.

8.4 Defining impact and push-off

Data collection in the laboratory had the advantage that the cameras could be triggered from activation of the force-plate. This enabled the video footage to be synchronised with the force-plate data, allowing time dependent information such as time of foot-strike, time of push-off and length of surface contact to be easily identified. When testing outside on natural turf, this information cannot be gained from force data and therefore had to be inferred from the results of the stereo-videogrammetry. 3D positional data from a sprint movement was collected both in the laboratory and outside on natural turf. The laboratory data set was synchronised with the force-plate and time of foot-strike was set to 0 s, as triggered from the force-plate. The laboratory data was compared to the natural turf data in order to identify features in the data set that can be used to identify foot-strike and push-off.

The vertical displacement of the impacting marker, P3 was examined in Figure 8.5.

Figure 8.5 - Vertical displacement of marker P3, Left: Laboratory; Right: Natural turf.

In both cases, P3 travelled downwards at a constant rate until contacting the surface. After initial foot-strike on to the soft ground, P3 continued to travel downwards, compressing or penetrating into the surface. Both surfaces showed a distinct change after the initial period of constant rate of displacement where the shoe is travelling through the air; calculation of velocity and acceleration was used to help identify this feature.

Figure 8.6 - Velocity and acceleration in the vertical direction (z) for marker P3, Left: Laboratory; Right: Natural turf.

Both the laboratory and natural turf acceleration results showed a peak in acceleration at the time of foot-strike. For the laboratory results, foot-strike was defined from the

force-plate with a 5 N threshold trigger. The confirmation between force-plate defined foot-strike and acceleration results suggested that it was appropriate to use the peak acceleration of the impacting marker in the vertical direction to define the time of impact when force-plate data is not available. This approach was also used by Hreljac and Marshall (2000) in determining event timing during walking using kinematic data.

At time of foot-strike, the coordinates of the impacting marker were set to the origin (0,0,0) and time set to 0 s.

For the sprint movement, time of push-off was also required. Using the laboratory data, time of push-off was defined as the time of maximum horizontal force in the posterior direction. The vertical displacement of marker P3 during the contact phase was different depending on the surface. As mentioned, the softer natural turf allowed the shoe to deform the surface and continue to travel vertically down after the time of impact. This did not occur on the hard laboratory surface as surface deformation was not possible.

Figure 8.7 - Using horizontal force (red) and vertical displacement (black) of marker P3 to define push-off, Left: Laboratory (push-off at 0.146 s); Right: Natural turf (push-off at 0.113 s).

Push-off for non-force data was defined as the time at which marker P3 moved above the previously defined origin level ($P3z > 0$).

8.5 Identifying variables for comparison

To improve the efficiency of the first stages of analysis when working with a larger sample size, the level of detail of the results needs to be reduced. From the case study (five repeats) the orientation of the shoe at foot-strike was calculated (Table 8.1).

	Pitch	Yaw	Roll
Mean \pm 1 SD	-10.7 \pm 2.1°	25.2 \pm 2.5°	16.3 \pm 1.4°

Table 8.1 - Orientation of the shoe on foot-strike.

The maximum standard deviation of $\pm 2.5^\circ$ was similar to the mean propagated error of $\pm 2.7^\circ$. As such, the pitch, yaw and roll at foot-strike were chosen as distinguishing variables for the larger set of results. It was anticipated that changing the movement (sprint, kick and side-cut) would change the orientation of the shoe on foot-strike.

8.6 Chapter summary

The limitations of the laboratory study were:

- A limited data set;
- A non-realistic surface;
- Restricted room for other movements;
- Additional external lighting sources required to lower the camera exposure;
- In a laboratory environment so subject to inherent change in participant movement due to testing conditions (i.e. non-realistic movement).

However, the reason the laboratory study was undertaken was to make use of the force-plate data to highlight event timings in the visual data. The study revealed that the peak acceleration of the impacting marker could be used to identify the time of foot-strike when force data is not available. The pitch, yaw and roll angles of the shoe at foot-strike were selected as the variables that could be used to differentiate between different movements; with the standard deviation of one participant being the equivalent to the maximum measurement error of the system after validation. Further advantages of the laboratory study were:

- Single participant allowed more in-depth analysis of results;
- More flexibility in time and duration of testing;

- No influence or restrictions of climatic conditions;
- No change to surface during testing;
- Force-plate also allowed cameras to be externally triggered reducing user error.

The laboratory study also provided information on the length of time to collect data from a single participant. This aided in planning the larger data collection study. Further information such as a detailed check-list of equipment required and time need to set-up and take down equipment was also fine tuned to allow more efficient data collection at Doncaster Rovers FC.

9 RESULTS AND ANALYSIS OF DONCASTER ROVERS FC DATA COLLECTION

9.1 Introduction

Using the information gained from the controlled study in the laboratory, a larger data collection study was undertaken at Doncaster Rovers FC. Eight participants from the youth team (17.1 ± 0.5 years) performed the sprint, kick and side-cut movements on a natural turf surface as detailed in Chapter 7. The study was undertaken to provide an example of how the proposed 3D measurement system can be used to obtain information on the shoe-surface interaction in an outdoor environment. The movements tested were similar to those performed in a warm-up drill before a game or training session. Testing took place mid-week on a low intensity training day for the players. Approximately five trials were obtained from each player for each movement.

The following terminology was used to designate a player number and movement trial number to the data collected (Table 9.1):

Example	Player, <i>i</i>	Movement	Trial,;
P,S,	<i>i</i> = 1 to 8	S = Sprint, K = Kick, C = Side-cut	<i>j</i> = 1 to 5
e.g. P3C4	Player 3	Side-cut	Trial 4

Table 9.1 - Player and movement trial terminology.

From the trials collected, the rear-foot section (three markers, P1-P3) was tracked. A trial was deemed successful if all three markers were visible throughout the desired frames. For the sprint movement, only forefoot strikers were considered for analysis (80% of trials). The number of successful trials for each movement and subsequent number of markers tracked is shown in Table 9.2.

Movement	Trials	Successful	Frames	Total markers tracked
Sprint	46	19	260	
Kick	40	34	40	23,520
Side-cut	42	22	70	

Table 9.2 - Results collected from Doncaster testing.

Post-processing analysis was then carried out on the results, primarily using the filtering techniques highlighted in Chapter 5. For each successful trial, the orientation of the rear-foot section, velocity and acceleration of the markers was determined. For comparison purposes, the time of initial foot-strike was chosen as a common reference point by resetting the time to zero at this event. Time of foot-strike was defined from the acceleration of the marker touching the ground first. In the case of the sprint, with forefoot landing, a notable change in the acceleration of marker P3 was used to define foot-strike. For the side-cut and planted foot in kicking, marker P1 was used. The controlled study results in Chapter 8 were used to verify the suitability of using this approach.

Statistical analysis was then used to determine if any outliers were present or further dichotomisation of the results was necessary. From the final set of results, a representative player trial for each movement or group was chosen. The representative player trial was selected by calculating the average absolute difference between the group mean and the trial value.

Marker P4 on the front of the foot was tracked in addition to the rear-foot markers for the representative player trials to enable the pitch of the forefoot and position of the forefoot studs to be determined. Table 9.3 shows the number of additional markers tracked and the resulting number of stud positions derived.

Trials	Frames	Markers	Stud coordinates
3	260	3,120	9,360

Table 9.3 - Results collected for complete shoe for representative player trials.

A more detailed analysis of the shoe-surface interaction for the representative trials was then undertaken using the visualisation and interpretation techniques described in Chapter 5.

9.2 Results

9.2.1 Orientation and velocity

The orientation of the shoe was calculated using the Euler method outlined in Chapter 5. The velocity of the shoe was derived from the smoothed displacement data using the 5-point central differencing method. The mean value, standard deviation and range (maximum and minimum values) for the orientation and velocity of the shoe for each movement at the time of initial foot-strike were calculated. For the sprint movement, shoe orientation and velocity at the time of peak push-off were also calculated.

The following terminology was used:

- +/- y = Anterior/Posterior
- + y = Direction of motion
- +/- x = Medial/Lateral
- +/- z = Vertical
- +/- Pitch = Toe-up/Toe-down
- +/- Yaw = Toe-in/Toe-out
- +/- Roll = Outward roll/Inward roll

a) Sprint results at foot-strike

	Pitch (°)	Yaw (°)	Roll (°)	$dxpj/dt$ (ms ⁻¹)	$dypi/dt$ (ms ⁻¹)	$dzpi/dt$ (ms ⁻¹)	Resultant (ms ⁻¹)
Mean	-15.0	-22.0	6.9	-0.44	0.27	-1.10	1.38
Standard deviation	5.7	8.3	8.0	0.58	0.46	0.38	0.50
Maximum	-4.6	2.8	23.2	0.68	1.11	-0.60	2.35
Minimum	-25.5	-29.3	-10.9	-1.76	-0.96	-1.75	0.73

Table 9.4 - Sprint results at foot-strike (N = 19).

The shoe was found to land in a toe-down and toe-out position (negative pitch angle, negative yaw angle) with outward roll (positive roll angle). Only participants landing forefoot first were included in the results (80%) giving the smaller standard deviation in pitch compared to the other angles. For the yaw and roll angles, only one participant landed in the opposite rotation to the rest of the data set. This led to the higher range for

the yaw and roll angles compared to the pitch. Further filtering of the data will help identify outliers and reduce the standard deviation and range seen in the results.

b) Sprint results at push-off

	Pitch (°)	Yaw (°)	Roll (°)	dx_{pi}/dt (ms ⁻¹)	$dypj/dt$ (ms ⁻¹)	$dzpj/dt$ (ms ⁻¹)	Resultant (ms ⁻¹)	Time (s)
Mean	-49.0	-27.2	18.9	-0.06	0.29	1.38	1.55	0.15
Standard deviation	12.1	8.4	8.9	0.55	0.42	0.72	0.74	0.03
Maximum	-27.7	-14.7	31.8	1.16	1.12	2.71	2.84	0.21
Minimum	-71.9	-39.2	4.4	-1.09	-0.41	0.58	0.58	0.11

Table 9.5 - Sprint results at push-off (N = 12).

At the time of peak push-off the shoe had further rotated about the x-axis to a higher pitch angle of 49°. The yaw and roll angles also increased, suggesting that participants pushed-off from the lateral side of the shoe. A higher standard deviation was seen compared to the results at foot-strike. This was possibly due to the potential errors in selecting the time of peak-push off, although a small standard deviation was seen in terms of movement time from initial foot-strike to peak push-off (0.15 ± 0.03 s). A greater velocity in the z-axis direction was seen compared to initial contact (in the opposite direction) giving rise to a slightly higher resultant velocity. This suggested that the participants were accelerating, with the shoe leaving the surface at a greater velocity than before initial contact.

c) Kick results at foot-strike

	Pitch (°)	Yaw (°)	Roll (°)	dx_{pj}/dt (ms ⁻¹)	$dypj/dt$ (ms ⁻¹)	$dzpi/dt$ (ms ⁻¹)	Resultant (ms ⁻¹)
Mean	21.1	-29.1	31.5	1.27	2.76	-1.74	3.66
Standard deviation	7.0	7.7	5.6	0.56	1.08	0.48	0.74
Maximum	35.9	-10.8	42.7	2.18	4.67	-0.71	5.21
Minimum	6.0	-40.4	18.7	0.13	0.23	-2.54	1.65

Table 9.6 - Kick results at foot-strike (N = 34).

All participants during the kick movement landed with the planted foot heel first in a toe-up position. Greater yaw and roll angles were seen compared to the sprint

movement, suggesting that the shoe was landing on the rear lateral studs of the heel with the toe externally rotated. A high range for all orientation angles was seen suggesting that further groupings may exist within the data set. The shoe was landing with a higher resultant velocity compared to the sprint movement, with a high velocity seen in the y-axis (i.e. in the dominant direction of travel).

d) Side-cut results at foot-strike

	Pitch (°)	Yaw (°)	Roll (°)	dx_{pi}/dt (ms ⁻¹)	dy_{pl}/dt (ms ⁻¹)	dz_{pj}/dt (ms ⁻¹)	Resultant (ms ⁻¹)
Mean	13.6	-22.3	-39.4	-1.53	0.03	-0.62	1.68
Standard deviation	6.4	10.6	8.2	0.56	0.25	0.39	0.64
Maximum	30.4	-7.1	-23.9	-0.33	0.73	-0.04	2.85
Minimum	3.9	-43.4	-54.1	-2.48	-0.26	-1.52	0.34

Table 9.7 - Side-cut results at foot-strike (N = 21).

Similarly to the kick movement, all participants landed heel first in a toe-up position although the pitch angle was lower indicating the shoe was impacting the surface at a flatter angle compared to the kick movement. A high inward roll angle was observed suggesting the shoe landed with the medial side of the shoe in contact first. This was different to the other movements where the lateral side was seen to contact first. A greater velocity was seen in the x-axis with an almost negligible velocity seen in the y-axis. This highlights the different movement directions experienced by the side-cut compared to the sprint movement.

9.3 Statistical analysis

Statistical analysis was firstly carried out on the largest data set, the kick movement, to determine if significant differences existed between participant results and if the kick movement could be divided into further groups. Similar analysis was then applied to the sprint and side-cut movement groups, although as the data sets were smaller, identification of outliers was the priority rather than further dividing into groups.

9.3.1 Kick analysis

The range of angles for pitch, yaw and roll orientations (30°, 29° and 24° respectively) were considered large in comparison to the mean value (Table 9.6). The analysis of variance (ANOVA) statistical test was used to distinguish if there were any significant differences between participants that might indicate that further dichotomisation of the data was required to best represent the boundary conditions.

	Sum of squares	<i>df</i>	Mean square	<i>F</i>	<i>P</i>
Between groups	324.8	26	12.5	14.86	<.01
Within groups (error)	1299.9	7	185.7		
Totals	1624.8				

Table 9.8 - Tabular report of analysis of variance for pitch angle.

	Sum of squares	<i>df</i>	Mean square	<i>F</i>	<i>P</i>
Between groups	383.0	26	14.7	15.27	<.01
Within groups (error)	1574.1	7	224.9		
Totals	1957.0				

Table 9.9 - Tabular report of analysis of variance for yaw angle.

	Sum of squares	<i>df</i>	Mean square	<i>F</i>	<i>P</i>
Between groups	486.3	26	18.7	4.26	<.01
Within groups (error)	558.2	7	79.7		
Totals	1044.5				

Table 9.10 - Tabular report of analysis of variance for roll angle.

Results from the ANOVA test indicated that there were significant differences (*p* < .01) between participant results in all three angles analysed from the kick movement. A

Scheffe's confidence interval test was used to determine which participants varied significantly.

	P1	P2	P3	P4	P5	P6	P7	P8
P1	0.00	10.23	11.91*	18.10**	0.95	12.31*	11.05	8.85
P2		0.00	1.68	7.87	11.18	2.08	0.82	1.38
P3			0.00	6.19	12.86**	0.39	0.86	3.06
P4				0.00	19.05**	5.80	7.05	9.25
P5					0.00	13.26**	12.00*	9.81
P6						0.00	1.26	3.45
P7							0.00	2.20
P8								0.00

Table 9.11 - Mean difference analysis for pitch angle. Note: * $p < .05$ ** $p < .01$

	P1	P2	P3	P4	P5	P6	P7	P8
P1	0.00	3.83	7.91	0.64	5.69	10.61	10.83	9.59
P2		0.00	4.08	4.46	1.86	6.78	14.65**	5.77
P3			0.00	8.54	2.22	2.70	18.74**	1.69
P4				0.00	6.32	11.24	10.19	10.23
P5					0.00	4.92	16.51**	3.91
P6						0.00	21.43**	1.01
P7							0.00	20.42**
P8								0.00

Table 9.12 - Mean difference analysis for yaw angle. Note: * $p < .05$ ** $p < .01$

	P1	P2	P3	P4	P5	P6	P7	P8
P1	0.00	0.27	0.16	7.25	5.22	2.50	5.41	4.60
P2		0.00	0.10	7.51	4.96	2.23	5.67	4.86
P3			0.00	7.41	5.06	2.33	5.57	4.76
P4				0.00	12.47	9.74	1.84	2.65
P5					0.00	2.73	10.63	9.82
P6						0.00	7.90	7.09
P7							0.00	0.81
P8								0.00

Table 9.13 - Mean difference analysis for roll angle. Note: * $p < .05$ ** $p < .01$

From this analysis it was clear that there were significant differences ($p < .01$) between player 5 and players 3, 4 and 6 for the pitch angle, although these differences were not evident in either the yaw or roll angle. With the yaw angle, player 7 differed from the other players by the highest degree. No significant differences between individual participants were evident for the roll angle when using the Scheffe's test. Using this approach alone it was difficult to identify whether there are clear differences between participants for all three angles that might benefit from further dichotomisation. A frequency plot of all participant results was used to assess the style of distribution and whether any groups within the results were evident.

Figure 9.1 - Relative frequency of pitch angle.

Figure 9.2 - Relative frequency of yaw angle.

Figure 9.3 - Relative frequency of roll angle.

All frequency curves (Figure 9.1 - 7.3) were slightly platykurtic in shape (i.e. kurtosis < 0) although not significantly so ($-2 < Z_{kurt} < 0$). The yaw angle results displayed a slight positive skew ($Z_{skew} = 1.70$), although again not significant ($0 < Z_{skew} < 2$). Due to the slight positive skew in the yaw angle data, it was thought that 2 groups of high yaw angle ($yaw < -28^\circ$) and low yaw angle ($yaw > -28^\circ$) may better represent the data set. The pitch and roll angles displayed a more normal distribution shape ($Z_{skew} = 0.10$ and 0.08 respectively), and as such it was harder to identify distinct groups within the individual angle sets. However, it was thought that there may be sets of results which display both higher pitch angles and higher roll angles.

Scatter plots of pitch-yaw, pitch-roll and yaw-roll data sets were used to identify any groupings between angles. Two potential groups for each angle combination were drawn by observation of the scatter plots.

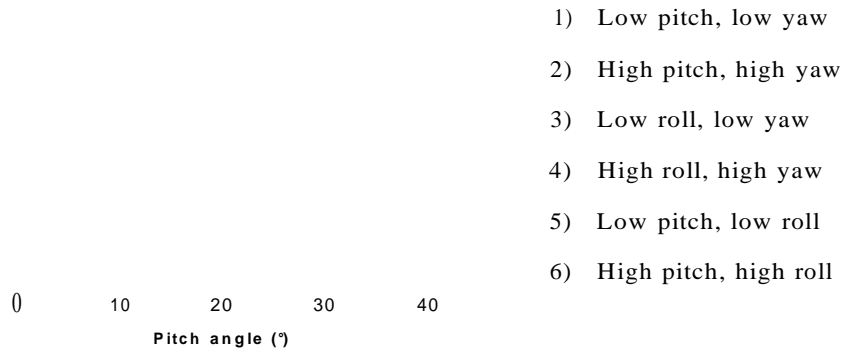


Figure 9.4 - Top left: Pitch and yaw angles; Top right: Yaw and roll angles; Bottom left: Pitch and roll angles; Bottom right: Possible groupings.

From the groupings observed in the scatter plots it was hypothesised that two groups of all three angles existed:

- 1) Low pitch, low yaw, low roll
- 2) High pitch, high yaw, high roll

The K-means clustering method was used to identify the centroids of the two groups and which results lay in them. The starting centroids were selected from the scatter plots and an iterative approach used to find the final centroid value. The following groups were formed:

	Group 1	Group 2
Centroid (Pitch, Yaw, Roll)	(15°, -21°, 27°)	(24°, -33°, 33°)
Standard deviation	(± 5°, ±7°, ±5°)	(± 6°, ±5°, ±5°)
Participant trials	P2K2 P4K1, P4K?, P4K3, P4K4, P4K5 p7k i? p7k 2, p7k 3, p7k 4, p7k 5	P, Kb P, K2, P, K3, P, K4, p, k 5 p2k 3, p2K4, p2k 5 p3k ,, p3k 2, p3k 3, p3K4 p5k ,, p5k 2, p5k 3, p5k 6 p6k ,, p6k 2, p6k 3 p8k ,, p8k 2, p8k 3, p8K4, p8k 5

Table 9.14 - K-means cluster method groups for kick movement.

With the exception of player 2, all participants fell exclusively into either group 1 or 2. Players 4 and 7 formed group 1, with the remaining players 1, 3, 5 and 6 forming group 2. This suggested that the individual players naturally displayed either high or low pitch, yaw and roll angles on foot-strike. The standard deviation of the pitch, yaw and roll angles when considering all results together were $\pm 7^\circ$, $\pm 6^\circ$, $\pm 8^\circ$ respectively; however the new standard deviations of the two groups were only slightly lower for each angle. If strong groupings existed, it was expected that the new standard deviations would be significantly lower than when considering all results combined. As this was not the case, a decision had to be made whether to represent the kick results as one data set, or as two sets of high and low angles. The scatter plots of pitch-yaw, pitch-roll and yaw-roll were redrawn using the new groupings (Figure 9.5).

• Group 2
x Group 1

Figure 9.5 - Scatter plots of kick impact angles after cluster groupings.

The problem with the K-means cluster method used above is that the number of groups and the starting centroid positions is very user subjective. It is possible that dichotomising the data into 3 or 4 groups may better represent the data set. This however may lead to the danger of forming a group that has a limited number of results that may, by other means, be considered as outliers rather than a group. The range of

the new groups has decreased ((17°, 20°, 15°) and (22°, 18°, 28°) respectively) which suggests a better distribution compared to using the complete data set.

9.3.2 Sprint analysis

Due to some data sets for participants only having one successful sprint trial, the ANOVA test could not be used to identify if any significant differences existed between participants. Instead, the K-means cluster analysis was used to see if the data set could be divided into smaller groups that reduced the range and standard deviation of the results.

The following groups were formed:

	Group 1	Group 2
Centroid (Pitch, Yaw, Roll)	(-17°, -26°, 4°)	(-11°, -13°, 12°)
Standard deviation	(± 5°, ±2°, ±7°)	(± 5°, ± 10°, ±9°)
Participant trials	P3S2 P5S1, P5S2, P5S3, P5S6 PfiS], P6S7, P6S3, P6S4 P8S2, P8S4, P8S5, P8^6	PjS], P1S2, P1S3, P1S4 P2S5 P5S5

Table 9.15 - K-means cluster method groups for sprint movement.

The centroid values of group 1 were close to the original mean values of the complete data set, but showed a reduced standard deviation. In contrast, group 2 centroid values for the pitch and yaw angles were lower than the original data set and the standard deviation for the yaw and roll angles was greater. Group 2 consisted primarily of the trials by player 1 and the single trial by player 2. With the exception of player 5, participants fell exclusively to either group 1 or 2. Due to the increased standard deviation and small group number of group 2, it was decided that group 2 would be considered as an outlier, and group 1 used to represent the sprint data set.

9.3.3 Side-cut analysis

The K-means cluster analysis method was used to identify outliers in the side-cut data set. The following groups were formed:

	Group 1	Group 2
Centroid (Pitch, Yaw, Roll)	(12°, -22°, -40°)	(29°, -17°, -38°)
Standard deviation	(± 4°, ± 12°, ± 8°)	(± 1°, ± 9°, ± 2°)
Participant trials	Pb P3, P5, P7, P8	P1C3, P1C5

Table 9.16 - K-means cluster method groups for side-cut movement.

The notable outliers after this form of analysis were two trials by player 1 which displayed higher pitch angles on initial contact compared to the rest of the data set. Removing these two results left group 1 which has a slightly smaller standard deviation than the original data set.

9.3.4 Analysis of relationships

Using the reduced data sets, further statistical analysis by means of the Spearman's rank correlation was carried out to investigate potential relationships that exist within the data sets. Results for each variable were ranked in value order and relationships between sets of ranked variables were assessed using the Spearman's rank correlation coefficient, r_s :

$$r_s = \frac{\sum d^2}{n(n^2 - 1)} \quad \text{Equation 9.1}$$

where d is the difference between ranked values.

The following variables were assessed:

- Pitch, yaw and roll angles at foot-strike;
- Resultant shoe velocity;
- Contact time between impact and peak push-off (sprint only);
- Ball velocity (kick only).

The ball velocity was calculated by tracking the centre of the ball in 3D coordinates and then using the central differencing method. The variables were assessed between movements and also between individual participants.

The following correlations were found to be significant using the Spearman's rank analysis:

Movement	First variable	Second variable	Level of significance
Sprint	Low pitch angle	High resultant shoe velocity	$p < .01$
Sprint	Low pitch angle	Shorter contact time	$p < .01$
Kick	Low pitch angle	High ball velocity	$p < .01$
Kick	High yaw angle	High ball velocity	$p < .05$
Side-cut	High pitch angle	High roll angle	$p < .05$

Table 9.17 - Significant relationships using Spearman's rank analysis.

No correlation was found between foot angles of players across different movements; for example, players that displayed high yaw angles on contact for the sprint movement did not necessarily show higher yaw angles for the kick or side-cut movement.

9.4 Foot placement during kicking

Additional information about the position of the shoe during kicking can also be gained from the 3D positional data. The literature review of biomechanics in football (section 2.5) identified that Lees and Nolan (1998) postulated that the placement of the planted foot during kicking may influence the performance. Using the same approach as McLean and Tumilty (1993), the position of one third the distance from heel to toe of the support foot at the moment of impact between the kicking foot and the ball was calculated for each of the kick trials (Figure 9.6).

The median position for the support foot during the kick was 39 ± 9 cm medially and 0 ± 6 cm posteriorly to the centre of the ball. McLean and Tumilty (1993) reported for a similar demographic that for right foot kicks the support foot was positioned 37 ± 4 cm medially and 8 ± 5 cm behind the ball. Similar results were observed for the medial position of the support foot but differed slightly on the anterior-posterior positioning.

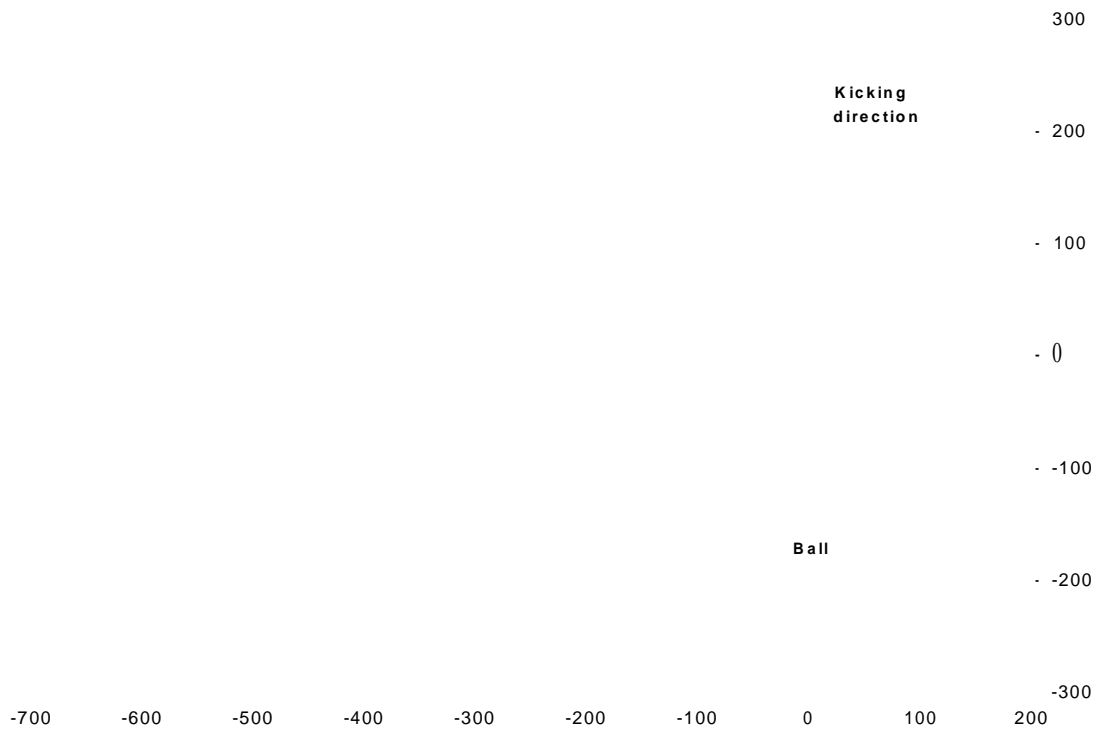


Figure 9.6 - Position of support foot during the kick; lines represent distance from heel to toe studs (distance values in mm, ball centre positioned at 0,0).

Lees and Nolan (1998) also hypothesised that the anterior-posterior positioning of the support foot is related to the type of kick and the intended trajectory. The ball trajectory and velocity was also observed for each kick trial but no relationship was apparent (Figure 9.7).

Figure 9.7 - Relationship between ball launch angle and position of the support foot.

9.5 Representative player trials

Representative player trials were selected for further analysis rather than averaging the complete data set as it was thought that averaging would potentially mask small levels of detail that may be important in describing the motion of the shoe.

The player trials that best represented each movement were selected using the absolute mean difference between the trial results for all three angles and the movement group's mean values. The trials were then ranked in order of smallest absolute difference to largest for each angle. The rank orders were then summed and ranked again. The player trial with the smallest final ranking number was selected as the player trial that best represented the mean of the group.

The limitation of using one trial is that it although the trial was selected to best represent the group there was still the possibility that the motion of the shoe during the interaction with the surface was unique to the participant. However, by using a single trial a thorough evaluation of the interaction could be undertaken in the same time period. The analysis of the representative player trial was used to provide an example of the level of detail that can be obtained from the 3D measurement system. The results from the analysis of each trial, although not statistically representative of the population, could be used to speculate how the shoe-surface interaction may influence traction testing procedures or the design of studded outsoles.

9.5.1 Representative sprint trial

After the cluster analysis, results from player 1 were removed as outliers. Table 9.18 shows the remaining data set, from which trial 2 of player 6 (P6S2) was chosen as the representative sprint trial.

	Pitch (°)	Yaw (°)	Roll (°)	$dxpj/dt$ (ms ⁻¹)	$dypi/dt$ (ms ⁻¹)	$dzpVdt$ (ms ⁻¹)	Resultant (ms ⁻¹)
Group Mean	-16.1	-25.6	5.6	-0.54	0.39	-1.01	1.32
Standard deviation	5.2	2.8	7.3	0.57	0.32	0.32	0.49
Representative trial (P6S2)	-18.3	-25.4	4.2	-0.46	0.68	-1.38	1.60

Table 9.18 - Representative players for the sprint movement.

The pitch of the representative trial is slightly lower than the mean value but the yaw and roll angles are very similar. A student's *t* test was used to evaluate the suitability of using the representative player, where *p* indicates the representative value:

$$t = \frac{\bar{X} - E}{SE_m} \quad \text{Equation 9.2}$$

where *SE_m* is the standard error of the mean (*X*) from the complete data set.

Angle	Group mean	Representative mean	<i>t</i> value	Significance
Pitch	-16.1	-18.3	1.53	<i>p</i> >.10
Yaw	-25.6	-25.4	-0.26	<i>p</i> >.10
Roll	5.6	7.0	0.69	<i>p</i> >.10

Table 9.19 - Student's *t* test results for sprint group mean and representative player trial.

There was no significant difference between the group mean and the representative player trial mean. It was therefore concluded that P6S2 could be used to represent the sprint movement.

9.5.2 Representative kick trial

A representative player trial was chosen for the kick movement in a similar fashion to the sprint group using group 2 identified through the K-means clustering. Group 2 was best represented by player 2 trial 3 (P2K3):

	Pitch (°)	Yaw (°)	Roll (°)
Centroid of Group 2	23.8	-32.8	33.4
Standard deviation	±6	±5	±5
Representative trial (P2K3)	25.0	-33.4	31.9

Table 9.20 - Representative player trial for the kick movement.

The representative player trial closely matched the centroid values for each group; the maximum absolute difference between group mean and representative angles was 1°.

9.5.3 Representative side-cut trial

After the cluster analysis, trials were removed as outliers leaving a group size of 19. The representative player trial, P2C4 was chosen from the new group.

	Pitch (°)	Yaw (°)	Roll (°)
Group mean	11.8	-21.7	-39.6
Standard deviation	4	11	9
Representative trial (P2C4)	12.6	-20.7	-36.3

Table 9.21 - Representative player trial for the side-cut movement.

The pitch and yaw angles of the representative trial closely matched the group mean (absolute difference of less than 1°). The roll angle showed a slightly larger difference 3°, but the standard deviation for the group for the yaw and roll were higher suggesting greater variability in these orientations.

9.6 Analysis of representative trials

The player trials selected to best represent the three movements were analysed using the visualisation techniques described in Chapter 5. The motion of the shoe during each movement was divided into three phases:

- Foot-strike
- Transition
- Push-off

For the sprint and side-cut movements, these phases were clearly defined with distinct transitions between each stage. For the kick movement, less emphasis was placed on the push-off stage and instead focus was placed on the motion of the shoe during ball impact. This was considered important as loss of traction during contact with the ball could affect the intended ball trajectory or speed.

For the transition phase, two types of shoe motion were selected as being significant to the traction behaviour of the shoe-surface interaction; the translation and rotation of the shoe. Changes in translation of the shoe when in contact with the surface could indicate that the shoe was slipping and that insufficient traction was available. This could compromise performance and in the most severe case lead to injury by the player

falling. The consequence of a slip is dependent upon the time at which it occurs during the movement and the distance of the slip. It has been hypothesised that the slip distance a human is able to perceive is > 30 mm (Gronquest *et al.* 2001). McGorry *et al.* (2007) classified slip distances into the following categories:

- Non-slip < 4 mm;
- 4 mm $<$ Micro-slip < 30 mm;
- 30 mm $<$ Slide < 93 mm;
- Slip > 93 mm.

Mechanical traction testing devices typically move the shoe in translation in a posterior direction to simulate slipping during the acceleration phase of sprinting. The standard protocol at adidas uses the coefficient of traction value during the dynamic phase of the translation; i.e. when the shoe is already slipping for outsole comparisons.

To characterise slip in the results collected, the movement of the shoe in the direction of motion can be used. Slip can be thought to occur when there is significant motion in the horizontal direction but no motion in the vertical or no change in the pitch angle; this eliminates the change in the horizontal motion being caused by the shoe lifting off the surface. For the side-cut and kick movements, slip in the medial/lateral direction is also significant although not often tested by traction testing methods.

The second motion that is regularly assessed during traction testing is the rotation of the shoe. Rotations during shoe-surface contact are more complex and can either be encouraged or prevented. Encouraging rotation could potentially help reduce ACL injuries suggested to be caused by the shoe locking into the surface and transferring the point of rotation to the knee. An alternative view-point is that rotations of the shoe during certain movements may compromise performance by reducing the efficiency of the movement. Whichever approach is used, the point of rotation is important and can influence traction testing procedures and shoe design. The Reuleaux method was used for each movement to determine where the centre of rotation was positioned for each time step, and if a common centre existed about which a significant degree of rotation occurs.

For each movement, the motion of the shoe during each phase was investigated as well as an overview of the complete shoe-surface interaction.

9.6.1 Sprint analysis

The sprint trial P6S2 was selected to best represent the data set based on the orientation of the shoe at foot-strike. The player landed with the forefoot first and as such, marker P3 (metatarsal-phalangeal) was initially used to assess the motion of the shoe. The coordinates of marker P3 were set to the origin (0, 0, 0) at the time of foot-strike as defined from the peak acceleration (Figure 9.9). The position of marker P3 and the orientation of the shoe were used to identify the three phases; foot-strike, transition and push-off.



Figure 9.8 - Visual image of the left foot at 20% (0.03 s) intervals during the sprint movement from -20 to 120% contact time (motion from right to left).

Time (s)

Figure 9.9 - Acceleration of marker P3 used to define time of impact (green marker indicates maximum vertical acceleration).

Figure 9.10 - Position of marker P3 in the yz (horizontal-vertical) plane during the sprint movement (1000 Hz); green to red marker = foot-strike phase, red to blue marker = transition phase, blue to purple marker = push-off phase (arrows indicate shoe motion direction, total contact time = 0.15 s).

Figure 9.11 - Horizontal (y) and vertical (z) displacement of marker P3 (1000 Hz; contact time = 0.15 s).

Figure 9.12 - Orientation of the shoe (200 Hz; contact time = 0.15 s).

The position of marker P3 in both the vertical and horizontal directions was used to identify the initial foot-strike, transition and push-off phases. During 20 to 60% contact time, both the horizontal and vertical motion appeared to remain constant; small changes in shoe orientation were also seen during this time period. The following phases were defined:

- Foot-strike = 0 to 20%
- Transition = 20 to 60%
- Push-off = 60 to 100%

a) Foot-strike

The participant landed in a toe-down position with a pitch angle of 16.2°. There was also slight toe-out rotation with a yaw angle of 24.8°. The roll angle was minimal (0.6°) suggesting the medial and lateral sides of the shoe came into contact with the surface at the same time. From time of initial foot-strike to 0.03 s (20%) after impact there was little change in the orientation of the shoe as seen in Figure 9.8. The pitch angle reduced slightly to 14.9°, yaw angle to 23.0° and roll angle to 1.0°. The change in the vertical position of marker P3 was more substantial; from 0 to 0.03 s there was a change of 14.8 mm. The motion in the horizontal (y) was more complex, with marker P3 first moving anteriorly to the point of first contact by 5.4 mm at 0.011 s (7.33%) and then posteriorly to be positioned 1.8 mm behind the point of first contact at 0.03 s. This was similar to the motion observed in the controlled participant study (Chapter 8).

The shoe impacted the surface with a resultant velocity of 1.53 ms⁻¹. The components of the velocity were: $v_x = -0.24$ ms⁻¹, $v_y = 0.81$ ms⁻¹, $v_z = -1.11$ ms⁻¹. Figure 9.13 illustrates the shoe orientation and velocity in the dominant yz plane.

Figure 9.13 - Velocity and orientation of shoe on foot-strike during sprint movement.

The location of the forefoot studs was found by additionally tracking the toe marker (P5). The positions of stud S3 located near the metatarsal-phalangeal joint and stud S11 at the toe end of the forefoot were also analysed. To normalise the data, stud S11 was set to the origin (0, 0, 0) at time of foot-strike (0 s).

Figure 9.14 - Position history of studs S3 and S11 in the yz plane during foot-strike phase (0 – 0.03 s) (Green markers indicate the time of initial foot-strike (0 s); red indicates 0.03 s after foot-strike; arrows represent stud motion direction).

Figure 9.14 illustrates that the toe studs were first to contact the surface and throughout the foot-strike phase due to the forefoot pitch angle of approximately 5° the toe studs remained approximately 10 mm deeper into the surface than the rear forefoot studs.

b) Transition phase

The transition phase was selected to be 20 – 60% contact time; for the sprint trial this was 0.03 to 0.09 s after initial foot-strike. During this phase, all forefoot studs were in contact with the surface. The first interaction investigated was whether the shoe was observed to slip during the transition phase. The position of stud S3 was initially analysed.

Figure 9.15 - Position of stud S3 in the horizontal (y) and vertical (z) directions (red markers indicate start of transition phase, 0.03 s and blue markers end, 0.09 s).

Shortly after the start of the selected transition phase, stud S3 reached maximum vertical displacement (at 0.04 s) travelling approximately 0.8 mm after the start of the transition. After reaching maximum vertical displacement, the shoe then travelled 7.4 mm vertically upwards until 60% contact time (0.09 s). During this time period the shoe also moved 9.2 mm posteriorly (-ve y direction) and 8.4 mm medially (+ve x direction). The pitch angle of the forefoot during this time period changed from 3.8° to 16.6° , giving an overall change in pitch of approximately 12.8° . Since a change in pitch angle affects the vertical position of stud S3 it was difficult to identify whether the horizontal displacement was due to a translation along the surface (slip) or simply the pitch rotation of the shoe. The position of the toe stud, S11 was additionally analysed was observed to move by the following amount during the transition phase:

- 3.9 mm medially (+ve x)
- 13.5 mm posteriorly (-ve y)
- 13.2 mm vertically down (-ve z)

Less medial movement of the toe stud was observed compared to the rear of the forefoot (S3). However, maximum vertical position was not reached until 0.115 s (76.7%) after contact resulting in the vertical downward displacement of 13.2 mm.

The posterior motion of the toe stud was greater than the rear of the forefoot stud suggesting that the horizontal movement of the forefoot may not be wholly attributed to the change in pitch angle of the forefoot. Figure 9.16 illustrates the respective yz plane motion of the toe, mid-forefoot and rear of forefoot.

Figure 9.16 - Relative positions of studs S11, S6 and S3 during contact phase (red markers indicates 0.03 s and blue markers 0.09 s after initial foot-strike; arrows indicate stud motion direction).

The motion paths of the three forefoot markers differed distinctly in the yz plane due to the change in the x position during the time period. Only a 1° change in yaw angle was observed during the contact phase suggesting that the shoe maybe translating rather the rotating to produce the change in x position.

The centre of rotation of the forefoot during the transition phase was calculated using the Reuleaux method. For this calculation an assumption was made that there was no movement of the stud in the vertical direction.



Figure 9.17 - Plan view (xy) of forefoot stud positions and corresponding centre of rotation during the transition phase (0.03 - 0.09 s) of the sprint movement (shaded circle represents ± 1 SD of centre of rotation; arrow indicates rotation direction).

The centre of rotation for the overall transition phase was positioned on the medial side of the shoe and anterior of the toe studs. The mean standard deviation of the intersection of the perpendicular bisectors was 5.8 mm. This was considered a reasonably small standard deviation suggesting good agreement on the centre of rotation. The angle of rotation of the centre stud, S8 about the centre of rotation was 3.8° . However, the change in pitch angle and vertical displacement of the shoe during the contact phase causes the centre of rotation to be only an estimate; i.e. shoe motion is occurring in all planes (3D) not only in the xy plane (2D approximation). The validity of the centre of rotation improves when the change in pitch or vertical displacement is minimal and motion of the shoe can be represented in 2D.

c) *Push-off phase*

The final push-off phase was selected as 60 – 100% movement time; representing 0.09 s to 0.15 s for trial P6S2. Studs S11 and S3 were selected for further analysis representing the toe end and the rear end of the forefoot respectively.

Time	S11x	S11y	S11z	S3x	S3y	S3z	Pitch	Yaw	Roll
60%	-11.4	74.4	-32.1	3.7	-12.8	-6.2	-30.1	-24.1	8.0
100%	-2.2	57.6	12.8	1.3	13.1	93.6	-76.8	-14.0	18.0
A	9.2	-16.8	44.9	-2.4	25.9	99.8	-46.7	10.1	10.0

Table 9.22 - Position of studs S3 and S11 and orientation of the shoe at push-off phase (position in mm, angle in °).

Figure 9.18 - Motion path of studs S3 and S11 in the yz and xz planes (Blue marker indicates start of push-off phase, purple marker end of push-off phase).

The position of the studs S3 and S11 relative to each other combined with the change in pitch and yaw angles suggested that the shoe was both rotating in the yz plane but also a small rotation in the xy plane causing stud S11 to move medially and stud S3 to move laterally. The pitch angle of the forefoot at the start of the push-off phase was 16.6° (toe-down). By the end of the movement the pitch angle had increased to 52.1°. This signified a rate of change in pitch angle of approximately 710°/s (12.4 rads). The change in pitch angle also affected the number of studs in contact with the surface. As

the pitch angle increased, the number of studs decreased until at 95% contact time, just the front two toe studs were in contact.

Observing the motion of the studs during the selected time period (Figure 9.18), the dominant motion appeared to be a rotation in the yz plane with the centre of rotation nearer the toe end of the forefoot, causing the rear of the forefoot (S3) to rise of the surface at a greater rate than the toe of the forefoot (SI 1). This was expected during a natural push-off movement. There was also movement in the xz plane caused by the change in yaw and roll of the shoe.

For the motion in the yz plane, the centre of rotation was calculated using the 2D Reuleaux method detailed in Chapter 5. This approach assumes that the movement in the x direction was negligible. The centre of rotation was calculated from the start of push-off (0.09 s) to the end of push-off (0.15 s).

Figure 9.19 - Centre of rotation and resulting path of movement; blue markers indicate start of push-off (0.09 s) and purple markers end of push-off phase (0.15 s); dashed lines represent the motion path assuming a rigid system rotating about the calculated centre of rotation (red marker).

**Point of
rotation**

Figure 9.20 – Fixed system rotation for forefoot during sprint movement in yz plane (blue indicates starting position and purple represents the position at the end of movement).

Figure 9.19 shows the centre of rotation for the push-off stage of the movement. The resulting motion path is also shown assuming a fixed system (Figure 9.20). As shown, for the rear forefoot stud (S3), the motion path resulting from a fixed centre of rotation provides a good match for the measured motion path. However, the toe stud (SI1) resulting path does not follow the exact shape of the measured path; whilst it appeared that the rear of the forefoot was rotating, the toe end of the forefoot potentially also underwent posterior translation which modified the curvature of the path in the yz plane.

One of the assumptions made using this approach was that the studs only moved in the yz plane; there was however 9.2 mm lateral and 2.4 mm medial of movement in the x direction seen in the rear forefoot (S3) and toe end of the forefoot (SI 1) respectively. The x displacement was approximately one third of the movement seen in the y and z directions.

The distance between studs S3 and SI1 in 3D was 91.9 ± 0.2 mm and in 2D in the yz plane 91.2 ± 0.2 mm. A difference of 0.7 mm was seen between the actual 3D position and the 2D approximation. This difference was considered negligible compared to the potential propagated error inherent in the stud position calculation (maximum ± 2.2 mm) suggesting that the dominant motion occurred in the yz plane.

A concern when observing the movement of the shoe during the push-off phase was that excessive flexion of the mid-foot could introduce error into the derivation of the forefoot stud positions. The distance between the marker P3 and P5 on the side of the shoe was calculated at each time step to ensure that the shoe was not flexing. The distance was 82.8 ± 3.1 mm ($\pm 1SD$). The standard deviation was approximately 3.6%

of the distance between the markers. This deviation was not deemed large enough to suggest that the shoe was flexing excessively during the movement.

The shoe left the surface with a resultant velocity of marker P3 of 3.37 ms⁻¹. The components of the velocity were: $v_x = -0.12$ ms⁻¹, $v_y = 1.57$ ms⁻¹, $v_z = 2.98$ ms⁻¹. The anterior-posterior and vertical velocity components were greater than those observed on impact. This could suggest that the acceleration was observed with the shoe leaving the surface at a greater velocity to impact.

9.6.2 Side-cut analysis

Player 2 side-cut trial 4 (P2C4) was chosen as the representative player for the side-cut movement. The vertical acceleration of marker P1 was used to identify the time of initial foot-strike. Initial foot-strike was in a toe-up position, predominantly on the lateral side of the shoe. After foot-strike, full shoe contact was observed until the participant had changed direction and underwent the push-off phase in a similar style to the sprint movement. For this reason, the position of stud S3 was used to identify the three stages of motion; foot-strike, transition and push-off as it was in contact with the surface for longer. Similar to the sprint movement, the orientation and position of the shoe was used to identify the phases.

Figure 9.21 – Visual image of the left shoe during the side-cut movement (from -20 to 120% contact time, at 20% (0.06 s) intervals; motion from right to left).

Time (s)

Figure 9.22 - Orientation of the shoe during the side-cut movement (200 Hz); green to red markers = foot-strike phase, red to blue markers = transition phase, blue to purple markers = push-off phase.

Time (s)

Figure 9.23 - Horizontal (y) displacement of stud S3 during the side-cut movement.

Time (s)

Figure 9.24 - Vertical (z) displacement of stud S3 during the side-cut movement.

Figure 9.25 - Horizontal (x) displacement of stud S3 during the side-cut movement.

The yaw and roll angle changed at a near constant rate during the movement whereas the pitch angle was observed to lessen the rate of change during the time phase 20 to 60% contact time. During this time there was also a decrease in the rate of change in the vertical direction of stud S3. Consequently, the following phases were identified:

- Foot-strike = 0 to 20%
- Transition = 20 to 60%
- Push-off = 60 to 100%

These are the same percentage contact time as the sprint movement. However, the duration of contact time for the side-cut movement was doubled; with the side-cut trial having a movement phase of 0.3 s compared to 0.15 s for the sprint trial (P6S2).

a) Foot-strike

The shoe initially landed in a toe-up position with a pitch angle of 14.3° . The shoe was also externally rotated with a yaw angle of 21.4° (toe-out) and an inward roll angle of 37.6° . The high inward roll angle resulted in the medial sided studs impacting the ground first. During the selected foot-strike phase, the pitch angle reduced to 4.9° and the roll angle reduced to 24.9° causing the shoe to be at a flatter angle on the surface, although still predominately on the medial side. The yaw angle increased during the foot-strike phase, further increasing the external rotation by 6.3° .

The shoe impacted the surface with a resultant velocity of 1.43 ms^{-1} . The components of the velocity were: $v_x = -1.38 \text{ ms}^{-1}$, $v_y = 0.15 \text{ ms}^{-1}$, $v_z = -0.33 \text{ ms}^{-1}$. This differed

significantly from the sprint movement with the dominant velocity component acting in the lateral (-ve x) direction as opposed to anteriorly (+ve y).

As the shoe impacted first on the medial side, stud S2 was the first stud to contact the surface. The motion of studs S1, S2 and S3 representing the lateral and medial sides of the heel and the lateral rear of the forefoot respectively, during the initial stages of foot-strike were analysed.

Time	S1x	S1y	S1z	S2x	S2y	S2z	S3x	S3y	S3z
0%	0	0	0	26.5	15.5	-18.7	-51.0	126.1	32.1
20%	-11.3	1.5	-4.7	17.6	17.8	-18.5	-76.4	125.0	5.9
A	-11.3	1.5	-4.7	-8.9	2.4	0.2	-25.4	-1.1	-26.2

Table 9.23 - Position of studs S1, S2 and S3 (in mm).

Over the 0.06 s of the initial foot-strike phase, the heel studs S1 and S2 moved less than 5 mm in the vertical (z) direction. Movement in the anterior-posterior (y) direction was similarly small. In comparison, significant motion was observed in the lateral (-ve x) direction. At 0.06 s after foot-strike, both studs S1 and S2 reach maximum lateral displacement. The rear of forefoot (S3) also had substantial lateral motion but also showed large displacements in the z direction. This was primarily due to the change in pitch angle of the shoe. The difference in vertical displacement between the medial stud (S2) and lateral studs (S1, S3) is likely to have occurred due to the change in roll angle of the shoe (-12.7°). In comparison to the changes in pitch and roll angles, the change in yaw angle was small (+6.3°) and although may contribute to the differences in lateral displacement of the studs it is unlikely to be the sole contributor. Stud S2 has very little motion in any direction other than laterally. This suggests that the shoe is slipping on the surface as it undergoes a change in orientation. The potential slip distance of the shoe was 8.9 mm. Using the McGorry *et al.* (2007) classification, the slip is described as a micro-slip but is unlikely to have been perceived by the participant. The speed of the slip was approximately 150 mms⁻¹. The lateral displacement of the heel studs is very rarely assessed when undergoing traction testing but slipping at the early stage in the side-cut movement could affect performance or injury.

b) Transition phase

The transition phase of the side-cut movement was selected to be 20 – 60% movement time (0.06 – 0.18 s after impact). During this time period there was little change in the pitch or yaw angles of the shoe (-6.5° and 5.6° respectively). There was however notable change in the roll angle of the shoe, reducing from 24.9° to 12.4°. The position of studs S1, S2, S3 and S11, representing the lateral and medial heel, rear of forefoot and toe respectively, were analysed to determine whether the shoe was slipping or rotating during the transition phase.

Time	S1x	S1y	S1z	S2x	S2y	S2z
20%	-11.3	1.5	-4.7	17.6	17.9	-18.5
60%	-5.8	-1.0	-3.9	23.5	18.0	-12.1
A	5.5	-2.5	0.8	5.9	0.1	6.4

Table 9.24 - Position of lateral (S1) and medial (S2) heel studs (in mm).

Time	S3x	S3y	S3z	S11x	S11y	S11z
20%	-76.4	125.0	5.9	-90.1	210.0	-7.4
60%	-82.7	115.9	-7.1	-106.9	200.8	-11.5
A	-6.3	-9.1	-13.0	-16.8	-9.2	-4.1

Table 9.25 - Position of rear of forefoot (S3) and toe (S11) studs (in mm).

The greater change in the vertical position of the medial heel stud compared to the lateral side emphasises the change in roll angle of the shoe. The forefoot studs displayed a greater vertical displacement than the heel studs which could be caused by the small change in pitch angle of the shoe. Very little change in the anterior-posterior direction was seen for either heel stud. However, both the forefoot and toe studs showed a displacement in the posterior direction of approximately 9 mm. All studs displayed a medial-lateral displacement, with the heel studs moving medially and the forefoot studs laterally. The toe stud (S11) also showed greater lateral displacement. Despite the small change in yaw angle of the shoe, the differences in medial-lateral position of the heel and forefoot studs suggested the shoe may be rotating. The observation of the greater lateral displacement at the toe end of the forefoot and the inverse in medial-lateral displacement between the heel and the forefoot suggested that the point of rotation may be situated nearer the heel.

Shoe rotation was therefore investigated in the xy plane assuming no vertical displacement; the centre of rotation was found using the Reuleaux method.

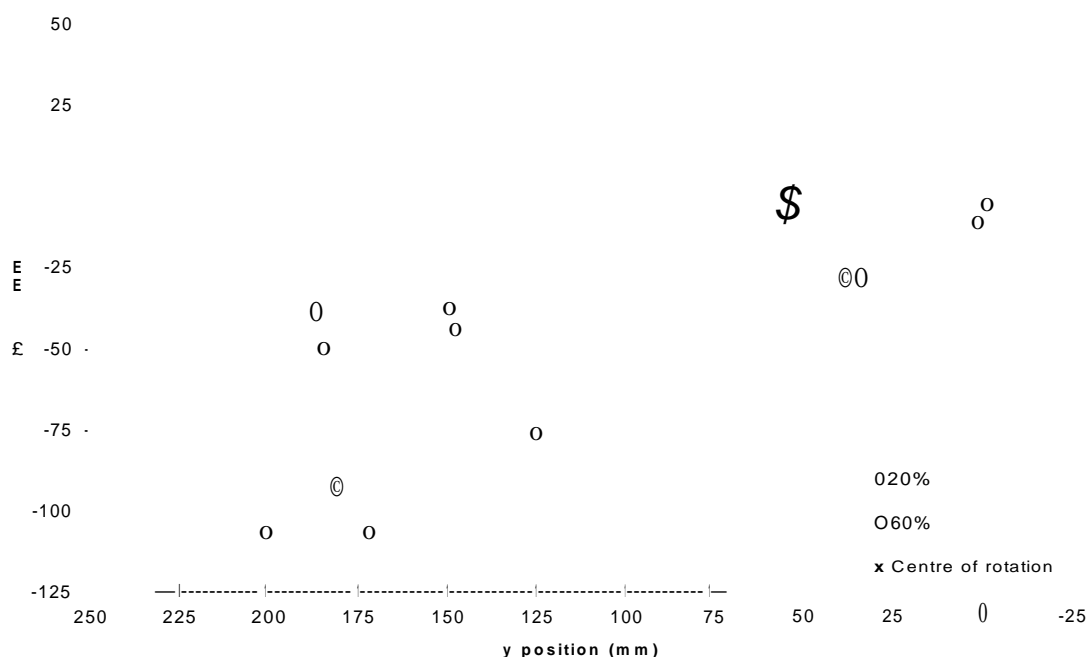


Figure 9.26 - Centre of rotation of the transition phase in the side-cut movement (shaded area indicates ± 1 SD for the calculation of the centre of rotation).

The centre of rotation was located on the medial side of the heel as anticipated. The standard deviation of the intersection of the perpendicular bisectors was ± 18.0 mm. This is greater than the standard deviation seen in the location of the centre of rotation in the sprint movement, but still only represents 8% of the distance from the rear heel to the front toe stud. Typically during traction testing, the centre of rotation is positioned in the middle of the forefoot, rotating about the heel is again not a movement often considered.

c) *Push-off phase*

The push-off phase was the final 60 - 100% movement time. During this stage, similar motion to the push-off phase in the sprint movement was observed. There was little change in the yaw and roll angles of the shoe ($+1.8^\circ$ and -4.8°) but notable change in the pitch angle of the shoe (49.1°) to a toe-down position. During this stage of the movement, the heel rotated off the surface leaving only the forefoot studs in contact. Table 9.26 and Figure 9.27 outline the change in position of the heel, rear of forefoot and toe studs (SI, S3 and Si1 respectively).

Time	S1x	S1y	S1z	S3x	S3y	S3z	S11x	S11y	S11z
60%	-5.8	-1.0	-3.9	-82.7	115.9	-7.1	-106.9	200.8	-11.5
100%	-15.1	48.9	152.8	-88.1	134.2	69.7	-109.4	197.3	11.0
A	-9.3	49.9	156.7	-5.4	-18.3	76.8	-2.5	3.5	22.5

Table 9.26 - Position of studs S1, S3 and S11 (in mm).

Figure 9.27 - Position of studs S1, S3 and S11 in the xz and yz planes (blue markers indicate start of push-off (0.18 s) and purple markers end of push-off (0.28 s)).

The dominant displacement was in the yz plane similar to the sprint movement. Figure 9.28 shows the difference in the motion paths of studs S3 and S11 during the push-off phase (60 – 100%) for each movement. The yaw position of the shoe was different for each movement (24.1° for the sprint and 33.3° for the side-cut) leading to potential discrepancies in the motion paths. However, despite the difference in yaw angle, the motion path of the rear of forefoot stud S3 was similar for both movements. The sprint movement started in a toe-down position, with the shoe in the side-cut movement being at a more neutral angle at the start of push-off. The most notable difference was in the motion path of the toe stud S11. The sprint movement showed a clear posterior translation of the shoe which also acted vertically downwards at the commencement of push-off. This was not as notable in the side-cut movement and could indicate that the slight posterior slip of the toe was seen in the sprint movement. The resultant direction in the sprint movement was also in the anterior-posterior direction whereas the side-cut intended trajectory was at 45° to this. However, small translations in the lateral direction of the forefoot studs were seen (> 5 mm) as noted in the sprint movement.

Figure 9.28 - Motion path of studs S11 and S3 during the push-off stage in the sprint and side-cut movements.

The shoe left the surface with a resultant velocity of marker P3 of 2.24 ms⁻¹. The components of the velocity were: $v_x = 0.14$ ms⁻¹, $v_y = 1.55$ ms⁻¹, $v_z = 1.61$ ms⁻¹. The horizontal velocity components were similar to the sprint push-off movement, with the lower resultant velocity caused by a significantly lower vertical component. This suggests that during the push-off movement, the participant was not accelerating away from the surface with the same emphasis as seen in the sprint movement.

9.6.3 Kick analysis

A representative trial (P2K3) from the larger group was selected for the kick movement. The shoe was observed to land in a toe-up position, as such, marker P1 was used to identify the time of initial foot-strike using the vertical acceleration. The kick movement differed from both the sprint and the side-cut movement as there was no defined time of push-off. During the kick movement, the important stage was during ball contact with the kicking foot. Slipping or loss of traction of the planted foot during

this time phase could affect the final trajectory or speed of the ball. Figure 9.29 illustrates the planted foot position at foot-strike, ball contact and end of the movement.

Figure 9.29 - Visual image of planted left foot during the kick movement at foot-strike, ball contact, end of ball contact and end of movement (motion from right to left).

For this trial, ball contact occurred at 0.127 s after impact (49% movement time). The pitch orientation of the shoe prior to this time was used to define the transition between the foot-strike phase and ball contact phase (Figure 9.30).

Time (%)

Figure 9.30 - Pitch angle of the planted foot during kicking.

During the time period 25 - 65% contact time, a change in pitch angle of only 8.9° was observed as the shoe moved from 1.1° (toe-up) to -7.8° (toe-down). Ball contact occurred at approximately 50% movement time where the shoe was at a pitch angle of -3.9° (toe-down). The change in pitch angle during this time was minimal compared to the initial change in pitch angle from 0 to 25% contact time (17.9°) and as such, the following phases were defined:

- Foot-strike = 0 to 25%
- Ball contact = 25 to 65%
- End phase = 65 to 100%

The initial foot-strike phase and ball contact phase were further analysed to investigate the interaction between the shoe and the surface for this movement.

a) Foot-strike

Similarly to the side-cut movement, the shoe was observed to land in a toe-up position, although at a slightly higher angle (19.0°). A toe-out position of the shoe was also seen with a yaw angle of 32.1°. The orientation of the shoe differed from the side-cut movement with the lateral side of the shoe coming into contact first with a roll angle of 29.8° (outward roll).

The shoe impacted the surface with a resultant velocity of 2.64 ms⁻¹. The components of the velocity were: $v_x = 1.47$ ms⁻¹, $v_y = 2.00$ ms⁻¹, $v_z = -0.91$ ms⁻¹. This was the highest resultant velocity seen out of the three movements analysed with significant influencing components in the medial and anterior directions.

During the selected foot-strike phase (0 – 25%) the shoe underwent changes in pitch, yaw and roll and in all three displacement directions. Table 9.27 and Table 9.28 highlight the difference in orientation and position of the lateral heel (S1), medial heel (S2) and rear forefoot (S3) during the selected time period.

Time	S1x	S1y	S1z	S2x	S2y	S2z	S3x	S3y	S3z
0%	0	0	0	26.4	9.8	22.3	-74.4	111.6	38.3
25%	42.3	24.6	-22.4	73.0	42.0	-14.9	-26.9	146.3	-20.0
A	42.3	24.6	-22.4	46.6	32.2	-37.2	47.5	34.7	-58.3

Table 9.27 - Position of studs S1, S2 and S3 (mm).

Time	Pitch	Yaw	Roll
0%	19.0	-32.1	29.8
25%	1.1	-29.7	11.4
A	17.9	2.4	18.4

Table 9.28 - Orientation of the shoe (°).

The most dominant displacement direction was medially with the shoe moving approximately 45 mm. Significant motion was also observed in the anterior direction with 25 – 35 mm of displacement recorded for the heel and forefoot studs respectively.

Vertical displacement of 22.4 mm was observed for the lateral heel stud, the vertical displacement of the medial stud was greater at 37.2 mm. This difference in vertical position between the medial and lateral heel studs is represented in the high outward roll angle observed on impact. By 25% movement time, the roll angle had lessened, reducing the medial-lateral heel difference to less than 10 mm. The forefoot stud showed a vertical change in position of 58.3 mm. This was notably greater than either of the heel studs. The difference in vertical motion of the forefoot and heel is due to the change in pitch angle of the shoe. Very little change in yaw angle was observed during the impact phase.

The consistency of horizontal displacement in both the medial and anterior directions of both medial and lateral heel studs and the forefoot stud suggests that although the shoe was undergoing changes in pitch and roll angle, it was also translating in a medial-anterior direction, predominantly on the lateral side of the shoe. This angle of shoe and translation direction is again a scenario rarely tested in traction assessments.

b) Ball contact

The motion of the planted foot during ball contact could influence the trajectory and resultant speed of the ball. For the selected trial, ball contact with the kicking foot occurred at 0.127 s (50%) after impact. The movement time 25 to 65% was analysed to assess for changes in orientation or shoe position of the planted foot.

Time	S1x	S1y	S1z	S2x	S2y	S2z	S3x	S3y	S3z
25%	42.3	24.6	-22.4	73.0	42.0	-14.9	-26.9	146.3	-20.0
50%	39.5	26.8	-12.0	71.4	43.0	-7.8	-22.9	151.9	-20.6
65%	31.8	24.0	-4.5	64.4	39.3	-2.2	-26.1	150.3	-21.9

Table 9.29 - Position of studs S1, S2 and S3 (mm).

Time	Pitch	Yaw	Roll
25%	1.1	-29.7	11.4
50%	-3.9	-26.5	8.5
65%	-7.8	-24.5	7.0

Table 9.30 - Orientation of the shoe (°).

From end of foot-strike (25%) to ball contact (50%) the most dominant displacement change was in the vertical direction. Approximately 2 mm of movement was seen in the horizontal directions compared to just less than 10 mm in the vertical motion of the heel. This suggests that as the kicking foot moved from behind the body to in line with the planted foot, the transfer of weight caused the planted foot to compress further into the surface. From the start to the end of the ball contact phase (50 – 65%) displacement in the horizontal direction was greater, but not notably so.

Throughout the ball contact phase, the pitch angle changed by 8.9° as the foot moved from a toe-up to a toe-down position. This change was minimal and together with the greater vertical displacement of the heel compared to the forefoot suggested the weight was being transferred from the heel to the forefoot as the kicking leg swung through. The yaw angle changed by 5.2° and the roll angle by 4.1° . Both changes were small compared to the initial change in angle during the impact phase.

Although slight translations and change in orientation were observed throughout the ball contact phase, the overall motion of the shoe was minimal suggesting that for this trial, the planted foot remained stable throughout the movement.

9.7 Chapter summary

Data collection

Approximately 60% of the trials captured using the Doncaster Rovers Youth team were suitable for tracking, resulting in over 23,000 marker coordinates. Post processing was then carried out on the tracked markers to give stud coordinates, shoe orientation and velocity at each time step (at 1000 fps). The acceleration of the impacting marker was used to normalise the time and marker coordinates were set to the origin at this time.

Statistical analysis

The orientation and velocity on foot-strike and push-off (sprint only) were identified for each successful trial. These values were then used as variables for comparison. Statistical analysis was performed on each group to identify outliers or further groupings. Due to the sample size for the sprint and the side-cut, only outliers were

identified. K-means cluster analysis on the kick results suggested that the data could be split into groups of high or low impact angles.

Movement analysis

Representative player trials for each movement were selected. The trial closest to the mean for all three angles was chosen. The representative player trial was then used in the next stage of post processing; visualisation and informatics. For each movement trial, the motion was divided into distinct stages based on the position and orientation of the shoe. For the sprint and side-cut movement, foot-strike, transition and push-off phases were highlighted. For the kick movement, the important phase was considered to be when the kicking foot made contact with the ball contact and so two phases, foot-strike and ball contact were selected. Particular attention was taken on the translation and rotation of the shoe during the transition stage; with changes in translation being early indicators of the shoe slipping during contact with the surface. The following conclusions were drawn for each movement.

During the sprint movement the shoe initially landed in a toe-down position. Immediately after foot-strike, there was slight posterior motion of the shoe but also change in yaw and roll angles lessening the significance of any displacement. The change in medial-lateral displacement during the transition phase was partially attributed to a rotation of the forefoot about a point positioned anterior of the medial toe studs. During the push-off phase a potential micro-slip of 16.8 mm of the toe studs was observed. During this phase the shoe was rotating in the yz plane causing the rear of the forefoot to rise at a greater rate than the front. Using the Reuleaux method, the centre of rotation was estimated to be slightly above the toe. The motion path of the rear of forefoot studs matched the predicted path using a fixed system about the calculated centre of rotation. However, the motion path for the front toe stud differed from the predicted path implying that the toe may be susceptible to posterior slip during this phase. In the final moments of push-off only the front two toe studs were in contact with the ground. The potential slip during this period could indicate that additional studs or a change in stud orientation is required to improve the traction performance.

For the side-cut movement the shoe was observed to land in a toe-up position with slight yaw (toe-out) and significant roll (inward) angles. This caused the medial side of the shoe to come into contact with the surface first. During the initial stages of foot-

strike significant motion in the lateral direction was seen (8.9 mm). Although the lateral motion was accompanied by a change in roll angle of the shoe, the displacement occurred predominantly on the medial side of the shoe. This is a direction and shoe orientation rarely assessed in traction testing but slip during this early stage in the side-cut movement could potentially cause injury or impede performance. During the transition phase, a greater medial-lateral displacement of the forefoot studs compared to the heel studs indicated that the shoe was rotating. The centre of rotation was estimated to be positioned on the medial side of the shoe, near the front heel stud. The standard deviation of the intersection of the perpendicular bisectors was 18.0 mm. This suggests that the centre of rotation is subject to some error due to the change in orientation of the shoe during this stage. It does however indicate a potential rotation configuration that again is not assessed in traction testing. The push-off phase of the side-cut movement was very similar to the sprint movement. The side-cut motion did not however display the posterior slip of the toe studs heightening the importance of that motion in the sprint movement.

The planted foot during kicking was also observed to land in a toe-up position with a notable yaw angle (toe-out). But for the kick movement, the shoe landed with outward roll rather than inward roll as observed in the side-cut. This lead the lateral heel studs to come into contact with the surface first. The resultant velocity on foot-strike was greatest for the kick movement and acted predominantly in the medial direction. During the initial stages of foot-strike, the pitch and roll angles reduced causing the shoe to be at a flatter angle to the surface with both the forefoot and heel in contact. During the phase leading to and directly following ball contact with the kicking foot, no notable movement of the planted foot occurred. Slight changes in pitch angle and vertical stud position were observed but attributed to the change in centre of mass as the kicking leg swung through.

The following figures summarise the motion of the shoe for each of the three movements.

	Foot-strike	Transition	Push-off
Sprint movement			
<i>Time (% contact):</i>	0-20%	20 – 60%	60- 100%
<i>Dominant movement direction:</i>	Posterior	Posterior & medial	Posterior
<i>Centre of rotation:</i>	N/A	Medial forefoot	N/A
<i>Orientation at start of phase:</i>	(-16.2°, -24.8°, 0.6°)	(-14.9°, -23.0°, -1.0°)	(-30.1°, -24.1°, 8.0°)
<i>Change in orientation:</i>	Reduction in pitch (+2°)	Increase in pitch (-15°), increase in roll (+9°)	Increase in pitch (-47°), decrease in yaw (+10°), increase in roll (+10°)

Figure 9.31 - Summary of shoe motion during the sprint movement.

	Foot-strike	Transition	Push-off
Side-cut movement			
<i>Time (% contact):</i>	0 – 20%	20 – 60%	60- 100%
<i>Dominant movement direction:</i>	Lateral	External rotation	Posterior
<i>Centre of rotation:</i>	N/A	Medial heel	N/A
<i>Orientation at start of phase:</i>	(14.3°, -21.4°, -37.6°)	(4.9°, -27.7°, -24.9°)	(-1.6°, -33.3°, -12.4°)
<i>Change in orientation:</i>	Decrease in pitch (-5°), increase in yaw (-6.3°), decrease in roll (+12.7°).	Decrease in roll (+12.5°).	Increase in pitch (-43°).

Figure 9.32 - Summary of shoe motion during the side-cut movement.

Foot-strike**Ball contact****Kick movement**

<i>Time (% contact):</i>	0-25%	25 – 65%	
<i>Dominant movement direction:</i>	Anterior & medial	Stationary	Anterior
<i>Centre of rotation:</i>	N/A	N/A	N/A
<i>Orientation at start of phase:</i>	(19.0°, -32.1°, 29.8°)	(1.1°, -29.7°, 11.4°)	(-7.8°, -24.5°, 7.0°)
<i>Change in orientation:</i>	Decrease in pitch (-18°), decrease in roll (-18°)	Minimal, slight decrease in pitch (-8.9°)	Increase in pitch.

Figure 9.33 - Summary of shoe motion during the kick movement.

The next stage of the study would be to expand the data collection to include a wider population with a range of different shoes, surfaces and movements. However, the intention of the study at this level was to provide an example of how the 3D measurement system can be used to aid in the understanding of the shoe-surface interaction. The results can have an implication on both the approach used in traction testing methodologies and in outsole design. The next chapter speculates on what these implications might be using the data collected at Doncaster Rovers FC as an example.

10 INFLUENCE OF SHOE-SURFACE INTERACTIONS ON TRACTION TESTING PARAMETERS

10.1 Introduction

Although the data set collected at Doncaster Rovers FC was limited in both sample size and test variables, the in depth analysis of the three representative movement trials was successfully used to give an indication on the level of detail available by using the 3D measurement system. The post processing analysis of the 3D marker coordinates enabled information on stud position and velocities to be obtained even though the studs were not visible due to penetration into the surface. This provided further understanding into the shoe-surface interaction giving rise to detailed information on possible translations and rotations during the foot-strike, transition and push-off stages in each movement.

The knowledge gained from the data collected to date was used to lay the foundations on how further understanding the shoe-surface interaction can influence the test parameters used in assessing the traction performance of outsoles. Three traction testing methodologies evaluated in Chapter 3 were further investigated in light of the results from player testing.

10.2 Mechanical traction testing

The adidas traction testing device was used as an example mechanical test method as detailed information on the current testing procedure and limits of the device were available (Table 10.1).

	Test distance	Maximum distance	Test speed	Maximum speed
Translation	50 mm	450 mm	10 mms ⁻¹	300 mms ⁻¹
Rotation	60°	180°	12°s ⁻¹	200°s ⁻¹

Table 10.1 - Current test parameters and limits of the adidas traction tester, total load = 69.3 kg.

A fixed last with shoe angle 18.1° (pitch) was used for the collection of data in Chapter 3. No set shoe angle is defined in the standard test procedure which can lead to inconsistencies within test repeats. A shoe angle of 18.1° generally enabled only the

forefoot of the shoe to be in contact with the surface, however, on softer ground or with shoes with longer stud length, the heel studs also came into contact. This again can cause differences between tests.

Two options present themselves when considering the realism of the current mechanical traction testing device and how the observations of the shoe-surface interaction during football related movements may influence the testing parameters:

- 1) Modification of the test parameters of the existing device to better suit the actual rotation and translation distances and speeds;
- 2) Redesign of the device to better mimic the complete shoe motion.

Both approaches were considered.

10.2.1 Recommendations for existing traction testing device

The current test set-up allows the shoe to be moved in translation or rotation. The angle of the shoe can be modified to account for different shoe orientations, although the shoe angle must remain fixed during testing. To ensure a full range of boundary conditions are tested, all three movements (sprint, kick and side-cut) need to be taken into consideration. Analysis of each movement showed that the motion of the shoe was complex and to fully replicate complete motion, changes in orientation and position must be applied simultaneously. This is not possible using the current traction tester and therefore the movement needed to be simplified. To do this, the critical time period was identified where it was estimated that the participant was at most at risk of slipping. The motion of the shoe during this time period was assessed and suitable approximations for the translation and rotation of the shoe were made. Loads were estimated from the force-plate data obtained in Chapter 8.

a) Selection of critical slip time

The first stage in identifying appropriate test parameters was to identify the time during each movement where the player was thought to be at greatest risk of slipping. This assessment can be very subjective and is strongly dependent on surface conditions and selection of footwear. The following approach used the single participant test data collected on a force-plate in the laboratory with artificial turf (Chapter 8).

Identifying risk factors

The following factors were selected as being influential on the likelihood of slipping:

1. Ratio of horizontal to vertical force;
2. Magnitude of horizontal force;
3. Magnitude of horizontal velocity;
4. Number of studs *not* in contact with the ground.

The ratio of horizontal to vertical force is often referred to as the required coefficient of friction (RCOF). As the required coefficient of friction becomes close to or greater than the available coefficient of friction (traction) the risk of slipping increases. However, as both the vertical and horizontal force approach zero (occurring on foot-strike and the later stages of push-off) the ratio increases rapidly, tending to infinity. This can mask other areas of importance during the movement. To overcome this, the magnitude of the horizontal force is also taken into consideration, with the hypothesis that the greater the horizontal force, the greater the risk of slipping. The ratio of horizontal to vertical force has been used in literature to indicate periods requiring high traction requirements (Shorten *et al.* 2003, Luo and Stefanyshyn 2011).

The horizontal velocity was included to incorporate the movement of the shoe during contact. If the horizontal velocity on foot-strike is greater than on push-off, this could indicate that the foot-strike has a greater risk of slipping than push-off. Slipping during surface contact would also be registered with an increase in velocity. The number of studs not in contact with the surface is an important consideration; ideally, to increase the level of traction, all available studs should be in contact.

Each factor was calculated as a percentage of the absolute maximum seen during the movement. For the side-cut and the planted foot in kicking, the number of studs not in contact was not included as it was not possible to see the studs due to the camera angles. For these two movements, the horizontal force and velocity in the medial-lateral direction in addition to the anterior-posterior direction was included.

Each risk factor was examined and an overall grip factor given by calculating the normalised mean of all contributors. A high grip factor indicated a high level of traction was required during the selected phase of the movement.

Sprint grip factor

For the sprint movement, the following were assessed:

- Horizontal force in the running direction;
- Ratio of horizontal to vertical force;
- Velocity of the lateral metatarsal-phalangeal stud in the running direction;
- Number of studs not in contact with the surface.

Figure 10.1 - Percentage of absolute maximum for contributing grip factors in the sprint movement.

The horizontal force reached a maximum at 70% contact time. This was previously termed time of peak push-off and corresponds to the time the foot is rotating with the forefoot in contact and the heel pitch angle increasing. The peak of the vertical force occurred earlier than this, leading to the later peak in the ratio of horizontal to vertical force (at 80%). There was also a peak in RCOF at the beginning of the movement when both horizontal and vertical forces were small. The velocity decreased from 20% of maximum to near stationary at 10% contact time but rapidly increased at the peak push-off (70 - 80% contact time). Similarly, as the heel pitch angle increased the number of studs in contact with the surface reduced; at the last moments of push-off, only the two toe studs were in contact.

An overall grip factor for the sprint movement was calculated from a normalised mean of the above contributors with equal weighting for each. Using a safety factor of 2 (i.e. grip factor of 0.5) the period most at risk from slipping was 60 - 100% contact time (Figure 10.2).

Figure 10.2 - Resulting grip factor for the sprint movement with a safety factor of 2.

The resulting grip factor indicated that the push-off phase of the sprint movement potentially required a higher level of traction than the initial foot-strike phase. The consequence of slipping during this time period could result in the player unable to accelerate to their full potential, or slip forwards onto the surface if their body weight was already committed to the movement.

Planted kicking foot grip factor

For the kick movement, the medial/lateral (x) force was also included as a contributing factor allowing two force ratios to be calculated, i.e. $RCOF_x = F_x/F_z$ and $RCOF_y = F_y/F_z$. Unlike the sprint movement, the kick movement displayed a high velocity in the medial direction on foot-strike. The velocity in the anterior direction was also high on foot-strike, but also showed a peak towards the end of the movement as the foot began to move off the surface. The anterior-posterior force reached a peak at 40% of the movement time, whereas the medial-lateral force peaked slightly earlier at 20% movement time. However, despite the early peaks in horizontal force, the ratio of horizontal to vertical was greatest at the latter stages of the movement. The normalised mean of the contributing factors was again calculated to see which stage was potentially at greatest risk of slipping.

Magnitude (%)

Magnitude (%)

Magnitude (%)

Figure 10.3 - Percentage of absolute maximum for contributing factors in the kicking movement.

Figure 10.4 - Resulting grip factor for kick movement with a safety factor of 2.

Figure 10.4 shows that the time of greatest risk of slipping was between 5 and 25% of contact time. This highlights that the important stage in terms of ensuring there is sufficient traction in the kick movement is on foot-strike, whereas for sprinting the push-off is potentially more important. For the kick movement, ball impact occurred at approximately 47% of contact time. This falls after the selected critical period but previous analysis of shoe motion during kicking indicated that minimal shoe motion was observed after 25% contact time (Chapter 9).

The consequence of slipping during the highlighted time period could affect the player's kicking performance as slip occurs before contact with the ball. A change in the positioning of the support foot could affect the trajectory and placement of the ball; this was most recently shown during the Wales v France Rugby World Cup 2011 semi-final where James Hook's planted foot slipped during the penalty kick causing the ball to go wide. A 'greasy' surface caused by a short rain shower before the game was primarily blamed for Hook's slip (Rugby World 2011). Figure 10.5 illustrates the high outward roll angle seen on foot-strike causing the traction requirements to be heavily weighted on the lateral side of the shoe. Using the diameter of the ball as a point of reference, an estimate on the slip distance of the planted foot was made. The foot was observed to slip approximately 24 cm in a medial-anterior direction; this was much higher than any translation distance observed during player testing, highlighting the effect of surface conditions on the shoe-surface interactions.

Figure 10.5 – Slip of the planted foot during Hook's penalty kick during the Wales v France World Cup semi-final, 2011 (Screen shots taken from video from ITV pic. 2011).

Side-cut grip factor

For the side-cut movement, the force and velocity in the medial-lateral direction (F_x) as well as anterior-posterior direction (F_y) were also included.

Figure 10.6 - Percentage of absolute maximum for contributing factors in the side-cut movement.

The magnitude of the force acting in the anterior/posterior direction (F_y) was less consistent than for the other movements. The medial/lateral force (F_x) shape was very similar to the kick movement, reaching a peak at approximately 40% contact time. The required coefficient of friction in the anterior/posterior direction was greatest at the beginning of the movement, whereas in the medial/lateral direction the RCOF remained at a level of 40% for the majority of the movement, with a minimum dip at the

beginning and a maximum rise at the end of the movement. This suggested that the motion in the medial/lateral direction is an important feature of this movement. The normalised mean of the contributing factors was calculated and is shown in Figure 10.7.

Figure 10.7 - Resulting grip factor for side-cut movement.

Using this approach, for the side-cut movement no clear time period of greatest risk was identified. Both the foot-strike and the push-off stage require a grip factor greater than 0.50. Chapter 9 identified the side-cut movement as showing the greatest amount of translation of the shoe during the contact period. The consequence of slipping at any selected time period is also an important consideration. The latter stages of the side-cut movement display a propulsive push-off similar to the sprint movement, slipping at this time period would compromise acceleration and stability in the anterior direction. Chapter 9 highlighted that the foot-strike motion of the shoe was unique to the side-cut movement, players were observed to land on the medial side of the shoe in a toe-up position. Slipping during this stage could cause the player to potentially fall on their medial side. During the transition phase, the shoe was observed to translate in the posterior-lateral direction. Slipping during this phase could lead to instability in the anterior-medial direction. Slipping during any of the aforementioned stages could compromise performance and potentially lead to injury by falling. The push-off phase was similar to the sprint critical time period. As such, two critical time periods for the side-cut movement were chosen: initial foot-strike (0 - 20%) and the transition phase (20 - 60%).

b) Traction testing parameters

The current traction testing device is limited to replicating the translation and rotation of the shoe independently. The orientation of the shoe during the motion cannot change. For each movement, the motion of the shoe during the aforementioned critical slip period was assessed only in terms of translation or rotation.

Translation

For the sprint movement, the final stages of push-off (60 - 100%) were considered the critical slip period. During this stage, the shoe appeared to pivot about a point just above the toe of the shoe, rotating in the yz plane. This rotation matched the rear of the forefoot motion well, but was unable to mimic the slight posterior translation of the toe that also occurred. Rotation of the shoe in the yz plane is not possible using current test procedures. The pitch angle of the forefoot increased from 16.6° to 52.1° and the y position of the toe stud, SI1 moved 17.4 mm posteriorly. The vertical change in the toe stud was also 17.4 mm. To ignore the change in pitch angle and vertical position change in the forefoot would not be fully representative of actual shoe motion; however, analysis of the critical slip factors indicated that if the participant were to slip during the sprint, the later stages of the push-off would potentially have the most consequences.

Taking the mean pitch angle during the critical time period and assuming no change in vertical motion, an approximation of the translation of the shoe was made giving the following test parameters:

- Shoe orientation: Pitch = 35°, Yaw = 0°, Roll = 0°
- Translation distance in y direction: 20 mm (posteriorly)
- Translation speed: 350 mm/s
- Load: 1.2 BW for 80 kg male = 96 kg

>-> 20 mm at 350 mms⁻¹

940 N

Figure 10.8 - Translation of shoe testing conditions to replicate motion during critical slip period during sprinting.

For the kick movement, the initial foot-strike phase was selected as the critical slip period. During this time, the shoe underwent changes in pitch, yaw and roll angles. The translation of the shoe was in both the anterior and medial direction. The shoe was in a toe-up position meaning that the heel studs were primarily in contact during this phase of the movement; this was significantly different to the sprint movement where the heel studs were rarely in contact with the surface. Similar to the sprint movement to estimate the test parameters, the pitch, yaw and roll angles were kept constant and the mean shoe angle throughout the critical time period was used. The resultant displacement direction was calculated from the medial and anterior displacement of the shoe; the orientation of the shoe was reset in order for the resultant direction to be represented by the translation of the traction tester.

- Shoe orientation: Pitch = 0°, Yaw = 105° (toe-out), Roll = 20° (outward roll)
- Translation distance in y direction: 15 mm (anteriorly)
- Translation speed: 300 mms⁻¹
- Load: 2.1 BW for 80 kg male = 168 kg

1650 N

Figure 10.9 – Translation of shoe testing conditions to replicate motion during critical slip period in the kick movement.

For the side-cut movement two important time periods were selected; the foot-strike and transition phases. During the foot-strike phase, the shoe was observed to land in a toe-up and toe-out position with notable inward roll. This caused the medial studs to come into contact with the surface first. The predominant translation direction was laterally, with the heel studs displacing 8.9 mm during the 0.06 s of the impact phase. During this phase changes in pitch, yaw and roll were observed. To simplify the movement, the average orientation was used giving the following test parameters:

- Shoe orientation: Pitch = 10° (toe-up), Yaw = 65° (toe-in), Roll = 30° (inward roll)
- Translation distance in y direction: 10 mm (anteriorly)
- Translation speed: 150 mms⁻¹
- Load: 0.9 BW for 80 kg male = 72 kg

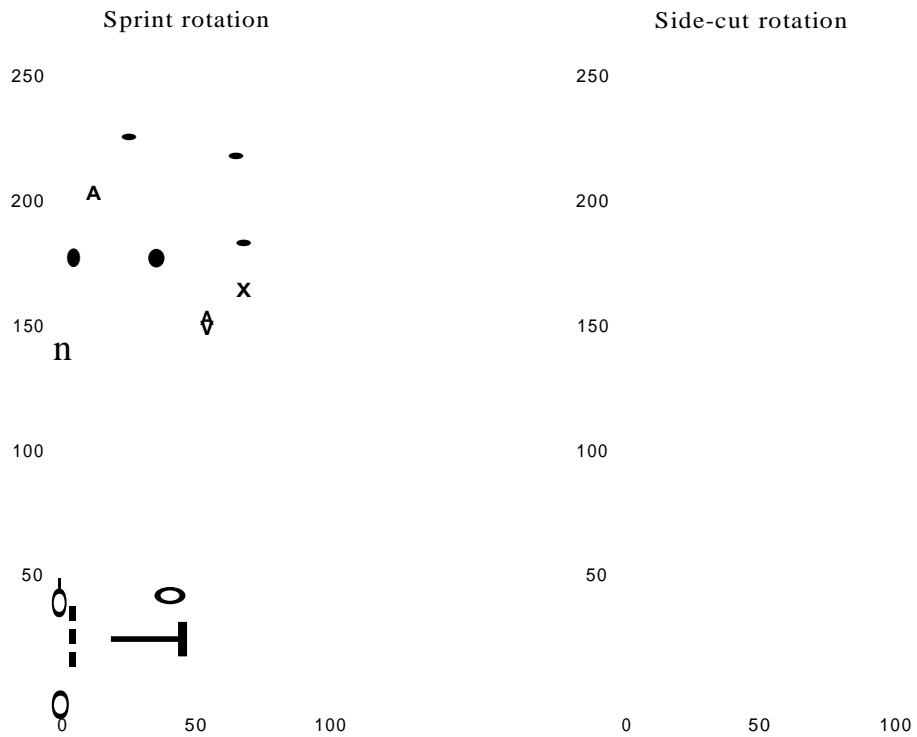
710 N

Figure 10.10 - Translation of shoe testing conditions to replicate motion during critical slip period in the side-cut movement.

Rotation

The second transition phase (20 - 60%) of the side-cut was also considered a period at high risk of slipping. During this time, the pitch and the yaw angles remained approximately level but notable change in the roll angle was observed. Greater translation of the forefoot studs compared to the heel studs implied that the shoe may be rotating during this phase. Rotation of the forefoot was also observed in the contact phase of the sprint movement; the centre of rotation of the two movements differed significantly suggesting that two rotation tests may be required to best represent realistic conditions. The rotation of the shoe during this phase is as equally as important as the motion of the shoe during the critical slip period; excessive shoe traction during rotation can lead to a greater risk of ACL knee injuries.

The following test parameters were derived from using the Reuleaux method to assess the centre of rotation for the sprint and side-cut movements.



Centre of rotation:	X(68.2, 165.2)	Centre of rotation	X (30.5, 49.1)
Orientation:	Forefoot only	Orientation	Complete shoe
Angle of rotation:	12° (externally)	Angle of rotation	6° (externally)
Speed of rotation:	60°s ⁻¹	Speed of rotation	60°s ⁻¹
Load:	1.7BW = 135 kg	Load	1.7BW = 135 kg

Table 10.2 - Test parameters for rotation of forefoot and complete shoe replicating the sprint and side-cut movements (stud positions for size UK 9.5, distances in mm).

Summary of test parameters

From the assessment of the motion of the shoe during the critical slip time periods for the three movements, five test scenarios were suggested. The translations of the shoe represent the push-off stage during sprinting, and the initial foot-strike phase for the kick and side-cut movements. The translation testing recommendations included posterior motion of the forefoot, anterior-lateral movement of the complete shoe and anterior-medial movement predominantly on the heel. The rotations represent the transition phase in both the sprint and the side-cut movements. For the sprint movement, the centre of rotation was situated near the medial side of the forefoot and included only rotation of the forefoot studs. For the side-cut rotation, the complete shoe was in contact and the point of rotation was situated on the medial side of the heel. Table 10.3 describes the test parameters for each of the five test scenarios.

	1	2	3	4	5
Orientation	(35°:0°:0°)	(0°:105°:20°)	(-10°:-65°:-30°)	Forefoot	Complete
Distance/Angle	- 20 mm	+ 15 mm	+ 10 mm	+ 12°	+ 6°
Speed	350 mms ⁻¹	300 mms ⁻¹	150 mms ⁻¹	170°s ⁻¹	60°s ⁻¹
Load	1.2 BW	2.1 BW	0.9 BW	1.7 BW	1.7 BW

Note: Orientation of the shoe = (Pitch:Yaw:Roll), , +/- Pitch = Toe-down/Toe-up, +/- Yaw = Toe-out/Toe-in, +/- Roll = Outward roll/Inward roll, +/- Displacement = Anterior/Posterior.

Table 10.3 - Five testing parameters to represent translations and rotations observed in the sprint, kick and side-cut movements.

From the three proposed translation tests, only the replication of the sprint movement translates the shoe in the same direction as the original test parameters. A smaller displacement distance is however recommended (20 mm instead of 50 mm). This is below the perceived slip distance of 30 mm (Perkins 1978). From assessment of the traction device in Chapter 3, the traction ranking of the shoes at 10, 20 and 50 mm was recorded. Out of the 12 trials tested (artificial, firm ground and soft ground with 4 shoes), between 10 and 20 mm 50% of the rankings had changed; primarily a switch of 2nd and 3rd place. Between 10 and 50 mm, 92% of the rankings had changed, and in some cases, switching from 1st to 4th place. Testing to 20 mm as proposed better represented the early traction rating of the shoe during translation.

One of the initial concerns about implementing realistic test conditions into the current traction testing device is for the speed of translation necessary to replicate the shoe motion. Assessment of the device in Chapter 3 revealed that as the speed increased above 100 mms⁻¹ the amount of noise present in the results also increased. This was potentially due to vibrations of the test device. Before fully adopting the modified test parameters, a full assessment of the repeatability of the results would need to be completed.

10.2.2 Suggestions for new traction testing device

One of the problems of the existing traction testing device was that it is limited to either a translational or rotational movement and during that movement, the orientation of the shoe remains fixed. Although suggestions were made on how more realistic test parameters could be used with the existing device; the advised parameters were still only an approximation and motion of the shoe was often simplified in order to meet the

test device constraints. An alternative method may be to design a new traction testing device based on the knowledge gained from player testing analysis. A potential approach is outlined below with further considerations to developing a new traction testing device detailed in Chapter 12.

a) Pendulum device

Pendulum type devices are one of the original traction testing methods and is still set as one of the FIFA test procedures and also employed by the UK Health and Safety Executive (Ferry 2005). They are however rarely used in research with many favouring the horizontal translation of the shoe to represent sliding during a forefoot push-off movement. The concept however is perhaps not as far from being representative of realistic movement as many critiques have stipulated. During the critical slip period in the sprint movement, a rotation of the forefoot in the yz plane was observed. Using the toe and rear of forefoot studs, the centre of rotation for the motion was calculated. Assuming a fixed system, Chapter 9 highlighted slight differences in the motion path for the toe stud, SI 1, but the motion path for stud S3 was very similar. This motion was also observed during the push-off phase in the side-cut movement where the toe stud better followed the predicted motion path of the fixed system.

A potential suggestion for a simple traction testing device to mimic the forefoot push-off movement is a pendulum device where the resistance to rotation can be used as a measure of traction. The point of rotation for the shoe motion studied in Chapter 9 was approximately 40 mm above and 20 mm in front of the toe stud. The positioning of a complete shoe with upper to fit with the centre of rotation may not be possible, and instead an additional plate with only the forefoot studs may be required. Figure 10.11 illustrates the potential test parameters for a pendulum traction testing device.

Figure 10.11 - Test parameters for pendulum device.

10.3 Analytical modelling

In Chapter 3 an analytical model was developed to estimate the likely interaction between a prototype stud and different hardness ground conditions. The impact conditions were initially the same as the drop hammer test used to define the ground condition ($m = 1.52 \text{ kg}$ and $v = -1.7 \text{ ms}^{-1}$). Modified boundary conditions were also used to attempt to replicate realistic loading conditions ($m = 19 \text{ kg}$ and $v = -0.7 \text{ ms}^{-1}$). Using the data collected in Chapter 9 a more detailed assessment of the modified boundary conditions can be made.

The impact velocity of the shoe in each of the three movements was calculated from the displacement data using the central differencing method. The impulse of the initial impact force collected in Chapter 8 was used with the vertical impact velocity and the number of studs in contact with the surface during the initial foot-strike phase to give an estimate on the weight of the mass (calculation described in Chapter 3).

Movement	Mass	Velocity
Sprint	1.4 kg	-1.27 ms^{-1}
Kick	20.2 kg	-0.91 ms^{-1}
Side-cut	44.5 kg	-0.33 ms^{-1}

Figure 10.12 - Modified test conditions from player testing results.

The initial modified conditions tested were calculated from literature with the intention to replicate a kick movement. The modified test conditions from player results for the kick movement were similar to the original estimation. For the sprint movement, more studs came into contact with the surface during the initial foot-strike phase, reducing the effective stud mass; the resulting boundary conditions were very similar to the drop hammer conditions. The side-cut movement displayed the lowest vertical component of velocity due to the lateral movement of the shoe.

Using the same approach as used in Chapter 3 to model the Smart Stud, a Copa Mundial stud was modelled using force-deflection data from Instron® testing. A non-linear equation for spring stiffness was defined and used with the original stiffness data for firm ground conditions to estimate the deformation of the stud and the surface for each of the three movements.

	Sprint	Kick	Side-cut
Stud	1.5 mm	4.3 mm	2.3 mm
Ground	4.0 mm	8.0 mm	5.2 mm
Time	6.4 ms	19.9 ms	33.1 ms
Sole clearance	4.5 mm	-0.3 mm	4.5 mm

Figure 10.13 - Relative deformation of a Copa Mundial stud (10 mm forefoot, 12 mm heel) on firm ground conditions using input parameters derived from player testing of a sprint, kick and side-cut movement.

The time to maximum deformation for each movement predicted by the analytical model was notably less than the impact phase defined in Chapter 9. However, the comparative ratio of impact time for each movement was similar. The analytical model

predicts that on firm ground conditions the Copa Mundial stud would not fully penetrate the surface in the sprint and side-cut movements, leaving a surface to sole-plate clearance of 4.5 mm for both studs due to the difference in height between the forefoot and heel studs (10 and 12 mm respectively).

Sprint Kick Side-cut

Figure 10.14 - Illustration of stud penetration depth for each movement using new input parameters.

Some of the limitations of the model described in Chapter 3 have not been overcome, such as using a stud stiffness derived from Instron® testing at controlled conditions. The use of realistic boundary conditions improves the model and also provides further information on potential Instron® test criteria for studs for future work.

10.4 Computational modelling

Finite element modelling provides the freedom to replicate the exact motion of the shoe during all three movements. One of the limitations of developing a finite element model is the feasibility of replicating the surface conditions. However the ability to accurately predict the exact traction force between the shoe-surface interactions is not necessarily required. An alternative approach is to ensure that the predicted traction ranking between shoe configurations is representative; for example, the traction results from mechanical testing can be used to rank the traction performance of a set of shoe configurations.

Using the data collected in player testing there are a number of potential options available to impart realistic shoe motion into a finite element model:

- Drive complete motion using stud coordinates;
- Model individual foot-strike, transition and push-off phases;
- Replicate mechanical traction testing test parameters.

10.4.1 Modelling complete shoe motion

The shoe motion can be driven by coordinate time-steps of three points on the shoe defining a rigid body section. The coordinate inputs can be taken directly from the difference between smoothed stud positional data at each time step. For example, Table 10.4 illustrates the boundary conditions required to mimic the motion of the shoe during the sprint movement at 0.01 s time steps.

Step	S1x	S1y	S1z	S2x	S2y	S2z	S3x	S3y	S3z	Increment
1	-2.71	-0.10	-8.11	-2.60	-0.27	-7.85	-1.82	0.94	-5.94	0.01
2	-4.19	-3.66	-5.27	-4.06	-4.10	-5.68	-2.97	-2.74	-3.98	0.01
3	-1.74	-2.33	-1.90	-1.53	-2.69	-1.39	0.11	-1.76	-2.87	0.01
4	0.23	-0.81	1.40	0.33	-0.96	1.57	0.95	-1.10	-0.80	0.01
5	2.62	-0.02	3.72	2.31	0.50	3.16	0.00	-2.14	0.77	0.01
6	3.89	0.68	6.25	3.67	1.26	6.46	2.23	-1.92	0.96	0.01
7	3.35	0.92	7.82	3.29	1.25	8.48	3.21	-1.70	1.38	0.01
8	1.10	1.50	8.71	1.08	1.65	9.23	1.90	-1.34	1.65	0.01
9	-0.37	2.68	9.73	-0.44	2.93	10.02	0.11	-1.00	2.65	0.01
10	-3.27	4.13	12.80	-3.08	3.71	12.78	-0.08	-0.66	3.07	0.01
11	-3.47	7.97	17.79	-3.33	7.72	18.31	0.89	0.52	5.67	0.01
12	-6.07	12.68	23.07	-5.92	12.28	22.81	-1.91	1.03	9.75	0.01
13	-8.15	19.25	30.80	-7.76	17.96	29.37	-4.09	3.42	17.55	0.01
14	-3.83	27.97	38.73	-3.78	27.58	37.98	0.10	9.20	27.73	0.01
15	-0.75	33.26	44.76	-0.99	33.66	44.09	2.64	12.34	36.02	0.01

Table 10.4 - Boundary conditions of 3 rigid nodes on the outsole during sprinting (displacements in mm, time increments in s).

Figure 10.15 - Coordinate position of stud S3 during the sprint movement (200 Hz).

Traction performance could be measured from the horizontal reaction force on the studs when in contact with the surface. This approach is valid when the surface and shoe interaction exactly replicates that seen in the field. The boundary conditions suggested represent one particular shoe-surface interaction and the resulting motion of the shoe is a consequence of the conditions at the time of testing. However, the intention of the FE model is to be able to make changes to the outsole configuration or surface conditions and estimate the influence on the traction behaviour. It logically follows that changing the conditions of the interaction would influence the motion of the shoe; for example reducing the stiffness of the surface could potentially cause the shoe to slip. This slip would not be seen in the FE simulation as the motion of the shoe is controlled and only a potential change in the horizontal reaction force would be seen.

Using the stud position to drive the motion of the shoe has limitations in the fact that the model would never reach equilibrium; the influence of changing shoe or surface conditions could only be measured by the reaction forces between the studs and the surface, the point at which this is measured is subjective and is depended on the stud configuration. Changing the stud configuration essentially changes the location where

the reaction force is being measured and can cause conflict between different outsole designs.

An alternative approach is to use the velocity and mass of the shoe to drive the motion and use the resulting trajectory as a measure of the traction performance as discussed below.

10.4.2 Modelling individual stages

Three distinct stages were identified in Chapter 9 for the sprint and the side-cut movement; foot-strike, transition and push-off. For the kick movement, a foot-strike and ball contact phase was identified. During the foot-strike phase, the resulting displacement of the shoe when in contact with the surface can be modelled by inputting the shoe velocity at the start of the phase and allow the model to reach equilibrium. The distance the shoe travels when in contact with the surface is effectively a measure of the traction performance of the shoe-surface interaction. This approach is similar to the analytical model, where the vertical velocity of the shoe was used to predict the penetration depth for each movement on impact. The advantage of using finite element analysis is that motion in three directions can be assessed and the orientation of the studs to the surface can be set to represent that observed in player testing.

Using the velocity of three studs on the shoe to ensure shoe rotation is also represented and the maximum vertical load from player testing, the following boundary conditions for the foot-strike stage of all three movements are shown in Table 10.5. Figure 10.16 illustrates the velocity boundary conditions applied to a Copa Mundial outsole for the impact phase of the sprint movement.

	Sprint	Side-cut	Kick
Orientation	(-16.2°:-24.8°:-0.6°)	(14.3°:-21.4°:-37.6°)	(19.0°:-32.1°: 29.8°)
Velocity S1	(-0.22, 0.26, -0.88) ms ⁻¹	(-0.97, -0.09, -0.43) ms ⁻¹	(1.32, 1.60,-1.22) ms ⁻¹
Velocity S2	(-0.21,0.25, -0.83) ms ⁻¹	(-0.84, -0.17,-0.32) ms ⁻¹	(1.37, 1.81,-1.40) ms ⁻¹
Velocity S3	(-0.13, 0.34, -0.74) ms ⁻¹	(-1.26, 0.08,-1.43) ms ⁻¹	(1.44,2.00, -2.21) ms ⁻¹
Load	1600N	1375 N	1965 N

Table 10.5 - Boundary conditions for replication of impact motion for sprint, side-cut and kick movements (orientation represents pitch, yaw and roll angles respectively; stud velocities represent x, y and z components).

Figure 10.16 - Example boundary conditions for the foot-strike phase of the sprint movement applied to rigid body nodes on the studs S1, S2 and S3.

During the transition phase for the sprint and side-cut movements the shoe was observed to rotate in the xy plane. For the sprint movement, only the forefoot studs were in contact with the surface and the resulting centre of rotation was situated on the medial side of the forefoot. For the side-cut movement, the heel and forefoot studs were in contact, with the centre of rotation on the medial side of the heel. Rotations can also be modelled using FE with boundary conditions similar to those recommended for mechanical traction testing (Table 10.2).

Using one set centre of rotation may however not be fully representative of the complete shoe motion. Analysis of sprint trial P5S1 which was observed to undergo a significant change in yaw angle during the contact phase revealed that the centre of rotation moved over each time-step (Figure 10.17).

The centre of rotations tended to lie on the medial side of the shoe, slightly outside of the forefoot. Over a duration of 0.09 s, the centre of rotation moved from the rear of the forefoot to the front. This suggests that at the beginning of the movement the forefoot is rotating about a point nearer to the ankle, but by the end of the movement, the heel and leg are rotating about a point near the forefoot which is fixed to the surface. This is potentially the mechanism that can cause ACL type injuries if the forefoot is unable to rotate.

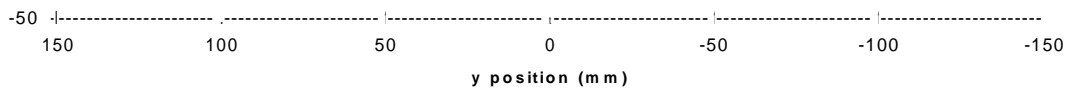


Figure 10.17 - Position of the centre of rotation during the contact phase for a sprint trial.

Bladed stud designs were initially heavily criticised in the press because of their inability to allow the foot to rotate when in contact with the surface (BBC 2005). Designs have since improved and tend to orientate the studs about a centre of rotation situated in the centre of the forefoot. Results from player testing suggested that a single centre of rotation may not exist but instead moved throughout the movement. It could, however be argued that the stud configuration and not the player motion controls the location of the centre of rotation. As such, orientating the studs about one centre of rotation will inherently cause the foot to rotate about that point. Whether this is desirable is a potential subject for further investigation but also highlights that a range of centre of rotations should be modelled. If design is based around a centre of rotation on the forefoot, the implications on the resistance to rotation about alternative points should be investigated with the concept of an acceptance zone to ensure rotation values do not get too high and cause a risk of injury.

10.4.3 Modelling mechanical test parameters

To validate an FE model the test parameters recommended for traction testing could be used. These can aid in developing a surface medium that is representative, if not realistic, of natural or artificial turfs. The traction ranking of a selection of outsoles

could be obtained for each test parameter using the mechanical traction tester. The same movement could be replicated using the FE model and the horizontal reaction force used to again rank the outsoles. An ideal solution would be for the traction force to be equal in both mechanical and FE modelling. This is a long term goal and an intermediate step would instead be to ensure that the traction ranking of the outsoles was consistent.

10.5 Chapter summary

Mechanical traction testing – modified test parameters

Five suggestions were made for test parameters for the current traction testing device that represented the three movements analysed; sprint, kick and side-cut. Initially, assessment of the time period during the movement where the player was considered to be most at risk of slipping was carried out. Factors such as ratio of horizontal to vertical force, number of studs in contact with the surface and velocity of the shoe were all taken into account. For the sprint movement, the final push-off phase was selected as the critical slip period; during this time, only the toe studs were in contact with the surface but a high ratio of horizontal to vertical force was observed. Analysis of shoe motion during this period suggested that the shoe was rotating in the yz plane about a point close to the toe. During the rotation, the toe studs were observed to undergo greater posterior translation than predicted by a fixed rotation point. This suggested that the toe studs were also sliding during push-off. The posterior translation was modelled to provide traction test parameters by assuming a fixed shoe position. A posterior translation of 20 mm at a pitch angle of 35° was recommended. For the kick movement the initial foot-strike phase was highlighted as the critical slip time period. The shoe was observed to land in a toe-up and toe-out position with notable outward roll. This led to the lateral heel studs coming into contact with the surface first. The shoe motion was simplified to recommend translational test parameters; translation in the medial direction was observed. Similarly the foot-strike phase for the side-cut movement was analysed. Again the shoe was observed to land in a toe-up position, but with substantial inward roll causing the medial heel studs to land first. The shoe was then observed to translate approximately 10 mm laterally giving the translation test parameters. The translation directions identified in the kick and side-cut movements are not traditionally tested in traction assessment. The posterior motion of the forefoot

during sprint is more commonly assessed, although the high pitch angle causing only the toe studs to be in contact with the surface is an important modification, highlighting the limited number of studs in contact with the surface during a potentially high-risk motion. The new speeds of translation are higher than originally tested; the speed could cause additional problems when implementing the new test parameters due to excessive vibration of the device. The rotation of the shoe during each movement was also analysed. Two sets of test parameters were derived to represent the forefoot rotation during the sprint movement and the complete shoe rotation during the side-cut movement. The rotation angles were smaller than originally tested (12° compared to 60°) but speeds of rotation were similar (60° s⁻¹). The point of rotation was found using the Reuleaux method; for the sprint forefoot rotation it was calculated to be on the medial side of the forefoot, and for the side-cut rotation, on the medial side of the heel. Both were rotation centres not normally assessed in traction testing. Implementation of the new recommended test parameters needs to be done with care; ensuring that the original test requirements of high repeatability, low standard deviation and clearly comparable results can still be achieved.

Mechanical traction testing – new device

An alternative to using the player testing results to modify the original traction tester is to instead develop a new test device to better represent shoe motion. The current traction testing device is limited to only translation and rotational movements and required the shoe orientation to be fixed throughout the motion. As observed in Chapter 9, this is not always the case; changes in pitch, yaw and roll were seen during impact, contact and push-off stages in all three movements. Using a concept often used to assess the frictional properties of two surfaces, a pendulum style device was recommended. This device aims to mimic the push-off stage in the sprint movement, where the dominant motion was a change in the pitch angle of the shoe. The resistance to rotation of the forefoot stud configuration on the surface could be used as a measure of the traction performance. More complex traction testing designs are introduced in Chapter 12.

Analytical modelling

An analytical model based on two non-linear springs in series was developed in Chapter 3 to predict the relative deformation of the stud and the surface leading to an estimate of penetration depth. The original test parameters for the mass-spring model were based on results from literature on the impact velocity (Kirk 2008) and impact force (Cavanagh *et al.* 1984) during a heel-strike in running. The results from player testing were instead used to estimate the stud penetration depth on impact during the sprint, kick and side-cut movements. Although the model requires further development to calculate the stud and surface spring stiffness during realistic load conditions, using representative test parameters suggested that the studs would not completely penetrate the surface during the sprint and side-cut movements on a firmer surface. This effectively reduces the contact surface area as sole-plate interaction would not occur, thus reducing the traction performance of the shoe.

Finite element modelling

Three approaches were identified for finite element modelling of the shoe-surface interaction; complete shoe movement, shoe movement during foot-strike, transition and push-off stages and shoe movement using mechanical test parameters. One of the limitations of using the complete trajectory to control the motion of the shoe is that the trajectory may be specific to the shoe-surface conditions at the time of testing. Developing a finite element model to follow the trajectory of the shoe and then changing the stud configuration or surface properties but maintaining the same trajectory would no longer be valid as the model would not reach equilibrium. A better approach may be to break the motion down into stages, use initial velocities and loads to set the boundary conditions for the movement, but use the resulting trajectory as a measure of traction. Replicating the test parameters recommended for mechanical traction testing would allow the model to be validated using the mechanical test results. Developing a realistic surface model is highly complex but ensuring that the same traction ranking is achieved between outsole configurations in both the finite element model and mechanical traction testing is an important intermediate step.

11 INFLUENCE OF SHOE-SURFACE INTERACTIONS IN OUTSOLE DESIGN

11.1 Introduction

A review of current literature (Chapter 2) revealed that there is very little published work available on the design of football boots, particularly the influence of player movement on outsole configurations. There have however been extensive studies into the measurement of traction to both classify surface conditions and rate outsole configurations. Attempts have been made to improve the realism of the measurement devices using biomechanical analysis, yet to date, the results have not been fully used to suggest outsole design modifications to enhance player performance or minimise the risk of injury.

When designing new outsole configurations player testing is normally performed after a prototype shoe has been developed (Figure 11.1). It is often considered the final stage before the shoe goes to market and can be used to gain feedback on comfort and performance. An alternative suggestion is to use the player testing to inform the initial idea conception; observations from the shoe-surface interaction under different conditions provide information on stud penetration angles or points of rotation.

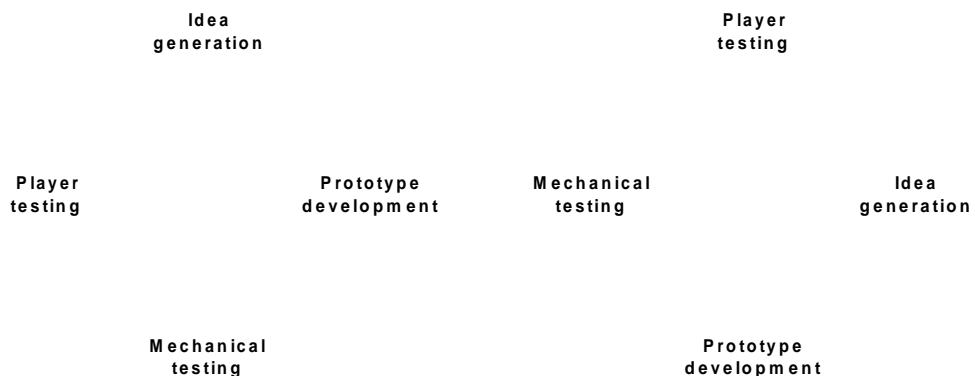


Figure 11.1 - Design cycle. Left: Traditional, player testing occurs after prototype development; Right: Modified, player testing is the starting point for idea generation.

The two main factors in traction assessment are movement in translation and rotation. These also form the primary design considerations. Current trends to meet the translational traction requirements are to increase the area of contact between the outsole and the surface; either through increasing the number of studs or increasing the

depth of penetration. Longer stud lengths do not necessarily lead to increased traction; sole plate interaction is also important helping to increase the contact area between the outsole and the surface (Clarke and Carre 2010). As such the selection of stud length for the surface condition is important; a long stud length on a hard surface will potentially display less traction than a shorter stud length due to the incomplete penetration and lack of sole-plate interaction. A range of stud profiles are available to suit varying pitch conditions; typically marketed as firm ground, soft ground and artificial turf outsoles. Soft ground studs are typically removable longer length studs made of metal. Firm ground and artificial turf outsoles often have a moulded sole with shorter, rubber studs. Interchangeable studs are still popular and allow players to keep the same shoe upper, but ensure that their stud selection is best matched to the ground conditions at the time. One of the latest innovations in stud technology to reach the market was the Nike pressure activated SENSE stud. The concept is similar to the adidas prototype Smart Stud, introduced in Chapter 3, whereby the stud length adjusts according to the surface hardness. This theoretically ensures that complete stud penetration, and hence maximum traction is achieved even when the surface conditions change during a match, or location on the pitch. This also eliminates the player decision making process required to select a suitable stud configuration and places the resulting traction performance in the hands of the manufacturer, not the player.

Figure 11.2 - Nike SENSE stud technology on the medial side of the forefoot on the Mercurial Vapor Superfly III (Nike INC. 2011).

Despite manufacturers recognising the importance of maximising translational traction, the availability of published work on the biomechanical validity behind the outsole designs is non-existent. This may in part be due to the confidentiality surrounding product generation but is also likely to be due to the considerable amount of time and resources required to conduct large scale player studies to obtain biomechanical data.

Kirk *et al.* (2007) used results from tracking the motion of the shoe in 2D during a heel-strike in low speed running 2D to suggest a change in stud design to increase penetration and surface area in contact. The suggested stud geometry aligned the central axis of the stud with the impacting velocity vector. This effectively improves the penetration of the stud, but the author noted that once penetrated, the depth of the stud is significantly reduced compared to if it was vertical, potentially reducing the translational traction. The author also expressed concerns over the effects of the modified stud geometry on other movements. The study was also limited by only being able to calculate stud angles in a 2D plane. The notion of using observations from player testing to influence design is important. Further knowledge on the interaction of all studs during a range of movements can help develop a wider picture on how player testing can influence design.

Rotational traction is also an important consideration and is more commonly associated with reducing injuries than improving performance. The influence of the shoe-surface interaction on lower limb injuries has been well researched; with Orchard *et al.* (2008) concluding that excessive traction between the shoe and the surface is one of the likely causes of ACL injuries. One of the earliest design suggestions resulting from assessment of player performance and injuries was by Cameron and Davis (1973). The authors developed a studded swivel plate attached to the outsole to allow the shoe to rotate about the studs when fixed into the surface. The design was based on biomechanical analysis from laboratory based player testing and observation of injuries to American Football players over a six year period. The resulting design was capable of turning 360° in either direction but required 10 lb torque to initiate the movement. The swivel shoe was trialled on a sample of 466 high school players over a complete football season. Results from 2373 players wearing conventional studded outsoles were also gathered. The results indicated that only 5% of the swivel shoe wearing players recorded an injury to the knee or ankle compared to 16% of the players wearing conventional shoes. This led the authors to conclude that at the time, the most effective method of reducing injuries caused by stud fixation is to wear a shoe with swivel studs and a stud-less heel. The design however has never made it to mass manufacture and the concept of swivel studs has been outweighed by the drive to have lightweight shoes.

Despite the knowledge that excessive rotational traction can lead to lower limb injuries (Cameron and Davis 1973), the 1990's saw the introduction of the first bladed stud

designs. The outsoles typically had wedge shaped studs orientated along the length of the shoe increasing the surface area for improved translational traction. These initial designs were not portrayed favourably by the press, with reports of calls to ban the design at both school and professional levels (BBC 2005).

More recently, bladed designs have curved or tapered studs orientated about the centre of the forefoot (Figure 11.7). These designs are in some ways taking note of the results from the study by Cameron and Davis (1973) but instead of having a swivel sole, the studs are orientated so to minimise rotation of the forefoot. Both the modern designs and the swivel plate shoe suggest that the centre of rotation of the lower limbs is about the centre of the forefoot. Chapter 9 identified the centre of rotation for two different movements performed wearing Copa Mundial shoes on natural turf. The centre of rotation for the sprint movement was identified to be on the medial side of the forefoot, with only the forefoot studs in contact, and for the side-cut movement, the centre of rotation was further back on the medial side of the heel, with the complete outsole in contact. The questions raised from this study and from reviewing relevant literature are: is the centre of rotation just an artefact of the stud position and which drives which? Should the natural centre of rotation be used to influence the stud configuration or should the stud configuration be designed to control the centre of rotation? Further work is required to answer the proposed questions, starting with an investigation to see how the centre of rotation changes depending on the choice of footwear. More details are outlined in Chapter 12.

An intermediate step is to use the knowledge gained from the player testing studies to suggest how the shoe-surface interaction may influence outsole designs. Understanding how the studs interact with the surface with a known stud configuration (Copa Mundial) can help to play an important part in the future design of outsoles. Both observations of the centre of rotation and translation direction vectors during the football specific movements can be used to aid in outsole design. The former being used to minimise rotational traction and reduce the risk of injury, and the latter to improve translational traction and increase player performance. The foot-strike and push-off shoe orientations are also analysed, building on the notion raised by Kirk *et al.* (2007) that improving the stud angle may improve penetration and hence increase traction. The proposed ideas are a suggestion on how biomechanical analysis can be incorporated in outsole design.

11.2 Influence of shoe orientation at foot-strike and push-off

The results from tracking the stud position and shoe orientation also allow the angle of stud on impact to be determined even though it is not visible from the video footage. This information could help answer question such as are additional studs needed on the tip of the toe or what angle should the studs be to improve traction on impact. Kirk *et al.* (2007) alluded to this when investigating the 2D forefoot angle on impact. The authors suggested a modified stud geometry to align the stud along the velocity vector. The results from player testing (Chapter 9) of three movements can be used to expand this idea in 3D to cover a wider range of scenarios. The orientation and velocity vector direction of the shoe and studs during impact and push-off for the sprint, kick and side-cut were investigated.

11.2.1 Sprint movement

During the foot-strike stage of the sprint movement, the shoe landed in a toe-down position with the forefoot coming into contact with the surface first. The pitch angle on foot-strike was 16.2° with a yaw (toe-out) angle of 24.8° while at push-off the angles were 30.1° and 24.1° respectively. Figure 11.3 and Figure 11.4 illustrate the orientation of the studs on foot-strike and push-off.

Foot-strike - Sprint

Figure 11.3 - Orientation and velocity vectors of the forefoot studs on foot-strike (sprint).

Figure 11.4 - Orientation and velocity vectors of the forefoot studs at push-off (sprint).

7.2.2 Kick movement

For the kick movement, all participants landed heel first in a toe-up and toe-out position. The shoe was also slightly outward rolled suggesting that the first studs to contact the ground were the lateral studs on the heel. Figure 11.5 illustrates the orientation of the heel studs on foot-strike.

Figure 11.5 - Orientation and velocity vectors of the heel studs on foot-strike (kick).

11.2.3 Side-cut movement

During the side-cut movement, the shoe was also observed to land in a toe-up and toe-out position but with substantial inward roll. As such, the medial heel studs were observed to come into contact with the surface first. Figure 11.6 illustrates the orientation of the heel studs on foot-strike.

Foot-strike - Side-cut

Pitch = 14°, Yaw = -24°, Roll = -38°

Figure 11.6 - Orientation and velocity vectors of the heel studs on foot-strike (side-cut).

11.2.4 Summary of shoe orientation

During foot-strike and push-off for the sprint movement, the resulting velocity vectors acted in opposing directions. Aligning studs to meet both requirements would be conflicting as in both cases it is the front forefoot studs that are predominantly involved in the interaction. The critical slip assessment of the sprint movement indicated that the latter moments of push-off were at a greater risk of slipping than the initial time of impact. It is therefore perhaps more important for the stud design to focus on the push-off angle and direction. Figure 11.4 illustrates that the toe area is the last point of contact with the surface. For the Copa Mundial outsole, no additional traction elements are present near the toe; future designs may either need additional studs or the use of surface texture to increase the traction in this zone.

For the heel plant during kicking, the shoe landed on the lateral edge, with substantial pitch (toe-down) and outward roll angles. The resultant velocity vector acted in an anterior-medial direction. Stud angle for the rear heel studs could be aligned along this

velocity vector to increase penetration during the initial contact stages. However, for the side-cut movement, the medial side of the shoe landed first and the resultant velocity vector predominantly acted in the lateral direction. The optimum alignment of studs for the side-cut movement would therefore be acting in the opposite direction to the kick movement. A potential solution would be to have opposing stud alignments on the medial and lateral sides of the heel. A side-effect of this design may be that the opposing stud may not penetrate the surface and instead lead to an increased roll angle. A compromise could be to lessen the alignment angles giving an improvement in penetration but also with consideration to other movements.

11.3 Influence of centre of rotation

The position of the centre of rotation can influence the stud shape and position on the outsole. Traditionally the centre of rotation is assumed to be in the centre of the forefoot for the forefoot studs and in the centre of the heel for the heel studs. Figure 11.7 illustrates the 2011 adidas F10 TRX AG outsole configuration; four centres of rotations are identified following the curvature and position of the forefoot and heel studs. Figure 11.8 shows the position of the calculated centre of rotation for the sprint and side-cut movements.

Figure 11.7 - Estimated centres of rotations (red markers) for the adidas F10 TRX AG outsole (adapted from adidas Group 2011); the dashed circles indicate the possible centre of rotation and corresponding motion path given the shape and orientation of the studs.

Figure 11.8 - Left: Centre of rotation in sprint movement; Right: Centre of rotation during side-cut movement with Copa Mundial stud configuration; red markers indicate the observed centre of rotation from player testing and the dashed lines represent the corresponding motion path for the forefoot or heel about the calculated centre.

Figure 11.8 illustrates that during the sprint movement, studs should be orientated to reduce rotational resistance about a point on the medial side of the forefoot. Only the forefoot studs are influenced by this centre of rotation. However, for the side-cut movement, the complete outsole is in contact and the centre of rotation located on the medial side of the heel. This could cause conflict between the rotation directions for the forefoot studs. A shape that allows a reduced rotational resistance along both rotation paths would be the optimal solution although could pose additional problems with regards translational traction.

11.4 Influence of translation vectors

The translation of the shoe during each movement was assessed using the positional data of the studs on the outsole of the shoe. Results suggested that the shoe did not slip such that it would have been perceived by the participants, but that the motion of the shoe for each of the three movements was distinctive for that movement. The sprint movement caused the shoe to move posteriorly after impact whereas the kick movement showed anterior and medial motion and the side-cut movement displayed both lateral and posterior motion. The movement directions of the studs when in contact with the ground could be used to aid in stud positioning and shape design. If the posterior slide during sprinting was deemed undesirable, a stud profile to enhance traction in that direction could be beneficial. However, other motions of the shoe aside from posterior sliding also occurred during the sprint movement; significant external rotation of the heel was also observed prior to the push-off stage. A stud profile that prevented posterior sliding would also need to allow for foot rotation to prevent the potential of knee or ankle injuries.

The stud translation vectors for each movement were created from the position history of the studs. The position history data was available for all the studs which also allowed the location of the studs at 0.02 s time intervals during contact with the ground to be viewed. Only the movement in the xy plane was investigated.

Figure 11.9 - Position history of forefoot studs for the sprint movement.

• 0 s 0.02 s 0.04 s 0.06 s *0.08 s *0.10 s *0.12 s *0.14 s

y position (mm)

Figure 11.10 - Position history of all studs for the kick movement.

Figure 11.11 - Position history of all studs for the side-cut movement.

The dominant change in position of the studs was used to create motion vectors for the shoe for each movement. The vector arrow represents the average displacement of the studs from foot-strike to the initial stages of push-off.

Figure 11.12 to Figure 11.14 illustrate the different stud motion pattern for the three movements. For the sprint movement, the dominant stud displacement was in the posterior direction, with only the forefoot studs in contact. During the kick movement, the complete outsole was in contact, but the heel motion was primarily in the medial direction and the forefoot also showing slight anterior motion. The side-cut dominant motion was in the lateral direction with the heel showing slight anterior sliding on impact and the forefoot dominant motion was slightly posterior but still acting laterally. To prevent potential sliding during contact, the stud surface area in the direction of motion needs to be maximised to increase translational traction. The conflicting motion vectors for each movement indicate that a conventional bladed stud with only one long axis would not be adequate. Circular studs may offer the optimum solution or triangular studs as long as care was taken to reduce sharp corners that could cause lacerations.

11.5 Design suggestion

Rubber directional scales on toe area to increase traction during push-off.

Surface area increased in anterior-posterior direction to improve translational traction.

Forefoot studs orientated to reduce rotational resistance during sprint movements.

Stud corners rounded to reduce risk of lacerations.

Rear forefoot stud shaped to have reduced rotational resistance from both forefoot and heel centre of rotations.

Medial heel studs orientated to reduce rotation during side-cut movements.

Profile of lateral heel stud angled to increase penetration during heel plant for kicking.

Figure 11.15 - Outsole design suggestion.

The above observations were then combined to develop an example outsole design (Figure 11.15) that combines the influences of the shoe-surface interactions from realistic football movements on natural turf. The translation vectors were used to shape the studs to increase the surface area in the direction of motion. Theoretically this should increase translational traction performance. The centre of rotation was taken into consideration to ensure that the studs were also positioned to reduce rotational resistance. It is hoped that this will minimise the risk of ACL injuries caused by excessive stud fixation. The orientation of the shoe on impact was used to change the profile of the studs to aid in penetration into the surface. The shoe orientation on push-off during the sprint movement highlighted that the tip of the toe was the last point of contact with the surface; this gave rise to the suggestion of additional toe traction elements.

12 FUTURE WORK

12.1 Introduction

There are three main areas for continued research resulting from the outcomes of the study:

- 3D methodology
- Data collection
- Implication of results

Each section has arisen from the progression of the study; from initial development of a 3D measurement system, evaluation of the system and collection of example data, to analysis of results and implications for testing and design. The following recommendations for future developments range from small modifications to the measurement system to improve efficiency and accuracy of data collection to the suggestion of new studies to answer longer term research goals.

12.2 3D methodology development

The aim and objectives of the 3D measurement system was to develop a method of obtaining the position of a shoe using a system that was portable, of minimal intrusion to the players, suitable for use both in a laboratory and outside and ultimately able to achieve high marker re-projection accuracy. Post processing methods were then developed to track the markers and obtain kinematic information. The main aims and objectives were achieved and the system successfully used to obtain shoe data from a single participant in the laboratory and from a larger sample size outside on natural turf. There are still however potential areas for development, namely to improve the efficiency of the data collection, speed of analysis and accuracy of re-projection. The following section outlines how the method can be developed for use in future research.

One current limitation of the measurement system is the small test viewing area. Players were required to place their left foot (tracked shoe) within **aim** zone for all three movements; after practice trials, for many players this was not an issue, but for some, their approach run was affected and additional repeats were necessary to ensure the shoe was within the filming zone. The viewing area was selected by assessing the

level of zoom, image size (in pixels) and resulting marker size. A larger test area could be generated by reducing the camera zoom and reducing the tracking marker size. Increasing the resolution would ensure that an adequate number of pixels remained in the marker to allow a high level of tracking accuracy. This however, would increase download time between repeats. An alternative approach would be to increase the number of cameras being used. One of the advantages of the measurement system developed was that only two high-speed cameras were required to track the shoe in 3D. With unlimited resources on equipment, additional cameras could be placed along the same plane as the original cameras to increase the viewing plane in the yz axis. Using additional cameras on the opposing side of the player would allow either the other shoe to be tracked, or the same shoe but through a greater range of motions. Figure 12.1 illustrates a modified camera set-up to capture wider viewing zone. This camera set-up is more representative of traditional laboratory based motion capture systems (Robertson *et al.* 2004) and in itself will have further limitations; for examples additional costs, extra cabling and more data to analyse. Increasing the viewing angle would also help identify markers when high roll or yaw angles obscured them from view.

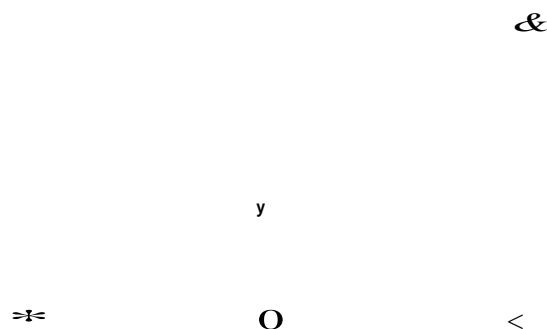


Figure 12.1 - Extended camera set-up for increased viewing area.

The time required to analyse the recorded video footage to obtain marker coordinates was reduced by the development of a semi-automated tracking algorithm. The algorithm was implemented in MATLAB™; the first step was to convert the *.cin* files saved by the Phantom camera software to *.avi* files. This step was time consuming and performed outside of MATLAB™. To increase the efficiency of the algorithm, the raw video files could be read directly into MATLAB™ using the *cineread* function. At the time the original tracking algorithm was developed, this function was not available but could be now used to improve the analysis efficiency (Phantom Zone 2010).

To identify the marker the image was converted to a binary image using a user defined threshold. This allowed the threshold to be modified depending on the light conditions of the image to be tracked. Testing outside in natural light gave varying light levels due to cloud cover or change in time. The same tracking algorithm needed to be used for all images. The manual adjustment of the conversion threshold potentially increased the analysis time for each video. The function *graythresh* could be used on the cropped image before conversion to obtain the global threshold of the image.

Original Level = 0.4 Level = 0.3 Level = 0.2 Level = 0.1 Level = 0.1353

Figure 12.2 - Use of *graythresh* function to identify appropriate binary conversion threshold.

The original image in Figure 12.2 is darker than average due to increased cloud cover, the standard threshold conversion of 0.4 is too high and the markers are not detected, reducing the threshold detects the markers, but the selection of the optimal threshold is experimental. The *graythresh* function selects the threshold to minimise the intraclass variance of the black and white pixels and reduces the manual input of the semi-automated tracking algorithm. The function can be applied at each loop to account for changing light during video capture; this will increase the computational requirements, but improve efficiency.

One of the greatest errors in propagation of marker coordinates to stud coordinates was obtained from measuring the relative stud location to marker position. An accuracy of ± 1 mm was estimated, this propagated to a maximum error of ± 2.2 mm. Alternative methods of obtaining the relative marker and stud positions are:

- 3D laser scanner
- CAD geometry
- 3D motion capture systems

Using CAD geometry was not possible at the time of testing, as the markers were positioned onto the shoe manually. If the markers were printed onto the shoe during the manufacturing process, the location of the markers relative to the stud geometry would be known as a full 3D CAD model would be produced. A 3D motion capture system

was used to validate the stud transformation calculation. To use the system to identify the marker and stud coordinates, the shoe would need to be mounted in the viewing plane allowing all markers and studs to be viewed from two or more cameras. The accuracy of measurements would then be as reliable as the measurement system. Commercially available biomechanical measurement systems are often used to obtain the relative coordinate locations of markers on the human body. The systems are typically electromagnetic and can achieve a root mean square error of less than 1 mm when measuring stationary markers (Richards 1999). This is similar to the estimated accuracy of the manual method, but would potentially be more time efficient and show greater reliability. 3D laser scanners can achieve similar results with a quoted accuracy of 15 μ m available on the more advanced scanners (Nikon Metrology NV 2011).

A potential source of random error in the measurement system arose from the flexion of the shoe changing the distance between markers. Two rigid bodies were defined on the shoe, and the distance between markers assessed to ensure that the shoe did not flex excessively during the movements. Increasing the number of markers and as such, the number of rigid bodies defining the shoe could reduce this potential error. Measuring the relative marker and stud position when the foot was in the shoe in both a neutral and flexed position could help quantify the potential error in assuming rigid body segments.

A long term goal of the study is to capture data in a real game scenario; reducing the need to have separate test days, the impedance on the players and influence on the test environment. In 2010 Sky Sports launched a dedicated 3D channel, with the broadcasting of top Premiership games being the main focus. The games were filmed using 3D cameras, and although the frame rate may not be high enough to obtain detailed information, the technology is a step towards being able to use TV footage to gather data. In order for the data collection to be remote, the shoe needs to be tracked without additional markers. The markers chosen for the current study were selected for their lack of impedance to the players and ease of tracking due to the high-contrast colour and shape. The markers were also positioned to define two rigid bodies on the shoe. Without additional markers, the shoe could be tracked using logos or designs already on the shoe. Knowing the location of the logo or design from the make, model and size would potentially allow the shoe to be tracked. In order for orientation of the shoe to be obtained, three markers defining a rigid body would be required. On some shoe designs this may be possible (for example, the three adidas stripes) but on others this is not possible without additional markers.

12.3 Data collection and analysis

Using the existing 3D measurement system and analysis tools or a future developed version, one of the long term goals of the study is to be able to populate the table of results on shoe-surface interactions by including a wider range of participants and test variables. Table 12.1 includes potential variables such as changing surfaces or player level to ensure that the full potential of the shoe-surface interaction is investigated. The results from these additional studies could be used to answer further research questions; such as, do female players require specific outsole configurations?

Test parameter	Potential variables
• Surface	• Natural turf (firm and soft), artificial, wet, dry
• Players	• Male, female, youth, professional, amateur, on pitch position
• Shoes	• Range of studded and non-studded outsole designs
• Movements	• Acceleration, braking, rotations (internal and external), cutting
• Sports	• Any, not restricted to those that wear studded footwear
• Location	• Countries – soil type, temperature, humidity, rainfall

Table 12.1 - Potential variables for investigation.

An additional study raised from the discussion on the centre of rotation of the shoe is whether the centre of rotation is influenced by the stud configuration, and which should be the driving factor. Using a range of stud configurations, included a no stud profile shoe, the centre of rotation from repeats of a set series of movements could be used to provide more information to help answer the research question.

One of the limitations of the data collected was that participants were not observed to or perceived that they were slipping during any of the movements tested. This indicates that the limits of the shoe configuration were not tested; small displacements during contact were instead used to extrapolate potential slip directions. Kinematic and kinetic information of the movements performed on a force-plate were then used to estimate the period of time though to be at greatest risk of slipping. To fully validate this estimate and the potential slip directions, a controlled study using a support harness should be

undertaken, gradually reducing the coefficient of traction between the outsole and the surface until the participant slips.

For each set of data collected, the surface conditions need to be classified to allow further conclusions to be drawn from the results. Classification could be through means of a Clegg hammer drop test, or replication of the standard FIFA surface test procedures.

To ensure that any additional data collected is a valid representation of the population, Cochran's (1977) equation can be used to estimate the required sample size given unlimited resources for player recruitment and time available for data collection.

Equation 12.1

where z = confidence interval, σ = estimate of standard deviation, d = margin of error.

Using the mean standard deviation from the Doncaster Rovers FC test results for the pitch, yaw and roll angles on impact from all three movements ($\pm 8^\circ$), a margin of error of $\pm 1^\circ$ and a 95% confidence interval, the recommended sample size is approximately 250.

The analysis tools developed in Chapter 5, 8 and 9 can be used to analyse the results from further data collection to obtain the following information:

- Stud location through matrix transformation;
- Shoe velocity and acceleration using central differencing;
- Shoe orientation (pitch, yaw and roll);
- Time of impact from acceleration of impacting marker;
- Centre of rotation using the Reuleaux method;
- Helical screw axis parameters.

This level of information will then provide a greater understanding on the shoe-surface interaction for a range of different test conditions allowing a more informed decision on resulting mechanical test parameters or potential designs.

12.4 Influence of results on traction test methods and outsole design

12.4.1 Traction testing

The results from each study variable can be used to identify potential test parameters for mechanical traction testing devices. The new testing parameters could be used to recommend modifications to the existing traction testing device, as suggested in Chapter 10. The increased sample size and range of variables would ensure that the new test parameters best represent the range of scenarios likely to be experienced by a player wearing the shoes to be tested. The test parameter for the existing traction testing device might also be dependent on the outsole being tested and the intended conditions of use. For example, statistical analysis can be used to identify if significant differences exist between the test parameters selected for natural turf to those for artificial turf. If differences exist the most appropriate test parameters for the intended surface of use should be used.

Alternatively a new traction device could be developed to replicate a range of motions. The limitation of the existing traction testing device is that simultaneous changes in the position and orientation of the shoe are not possible. A new traction testing device could be designed to overcome this. When designing a new traction testing device, it should:

- Represent realistic movements;
- Produce results that are easy to compare;
- Produce results with a high repeatability;
- Be portable for use in different test environments (laboratory and outside);
- Have a short test time;
- Be easy to use.

This ensures that the device is applicable to traction assessment for manufacturers and also researchers.

One method to obtain both rotation and translation is to use a robotic arm with shoe attached on the end. To control a rigid body with six degrees of freedom (translation and rotation) either requires input data of nine coordinates of three points on the rigid body, or the helical axis parameters (Pliicker coordinates, translation displacement and angle of rotation). The use of helical axis parameters in robotic motion and

computational animations is becoming more popular due to the reduced number of input parameters required to describe the motion (Murray *et al.* 1994). Appendix A describes the helical screw axis parameters used to define the motion of the shoe through the sprint, kick and side-cut movements.

The potential limitation of this type of device is that the motion being represented by the shoe may only be specific to one particular scenario. Analysis of the extended data collection could be undertaken to deduce the effect of changing the shoe or surface conditions on the resulting shoe motion. The use of risk ratings to identify the time during the motion the participant is at most risk of slipping could be used to break the movement down into smaller motions. Assessment of only these motions instead of the complete movement may help reach the design goals of the new traction tester.

12A.2 Outsole design

In Chapter 11, an example of how further information on the shoe-surface interaction could be used to influence the design of outsoles. Using the additional information gained from the extended data collection, outsoles unique to specific conditions could be designed. For example, an outsole suited to attacking players on a natural grass surface may require greater influence on translational traction.

Further considerations on the designs of outsoles are:

- The location of the flex point on sole; this can influence metatarsal injuries and is often governed by the stud configuration and outsole design.
- Influence of plantar pressure; stud positions have been shown to influence the pressure points on the sole of the foot and are a prime factor in injuries or perceived comfort.
- Clogging; ploughing effects created by certain stud configurations and outsole materials may be more resistant to clogging than other designs; mechanical traction testing methods could be used to evaluate this.
- Weight: lightweight shoes are becoming more popular, the number and size of the studs and material selection of the outsole can affect the overall shoe weight.

Rapid manufacture can be used to produce prototype designs which can be mounted to lasts for mechanical traction testing using the realistic test parameters. The designs can then be developed into a test shoe for biomechanical assessment.

12.5 Chapter summary

Further work relating to the 3D measurement system, data collection approach and potential use of results was discussed leading to the identification of three main projects:

1. Fine tune the test protocol: improve viewing area and speed of analysis.
2. Undertake a large scale data collection: more variables, increased sample size.
3. Develop a new traction testing device: use new test parameters.

The projects outline the long term goal of the study; to develop or modify a traction testing device to fully replicate movements seen in match play situations. Short term projects can be carried out using the existing measurement system and analysis tools. An intermediate step in terms of current traction testing may be to assess the implications of modifying the test parameters to meet those recommended in Chapter 10.

14 CONCLUSIONS

This final chapter summarises the major findings from the research undertaken in this project. The aim of the project was to identify appropriate test parameters for traction testing of studded footwear. In order to fulfil this aim, the first stage of the project was to review current traction testing methods and define the requirements for appropriate test parameters. To identify the test parameters a 3D measurement system was developed to capture the shoe-surface interaction. A series of post processing steps were established to infer the shoe orientation, kinematics and kinetics. Data collection was undertaken both in the laboratory and outside on natural turf. The results from the data collection were used to provide an example of how appropriate test parameters can be obtained. Implications for traction testing and outsole design were discussed.

14.1 Assessment of current traction testing methodologies

A selection of traction testing methodologies was assessed to identify the advantages and disadvantages of experimental testing. Mechanical traction testing, identification of surface shear stresses and two modelling techniques were investigated to cover a range of the potential drawbacks of experimental testing; namely the use of non-representative movements and non-representative surfaces.

The adidas mechanical traction tester was used to investigate the translational and rotational traction values of a range of studded outsoles and a studded plate on natural and artificial turf. The following conclusions were made:

- The first advantage of mechanical testing was that the tests were controlled and repeats were easy to conduct.
- The device was also portable allowing realistic surfaces to be tested; soft and firm natural turf and an artificial turf were assessed.
- Although the surfaces were thought to be representative, one of the first findings from the study was the complexity of testing natural surfaces; a greater standard deviation in both traction and hardness readings was found compared to artificial surfaces.
- A plate with similar stud configurations to a range of outsoles was also tested to investigate the use of a plate to test experimental new stud configurations. However, the resulting traction value and traction curve for the plate was not

similar to the counterpart shoe. The primary reason for this was the additional surcharge pressure applied from the increased surface area of the plate. The orientation and centre of rotation of the plate and shoe also differed.

- One of the most important findings from the study was the change in traction ranking of the shoes when comparing the value at different displacements.

A photoelastic device was developed to identify the shear stresses between a studded outsole and the surface. Participants wearing studded footwear ran across a glass force-plate with photoelastic material on the surface. A high-speed camera was used to capture the dynamic photoelastic shear stress patterns; image processing was then used to identify the individual fringes and estimate the resulting shear stress. The images provided a visual aid for identifying the interaction between the surface and the studs. Although the movements of the participants were intended to be representative, the non-realistic surface raised concerns that participants were unable to move naturally. The non-realistic surface also limited the use of the technique for traction analysis.

Analytical and computation models were developed to provide a tool to estimate the vertical interaction between a stud and a surface. This was the first stage to developing a model that can represent the full shoe motion included translation. Both models were able to estimate the relative deformation of the stud and the surface, providing a prediction on the likely depth of penetration. The main limitation of the approach was that although individual sections of the model were validated against mechanical test results, the complete model under actual test loading conditions was not validated.

The main finding from the assessment of the three techniques was that in all approaches, prior knowledge of realistic test parameters would help improve the validity of the results and their suitability for traction measurements.

14.2 Development and validation of 3D measurement system

The first aim for the project was to develop and validate a 3D measurement system to capture the shoe-surface interaction during realistic football movements. A self-developed measurement system was chosen over commercially available motion capture packages as it allowed the system to be customised to suit the demands of the test environment and its intended application. The following system was developed:

- Two high-speed Phantom v4.3 cameras were chosen, filming at 1000 Hz with a resolution of 512 x 386.
- The cameras were calibrated using the checkerboard approach.
- Five white retro-reflective markers were painted onto the side of a Copa Mundial shoe to represent two rigid bodies (forefoot and rear-foot).
- A semi-automated tracking algorithm was developed using the self-windowing and image processing techniques to identify the markers in each frame.
- The consistency in locating the marker using the semi-automated algorithm was ± 0.24 pixels.
- The marker image coordinates were converted to global 3D coordinates using stereo-triangulation with the origin set near the centre of the filming zone (± 0.5 mm).
- The mean difference in mean position of an object tracked using the developed 3D measurement system and a commercially available system was 1.2 mm but the standard deviation of the developed system was lower.
- The marker coordinates were filtered using a 5-point moving average filter to reduce the influence of noise.
- A transformation matrix was used to convert the marker positions to stud coordinates (maximum propagated error ± 2.2 mm).
- The stud coordinates were then used to calculate the kinematics and orientation of the shoe.
- Matrix transformation was used to calculate the pitch, yaw and roll angles of the shoe at each time step (mean maximum propagated error $\pm 2.5^\circ$).
- The velocity was calculated using a 5-point central differencing method and then smoothed using a 5-point moving average filter (maximum propagated error ± 0.3 ms⁻¹).
- The acceleration was found from the pre-filtered velocity data using the 3-point central differencing method.
- The Reuleaux method was used to identify the 2D centre of rotation of the shoe when in contact with the surface using the intersection of the perpendicular bisectors from two consecutive time steps.

The 3D measurement system was concluded to have suitable levels of accuracy and reliability compared to commercial systems. The post processing techniques identified

allowed results to be analysed in depth to aid in understanding the shoe-surface interaction.

14.3 Data collection and analysis

Two data collection studies were carried using the developed 3D measurement system. The primary aim of the data collection process was to provide an example of the level of detail that could be obtained on the shoe-surface interaction and suggest how these results can be used to identify appropriate test parameters to meet the sponsors requirements.

The first data collection study took place in the laboratory using a single participant. This allowed more time to be taken over the data collection and the additional use of a force-plate was also available. The following findings were made:

- Using only one participant allowed a detailed discussion of the shoe kinematics, specifically identifying the changes in orientation of the shoe during impact.
- Force-plate data was used to compare shoe kinematics to kinetic information to help identify key event timings during the movement.
- The peak acceleration of the impacting shoe marker coincided with the activation of the force-plate identifying the time of initial foot-strike.
- The pitch, yaw and roll angles of the shoe were selected as variables that could be used as the first stage of larger sample size data analysis.

Using the knowledge gained from the controlled laboratory study, a larger cohort of eight youth team players from Doncaster Rovers FC participated in the study on a natural turf surface. The participants were asked to perform three movements (acceleration phase of sprinting, 45° lateral side-cut and a long range kick) five times. Only 60% of the trials collected were suitable for analysis. The following points summarise the data collected:

- Each trial was normalised setting the time of the peak acceleration of the impacting marker to zero.
- Statistical analysis was performed on each movement group to identify outliers or potential further groups.

- For the kick movement, K-means cluster analysis indicated that the group could be divided into two; a group with high pitch, yaw and roll angles, and one with low angles.
- A representative player trial was selected from each movement group using the minimum difference between the pitch, yaw and roll angles of each trial and the mean of the group. Full post processing analysis was carried out on each representative trial.
- Each movement was divided into three phases: foot-strike, transition and push-off.
- During the sprint movement, the shoe landed in a toe-down position, and immediately after foot-strike there was slight posterior motion and a change in the yaw and roll angles of the shoe. During the transition phase, change in the yaw angle related to the shoe rotating in the xy plane. The centre of rotation was calculated to be on the outer medial side of the forefoot. During push-off, the toe studs were observed to slip 16.8 mm posteriorly.
- During the kick movement, the planted foot landed in a toe-up and toe-out position, with substantial outward roll. As such, the lateral heel studs contacted the surface first. The resultant velocity on foot-strike acted in the medial direction. During transition, the pitch and roll angles reduced causing the shoe to be at a flatter angle to the surface; increasing the number of studs in contact. At the time of ball contact with the opposing foot, the planted foot was not observed to be in motion.
- During the side-cut movement, the shoe also landed in a toe-up position, but with inward roll. This caused the medial heel studs to contact the surface first. During initial foot-strike, lateral motion of 8.9 mm was observed. Full shoe rotation was observed during the transition phase, with the centre of rotation located on the medial side of the heel.

14.4 Influence of results

The findings from both data collection studies were used to identify potential test parameters for mechanical, analytical and computational traction testing methods.

For the mechanical traction tester, the shoe motion for each movement needed to be simplified to a translational or rotational movement. To identify which time period

during the movement should be represented, the critical slip time was estimated. This was found using the ratio of horizontal to vertical force, the velocity of the studs and the number of studs in contact with the surface during each movement. The normalised magnitude of each contributing factor was combined to identify the time at which the participant was thought to be at greatest risk of slipping. The following five sets of key test parameters were identified:

1. *Posterior translation of 20 mm at 350 mms⁻¹ with a pitch angle of 35°*: The final push-off phase was selected as the critical slip time for the sprint movement. During this time the shoe rotated in the yz plane about a point close to the toe. A potential slip of the toe when in contact with the surface was observed; this posterior slip was selected as the key motion for the sprint movement.
2. *Anterior translation of 15 mm at 300 mms⁻¹ with a pitch angle of 0°, yaw angle of 105° and roll angle of 20°*: For the kick movement, the initial moments of foot-strike were selected as the critical slip time. The shoe landed with lateral heel studs first and was observed to translate in a medial-anterior direction.
3. *Anterior translation of 10 mm at 150 mms⁻¹ with a pitch angle of -10°, yaw angle of -65° and roll angle of -30°*: The foot-strike phase for the side-cut movement was also selected as the critical slip time. The shoe landed with substantial inward roll and was observed to move approximately 10 mm laterally.
4. *External rotation of 12° at 170°s⁻¹ about the medial side of the forefoot (forefoot studs only)*. During the transition phase of the sprint movement, the centre of rotation of the change in yaw (toe-out) angle of the shoe in the xy plane was on the medial side of the forefoot.
5. *External rotation of 6° at 60°s⁻¹ about the medial side of the heel (complete shoe)*: The centre of rotation during the transition phase of the side-cut movement was close to the medial side of the heel.

The direction and orientation of the shoe during the kick and side-cut movements is one of the key findings from the results collected. The translation direction is rarely tested in traction assessment, yet is representative of the movement of the shoe during the time at which the player is at greatest risk of slipping.

For the analytical model, the velocity and effective mass of the stud on impact with the surface was calculated for each of the movements tested. The modified test parameters were applied to the existing analytical model and the predicted penetration depth

estimated. Results suggested that on a firmer surface the stud during the side-cut and sprint movements would not fully penetrate the surface during initial impact; this effectively reduces the contact area as the sole-plate is not in contact and potentially reduces the resulting traction.

To integrate the test parameters into a finite element model, three potential approaches were identified:

1. Mimic the complete motion of the shoe for each movement;
2. Use the motion of the shoe during the foot-strike, transition and push-off stages individually;
3. Replicate the test parameters identified for mechanical traction testing.

Each approach has its advantages and disadvantages. Using the complete trajectory of the shoe ensures that the movement is representative; but is specific only to one shoe-surface combination. The displacement of the shoe would be used to drive the model, preventing natural equilibrium from being reached; the effect of changing the stud configuration or surface conditions would be harder to identify. Using the individual stages improves the functionality of the model; the velocity of the shoe could be used instead of the displacement to drive the model. This would mean the resulting movement of the shoe into the surface would represent the traction properties. Using the same test parameters as the mechanical test device allows the finite element model to be validated but does not make use of the models ability to simultaneously change the orientation and position of the shoe during the movement; one of the limitations of the mechanical traction tester.

The observation of the shoe-surface interaction can also play a part in the future design of outsoles. Knowing the translation directions and the centre of rotations allows the studs to be shaped and positioned to enhance translational traction but minimise rotational resistance. In theory, this will help meet the balance for improving performance but minimising the risk of injury.

14.5 Limitations of the research

The following limitations were stated throughout the research:

- The shoe was approximated to two rigid bodies (forefoot and rear-foot).

- Circular tracking markers were used and have the potential to introduce eccentricity errors.
- The use of two cameras reduced the viewing area and restricted the range of rotational motion that could be tracked.
- Calculation of the 2D centre of rotation assumed no movement occurred in the other plane.
- A limited sample size was used for event detection (definition of time of foot-strike and push-off) which was applied to all collected data.
- A representative player was chosen for the in-depth analysis in Chapter 9; as such all conclusions drawn in further chapters relate only to that player trial.
- The results are representative only for the shoe-surface combination tested.

14.6 Future research

Three main projects were identified as long term research goals from the assessment of the development and application of the 3D measurement system and analysis of the results collected:

1. Improvements to the measurement system;
2. Large scale collection of results;
3. Implement data in traction testing devices and outsole design.

The main improvements in the measurement system involved the efficiency of the semi-automated tracking algorithm. Additional functions could be applied to aid in image processing and ultimately the effectiveness of the tracking ability. Using either the existing measurement system or a modified version of, large scale data collection studies could be undertaken to investigate a wider range of variables with a statistically significant sample size. Using the post processing and analysis techniques employed in this thesis, appropriate test parameters for a new traction tester could be identified for each of the variables collated.

REFERENCES

- Adidas Group, 2009. *Spirit of Sport* [online]. Available from: http://www.adidas-group.com/en/spiritofsports/story_1954.aspx [Accessed 28 October 2011].
- Adidas Group, 2011. *F10 TRX AG* [online]. Available from: <http://shop.adidas.co.uk/product/KU905/G40252/Sports/Men%27s-i-F10+TRX+AG/detail.jsf> [Accessed 28 October 2011].
- Agbinya, J.I. and Rees, D., 1999. Multi-object tracking in video. *Real-Time Imaging*, 5(5), pp.295-304.
- Ahmadi, A., Rowlands, D. and James, D.A., 2010. Towards a wearable device for skill assessment and skill acquisition of a tennis player during the first serve. *Sports Technology*, pp.1-8.
- Ahn, S.J., Warnecke, H.J. and Kotowski, R., 1999. Systematic Geometric Image Measurement Errors of Circular Object Targets: Mathematical Formulation and Corrections. *The Photogrammetric Record*, 16(93), pp.485-502.
- Andreasson, G., Lindenberger, U., Renstrom, P. and Peterson, L., 1986. Torque developed at simulated sliding between sports shoes and an artificial turf. *The American Journal of Sports Medicine*, 14(3), pp.225-230.
- Arcan, M. and Brull, M.A., 1976. A fundamental characteristic of the human body and foot, the foot-ground pressure pattern. *Journal of Biomechanics*, 9, pp.453-457.
- Baker, S.W., 1991. Temporal variation of selected mechanical properties of natural turf football pitches. *Journal Sports Turf Research Institute*, 67, pp.83-92.
- Barnett, S., Cunningham, J. L. and West, S., 2000. A comparison of vertical force and temporal parameters produced by an in-shoe measuring system and a force platform. *Clinical Biomechanics*, 15 (10), pp.781-785.
- Baroon, J. and Ravani, B., 2006. A three-dimensional generalization of Reuleaux's method based on line geometry. *Proceedings of IDETC/CIE 2006*, 10-13 September 2006 Philadelphia. Pennsylvania: ASME, pp.1-8.
- Baroon, J. and Ravani, B., 2009. A computational geometric solution of the kinematic registration problem using the bisecting linear line complex. *Computer-Aided Design and Applications*, 6(1-4), pp.1-13.
- Barry, E.B. and Milburn, P.D., 1999. A mechanism explaining traction of footwear on natural surfaces. *Proceedings of the 4th Symposium on Footwear Biomechanics* [online]. Available from: <http://www.staffs.ac.uk/isb-fw/Manuscr/Barry16.pdf> [Accessed 29 October 2011].
- BBC, 2005. *Ferguson wants bladed boot ban* [online]. Available from: http://news.bbc.co.uk/sport1/hi/football/teams/rn/man_utt/4277722.stm [Accessed 31 October 2011].
- Bentley, J.A., Ramanathan, A.K., Arnold, G.P., Wang, W. and Abboud, R.J., 2011. Harmful cleats of football boots: A biomechanical evaluation. *Foot and Ankle Surgery*, 17, pp.140-144.

- Blickhan, R., 1989. The spring-mass model for running and hopping. *Journal of Biomechanics*, 22, pp.1217-1227.
- Bloomfield, J., Polman, R. and O'Donoghue, P., 2007. Physical demands of difference positions in FA Premier League soccer. *Journal of Sports Science and Medicine*, 6, pp.63-70.
- Bloomfield, J., Polman, R., O'Donoghue, P., 2004. The 'Bloomfield Movement Classification': Motion analysis of individual players in dynamic movement sports. *International Journal of Performance Analysis in Sport*, 4(2), pp.20-31.
- Bobrowitsch, E., Hurschler, C., Olender, G., Plaass, C., Waizy, H., Arnold, H. and Stukenborg-Colsman, C., 2011. Digital stereophotogrammetry based on circular markers and zooming cameras: evaluation of a method for 3D analysis of small motions in orthopaedic research. *BioMedical Engineering* [online], 10. Available from: <http://www.biomedical-engineering-online.com/content/pdf/1475-925X-10-12.pdf> [Accessed 31 October 2011].
- Bouguet, J.Y., 2010. *Camera Calibration Toolbox for Matlab* [online]. Available from: http://www.vision.caltech.edu/bouguetj/calib_doc/ [Accessed 28 October 2011].
- Brighton, J.L. and Godwin, R.J., 2006. *Ground assessment*. US patent number: US 6,983,643 B2.
- Brinkgreave, R., 2005. Selection of soil models and parameters for geotechnical engineering applications. In: J.A. Yamamuro and V.N. Kaliakin eds. *Geotechnical Special Publication No. 128*. ACSE, pp.69-98.
- Brizuela, G., Ferrandis, R., Alcantara, E., Martinez, A. and Forner, A., 1998. Biomechanical design of football boots: Effect of studs on performance and injury prevention. In: H.J. Riehle and M.M. Vieten, eds. *16th International Symposium on Biomechanics in Sport*, 21-25 July 1998 Konstanz.
- Brouwer, C., Goffeau, A., and Heibloem, M., 1985. *Irrigation Water Management: Training Manual No. 1 – Introduction to Irrigation* [online]. Food and Agriculture Organisation of the United Nations. Available from: <http://www.fao.org/docrep/R4082E/r4082e00.htm#Contents> [Accessed 31 October 2011].
- Cameron, B.M. and Davis, O.M.D., 1973. The swivel football shoe: A controlled study. *The Journal of Sports Medicine*, 1(2), pp. 16-27.
- Canaway, P.M. and Baker, S.W., 1993. Soil and turf properties governing playing quality. In: R.N. Carrow, N.E. Christians and R.C. Shearman, eds. *International Turfgrass Society Research Journal 7*. Kansas: Intertec Publishing Corp., pp. 192-200.
- Canaway, P.M., Bell, M.J., Holmes, G. and Baker, S.W., 1990. Standards for the playing quality of natural turf for association football. In: R.C. Schmidt, E.F. Hoerner, E.M. Milner and C.A. Morehouse, eds. *Natural and Artificial Playing Fields: Characteristics and Safety Features*. Philadelphia: American Society for Testing and Materials, pp.29-47.
- Carre, M.J., Haake, S.J., Baker, S.W. and Newall, A., 1998. The analysis of cricket ball impacts using digital stroboscopic photography. In: S.J. Haake, ed. *The Engineering of Sport – Design and Development*. Sheffield: Blackwell Publishing, pp.379-386.

- Carre, M.J., James, D.M. and Haake, S.J., 2006. Hybrid method for assessing the performance of sports surfaces during ball impacts. *Proceedings of the Institution of Mechanical Engineers, Part L: Journal of Materials: Design and Applications*, 220, pp.30-39.
- Cavanagh, P.R., Valiant, G.A. and Misevich, K.W., 1984. Biological aspects of modelling shoe-foot interaction during running. In: E.C. Frederick, ed. *Sport Shoes and Playing Surfaces*. Illinois: Human Kinetic Publishers, Inc., pp.24-46.
- Cavanga, G.A., 1970. Elastic bounce of the body. *Journal of Applied Physiology*, 29(3), pp.279-282.
- Chen, X. and Davis, J., 2000. *Camera placement considering occlusion for robust motion capture*. Stanford University Computer Science Technical Report, CS-TR-2000-07.
- Choppin, S., Goodwill, S. and Haake, S., 2011. Impact characteristics of the ball and racket during play at the Wimbledon qualifying tournament. *Sports Engineering*, 13(4), pp.163-170.
- Choppin, S.B., 2008. *Modelling of tennis racket impacts in 3D using elite players*. Thesis (Ph.D.). The University of Sheffield.
- Clarke, J.D. and Carre, M.J., 2010. Improving the performance of soccer boots on artificial and natural soccer surfaces. In: A. Sabo, S. Litzengerger, P. Kafka and C. Sabo, eds. *8th Conference of the International Sports Engineering Association*, 11-14 July 2010 Vienna. London: Elsevier Ltd., pp.2775-2781.
- Cochran, W.G., 1977. *Sampling Techniques*. 3rd ed. Toronto: John Wiley & Sons.
- Dally, J.W. and Riley, W.F., 1991. *Experimental stress analysis*. 3rd ed. McGraw-Hill.
- Davis, B.L., Perry, J.E., Neth, D.C. & Waters, K.C., 1998. A device for simultaneous measurement of pressure and shear force distribution on the plantar surface of the foot. *Journal of Applied Biomechanics*, 14, pp.93-104.
- Di Salvo, V., Collins, A., McNeill, B. and Cardinale, M., 2006. Validation of Prozone: A new video-based performance analysis system. *International Journal of Performance Analysis in Sport*, 6(1), pp.108-119.
- DiDomenico, A., McGorry, R.W. and Chang, C.C., 2007. Association of subjective ratings of slipperiness to heel displacement following contact with the floor. *Applied Ergonomics*, 38, pp.533-539.
- Dixon, S. J., James, I.T., Blackburn, K., Pettican, N. and Low, D., 2008. Influence of footwear and soil density on loading within the shoe and soil surface during running. *Proceedings of the Institution of Mechanical Engineers, Part P: Journal of Sports Engineering and Technology*, 222(1), pp.1-10.
- Doncaster Weather Station, 2010. *Graphs* [online]. Available from: <http://doncasterwx.co.uk/graph.htm> [Accessed 13 October 2010],
- Doyle, F., 2004. *Modern Experimental Stress Analysis: Completing the solution of partially specified problems*. Chichester: John Wiley & Sons Ltd.
- Dr Baden Clegg Pty Ltd, 2011. *Impact Soil Tester* [online]. Available from: <http://www.clegg.com.au/index.asp> [Accessed 28 October 2011].

- Dvorak, J. and Junge, A., 2000. Football Injuries and Physical Symptoms. *The American Journal of Sports Medicine*, 28(5), pp.3-9.
- Eberharter, J.K. and Ravani, B., 2006. Kinematic registration in 3D using the 2D Reuleaux method. *Journal of Mechanical Design*, 128, pp.349-355.
- Edgerton, H., 2011. *Iconic images* [online]. Massachusetts: MIT. Available from: <http://edgerton-digital-collections.org/galleries/iconic/athletics> [Accessed 28 October 2011].
- Ehara, Y., Fujimoto, H., Miyazaki, S., Mochimaru, M., Tanaka, S. and Yamamoto, S., 1997. Comparison of the performance of 3D camera systems II. *Gait and Posture*, 5, pp.251-255.
- Ehara, Y., Fujimoto, H., Miyazaki, S., Tanaka, S. and Yamamoto, S., 1995. Comparison of the performance of 3D camera systems. *Gait and Posture*, 3(3), pp.166-169.
- Fenton, R.G. and Shi, X., 1990. Comparison of methods for determining screw parameters of finite rigid body motion from initial and final position data. *Transactions of the ASME*, 112, pp.472-479.
- Ferry, S., 2005. Slip testing of floorings. *SATPA Spotlight*, pp.6-7.
- FIFA, 2007. *FIFA Big Count 2006* [online]. Available from: http://www.fifa.com/mm/document/fifafacts/bcoffsurv/bigcount.statspackage_7024.pdf [Accessed 28 October 2011].
- FIFA, 2008. *FIFA Quality Concept for Football Turf: Handbook of test methods* [online]. Available from: http://www.uefa.com/MultimediaFiles/Download/uefa/UEFAMedia/74/52/07/745207_DOWNLOAD.pdf [Accessed 28 October 2011].
- Figuroa, P.J., Leite, N.J. and Barros, R.M.L., 2006. Tracking soccer players aiming their kinematical motion analysis. *Computer Vision and Image Understanding*, 101(2), pp.122-135.
- Ford, K. R., Manson, N.A., Evans, B.J., Myer, G.D., Gwin, R.C., Heidt, R.S. and Hewett, T.E., 2006. Comparison of in-shoe foot loading patterns on natural grass and synthetic turf. *Journal of Science and Medicine in Sport*, 9, pp.433-440.
- Frederick, E.C., 1986. Biomechanical consequence of sport shoe design. *Exercise and Sport Science Reviews*, 14, pp.365-400.
- Fujikaka, K., Yamamoto, T. and Takemura, M., 2007. A comparison of the mechanical characteristics of natural turf and artificial turf football pitches. *Football Science*, 4, pp.1-8.
- Garcia, A. C., Martinez, A., Solaz, J.S., Montero, J., Dura, J.V. and Ramiro, J.F., 1999. Development of a method for measuring horizontal forces in soccer boots studs during skills performance. *Forth Symposium of Footwear Biomechanics*, 5-7 August Canmore.
- Glowtec, 2011. *Starglow Deflective Paint* [online]. Available from: <http://glowpaints.co.uk/reflective-paint-info.htm> [Accessed 1 November 2011].
- Gonzalez, J. C., Martinez, A., Montero, J., Alemany, S. & Gamez, J., 2003. *Analysis of the horizontal forces in soccer boot studs for specific movements* [online]. Available from: http://www.staffs.ac.uk/isb-fw/Abstracts/GONZALEZ_ANALYSIS_OF.pdf [Accessed 28 November 2008].

- Gronqvist, R., Chang, W.R., Courtney, T.K., Leamon, T.B., Redfern, M.S. and Strandberg, L., 2001. Measurement of slipperiness: fundamental concepts and definitions. *Ergonomics*, 44(13), pp.1102-1117.
- Grund, T. and Senner, V., 2010. Traction behaviour of soccer shoe stud designs under different game-relevant loading conditions. In: A. Sabo, S. Litzenberger, P. Kafka and C. Sabo, eds. o *Conference of the International Sports Engineering Association*, 11 -14 July 2010 Vienna. London: Elsevier Ltd., pp.2783-2788.
- Grund, T., Senner, V. and Gruber, K., 2007. Development of a test device for testing soccer boots under game-relevant high-risk loading conditions. *Sports Engineering*, 10, pp.55-63.
- Haake, S.J., 1991. The impact of golf balls on natural turf II Results and conclusions. *Journal of Sports Turf Research Institute*, 67, pp.128-134.
- Haake, S.J., Carre, M.J., Kirk, R.F. and Senior, T., 2004. Traction of studded boots on turf. *Sports Engineering*, pp.544-551.
- Hall, M.J. and Riou, P., 2004. Football blades: a cause for concern. *British Journal of Sports Medicine*, 38, pp.642-644.
- Hennig, E.M., 2011. The influence of soccer shoe design on player performance and injuries. *Research in Sports Medicine*, 19(3), pp.186-201.
- Hreljac, A. and Marshall, R.N., 2000. Algorithms to determine event timing during normal walking using kinematic data. *Journal of Biomechanics*, 33, pp.783-786.
- ITV pic., 2011. *Rugby World Cup 2011 Semi Final* [online]. Available from: <http://www.itv.com/itvplayer/video/?Filter=281374> [Accessed 17 October 2011].
- Johnson, G.R., Dowson, D. and Wright, V., 1976. A biomechanical approach to the design of football boots. *Journal of Biomechanics*, 9, pp.581-585.
- Kaila, R., 2007. Influence of modern studded and bladed soccer boots and sidestep cutting on knee loading during match play conditions. *The American Journal of Sports Medicine*, 35(9), pp.1528-1536.
- Keefe, D.F., O'Brien, T.M., Baier, D.B., Gatesy, S.M., Brainerd, E.L. and Laidlaw, D.H., 2008. Exploratory visualisation of animal kinematics using instantaneous helical axes. In: A. Vilanova, A. Telea, G. Scheuermann and T. Moller, eds. *Eurographics/IEEE-VGTC Symposium on Visualisation 2008*, 26-28 May 2008 Eindhoven. Oxford: Blackwell Publishing, pp.863-870.
- Kelley, J., Choppin, S.B., Goodwill, S.R. and Haake, S.J., 2010. Validation of a love, automatic ball velocity and spin rate finder in tennis. In: A. Sabo, S. Litzenberger, P. Kafka and C. Sabo, eds. *8th Conference of the International Sports Engineering Association*, 11 -14 July 2010 Vienna. London: Elsevier Ltd., pp.2967-2972.
- Kelley, J.W., 2011. *Measuring ball spin rates in match play tennis*. Thesis (Ph.D.). Sheffield Hallam University.
- Kingston Museum and Heritage Service, 2010. *Eadweard Muybridge: Defining Modernities* [online]. London: Kingston University. Available from: http://www.eadweardmuybridge.co.uk/muybridge_image_and_context/animalJn_motion/# [Accessed 31 October 2011].

- Kirk, R. F., 2008. *Traction of association football boots*. Thesis (Ph.D.). The University of Sheffield.
- Kirk, R.F., 2005. *Summary of Internship*. Unpublished Presentation.
- Kirk, R.F., Noble, I.S.G., Mitchell, T., Rolf, C., Haake, S.J. and Carre. M.J., 2007. High-speed observations of football-boot-surface interactions of players in their natural environment. *Sports Engineering*, 10, pp.129-144.
- Kistler, 2011. *Multicomponent portable force plate* [online]. Available from: http://www.kistler.com/mediaaccess/9286B_BP__000-713e-10.11.pdf [Accessed 14 September 2011].
- Klanecki, B.E., 2001. *ME5247 Concepts underlying photoelasticity* [online]. Minneapolis: University of Minnesota. Available from: <http://www.me.umn.edu/education/courses/me5247/Photoelasticity/BasicConcepts/basicconcepts.html> [Accessed 15 July 2009].
- Koerger, H., 2007. *Smart Stud update: Summary from Biolab*. Unpublished Presentation.
- Kuhlman, S., Sabick, M., Pfeiffer, R., Cooper, B. and Forhan, J., 2009. Effect of loading condition on the traction coefficient between shoes and artificial turf surfaces. *Proceedings of Proceedings of the Institution of Mechanical Engineers, Part P: Journal of Sports Engineering and Technology*, 224, pp.155-165.
- Lees, A. and Nolan, L., 1998. The biomechanics of soccer: A review. *Journal of Sports Sciences*, 16, pp211-234.
- Livesay, G.A., Reda, D.R. and Nauman, E.A., 2006. Peak torque and rotational stiffness developed at the shoe-surface interface. *The American Journal of Sports Medicine*, 34(3), pp.415-421.
- Luo, G. and Stefanyshyn, D., 2011. Mechanically available traction as a limiting factor to curve sprinting performance. *Footwear Science*, 3(sup1), pp.100-101.
- Maiwald, C., (christian.maiwald@hsw.tu-chemnitz.de), 18 July 2011. *FBS2011 Presentation*. Email to H.F. Driscoll (H.F.Driscoll@shu.ac.uk).
- Manal, K.T. and Buchanan, T.S., 2004. *Biomechanics of human movement* [online]. McGraw-Hill. Available from: http://unhas.ac.id/tahir/BAHAN-KULIAH/BIO-MEDICAL/NEW/HANBOOK/0071449337_ar005-Biomechanics_Of_Human_Movement.pdf [Accessed 17 June 2011].
- Mason, M.T., 2011. *Lecture 8 – Representing displacements (Plucker coordinates of a line)* [online]. Pittsburgh: Carnegie Mellon University. Available from: <http://www.cs.cmu.edu/afs/cs/academic/class/16741-s07/www/lecture8.pdf> [Accessed 31 October 2011].
- Maxwell, J.C., 1853. On the Equilibrium of Elastic Solids. *Transactions of the Royal Society of Edinburgh*, 20(1), pp.30-73.
- McGorry, R.W., DiDomenico, A. and Chang, C.C., 2007. The use of a heel-mounted accelerometer as an adjunct measure of slip distance. *Applied Ergonomics*, 38(3), pp.369-376.

- McLean, B.D. and Tumilty, D.M., 1993. Left-right asymmetry in two types of soccer kick. *British Journal of Sports Medicine*, 27(4), pp.260-262.
- McNitt, A. S., Middour, R. O. and Waddington, D. V., 1997. Development and evaluation of a method to measure traction on turfgrass surfaces. *Journal of Testing and Evaluation*, 25(1), pp.99-107.
- McNitt, A., 2000. Traction on turf. *Grounds Maintenance*, 35(9), pp.4-9.
- MIT Museum, 1998. *Stroboscopic* [online]. Massachusetts: MIT. Available from: <http://edgerton-digital-collections.org/techniques/stroboscope> [Accessed 31 October 2011].
- Motion Analysis Corporation, 2011. *Movement analysis products* [online]. Available from: <http://www.motionanalysis.com/html/movement/products.html> [Accessed 31 October 2011].
- Muller, C., Sterzing, T., Lake, M. and Milani, T., 2010. Different stud configurations cause movement adaptations during a soccer turning movement. *Footwear Science*, 2(1), pp.21-28.
- Mumford, C., 2006. *The optimization of going management on UK racecourses using controlled water applications*. Thesis (EngD). Cranfield University.
- Muncaster, R., 1981. *A-level Physics*. Cheltenham: Stanley Thornes (Publishers) Ltd.
- Murray, R.M., Li, Z. and Sastry, S.S., 1994. *A mathematical introduction to robotic manipulation* [online]. California: CRC Press. Available from: <http://www.cds.caltech.edu/~murray/books/MLS/pdf/mls94-complete.pdf> [Accessed 31 October 2011],
- Nicon Metrology NV, 2011. *ModelMaker for articulated arm scanning*. Available from: http://www.nikonmetrology.com/handheld_scanners/mmdx_mmc/ [Accessed 31 October 2011].
- Nigg, B.M. and Liu, W., 1999. The effect of muscle stiffness and damping on simulated impact force peaks during running. *Journal of Biomechanics*, 32, pp.849-856.
- Nigg, B.M. and Yeadon, M.R., 1987. Biomechanical aspects of playing surfaces. *Journal of Sports Science*, 5, pp.117-145.
- Nigg, B.M., 1990. The validity and relevance of tests used for the assessment of sports surfaces. *Medicine and Science in Sports and Exercise*, 22(1), pp.131-139.
- Nike, INC., 2011. *Nike Mercurial Vapor Superfly III* [online]. Available from: http://store.nike.com/gb/en_gb/?l=shop,pdp,ctr-inline/cid-102602/pid-421306/pgid-392358 [Accessed 31 October 2011].
- Nishizawa, Y., Fujita, T., Matsuoka, K. and Nakagawa, H., 2006. Contact pressure distribution features in Down syndrome infants in supine and prone positions, analysed by photoelastic methods. *Pediatrics International*, 48, pp.484-488.
- Olshausen, B.A., 2010. *Aliasing [onWne]*. Berkley: University of California. Available from: <http://redwood.berkeley.edu/bruno/npb261/aliasing.pdf> [Accessed 31 October 2011].
- Orchard, J., 2001. The AFL Penetrometer Study: Work in Progress. *Journal of Science and Medicine in Sport*, 4(2), pp.220-232.

- Orchard, J., Rodas, G., Til, L., Ardevol, J. and Chivers, I., 2008. A hypothesis: could portable natural grass be a risk factor for knee injuries? *Journal of Sports Science and Medicine*, 7(1), pp.184-197.
- Orr, J.F. and Shelton, J.C., eds., 1997. *Optical measurement methods in biomechanics*. Bury St. Edmunds: Chapman & Hall.
- Perkins, P.J., 1978. Measurement of slip between the shoe and ground during walking. In: C. Anderson and J. Senne, eds. *Walkway Surfaces: Measurement of slip resistance*. American Society for Testing and Materials, pp.71-87.
- Persson, B.N.J., 1998. *Sliding friction: physical principles and applications*. London: Springer.
- Phantom Zone, 2010. *Matlab Cine Reader* [online]. Available from: <http://www.visionresearch.com/phantomzone/viewtopic.php?f=4&t=738> [Accessed 1 November 2011].
- Potthast, W., Verhelst, R., Hughes, M., Stone, K. and De Clercq, D., 2010. Football-specific evaluation of player-surface interaction on different football turf-systems. *Sports Technology*. 3(1), pp.5-12.
- Price, D., 2008. *Smart Stud Development*. Unpublished Presentation.
- Prozone, 2009. *Prozone3 – Precise player tracking* [online]. Available from: <http://www.prozonesports.com/product-prozone3.html> [Accessed 31 October 2011].
- Queen, R. M., Charnock, B.L., Garrett, W.E., Hardaker, W.M., Sims, E.L. and Moorman, C.T., 2008. A comparison of cleat types during two football-specific tasks on FieldTurf. *British Journal of Sports Medicine*, 42, pp.278-284.
- Quintic Consultancy Ltd., 2011. *Markers -Automatic digitisation* [online]. Available from: <http://www.quintic.com/software/biomechanics/markers.htm>. [Accessed 31 October 2011].
- Redfern, M.S., Cham, R., Gielo-Periczak, K., Gronqvist, R., Hirvonen, M., Lanshammar, H., Marpet, M. and Pai, C.Y.C., 2001. Biomechanics of slips. *Ergonomics*, 44(13), pp.1138-1166.
- Rennie, D., 2010. The association between ground hardness and injury over the course of a season in professional football. *The 2nd SportSURF Conference* [online], 21-22 April 2010 Loughborough. Available from: <http://sportsurf.lboro.ac.uk/workshops/STARSS/SE/DR.pdf> [Accessed 31 October 2011].
- Rhodes, A., Sherk, H.H., Black, J. and Margulies, C., 1988. High resolution analysis of ground foot reaction forces. *Foot & Ankle*, 9(3), pp.135-138.
- Richards, J.G., 1999. The measurement of human motion: A comparison of commercially available systems. *Human Movement Science*, 18, pp.589-602.
- Robertson, D.G.E., Caldwell, G.E., Hamil, J., Kamen, G. and Whittlesey, S.N., 2004. *Research methods in biomechanics*. Leeds: Human Kinetics.
- Rogers, J.N. and Waddington, D.V., 1989. The effect of cutting height and verdure on impact absorption and traction characteristics in tall fescue turf. *Journal of Sports Turf Research Institute*, 65, pp.80-90.

- Rugby World, 2011. *France 9 Wales 8* [online]. Available from: <http://www.rugbyworld.com/news/france-9-wales-8-oh-the-agony/> [Accessed 17 October 2011].
- Sallam, A., 2009. Application of finite element analysis in geotechnical engineering. *Florida Engineering Society Journal*, 5, pp.29-31.
- Seeley, 2009. *Filtering considerations* [online]. Brigham Young University. Available from: [http://iodine.byu.edu/~seeley/exsc663\(seeley\)/filtering_considerations.pdf](http://iodine.byu.edu/~seeley/exsc663(seeley)/filtering_considerations.pdf) [Accessed 21 June 2011].
- Setterwall, D., 2003. *Computerised Video Analysis of Football – Technical and Commercial Possibilities for Football Coaching*. Thesis (MSc). University of Stockholm.
- Shorten, M., Hudson, B. and Himmelsbach, J., 2003. Shoe-surface traction of conventional and in-filled synthetic turf football surfaces. In: P. Milburn ed. *Proceedings of the XIX Congress of Biomechanics*, New Zealand. University of Otago.
- Slabaugh, G.G., 1999. *Computing Euler angles from a rotation matrix* [online]. Available from: <http://www.gregslabaugh.name/publications/euler.pdf> [Accessed 30 October 2011].
- Spoor, C.W. and Veldpaus, F.E., 1980. Rigid body motion calculated from spatial co-ordinates of markers. *Journal of Biomechanics*, 13, pp.391-393.
- Stein, G.P. and Shashua, A., 1997. On degeneracy of linear reconstruction from three views: Linear line complex and applications. *IEEE Transactions on Pattern Analysis and Machine Intelligence*, 21(3), pp.244-254.
- Sterzing, T. and Hennig, E.M., 2008. The influence of soccer shoes on kicking velocity in full-instep kicks. *Exercise and Sport Science Reviews*, 36(2), pp.91-97.
- Sterzing, T., Muller, C. and Milani, T.L., 2010. Artificial Soccer Turf – What shoes to wear. In: P.R. Fleming and S.E. Forrester, eds. *2nd International Conference of the SportSURF Network*, 21-22 April 2010 Loughborough. Loughborough: Loughborough University.
- Stiles, V.H., James, I.T., Dixon, S.J. and Guisasola, I.N., 2009. Natural Turf Surfaces; The case for continued research. *Sports Medicine*, 39(1), pp.65-84.
- Strainoptics Technologies Inc., N.D. *Fundamentals of photoelasticity* [online]. Available from: http://www.strainoptics.com/page.asp?page_id=87 [Accessed 8 June 2009].
- Sun, Z., Howard, D. and Moatamedi, M., 2005. Finite-element analysis of footwear and ground interaction. *Strain*, 41, pp.113-115.
- Taylor, J.R., 1997. *An introduction to error analysis: the study of uncertainties in physical measurements*. 2nd ed. Sausalito: University Science Books.
- Taylor, L., 2010. Steve Bruce demands inquiry into modern boots as cause of injury spate. *The Guardian* [online]. Available from: <http://www.guardian.co.uk/football/2010/sep/16/steve-bruce-boots-injuries> [Accessed 31 October 2011].
- Tipler, P.A. and Mosca, G., 2004. *Physics for Scientists and Engineers*. 5th ed. New York: W.H. Freeman and Company.
- Torell, V.B., 2011. As fast as possible rather than well protected: experiences of football clothes *Journal of Cultural Research*, 3, pp.83-99.

- Twomey, D.M., Otago, L. and Saunders, N., 2011. Challenges in the development of standards for synthetic turf for Australian football and cricket. *Proceedings of the Institution of Mechanical Engineers, Part P: Journal of Sports Engineering and Technology*, 225, pp.93-101.
- Urry, S., 1999. Plantar pressure-measurement sensors. *Measurement Science and Technology*, 10, pp.16-32.
- Utsumi, O., Miura, K., Ide, I., Sakai, S. and Tanka, H., 2002. An object detection method for describing soccer games from video. *2002 IEEE International Conference on Multimedia and Expo*, pp.45-48.
- Vachon, F., 2005. Football boot sole configurations and their influence upon surface adhesion. *International Association for Sports Surface Science* [online]. Available from: http://www.iss-sportsurfacescience.org/downloads/documents/G616R0ZADF_Sole_Mat_Friction_Vachon.pdf [Accessed 29 October 2011].
- Valiant, G.A., 1993. Friction – Slipping – Traction. *Sportverletz Sportschaden*, 7, pp.171-178.
- Whyld, N., 2004. *3D image reconstruction from a stereo camera pair: Assessment of calibration techniques*. Sheffield: The University of Sheffield.
- Winner, D., 2005. *Those Feet*. London: Bloomsbury.
- Winter, D.A., 2005. *Biomechanics and motor control of human movement*. 3rd ed. Hoboken: John Wiley & Sons, Inc..
- Zhang, Z., 1999. Flexible camera calibration by viewing a plane from unknown orientations. *Proceedings of the 7th IEEE International Conference on Computer Vision*, 20-27 September 1999 Corfu, Greece: IEEE, pp.666-673.

PERSONAL BIBLIOGRAPHY

Driscoll, H., Koerger, H., Senior, T. and Haake, S., 2010. The use of photoelasticity to identify surface shear stresses during running. *In: A. Sabo, S. Litzenberger, P. Kafka and C. Sabo, eds. 8th Conference of the International Sports Engineering Association, 11 -14 July 2010 Vienna.* London: Elsevier Ltd., pp.3047-3052.

Driscoll, H., Kirk, B., Holmes, C., Koerger, H. and Haake, S., 2011. Tracking of foot movement during sprinting in studded footwear. *Footwear Science*, 3(sup1), pp.S51-S53.

A. APPENDICES

A.1 Helical screw axis

The helical screw axes were analysed for each movement to investigate whether they aided in the understanding of the shoe-surface interaction. The Euler angle approach used to define the orientation of the shoe could also be used, but the helical screw axis has the advantage that it lends itself well to animations which is an important aid to visualisations. The helical screw axis also eliminates the problem of Gimbal lock and is less prone to error when rotations are small. However, the downsides are that it is sensitive to noisy data and does not directly represent anatomical features (Robertson *et al.* 2004).

A method of calculating the helical screw axis from positional data over a series of time-steps needed to be implemented in order to apply it to the motion of the shoe. Various approaches have been developed to find the screw parameters from only three points; the most frequently used methods are the least squares technique, Rodrigues' formula and Begg's method of solving a set of simultaneous equations (Fenton and Shi 1990). The bisecting linear line complex method was chosen for its computational efficiency and similarities with the 2D Reuleaux method.

A. 1.1 Linear line complex

A computational method for identifying the screw parameters was developed based on the linear line complex solution outlined by Baroon and Ravani (2009). A linear line complex is a set of lines in space intersecting at a common line (Stein and Shashua 1999). Figure A.1 shows two positions of a rigid body (F, F'); there always exists a shortest helical screw displacement between these two positions (axis, A) (Eberharter and Ravani 2006). Computing the midpoint, M_i between two points in the first and second positions (F, F') allows lines incident with the midpoint and orthogonal to the connecting line (G_i) to define a bisecting plane. The union of these lines on the bisecting plane is a linear line complex $(C:(C,C))$ (Eberharter and Ravani 2006).

Figure A.1 - Left: Bisecting linear line complex; Right: The linear line complex of path normal (adapted from Eberharder and Ravani 2006).

Helical screw axes are typically given in terms of Plucker coordinates. Plucker coordinates are used as a way to specify a line in a 3D space using the direction of the line and a vector direction from the origin to the nearest point on the line. A Plucker coordinate is written as $Q \setminus (q ; q0)$ where

p is a point on the line

q is the direction vector to the line

and $q\$ = p \times q$ is the moment vector; this gives the six Plucker coordinates (Mason 2011).

The following method was used to calculate the helical screw axis and parameters:

a) Rigid body points before and after displacement

$$\begin{array}{r}
 P_i^* \quad p_{2x} \quad p_{3x} \\
 P_i = \begin{array}{l} P_{iy} \\ LP_i^{\wedge} J \end{array} ; P_2 = \begin{array}{l} P_{zy} \\ \setminus . P_2 Z \setminus \end{array} ; P_3 = \begin{array}{l} P_{ay} \\ LP_a^{\wedge} J \end{array} \\
 \\
 P_i^* \quad P_{l^*} \quad P_a^* \\
 P_i^* = \begin{array}{l} P_{iy}' \\ -P_{iz}' \end{array} ; P_2' = \begin{array}{l} P_{2y}' \\ -P_{2z}' \end{array} ; P_3 = \begin{array}{l} P_{ay}' \\ . P_a < \end{array}
 \end{array}$$

a) Define midpoints between original and displaced points

$$\text{II) } = \frac{(P_i + P_i^*)}{\text{-----}}$$

b) Define connecting vector line between original and displaced points

$$g_i = p'_i - p_i$$

c) Every midpoint of a pair with its connecting line forms a null plane of the bisecting linear line complex; $C = (c, \bar{c})$

$$\bar{c} = - \begin{bmatrix} m_1 \\ m_2 \\ m_3 \end{bmatrix}^{-1} \begin{bmatrix} m_1 \cdot g_1 \\ m_2 \cdot g_2 \\ m_3 \cdot g_3 \end{bmatrix}$$

d) The direction vector, c of the bisecting linear line complex is found from

$$c = \begin{bmatrix} g_1 \times m_1 \\ g_2 \times m_2 \\ g_3 \times m_3 \end{bmatrix}^{-1} \begin{bmatrix} (g_1 + \bar{c}) \cdot g_1 \\ (g_2 + \bar{c}) \cdot g_2 \\ (g_3 + \bar{c}) \cdot g_3 \end{bmatrix}$$

e) Pitch of bisecting linear line complex

$$P_{blc} = \frac{c \cdot \bar{c}}{c^2}$$

f) The line part of the screw axis of the helical motion between two positions is the line of the bisecting linear line complex axis. The Plücker coordinates of the helical axis are $A = (a, \bar{a})$

$$a = \frac{-c}{|-c|}$$

$$\bar{a} = \frac{P_{blc} * c - \bar{c}}{|-c|}$$

g) The translation distance along the axis is

$$d = (p'_i - p_i) \cdot a$$

h) The angle of rotation around the axis is

$$\varphi = 2 \tan^{-1} \left(\frac{d}{2P_{blc}} \right)$$

i) The pitch of the screw axis displacement is

$$P = \frac{d}{\varphi}$$

Once the helical screw parameters have been identified, a visual representation of the helical screw motion can be obtained. To plot the screw axis, a point lying on the axis is first found, I . Projecting the vectors between points onto one plane and applying the 2D Reuleaux method can be used to define the location of I . Using the knowledge that $a = a \times I$ (Eberharter and Ravani 2006), product identities can be used to solve for I .

j) Point on helical screw axis

$$(a \times a)$$

$$(a \ a)$$

The calculations in the methodology were validated using the following example in the literature (Eberharter and Ravani 2006):

$$\begin{array}{r} \mathbf{T} \quad \quad \quad '4' \quad \quad \quad 7' \\ \mathbf{P1} = \begin{array}{l} 1 \\ .7. \end{array} ; \mathbf{p2} = \begin{array}{l} 7 \\ .1. \end{array} ; \mathbf{Ps} = \begin{array}{l} 10 \\ 10. \end{array} \end{array}$$

$$\begin{array}{r} \quad \quad \quad 7' \quad \quad \quad '3' \quad \quad \quad 10' \\ \mathbf{P1}' = \begin{array}{l} 1 \\ .7. \end{array} ; \mathbf{p2}' = \begin{array}{l} 9 \\ .6. \end{array} ; \mathbf{Ps}' = \begin{array}{l} 10 \\ .13. \end{array} \end{array}$$

The computational method gives a helical axis with Pliicker coordinates, $A : (0.57735 : 0.57735 : 0.57735 ; 0.0 : 0.0 : 0.0)$, a displacement angle of ($p = 60.0^\circ$ and translation of $d = 3.4641$ giving a pitch of $P = 3.308$). These parameters are in agreement with the values given by Eberharter and Ravani (2006). The helical axis also passes through the origin, $I = (0, 0, 0)$.

The results produced by the described methodology were validated by comparison with the Rodrigues' method outlined by Spoor and Veldpaus (1980) where

$$Q = a \tan \frac{\langle p \rangle}{2} \quad \text{Equation A.1}$$

$$\mathbf{P1} - \mathbf{P2} - \mathbf{P1} + \mathbf{P2} = \quad \times (\mathbf{p1} - \mathbf{P2} + \mathbf{P1} - \mathbf{Pz}) \quad \text{Equation A.2}$$

$$\mathbf{P1} - \mathbf{P3} * \mathbf{P1} + \mathbf{P3} = \quad \times (\mathbf{P1} - \mathbf{P3} + \mathbf{P1} - \mathbf{Pz}) \quad \text{Equation A.3}$$

Using the results from the previous example ($\langle p \rangle = 60.0^\circ$), the value for Q was calculated. Using this, the values of both the left and the right-hand side of equation 5.9 were then

determined. The values were found to be equal and thus, the results from the described methodology were shown to be the same as other methods.

Errors can arise from using the helical screw axis method when either the angle of rotation or displacement distance are small. To check that the helical screw axis generated for each set of data was appropriate, the distances of the 3 points before and after displacement from the helical axis were calculated. The consistency of the distances before and after displacement gave indication to the suitability of the helical axis position.

To graphically view the change in helical screw axis parameters over series of time steps; an approach similar to Keefe *et al.* (2008) was chosen. The helical screw axis direction vector is represented by an arrow originating from position I. A cylinder around the direction vector symbolises the helical axis parameters; the length of the cylinder corresponds to the displacement and the radius of the cylinder represents the angle of rotation (Figure A.2).

6

5.

Figure A.2 - Visual representation of helical screw axis parameters; arrow represents the direction of the helical screw axis, radius of the cylinder relates to the angle of rotation and length of cylinder to the displacement along the axis.

This approach is well suited to computational methods, whereby the movement of a rigid body can be described by its helical screw axis parameters reducing the number of input variables.

A. 1.2 Helical screw axis for the sprint movement

The helical screw axis parameters were derived for the sprint movement PeS? for 0.01 s before to 0.15 s after impact at 0.01 s intervals using the three markers on the side of the shoe. Table A.1 shows helical screw parameters at each time step. The direction of the helical axes varied throughout the movement but tended to be predominately in the anterior-posterior direction during the early stages of the movement and in the medial-lateral direction towards the latter. From time impact to 0.04 s after, the helical axis was mostly in the anterior-posterior direction. During this time frame, the rotations about the axis were small, and although translation distances are not large, they suggest that the shoe is predominantly moving in the anterior-posterior direction. Towards the end of the movement (0.11 to 0.14 s after impact), the helical screw axis was principally in the medial-lateral direction. Rotations during this time period were significantly larger than the rest of the movement. This suggests the shoe was rotating in the yz plane; as expected during the push-off phase of the movement. Figure A.3 illustrates the position of the helical axis relative to the shoe during the sprint movement.

Time step (s)	<i>a</i> (direction vector)			<i>d</i> (mm)	<P(°)	Pitch (mm/rad)
-0.01 -0.00	0.803	-0.400	-0.441	0.54	-0.19	-167.88
0.00-0.01	-0.046	0.975	-0.218	-1.88	1.01	-106.89
0.01-0.02	0.352	-0.930	-0.105	3.70	1.92	110.64
0.02 - 0.03	-0.282	0.756	-0.591	1.41	-1.53	-52.95
0.03 - 0.04	-0.413	-0.871	0.266	0.02	0.03	28.73
0.04 - 0.05	-0.695	0.603	0.391	-0.48	1.67	-16.33
0.05 - 0.06	-0.454	-0.112	0.884	3.35	3.06	62.78
0.06 - 0.07	-0.266	-0.946	-0.184	-4.17	12.22	-19.53
0.07 - 0.08	-0.676	-0.453	0.582	2.13	4.91	24.82
0.08 - 0.09	-0.997	0.025	-0.072	1.01	2.39	24.34
0.09-0.10	-0.811	-0.584	0.023	-0.74	-1.41	30.00
0.10-0.11	-0.638	-0.770	-0.012	-3.22	4.27	-43.17
0.11 -0.12	-0.969	0.225	-0.106	7.85	10.34	43.52
0.12-0.13	-0.876	-0.474	0.093	-1.94	8.86	-12.55
0.13-0.14	-0.945	-0.195	-0.261	-8.11	11.33	-41.02
0.14-0.15	-0.854	-0.273	0.443	7.97	10.87	42.02

Table A.1 - Helical screw axis parameters for the sprint movement (bold indicates dominant direction).

Figure A.3 - Helical axis position for the sprint movement.

A. 1.3 Helical screw axis for the kick movement

The helical screw axis parameters were found for time steps of 0.01 s for 0.02 s before to 0.24 s after impact.

The helical screw axis was predominantly in the medial-lateral direction throughout the majority of the kick motion. Screw axis parameters were more varied compared to the sprint movement and in some case extremely small displacements and rotations were observed. The accuracy of the helical screw axis is compromised when displacements and rotations are small which questions its validity at a number of time steps during the kick movement.

Time step (s)	a (direction vector)			d (mm)	$\langle P \rangle$ (°)	Pitch (mm/rad)
-0.02--0.01	-0.278	-0.719	-0.637	-18.3	15.1	-69.1
-0.01 -0.00	-0.859	0.491	0.148	-1.1	-66.0	1.0
0.00-0.01	0.886	-0.206	0.416	21.8	18.5	67.5
0.01-0.02	0.958	0.265	0.113	9.8	94.4	5.9
0.02 - 0.03	-0.819	0.547	-0.172	-1.1	-18.6	3.5
0.03 - 0.04	-0.882	-0.196	-0.428	4.1	-40.0	-5.8
0.04 - 0.05	0.566	0.694	0.444	2.4	1.2	114.6
0.05 - 0.06	-0.780	-0.609	-0.149	-1.2	0.6	-125.0
0.06 - 0.07	0.625	-0.551	-0.553	-1.8	1.8	-55.1
0.07 - 0.08	0.996	0.089	0.006	-0.3	-16.9	0.9
0.08 - 0.09	-0.827	0.563	0.000	2.1	13.2	9.1
0.09-0.10	-0.962	-0.272	-0.022	-0.8	18.0	-2.6
0.10-0.11	-0.482	0.875	-0.054	0.0	0.0	5.8
0.11-0.12	-0.875	0.403	0.270	1.9	0.2	531.8
0.12-0.13	-0.737	0.079	-0.671	1.0	1.1	50.9
0.13-0.14	-0.946	-0.313	0.086	1.4	51.3	1.6
0.14-0.15	-0.779	0.628	-0.010	1.8	2.7	39.2
0.15-0.16	-0.052	-0.998	-0.039	-1.3	1.9	-39.1
0.16-0.17	-0.910	-0.138	-0.391	0.0	-1.0	1.5
0.17-0.18	-0.880	0.091	0.467	7.7	38.2	11.5
0.18-0.19	-0.925	0.056	0.375	7.9	29.1	15.6
0.19-0.20	-0.861	0.321	0.394	11.6	28.4	23.3
0.20-0.21	-0.864	-0.487	0.128	2.4	-33.8	-4.1
0.21-0.22	-0.633	-0.628	0.454	0.0	0.0	36.3
0.22 - 0.23	-0.502	0.417	0.758	15.2	8.9	98.3
0.23 - 0.24	-0.278	-0.719	-0.637	-18.3	15.1	-69.1

Table A.2 - Helical screw axis parameters for the kick movement.

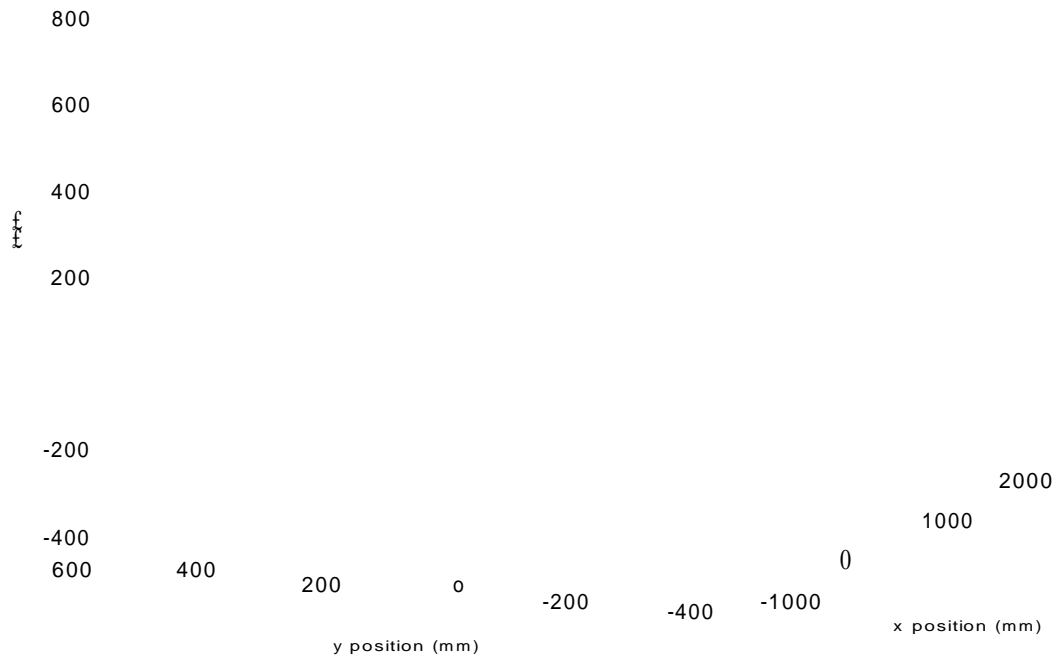


Figure A.4 - Helical screw axis positions throughout kick movement (kick positions in red).

A. 1.4 Helical screw axis for the side-cut movement

The side-cut helical screw axis parameters are also varied, similar to the kick movement and showed a range of large and small displacements and rotations. At the beginning of the movement, the helical screw axis was mostly in the medial-lateral direction, but appeared to rotate to a more anterior-posterior direction in the middle stages of the movement. This was apparent in the xy view of the helical screw axis positions shown in Figure A.5. Unlike the kick movement, the helical axis is situated close to the leg/foot and appears to rotate about this position as the movement progresses.

Time step (s)	a (direction vector)			d (mm)	$\langle P \rangle$ (°)	Pitch (mm/rad)
-0.01 -0.00	-0.678	-0.684	-0.269	10.9	11.3	55.3
0.00-0.01	-0.972	0.161	-0.172	10.6	50.7	12.0
0.01-0.02	0.951	-0.273	0.147	-3.5	167.5	-1.2
0.02 - 0.03	0.685	-0.103	-0.721	-4.3	-44.8	5.5
0.03 - 0.04	-0.860	0.429	-0.275	-0.9	-4.3	12.5
0.04 - 0.05	0.893	0.098	0.438	-3.6	51.1	-4.1
0.05 - 0.06	-0.032	-0.999	0.038	-0.9	6.7	-7.3
0.06 - 0.07	0.898	-0.151	0.414	-2.1	10.0	-12.2
0.07 - 0.08	-0.167	-0.522	-0.837	-0.5	-1.5	17.8
0.08 - 0.09	-0.373	0.751	0.546	-1.1	3.2	-20.7
0.09-0.10	0.588	-0.644	-0.489	-0.9	1.4	-38.1
0.10-0.11	-0.906	-0.392	0.159	1.1	13.3	4.9
0.11-0.12	-0.470	0.854	-0.223	-0.8	9.4	-5.0
0.12-0.13	-0.511	-0.727	0.458	0.3	1.2	15.8
0.13-0.14	-0.244	-0.967	-0.077	1.4	4.4	18.0
0.14-0.15	-0.087	0.334	0.939	-0.8	4.8	-9.2
0.15-0.16	-0.354	-0.899	-0.258	-0.8	1.9	-23.5
0.16-0.17	-0.556	0.757	-0.343	-0.1	-0.2	36.6
0.17-0.18	-0.643	0.718	0.268	0.3	1.1	14.4
0.18-0.19	-0.958	-0.148	0.245	2.9	-28.2	-5.8
0.19-0.20	-0.447	0.511	-0.734	-1.8	-7.5	13.9
0.20-0.21	-0.003	-0.973	-0.230	-3.5	8.0	-24.8
0.21 -0.22	-0.926	-0.375	-0.044	-0.4	4.1	-4.9
0.22-0.23	-0.394	0.260	0.882	14.9	34.4	24.8

Table A.3 - Helical screw axis parameters for the side-cut movement.

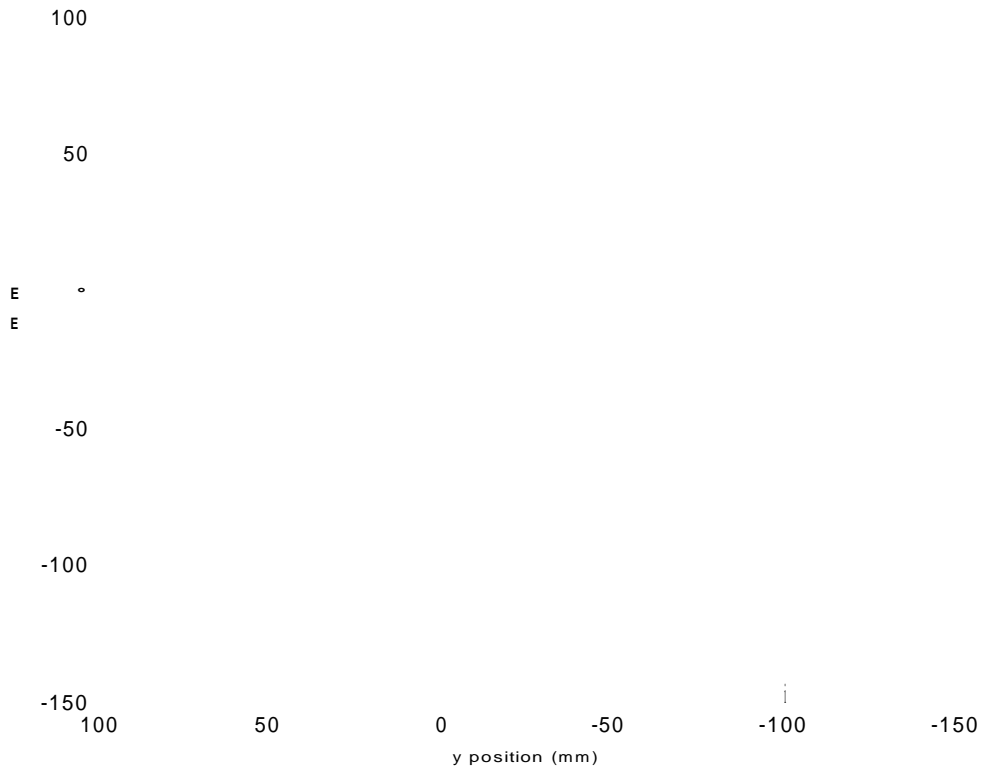


Figure A.5 - Helical screw axis position for side-cut movement.

A. 1.5 Summary helical screw axis

Analysis of the resultant helical screw axis for each movement indicates that both the sprint and the side-cut axes act predominantly in the anterior-posterior direction but for the kick the medial-lateral direction is the most dominant. The sprint helical axis parameters indicated greater translation and rotation than the other movements. The translation was primarily in the anterior direction as expected.